THE
PHYSICAL REVIEW
A Journal of Experimental and Theoretical Physics Established by E. L. Nichols in 1893
VOL. 57, NO. 9 MAY 1, 1940 SECOND SERIES

The Electric Quadrupole Moments of Ga^{69} and Ga^{71}

An Atomic Beam Study of the Hyperfine Structures of the $^2P_{1/2}$ and $^2P_{3/2}$ States of Ga^{69} and Ga^{71} *

NICHOLAS AUGUSTUS RENZETTI
Columbia University, New York, New York
(Received February 23, 1940)

An investigation of the hyperfine structures of the ground $^2P_{\frac{1}{2}}$ state, and the metastable $^2P_{3/2}$ state of the two isotopes 69 and 71 of gallium has been made with the zero-moment method of atomic beams. Six zero-moment peaks, three for each isotope, of the metastable state and two, one for each isotope, of the ground state have been observed. It has been found that the h.f.s. energy levels for the higher state can be described by an equation of the form $E=aC/2+bC(C+1)$, where "a" and "b" are the interval rule and quadrupole interaction constants, respectively.

Ga^{69}: $b/a=0.0136\pm0.0004$; $b=(8.69\pm0.43)\times10^{-5}$ cm^{-1}; $a=(6.39\pm0.12)\times10^{-3}$ cm^{-1}

Ga^{71}: $b/a=0.0068\pm0.0004$; $b=(5.51\pm0.39)\times10^{-5}$ cm^{-1}; $a=(8.11\pm0.11)\times10^{-3}$ cm^{-1}.

From these the h.f.s. separations are

Ga^{69}: $\Delta\nu=(0.0362\pm0.0007)$ cm^{-1}; Ga^{71}: $\Delta\nu=(0.0474\pm0.0007)$ cm^{-1}

and the quadrupole moments are

$Q^{69}=0.20\times10^{-24}$ cm^2; $Q^{71}=0.13\times10^{-24}$ cm^2.

The nuclear spins are verified to be $\frac{3}{2}$. From the zero-moment peaks of the normal state we obtain $\mu_{71}/\mu_{69}=\Delta\nu_{71}/\Delta\nu_{69}=1.270\pm0.006$ and these separations are

Ga^{69}: $\Delta\nu=(0.0897\pm0.0011)$ cm^{-1}; Ga^{71}: $\Delta\nu=(0.1139\pm0.0019)$ cm^{-1}

and from these the nuclear moments are

$\mu_{69}=2.11$; $\mu_{71}=2.69$.

INTRODUCTION

THE nuclear properties of the two isotopes of gallium ($_{31}Ga^{69}$ and $_{31}Ga^{71}$) have been measured by various experimenters. Jackson[1] worked with the GaI spectrum and found the value $\frac{3}{2}$ for each of the spins. Campbell,[2] working with the GaII spectrum, substantiated these values and found the ratio of the nuclear moments to be 1.27. Schüler and Korsching[3] studied the GaII spectrum and in addition to obtaining agreement with the above measurements ob-

* Publication assisted by the Ernest Kempton Adams Fund for Physical Research of Columbia University.
[1] D. A. Jackson, Zeits. f. Physik **75**, 229 (1932).
[2] J. S. Campbell, Nature **131**, 204 (1933).
[3] H. Schüler and Korsching, Zeits. f. Physik **103**, 434 (1936).

served that the hyperfine structure separations of various P states did not follow the interval rule. From this they concluded that the gallium nuclei possessed electrical quadrupole moments and obtained the values $Q^{69}=1\times10^{-24}$ cm^2 and $Q^{71}=0\pm0.5\times10^{-24}$ cm^2. Because of the large uncertainty in these numbers, it was thought interesting to check the quadrupole hypothesis by a study of some other state with the atomic beam method of zero-moments.

Gallium possesses many features which make it suitable for investigation by this method. Its ionization potential is not too high for the surface ionization method used in detecting atomic beams of the nongaseous elements and its boiling point is low enough to get appreciable beam intensities at reasonable temperatures (1400°K–1600°K). Furthermore, as a consequence of the relatively small doublet fine structure, there are present in the beam atoms in the metastable $^2P_{3/2}$ state as well as those in the ground $^2P_{1/2}$ state. The separation of these states is 826.0 cm^{-1} and the ratio of the number of atoms in the higher state to those in the ground state is given by the Boltzman factor multiplied by the ratio of the statistical weights, i.e., $2\cdot e^{-hc\Delta\nu/kT}$. At an absolute temperature of 1600°, since the excitation of the other states is negligible, the abundance of atoms in the upper state is 50 percent. This circumstance gives the opportunity for studying the quadrupole moment of gallium since in the higher P state, with $J=\frac{3}{2}$, one can seek deviations from the interval rule produced by the interaction of the electrons with a quadrupole. S states and $P_{1/2}$ states, because they possess spherically symmetrical electronic charge distributions show no effect of quadrupole moment in their h.f.s. even though the nucleus may have a nonspherical charge density.

Method

The atomic beam method of zero-moments[4] is based upon the behavior of the atomic energy states in a magnetic field. If one considers the progress of the energies of the states into which the h.f.s. levels split on applying a magnetic field, H, then for certain states there will be a value of $H=H^\circ$ (different for different states) at which the energy is a maximum or a minimum, i.e., $dE/dH=0$. An atom for which dE/dH is zero experiences no net translational force at a point in an inhomogenous field for which $H=H^\circ$. If a beam of atoms is made to traverse this field and the intensity at the position of zero deflection is observed as a function of H, "peaks" are found at the zero-moment fields of the various states. Actually the occurrence of such peaks is brought about by the progressive reorientation of J, the electronic angular momentum, by the external field, H. As the field is strengthened there is a decoupling of I, the nuclear angular momentum, and J, and during that process there may be some value of H such that the time average direction of J is perpendicular to H. The strength of the field necessary to bring this about is proportional to the strength of the interaction of the electrons and the nuclear magnetic dipole moment if one neglects the quadrupole interaction. If now the nucleus has a quadrupole moment, another torque in addition to that exerted by the nuclear magnetic moment acts upon J with a different dependence on the relative orientations of I and J. As a result, the value of the field necessary for the reorientation is greater or less depending upon whether or not the process has been hindered or helped by the added torque. Thus a measurement of the relative values of the fields at which the zero-moment peaks occur determines the relative strengths of the magnetic dipole and electric quadrupole interactions. The real advantage of the zero-moment method lies in the fact that the peaks are indeed shifted by large amounts (from 10 percent to 50 percent in the present experiment). On the other hand, the optical spectroscopist relies on the small differences between the wave-lengths of the components of a well-resolved spectral line. The calculation of Q is based upon the deviation of these differences from the interval rule and in many cases these deviations are not much larger than the limit of the experimental method.

Apparatus and Procedure

The high resolution apparatus used in this experiment is essentially the same as that in the experiment of Hamilton.[5] A schematic top view

[4] V. W. Cohen, Phys. Rev. **46**, 713 (1934).

[5] D. R. Hamilton, Phys. Rev. **56**, 30 (1939).

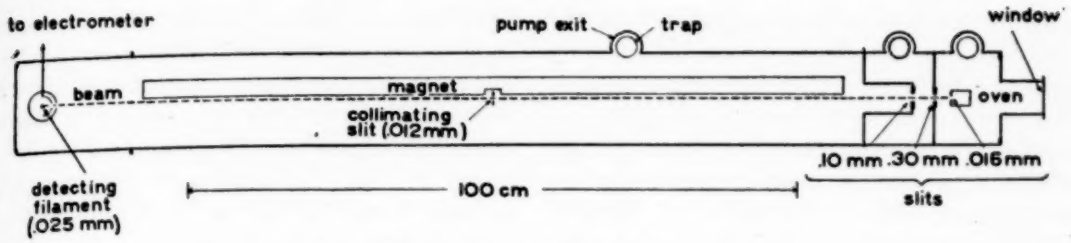

FIG. 1. Schematic top view of the apparatus.

is shown in Fig. 1. It consists of a brass can 6″ o.d., $5\frac{3}{4}$″ i.d. separated into three chambers which are pumped out in parallel. The high temperatures necessary for an appreciable intensity of gallium atoms require good separation and high pumping speeds. With this arrangement it is possible to maintain a pressure of better than 10^{-6} mm of Hg in the main chamber with a pressure of 5×10^{-5} in the oven chamber.

A preliminary investigation was made to determine whether gallium could be detected with an oxide-coated filament (tungsten). This experiment consisted of evaporating the gallium from a tungsten coil about 10 cm from the detector. A continual stream of oxygen was played upon the detector in a manner first developed by Manley and Millman[6] to raise the work function of the tungsten surface to that of the ionization potential of the atom which makes the detection possible. For gallium this potential has a value 5.97, and is 0.27 volt higher than the highest previously detected by this means. Another feature of this experiment was the use of a graphite oven in which the gallium was placed. Attempts to use other materials all met with failure. At first we utilized a molybdenum block as in the experiment of Millman, Rabi and Zacharias[7] on indium. Slit jaws both of molybdenum and tantalum were used. However, in each case, the gallium combined with the molybdenum to give an extremely hard compound which a surface grinder had difficulty in removing. A beam of molecules was observed for a short time. Tantalum was used in the form of a rod with a hole drilled into it and inserted diagonally down in the molybdenum and also as material for the slits. In this case the liquid gallium crept up on to the slits giving a broad beam for a short time. Ovens made completely of iron and nickel gave no beam at all; the gallium combined with the material of the oven and closed the slit jaws. A complete graphite oven gave considerable difficulty by a continual evolution of gas. The oven ultimately used had a graphite rod with a hole drilled into it and inserted diagonally into a molybdenum block and graphite slits. The heating coils (in the molybdenum) with the aid of 1-mil molybdenum sheets wrapped around the oven acting as a radiation shield gave temperatures of the order of 1600°K.

Figure 2 shows a cross section of the deflecting magnet at right angles to the plane of the beam. It consists of two copper tubes 0.144″ o.d. and 0.066″ i.d. each set in the face of a Duralumin block 3.5 by 5 by 115 cm. The tubes are insulated from each other and the block by mica sheets and carry the same current in opposite directions and are water cooled. This two-wire type of field[8] without iron has the advantage of having no magnetization difficulties. After placing the wires in the block, we found the average deviation of the surface tangent to the wires to the mean tangent plane to be about 0.007 mm. The current supply (at times as high as 1500 amperes) for this magnet was furnished by a bank of six-volt storage batteries which had a normal capacity of 3500 ampere-hours. A Leeds and Northrup Type K potentiometer across a 50-millivolt, 1500-ampere shunt was used to measure the current. The calibration of the field at the position of the beam is made with the aid of a beam of caesium atoms in the manner described below.

The requirements of high resolution are met by making the beam long and narrow. The total

[6] J. H. Manley and S. Millman, Phys. Rev. **51**, 19 (1937).
[7] S. Millman, I. I. Rabi and J. R. Zacharias, Phys. Rev. **53**, 384 (1938).
[8] I. I. Rabi, M. J. B. Kellogg and J. R. Zacharias, Phys. Rev. **46**, 157 (1934).

beam length is 165 cm; the oven and collimating slit (the latter at the center of the beam path) which define the beam are set at about 0.01 mm, and the path in the deflecting region is 115 cm. This symmetrical arrangement has the advantage of making the results independent of the parallelism of the beam plane to the surface of the field wires within wide limits. The slits and the detector (0.025 mm in diameter) are movable under vacuum so that the beam could be put at any desired distance from the field wires. For this purpose the oven is seated on three tungsten pegs set in a dovetail slide operated from outside the can by an Invar screw and the collimating slit and the detector are mounted eccentrically on ground joints. All the runs were made with the beam 0.1 mm inside the surface tangent to the wires.

It is important (see next section) that the detecting filament be accurately centered with respect to the beam. This is done by placing the filament midway between two points of equal intensity on the sides of the beam. During the course of the experiment, the position of the beam at zero field is recorded before and after two or three peaks are observed. The position of the filament, given by a microscope, and thus the relative position of the beam could be observed to 0.0005 mm. Ordinarily, the average shift of the beam was 0.001 mm or less and corrections for this are negligible.

Experimental Data

Figure 3 shows the beam intensity as a function of the magnet current. The $^2P_{3/2}$ peaks are superimposed upon a sloping background which is made up of the undeflected atoms in the ground state. The atoms in this latter state have an over-all magnetic moment of $\frac{1}{3}$ Bohr magneton as compared with 2 Bohr magnetons for the atoms in the $^2P_{3/2}$ state and therefore higher fields are required to sweep them out of the beam. To locate the exact positions of these peaks this background is represented by an empirically drawn smooth curve which is then subtracted from the total intensity. The results of this last operation are given in Fig. 4 which shows the intensity of the atoms in the $^2P_{3/2}$ state alone.

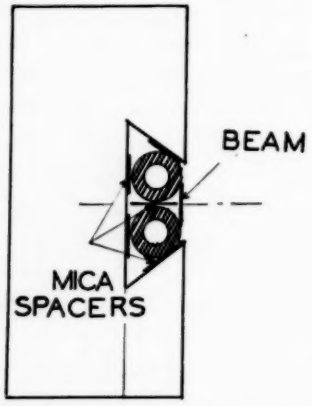

Fig. 2. Cross section of the deflecting magnet. Field wires enlarged relative to the Duralumin block. The direction of the beam is perpendicular to the plane of the paper.

For reasons to be mentioned shortly, it was also found necessary to observe the changes in the pattern produced when the detector is shifted slightly away from its position of zero deflection, i.e., away from the "beam plane" or plane defined by the source and collimating slits. In these observations, complete curves were obtained as in Fig. 3 and the resulting positions of the peaks as a function of the position of the detector are shown in Fig. 5. It should be noted that the maximum lateral displacement given to the detector was only 0.04 mm. The reason for the shifts in the peak positions is given in the following discussion. As explained previously,[4] any zero-moment peak may be classified as a "focusing" or a "nonfocusing" peak, according to whether d^2E/dH^2 is positive or negative at H°. In the former, or focusing case, the atoms of the state in question are attracted toward that region of the field where $H=H^\circ$, and hence travel along a potential valley whose center is the so-called "zero-moment plane," the locus of points for which $H=H^\circ$. Correspondingly, the atoms of a nonfocusing state are repelled from the zero-moment plane and travel along a potential ridge with its center at the zero-moment plane. As the exciting current in the magnet is increased, the zero-moment plane for a given state moves away from the deflecting magnet; i.e., the center of the potential ridge or valley moves toward the beam plane. When the zero-moment plane of a given state and the beam plane coincide, atoms in that state are not deflected and a zero-moment peak is observed. Considering the atoms in a nonfocusing state, we see that when the field at the beam plane has a value less than the zero-moment value, i.e., the

zero-moment plane has not yet reached the beam plane, the atoms are deflected from the beam plane in a direction away from the magnet; this deflection decreases as the zero-moment plane approaches the beam plane. If the detecting filament is laterally displaced from the beam plane in a direction away from the deflecting magnet, the atoms will reach the detector at smaller magnet currents, i.e., the peak will appear to have been shifted to lower current

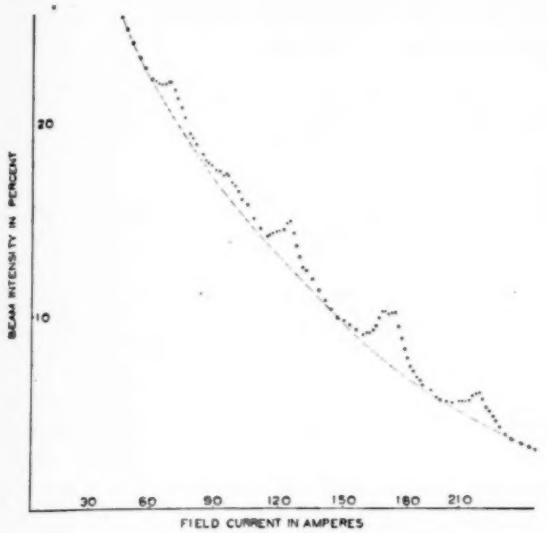

FIG. 3. Beam intensity at the position of zero deflection as a function of the current in the field wires. Background of the $^2P_{\frac{1}{2}}$ atoms is included.

values. A similar argument shows that the focusing peaks are displaced toward higher current values. This last statement is true even when the sides of the potential valley are so steep that the atom may pass from one side of the zero-moment plane to the other several times in the course of its passage through the deflecting field.

The advantage of these considerations is brought out in the case of the fourth and fifth peaks, which as Fig. 4 shows, are quite close together and therefore difficult to locate exactly. However, the procedure described above disclosed that the fourth is a nonfocusing and the fifth a focusing peak and therefore a shift of the detector away from the magnet separates these two peaks. By observing the separation for a number of positions of the detector, an extrapolation back to zero displacement may be made with considerable accuracy. (See Fig. 5.)

The second use of the data shown in Fig. 5 is as an aid to later identification of the experimental peaks. From the criterion given above and the data of the figure, it is known which of the peaks are focusing and which are nonfocusing. (An upward slant to the right in Fig. 5 indicates a focusing peak.) Likewise one can determine from the calculations described later whether d^2E/dH^2 is positive or negative for each of the theoretically predicted peaks. Then any fit of the two sets of peaks must identify a "focusing" experimental peak with a "focusing" theoretical peak.

The procedure which was followed in interpreting the data obtained from the various runs consisted of locating for each run a most probable position of each of the observed peaks, using the

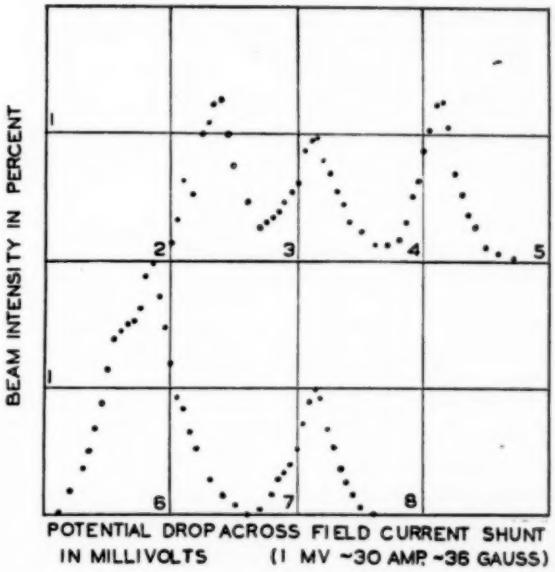

FIG. 4. Beam intensity, at the position of zero deflection, of the $^2P_{3/2}$ atoms alone.

methods described above. From the identification of the peaks and the theoretical interpretation of their positions (to be discussed in the next section) values of the desired h.f.s. constants were obtained; the numerical values will be discussed following the presentation of the method by which they were calculated.

Zero-moment peaks arising from atoms in the ground state are also observed. These are shown in Fig. 6. For the large values of the field here

beam length is 165 cm; the oven and collimating slit (the latter at the center of the beam path) which define the beam are set at about 0.01 mm, and the path in the deflecting region is 115 cm. This symmetrical arrangement has the advantage of making the results independent of the parallelism of the beam plane to the surface of the field wires within wide limits. The slits and the detector (0.025 mm in diameter) are movable under vacuum so that the beam could be put at any desired distance from the field wires. For this purpose the oven is seated on three tungsten pegs set in a dovetail slide operated from outside the can by an Invar screw and the collimating slit and the detector are mounted eccentrically on ground joints. All the runs were made with the beam 0.1 mm inside the surface tangent to the wires.

It is important (see next section) that the detecting filament be accurately centered with respect to the beam. This is done by placing the filament midway between two points of equal intensity on the sides of the beam. During the course of the experiment, the position of the beam at zero field is recorded before and after two or three peaks are observed. The position of the filament, given by a microscope, and thus the relative position of the beam could be observed to 0.0005 mm. Ordinarily, the average shift of the beam was 0.001 mm or less and corrections for this are negligible.

Experimental Data

Figure 3 shows the beam intensity as a function of the magnet current. The $^2P_{3/2}$ peaks are superimposed upon a sloping background which is made up of the undeflected atoms in the ground state. The atoms in this latter state have an over-all magnetic moment of $\frac{1}{3}$ Bohr magneton as compared with 2 Bohr magnetons for the atoms in the $^2P_{3/2}$ state and therefore higher fields are required to sweep them out of the beam. To locate the exact positions of these peaks this background is represented by an empirically drawn smooth curve which is then subtracted from the total intensity. The results of this last operation are given in Fig. 4 which shows the intensity of the atoms in the $^2P_{3/2}$ state alone.

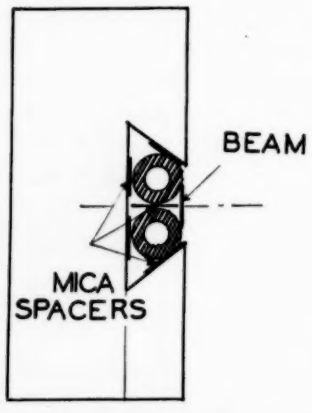

Fig. 2. Cross section of the deflecting magnet. Field wires enlarged relative to the Duralumin block. The direction of the beam is perpendicular to the plane of the paper.

For reasons to be mentioned shortly, it was also found necessary to observe the changes in the pattern produced when the detector is shifted slightly away from its position of zero deflection, i.e., away from the "beam plane" or plane defined by the source and collimating slits. In these observations, complete curves were obtained as in Fig. 3 and the resulting positions of the peaks as a function of the position of the detector are shown in Fig. 5. It should be noted that the maximum lateral displacement given to the detector was only 0.04 mm. The reason for the shifts in the peak positions is given in the following discussion. As explained previously,[4] any zero-moment peak may be classified as a "focusing" or a "nonfocusing" peak, according to whether d^2E/dH^2 is positive or negative at H°. In the former, or focusing case, the atoms of the state in question are attracted toward that region of the field where $H=H^\circ$, and hence travel along a potential valley whose center is the so-called "zero-moment plane," the locus of points for which $H=H^\circ$. Correspondingly, the atoms of a nonfocusing state are repelled from the zero-moment plane and travel along a potential ridge with its center at the zero-moment plane. As the exciting current in the magnet is increased, the zero-moment plane for a given state moves away from the deflecting magnet; i.e., the center of the potential ridge or valley moves toward the beam plane. When the zero-moment plane of a given state and the beam plane coincide, atoms in that state are not deflected and a zero-moment peak is observed. Considering the atoms in a nonfocusing state, we see that when the field at the beam plane has a value less than the zero-moment value, i.e., the

zero-moment plane has not yet reached the beam plane, the atoms are deflected from the beam plane in a direction away from the magnet; this deflection decreases as the zero-moment plane approaches the beam plane. If the detecting filament is laterally displaced from the beam plane in a direction away from the deflecting magnet, the atoms will reach the detector at smaller magnet currents, i.e., the peak will appear to have been shifted to lower current

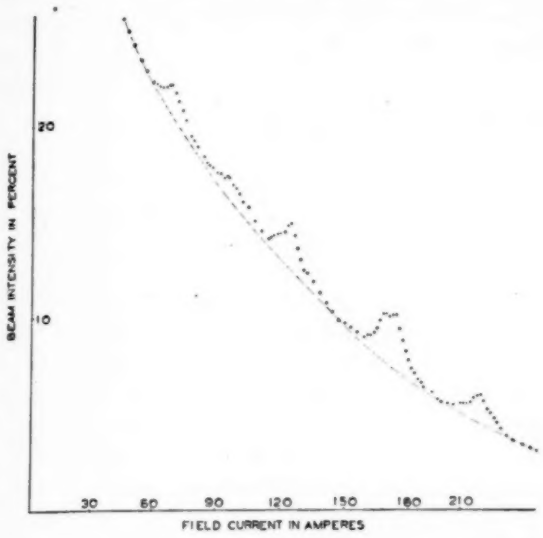

FIG. 3. Beam intensity at the position of zero deflection as a function of the current in the field wires. Background of the $^2P_{\frac{1}{2}}$ atoms is included.

values. A similar argument shows that the focusing peaks are displaced toward higher current values. This last statement is true even when the sides of the potential valley are so steep that the atom may pass from one side of the zero-moment plane to the other several times in the course of its passage through the deflecting field.

The advantage of these considerations is brought out in the case of the fourth and fifth peaks, which as Fig. 4 shows, are quite close together and therefore difficult to locate exactly. However, the procedure described above disclosed that the fourth is a nonfocusing and the fifth a focusing peak and therefore a shift of the detector away from the magnet separates these two peaks. By observing the separation for a number of positions of the detector, an extrapolation back to zero displacement may be made with considerable accuracy. (See Fig. 5.)

The second use of the data shown in Fig. 5 is as an aid to later identification of the experimental peaks. From the criterion given above and the data of the figure, it is known which of the peaks are focusing and which are nonfocusing. (An upward slant to the right in Fig. 5 indicates a focusing peak.) Likewise one can determine from the calculations described later whether d^2E/dH^2 is positive or negative for each of the theoretically predicted peaks. Then any fit of the two sets of peaks must identify a "focusing" experimental peak with a "focusing" theoretical peak.

The procedure which was followed in interpreting the data obtained from the various runs consisted of locating for each run a most probable position of each of the observed peaks, using the

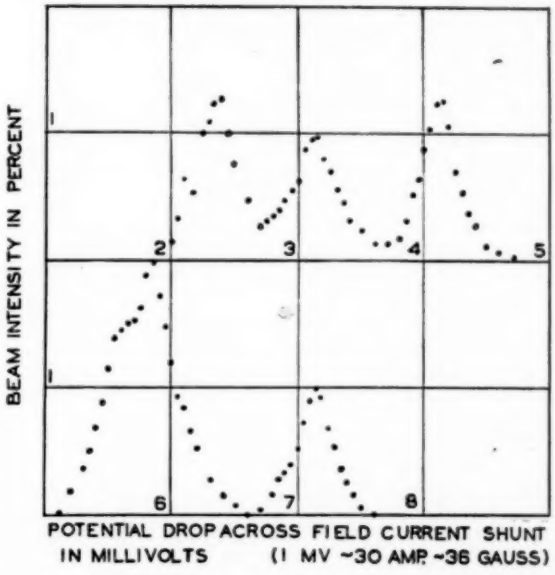

FIG. 4. Beam intensity, at the position of zero deflection, of the $^2P_{3/2}$ atoms alone.

methods described above. From the identification of the peaks and the theoretical interpretation of their positions (to be discussed in the next section) values of the desired h.f.s. constants were obtained; the numerical values will be discussed following the presentation of the method by which they were calculated.

Zero-moment peaks arising from atoms in the ground state are also observed. These are shown in Fig. 6. For the large values of the field here

involved, the peaks occur without any background. There are no peaks of either state in the region between 7.5 and 35 millivolts. The theory involved in the interpretation of their positions and the information to be derived therein are discussed in the section devoted to the $^2P_{1/2}$ state. The data are summarized in Table I.

Finally, the ratio of the zero-moment peaks arising from the atoms in the ground states of

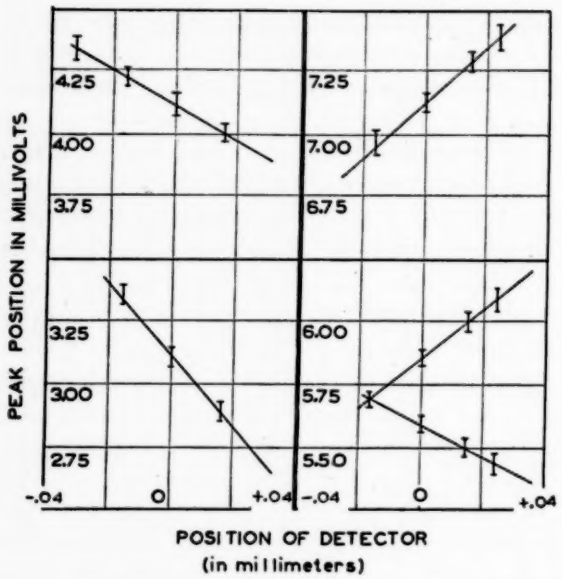

FIG. 5. Peak position as a function of the position of the detector. The positive numbers indicate that the detector was moved away from the magnet.

sodium and lithium was measured as a check on the accuracy of the apparatus. This ratio is very accurately known from the ratio of the h.f.s. $\Delta\nu$'s measured by the new magnetic resonance method by Kusch, Millman, and Rabi.

THEORY AND EVALUATION OF THE EXPERIMENTAL RESULTS—$^2P_{3/2}$ STATE

In this section we shall first discuss the effect of a quadrupole moment on the h.f.s. energy levels. Then we shall describe the behavior of these levels in a magnetic field and discuss the calculations necessary for the evaluation of the h.f.s. constants. Finally, we shall show how the experimental peaks are fitted to the theoretical curves and give the numerical results.

In the presence of an interaction with a quadrupole moment the h.f.s. energy levels are described by the equation

$$E=aC/2+bC(C+1) \tag{1}$$

where $C=F(F+1)-I(I+1)-J(J+1)$ and F is the total angular momentum, nuclear plus electronic. The first term in this equation gives the interval rule which arises from the cosine interaction of the nuclear magnetic dipole and the field at the nucleus produced by the electrons. The second term gives the quadrupole interaction with[9]

$$b=-\left\langle\left[\frac{3\cos^2\theta-1}{r^3}\right]_{JJ}\right\rangle_{Av} \times\frac{\frac{3}{8}Q}{ij(2i-1)(2j-1)}2R\alpha^4\ \text{cm}^{-1}. \tag{2}$$

The expression in the brackets is the average value for the electronic state $M_j=J$; the mean value of $(3\cos^2\theta-1)$ is a measure of the deviation from spherical symmetry of the charge density of the electrons. Q itself is defined as the average of $(3z^2-r^2)$ over the nuclear charge density for the state $M_i=I$, i.e.,

$$eQ=\int\rho(3z^2-r^2)d\tau$$

where $\int\rho d\tau=Ze$. Thus Q is a measure of the quadrupole moment of the nuclear charge distribution and leads to a cosine squared interaction with the electrons.

In order to obtain the positions of the zero-moment peaks arising from the atoms in the $^2P_{3/2}$ state and their dependence on Q, one must study the behavior of the energy levels in a magnetic field. To do this, one first obtains the Hamiltonian for the interactions and puts it into the secular equation for the energy. If we take the direction of the field as z, and omit constant terms independent of F, this Hamiltonian is given by[9]

$$\mathcal{H}=\mu_0H(g_jJ_z+g_iI_z)+a\mathbf{I}\cdot\mathbf{J} +b2\mathbf{I}\cdot\mathbf{J}(2\mathbf{I}\cdot\mathbf{J}+1). \tag{3}$$

The terms are, in order, the interaction of the

[9] H. B. G. Casimir, "On the interaction between atomic nuclei and electrons," Prize Essay published by Teyler's Tweede Genootschap (1936).

external field with the electrons and with the nucleus; the electron-nuclear interaction due to the nuclear magnetic dipole and due to the nuclear electric quadrupole. The h.f.s. energy levels in zero field are specified by the F values 3, 2, 1, and 0, since $I=\frac{3}{2}$ and $J=\frac{3}{2}$ and $F=I+J$, $I+J-1$, $\cdots I-J$. In a magnetic field each F state splits into $2F+1$ states, a total of 16 in all. Thus we must solve a 16-rowed determinant for the energies. However, in the (M_f, F) representation $\mathcal{H}$ is diagonal in $M(\equiv M_f)$, the z component of the total angular momentum and since at most 4 states have the same M, the determinant, which reads as follows

$$|(F'M|\mathcal{H}|F''M)-\delta(F', F'')E|=0 \qquad (4)$$

factors into 4 smaller determinants. In addition, in this representation, the last two terms of Eq. (2) are diagonal with matrix elements given by $aC/2+bC(C+1)$ from which Eq. (1) arises. In the calculations it is found convenient to express energies in terms of "a." Therefore we define

$$x=g_j\mu_0 H/a \qquad (5)$$

and Eq. (3) now becomes

$$\mathcal{H}/a=x(J_z+I_z g_i/g_j)+\mathbf{I}\cdot\mathbf{J} +b/a\mathbf{2I}\cdot\mathbf{J}(\mathbf{2I}\cdot\mathbf{J}+1). \qquad (6)$$

The matrix elements of I and J are well known and are given by Condon and Shortley.[10] After the numerical values of the elements involving the angular momenta are calculated, the equations to be solved for the energies contain as parameters x, g_i/g_j, and b/a. Given any particular state, one desires the value of x, say x_0, at which $\delta E/\delta x=0$ (provided x_0 exists). x_0 will depend on the values of g_i/g_j and b/a; numerical calculation of this dependence is necessary—i.e., one assumes values for g_i/g_j and b/a, calculates $\delta E/\delta x$ for several values of x, and interpolates to find x_0. This process must be repeated to obtain x_0 for as many values of g_i/g_j and b/a as are necessary.

TABLE I. *Final determination of peak positions.*

	Peak (M,F)	$^2P_{3/2}$ Peak Position millivolts	$^2P_{1/2}$ Peak Position millivolts
Ga^{71}	$(-1,3)$	7.12 ± 0.01	
	$(0,1)$	5.57 ± 0.02	47.20 ± 0.10
	$(+1,1)$	3.12 ± 0.03	
Ga^{69}	$(-1,3)$	5.84 ± 0.02	
	$(0,1)$	4.12 ± 0.02	37.14 ± 0.03
	$(+1,1)$	2.27 ± 0.03	

The effect of g_i/g_j is actually so small in this case that the theoretical calculations were made with the g_i's set equal to zero. The effect of the approximately known values of g_i^{69} and g_i^{71} is discussed later. The results of the calculations are shown in Figs. 7 and 8. To take care of the fact that perturbations might reduce the value of "a," the pattern was calculated for values of b/a from minus infinity to plus infinity.

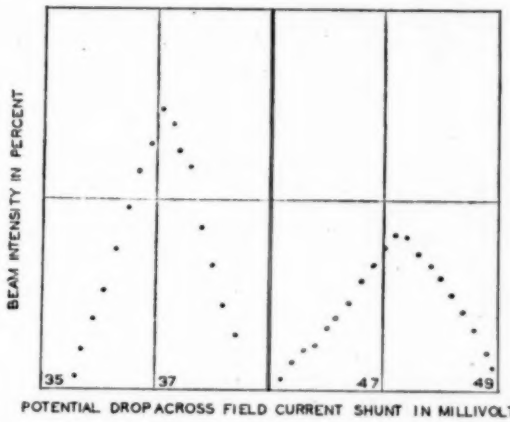

FIG. 6. Beam intensity, at the position of zero deflection, of the $^2P_{\frac{1}{2}}$ atoms.

It is found that for $b/a=0$, i.e., for zero quadrupole, the states $M=0$, $F=1$; $M=+1$, $F=1$; and $M=-1$, $F=3$ have zero moments at different values of the field. As b/a assumes values different from zero, some states which at first had no zero-moment now do, and, in some cases, (i.e., the closed curves in Fig. 7) one state has zero-moments for two different values of x. This situation is explained with the aid of Figs. 9 and 10. In the first of these the relative positions of the field free energy levels are plotted as a function of b/a. These curves are a plot of Eq. (1) (it must be noted, however, that actually the center of gravity of the fine structure level (n, j) is not altered by the quadrupole interaction). It is observed that the interval rule pattern is completely disrupted with the F levels freely exchanging their order. As the levels

[10] E. U. Condon and G. H. Shortley, *Theory of Atomic Spectra* (Cambridge, 1935).

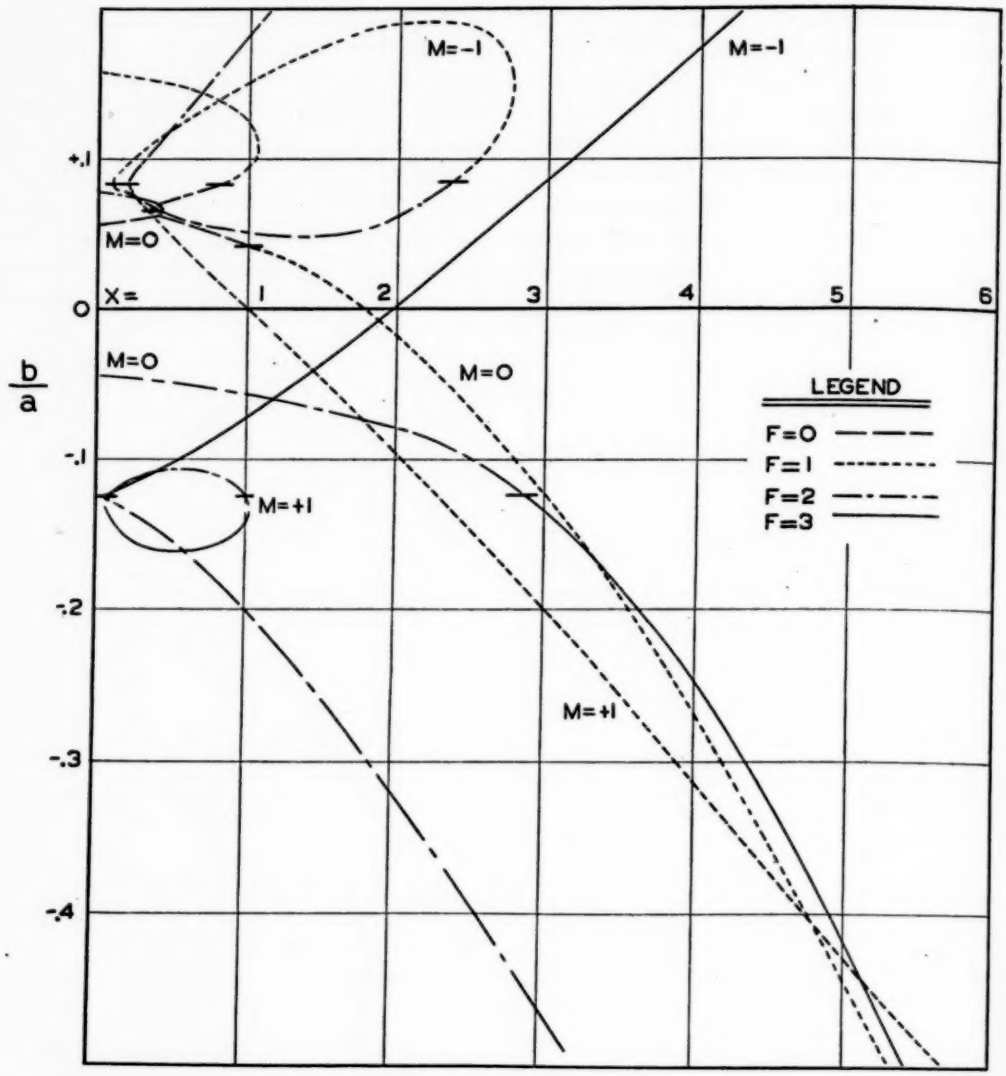

FIG. 7. Theoretical peak position in x as a function of the quadrupole interaction constant where $x \sim 7 \times 10^{-3} H$. Peaks are denoted by their (M,F) values and the short heavy horizontal lines indicate that at this point of the curve there is a transition of the F state involved. These transitions occur where the F states cross in Fig. 9.

$F=1$ and $F=2$ approach each other at $b/a=1/12$, their behavior in the field changes considerably. This is shown in Fig. 10. In this diagram the slope of the energy curve as a function of x is plotted against x for each of the two states for various values of b/a. Plotted in this way, i.e., the effective moment against x, the effect is brought out more strikingly. As the states approach each other, the repulsion between them becomes large compared with the interactions with the field and the upper of the two moment curves is pushed up toward smaller values. As the transition point $(b/a=0.0825)$ is reached, the upper curve is pushed up more sharply until it crosses the zero line. In this region the state in question shows zero-moment values corresponding to a minimum and a maximum in the energy curve. This phenomenon continues after the states have crossed and are still close to each other. Once we get past $b/a=0.2$ the mutual interaction becomes small and no zero-moments occur. In each case there is included in the diagram the corresponding curve of the $M=-1$, $F=3$ state which has the property that it crosses

the zero line at higher values of x as b/a is increased. The states $M=+1$, $F=1$, 2 and the $M=-1$, $F=2$, 3 are expected to show the phenomenon of zero-moment since they start out with moments of one sign in the Zeeman region and finish with moments of the opposite sign in the Paschen-Back region. All the other zero-moments occur as a result of considerations similar to the above. The numerical calculations, which involved quartic equations for $M=0$ and cubic for $|M|=1$, were made for values of b/a differing by 0.01 in the region $+0.2>b/a>-0.3$ and at more widely separated values in the remaining regions.

Evaluation of b/a

To identify the peaks one has to begin with the data of Fig. 7 (replotted with the same ordinates but with abscissae corresponding to ratios of lower theoretical peaks to highest peak). One then plots the experimentally known peaks to the same scale and records all those values of b/a, within or nearly within the experimental error, for which there is a coincidence of the two sets of peaks. These correspond to a number of tentative classifications of two or more peaks as belonging to a given isotope. Furthermore, an analysis of the half-widths of the theoretically predicted peaks indicates that none of the peaks should be unobservable unless, of course, two peaks nearly coincide and appear as one. This possibility is taken into consideration. In no instance is it found possible to assign more than three peaks to a given isotope.

As shown in reference 5, the various zero-moment peaks for a given isotope may have considerable differences in maximum intensity or in area under a peak, although the states which give rise to the various peaks are equally populated for a given isotope. Because of this variation in intensity among the peaks of a given isotope, and because the isotopes are present to the same order of magnitude (i.e., to the ratio of 3 : 2), it is impossible to distinguish between peaks by intensity considerations alone. Thus three peaks might belong to each isotope, or the division might be 1 and 5.

The simple criterion of consistency removes many of the possible values of b/a; i.e., a classification of the first, fifth and sixth peaks as belonging to one isotope must be false unless there is a corresponding tentative identification of the second, third and fourth as belonging to the other. A further criterion is provided by the experimental classification (see Fig. 5), previously discussed, of all except the first peak as focusing or nonfocusing peaks. Thus any value of b/a which is associated with the coincidence of a focusing and a nonfocusing peak is discarded.

In this manner all but two of the possible assignments are removed. For each of the remaining, the values of "a" for the two isotopes are calculated. A ratio of the "a's" of the two isotopes is obtained for each of the assignments; this ratio should be the same as the ratio of the magnetic moments of the two isotopes. Since the spins are the same, and any perturbations arising from an electronic source must be the

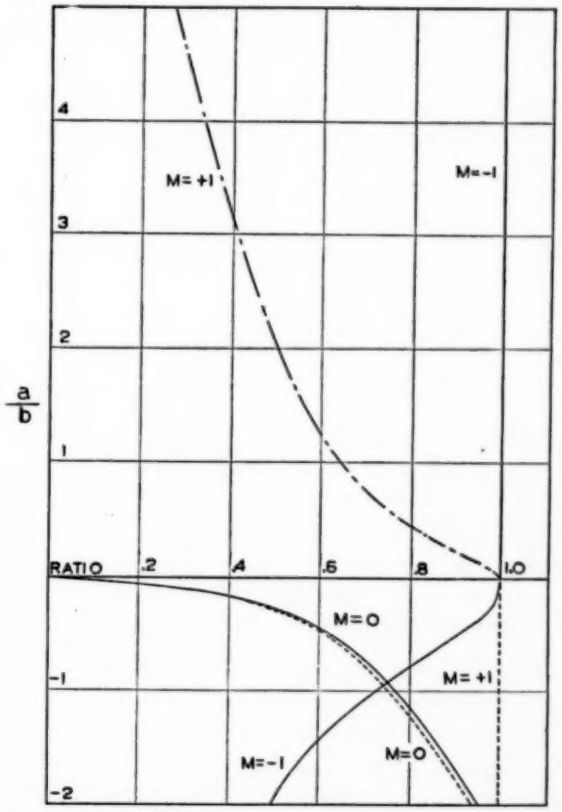

FIG. 8. Theoretical peak position as a function of the reciprocal of the quadrupole interaction constant plotted as ratios, taking the ratio of each peak in x to the highest peak. This was also done for Fig. 7 in obtaining the final results and together with 7 cover the entire range of b/a from minus infinity to plus infinity. The same notation indicates the F states involved.

same for the two isotopes, the ratio of the moments is equal to the ratio of the magnetic dipole interaction constants. The two ratios thus calculated are 1.020 and 1.268. As mentioned above, the true value of this ratio is 1.270 both from spectroscopic data[2,3] and measurements with the present apparatus (see the results for the $^2P_{1/2}$ state). There is thus no doubt that only one assignment of the peaks to the two isotopes is possible and the values of b/a obtained are unique. These are

$$\mathrm{Ga}^{71}\colon\ b/a=0.0068\pm0.0004;$$
$$\mathrm{Ga}^{69}\colon\ b/a=0.0136\pm0.0004.$$

It is to be emphasized that the method of determining b/a makes these ratios independent of an absolute measurement of the magnetic field.

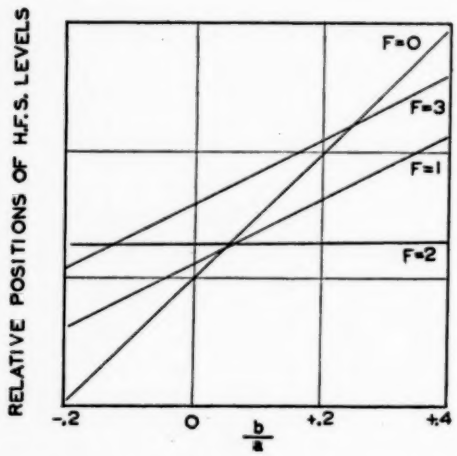

FIG. 9. This is a plot of the equation $E/a=C/2+b/a$ $C(C+1)$. It is understood that actually the center of gravity of the h.f.s. levels is not altered by this type of interaction, i.e., $\Sigma_f(2f+1)\Delta_f\nu=0$. Ordinates correspond to energy in units of "A."

The hyperfine structure separations

Knowing b/a, we may now determine from the calculations upon which Figs. 7 and 8 are based the value of x at which any given peak occurs. A measure of the value of the field at this peak then gives a/g_j directly, by Eq. (5). As mentioned above, the most accurate way of calibrating the field is to run another element whose peaks occur at known fields. In this case a beam of caesium atoms is used. For practical purposes it was found necessary to make a caesium run between two gallium runs. The $\Delta\nu$ of the $^2S_{1/2}$ ground state of caesium has been measured spectroscopically.[11] A value of 0.3067 ± 0.0004 cm^{-1} was obtained. Millman and Fox,[12] using atomic beam methods, found a value of 0.307 ± 0.003 cm^{-1} for the $\Delta\nu$ and a value of $7/2$ for the nuclear spin. With this information the field at any zero-moment peak is known. If we follow exactly the same procedure used in evaluating the results for the ground state of gallium (see later), we see that the first peak of caesium occurs at a field, $H'=0.3067hc/8\mu_0$ (since $y=-2M/2i+1=1/4$ for $M=-1$, $i=7/2$ and $y=g_j\mu_0H'/hc\Delta\nu$). The most accurately reproducible gallium peak is the $M=-1$, $F=3$, for which the above assignment of b/a gives an x value of 2.075 ± 0.010 belonging to the isotope 71. From Eq. (5) the field at this peak $H''=2.075a_{71}hc/g_j\mu_0$. Experimentally the ratio of H'' to H' is 0.3294 ± 0.0012. From these numbers one obtains $a_{71}/g_j=(6.086\pm0.062)\times10^{-3}$ cm^{-1}. If one assumes this state is a pure one, then $g_j=4/3$ and $a_{71}=(8.11\pm0.082)\times10^{-3}\,\mathrm{cm}^{-1}$. However, because of the possible influence of perturbations on g_j (see later), we increase the limits of error and take $a_{71}=(8.11\pm0.11)\times10^{-3}$ cm^{-1}. From the discussion given above $a_{71}/a_{69}=1.270\pm0.006$. Therefore,

$$a_{69}=(6.39\pm0.12)\times10^{-3}\ \mathrm{cm}^{-1}.$$

If there were no quadrupole moments, the h.f.s. separations would be

$$\Delta\nu_{71}'=6a_{71}=0.0487\pm0.0007\ \mathrm{cm}^{-1};$$
$$\Delta\nu_{69}'=6a_{69}=0.0383\pm0.0007\ \mathrm{cm}^{-1}.$$

However, its presence shifts the top and bottom levels by different amounts so that making use of the values $b_{71}=(5.51\pm0.39)\times10^{-5}$ cm^{-1} and $b_{69}=(8.69\pm0.43)\times10^{-5}$ cm^{-1}, the true separations are

$$\Delta\nu_{71}=0.0474\pm0.0007\ \mathrm{cm}^{-1};$$
$$\Delta\nu_{69}=0.0362\pm0.0007\ \mathrm{cm}^{-1}.$$

Nuclear spin and nuclear g factors

The previously measured[1,2] values of the spins for each isotope (3/2) are used in the theoretical

[11] L. P. Granath and R. K. Stranathan, Phys. Rev. **48**, 725 (1935).
[12] S. Millman and M. Fox, Phys. Rev. **50**, 220 (1936).

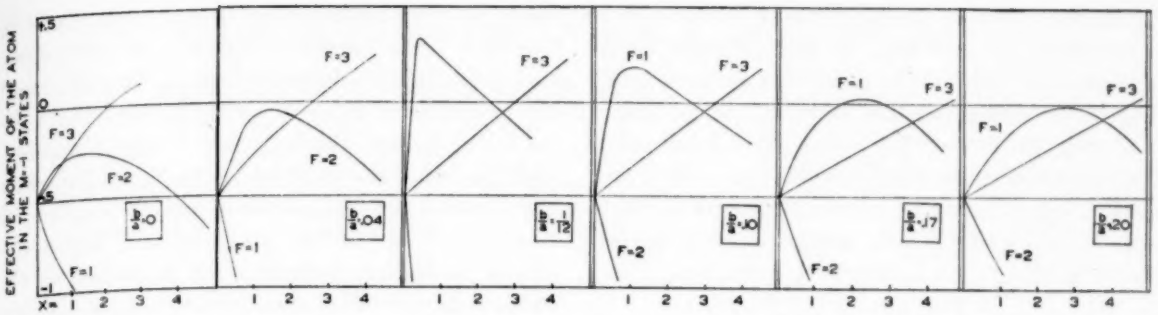

FIG. 10. The slope of the energy curve (i.e., effective moment), dE/dx, as a function of x for various values of b/a on either side of the transition $F=1$, $F=2$ at $b/a=1/12$. All the curves correspond to $M=-1$ states.

calculations upon which Figs. 7 and 8 are based. The fact that we can make the above unambiguous identifications is a verification of these values.

The nuclear g factors as calculated from the hyperfine structure separations of the ground state are more accurate than from the $^2P_{3/2}$ state. The effect of g_i/g_j on the relative positions of the peaks is indeed very slight. The theoretical calculations were made with the g_i's set equal to zero. If we take $g_i=-0.000907$ for Ga^{71} and $g_i=-0.000725$ for Ga^{69} corresponding to $\mu_{71}=2.5$ and $\mu_{69}=2.0$ nuclear magnetons, the resulting changes in the values of b/a are 1.4 percent and 0.7 percent, respectively. The basis for the calculation of these effects is given in reference 5. These results are utilized in the final determination of b/a.

The quadrupole moments

The relation between Q and "b" for the $^2P_{3/2}$ state is given by[9, 5]

$$Q=b\frac{i(2i-1)Z_iIIC}{\delta R'}\frac{60}{e^2}\mu_0^2.$$

In this expression δ is the doublet separation, 826.0 cm^{-1}. It occurs because it is proportional to $\langle r^{-3}\rangle_{Av}$ of Eq. (2). H, R' and C are relativistic correction factors which enter because of the use of δ to give $\langle r^{-3}\rangle_{Av}$. Calculations of these quantities have been made by Casimir, from whose tables we obtain $H=1.018$ and $R'=1.028$. C is a correction for the fact that in calculating H and R' the difference in the normalization integrals of the $^2P_{1/2}$ and $^2P_{3/2}$ states, caused by the difference in the energies of these states, was neglected. Casimir gives an analytic expression for this effect from which we obtain $C=1.013$. Z_i is the effective nuclear charge. On the basis of the relativistic wave functions from which H, R', and C are calculated, Casimir obtains an expression for δ which depends on Z_i. From the doublet separations and the term values of the series $4s^2np$, a value of Z_i may be obtained for $n=5$, 6, and 7. We find as the average $Z_i=26.4=Z-4.6$, with an average deviation of 0.4. Finally in the calculation of μ_0/e, in which μ_0 and e are the Bohr magneton and the electronic charge, respectively, we have taken $h/e=1.3759\times10^{-7}$ e.s.u. and $e/m=1.7591\times10^7$ e.m.u. "b" is in cm^{-1}. Substitution of these numerical values gives

$$Q^{71}=+0.13\times10^{-24}\ cm^2;$$
$$Q^{69}=+0.20\times10^{-24}\ cm^2.$$

In assigning the deviations from the interval rule to the effect of a quadrupole moment of the nucleus, one must consider the effect of perturbations on this term. In view of the large fine structure separation, the deviations arising from a second-order effect in the magnetic interaction are very small. Casimir has shown that the order of magnitude of these deviations is given by the hyperfine structure splitting squared divided by the fine structure separation.

However, in the consideration of the magnitude of "b," one must study the effect on the $4s^24p\ ^2P_{3/2}$ state in question, of the electrostatic coupling with the states of the same total angular momentum in higher configurations, notably the states with $J=\frac{3}{2}$ in the $4s4p5s$ configuration. From the discussion on the closely

analogous cases of thallium[13] and indium,[5] it is concluded that although the perturbation on $\Delta\nu$ is large, it is only of the order of 1 percent on Q. The latter occurs because in both configurations it is only the $4p$ electron which gives quadrupole contributions to the energy levels; the s electrons, having spherically symmetric wave functions, do not. As concerns g_j, the same considerations show that it might be increased by 0.3 percent.

Theory and Evaluation of Experimental Results—$^2P_{1/2}$ State

The positions of the zero-moment peaks arising from the atoms in the $^2P_{1/2}$ state are described by the Breit-Rabi formula[14] which is valid for the case where either I or $J=\frac{1}{2}$. Since $J=\frac{1}{2}$, there is no quadrupole effect in this term. One gets that the magnetic moment of an atom with $J=\frac{1}{2}$, nuclear spin "I," and positive nuclear moment, in a magnetic field H is, in units of the Bohr magneton μ_0

$$\mu_M=\mp\frac{y+(2M/2I+1)}{2[1+(4M/2I+1)y+y^2]^{\frac{1}{2}}}g_J.$$

In this formula M is the total magnetic quantum number as above and y is defined by the equation

$$y=g_j\mu_0 H/hc\Delta\nu \qquad (7)$$

where $\Delta\nu$ is the separation in wave numbers between the hyperfine levels $F=I+\frac{1}{2}$ and $F=I-\frac{1}{2}$. In this approximation ($g_i=0$), it is seen that, for negative values of M, there are certain values of y for which $\mu_M=0$ in two of the $2(2I+1)$ levels. These come at $y=-2M/2I+1$, $M=-\frac{1}{2}$, $-\frac{3}{2}\cdots(I-\frac{1}{2})$ if the spin is integral, and -1, -2, $\cdots-(I-\frac{1}{2})$ if the spin is a half-integer. Since the spin of each isotope is known to be $\frac{3}{2}$, there is one zero-moment peak for each. These have the same $y(\frac{1}{2})$, but because the $\Delta\nu$'s are the different, the peaks occur at different values of the magnetic field.

The hyperfine structure separations

It is seen from Eq. (7) that if we know the field at the peak arising from this state, the h.f.s. $\Delta\nu$ is known because there $y=-2M/2I+1$. Since $y=\frac{1}{2}$ for each isotope, the ratio of the fields at the peaks gives directly the ratio of the $\Delta\nu$'s. This number is equal to 1.270 ± 0.006 and is of course independent of any measurement of the absolute value of the field. Moreover, the $\Delta\nu$ is due only to the magnetic dipole interaction and therefore the ratio of the $\Delta\nu$'s gives directly the ratio of the nuclear moments. To obtain the absolute values of the $\Delta\nu$'s, the field was determined in the same manner as described in the results for the $^2P_{3/2}$ state. From that discussion we saw that the field at the caesium peak is given by $H'=0.3067hc/8\mu_0$ and the field at the first gallium peak which is due to Ga^{69} is $H''=\Delta\nu hc/2g_j\mu_0$. Experimentally this ratio is $H''/H'=1.754\pm0.012$. From these numbers

$$\Delta\nu_{69}/g_j=(0.1345\pm0.0016)\ \text{cm}^{-1}.$$

If this state is pure, $g_j=\frac{2}{3}$ and, therefore,

$$\Delta\nu_{69}=(0.0897\pm0.0011)\ \text{cm}^{-1};$$
$$\Delta\nu_{71}=(0.1139\pm0.0019)\ \text{cm}^{-1}.$$

The nuclear moments

With the information given above and the assistance of the Goudsmit[15] and Fermi-Segrè[13] formulae which relate the magnetic moment to the $\Delta\nu$ we are able to calculate these moments. We obtain as a consequence that

$$\mu_{69}=2.11;\quad \mu_{71}=2.69$$

in nuclear magnetons.

Discussion

Schüler and Korsching, who worked on the $^3P_{2,1,0}$ states of GaII obtained values of $Q^{69}=1.0\times10^{-24}$ cm^2; $Q^{71}=(0\pm0.5)\times10^{-24}$ cm^2. Because they observed deviations from the interval rule of the order of 0.001 cm^{-1} for an S state where there should be none, these authors set this number as the limit of error of the experimental method for well resolved lines. If one applies this criterion to their observations, the values of "b" and therefore Q are changed by factors ranging from 1.5 to 9. In the light of these observations one can say there is no real disagreement.

From the hyperfine separations of various levels these authors conclude that the ratio of the nuclear moments is $\mu_{71}/\mu_{69}=1.269$ and that

[13] E. Fermi and E. Segrè, Zeits. f. Physik **82**, 729 (1933).
[14] G. Breit and I. I. Rabi, Phys. Rev. **38**, 2082 (1931).
[15] S. Goudsmit, Phys. Rev. **43**, 636 (1933).

these moments are $\mu_{71}=2.5$ and $\mu_{69}=2.0$. The agreement in the ratios is excellent and the values of the moments agree as well as this method of calculation allows. The values of the moments one gets from the $^2P_{3/2}$ $\Delta\nu$'s are too small by a factor 1.36. This number is obtained by taking the ratio of the expected $\Delta\nu$'s from the Goudsmit formula and comparing it with the experimental results. However, from the considerations given above, the diminished $\Delta\nu$ may be due to the effect of a perturbation by a higher configuration.

The experiment on gallium depended, as was seen, very critically on the ratios of the zero-moment peaks. We had occasion on this same apparatus to measure the ratio of the sodium and lithium hyperfine $\Delta\nu$'s given directly by the ratio of the zero-moment peaks. We obtained for this ratio $\Delta\nu_{Na}/\Delta\nu_{Li}=2.2098\pm0.0035$. Millman, Kusch and Rabi,[16] using the new and very accurate molecular beam resonance method, obtained the value $\Delta\nu_{Na}/\Delta\nu_{Li}=2.2052\pm0.0002$. The discrepancy of $\frac{1}{2}$ of 1 percent implies a systematic error of this magnitude in the zero-moment experiments. We believe, therefore, that this gives a good indication of the precision of the apparatus in locating zero-moment peaks.

The author wishes to thank Professor I. I. Rabi for suggesting this application of atomic beams to the measurement of quadrupole moments. He also wishes to express his great indebtedness to Mr. D. R. Hamilton for his continuously invaluable assistance during the course of the research. The other members of the molecular beam laboratory were generous in making available their valuable experience.

[16] The author is indebted to these authors for the communication of this result before its publication.

MAY 1, 1940 PHYSICAL REVIEW VOLUME 57

The Radiofrequency Spectra of Atoms

Hyperfine Structure and Zeeman Effect in the Ground State of Li^6, Li^7, K^{39} and K^{41} *

P. Kusch, S. Millman and I. I. Rabi
Columbia University, New York, New York

(Received February 26, 1940)

The molecular beam magnetic resonance method previously used for the study of molecules has been extended to the study of atoms. Transitions between the members of hyperfine structure multiplets of the ground state of atoms have been observed directly. In this way the hyperfine structure intervals of the normal states of Li^6, Li^7, K^{39} and K^{41} have been measured. Since the measurement of frequency alone is involved, the results are of very high precision. These spectra have been observed in external magnetic fields varying from 0.05 to 4000 gauss, i.e., from the ordinary Zeeman to the complete Paschen-Back region. The lines in the pattern are completely resolved even at the low fields. The h.f.s. separations derived from measurements at different fields are in excellent agreement. Comparison is made between the ratio of the nuclear moments of Li^7 and Li^6 as derived from the h.f.s. measurements with the directly measured ratio. The two ratios are 3.9610 and 3.9601, respectively. They agree within the experimental error of 0.04 percent. The h.f.s. separations are given both in absolute frequency units and in wave numbers.

	$sec.^{-1}\times10^{-6}$	cm^{-1}
Li^6	228.22	0.007613
Li^7	803.54	0.026805
K^{39}	461.75	0.015403
K^{41}	254.02	0.008474

Introduction

BECAUSE of the existence of nuclear spin the ground states of many atoms consist of a set of closely spaced energy levels. Each level of this hyperfine structure multiplet corresponds to a value of the total angular momentum of the atom. The spacings are caused chiefly by the feeble interactions of the magnetic and electric fields of the electrons with the nuclear magnetic moment and the electrical quadrupole moments,

* Publication assisted by the Ernest Kempton Adams Fund for Physical Research of Columbia University.

respectively. Since the magnitudes of these interactions depend on the angle between the angular momentum of the nucleus and that of the electronic configuration, the states of different total angular momentum, F, will differ in energy.

Left to themselves, the atoms would radiate this energy in the form of electromagnetic radiation of frequency given by the Bohr formula,

$$W_F - W_{F'} = h\nu \qquad (1)$$

and settle down to their lowest energy state. Since the different F states correspond to different orientations of the atomic magnetic moment, this radiation has the character of magnetic dipole radiation.

The region of frequency in which these radiations are emitted lies in the rapidly developing upper end of the technical radiofrequency range, as most hyperfine structures of ground states which have been observed are included between the limits of 0.005 cm^{-1} and 0.4 cm^{-1}, i.e., between frequencies of 1.5×10^{8} and 1.2×10^{10} $sec.^{-1}$ or between wave-lengths of 200 and 2.5 cm. Because of these low frequencies the lifetime of a hyperfine structure level is very long and the intensity of spontaneous emission very feeble. Direct observation of this radiation would be very difficult.

However, it is possible to illuminate the atom with electromagnetic radiation of the correct frequency and of such intensities as to cause it to absorb, or, by the Einstein process of stimulated emission, to emit a quantum of this frequency in the reasonably short time of about 10^{-4} second. If such a process is detected it offers a direct method of measuring hyperfine structure. Such a method has many important advantages over existing optical methods. Firstly, the results are simple to interpret since we are concerned with only one atomic energy level; secondly, the accuracy is very high because only the measurement of the frequency of a radio wave is involved; thirdly, it is possible to measure extremely small energy separations. It is, of course, clear that similar considerations apply to all metastable states which have sufficiently long lifetimes, as well as to the ground states of atoms.

The problem of the detection of the induced transitions between the hyperfine structure levels of the atom has been solved by the utilization of atomic beams in a manner similar to that of the molecular-beam magnetic-resonance method.[1]

In practice these methods have proved superior to the older optical methods as well as to the atomic beam method of zero moments. Measurements of hyperfine structure with an accuracy of 0.005 percent are made without difficulty. The high resolution which can be obtained is exemplified by the fact that it was possible to observe a clearly resolved Zeeman pattern of a hyperfine structure line in a magnetic field of 0.05 gauss, and to obtain half-widths of observed lines of 10^{-6} cm^{-1}.

The principal physical question to which we have applied these methods is the accurate measurement of the hyperfine structures of Li^7 and Li^6 and the comparison of the ratio of the nuclear moments of Li^7 and Li^6 deduced from such measurements with that obtained from the moment values directly measured by the molecular-beam magnetic-resonance method.[1] Present theory accounts for the h.f.s. of an atomic energy level by the assumption that h.f.s. is due solely to the magnetic interaction of the nuclear moment with the external electrons. On the basis of this assumption, the ratio, $(\Delta\nu)_1/(\Delta\nu)_2$, of the h.f.s. separations of a given atomic energy state of two isotopes should yield the ratio, μ_1/μ_2, of the nuclear moments, in a manner which does not involve the electronic wave functions since they are the same for the two isotopes. If there are nonelectromagnetic interactions between the electrons and the nucleus, the directly measured ratio of moments may be expected to differ from that obtained from h.f.s. They would be the same only if the additional interactions were proportional to the magnetic moment, which is hardly likely. Since the two nuclei (Li^6 and Li^7) differ widely in structure it seems that this case is a particularly favorable one for searching for nonelectromagnetic interactions, particularly since the ratio of the moments of the lithium isotopes is accurately known from direct measurements.

This question has already been discussed in an earlier paper[1] where a comparison was made between the directly measured moment ratio and

[1] I. I. Rabi, S. Millman, P. Kusch and J. R. Zacharias, Phys. Rev. **55**, 526 (1939).

the ratio obtained by Manley and Millman[2] from the h.f.s. ratio measured by the atomic-beam zero-moment method. The ratio of moments as determined from h.f.s. was subject to considerable uncertainty, and the discrepancy of about 2 percent between the two ratios, although outside the experimental error, was not considered sufficiently great to give conclusive indication of a real physical effect.

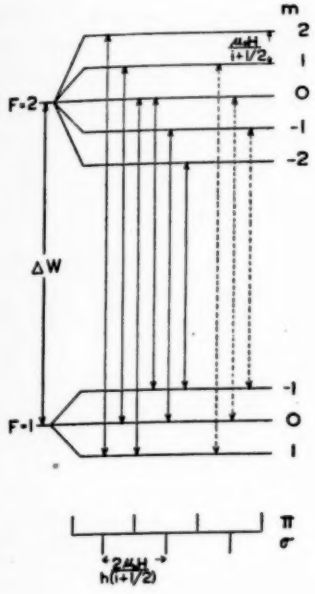

FIG. 1. The magnetic levels, at low field, of the h.f.s. doublet of a $^2S_{\frac{1}{2}}$ state for a nuclear spin of $\frac{3}{2}$ and the allowed transitions between these levels. The lower part of the figure indicates the spectrum resulting from these transitions.

THEORY OF THE EXPERIMENT

The levels which compose an h.f.s. multiplet are, by the rules of quantum mechanics, characterized by total angular momenta, $F=i+J$, $i+J-1$, $i+J-2$, $\cdots$, where i is the nuclear and J the total electronic angular momentum. The lowest F is $J-i$ if $J>i$ and $i-J$ if $i>J$. Transitions between the levels are governed by the selection rules for magnetic dipole radiation,

$$\Delta F=0,\ \pm 1;\quad \Delta m=0,\ \pm 1,$$

where m is the magnetic quantum number.

Only in the absence of an applied magnetic field will the transition $|F-F'|=1$ result in a single line. In a magnetic field the Zeeman effect of this line will be observed. For sufficiently weak fields the Zeeman pattern can be calculated in the usual way by the Landé g formula:

$$g_F=g_J\frac{F(F+1)+J(J+1)-i(i+1)}{2F(F+1)}+g_i\frac{F(F+1)-J(J+1)+i(i+1)}{2F(F+1)}. \quad (2)$$

Neglecting the second term and restricting ourselves to atoms for which $J=\frac{1}{2}$ we have for the two F states, $i+\frac{1}{2}$ and $i-\frac{1}{2}$,

$$g_{i+\frac{1}{2}}=\frac{g_J}{2i+1}\quad\text{and}\quad g_{i-\frac{1}{2}}=-\frac{g_J}{2i+1}, \quad (3)$$

respectively. The weak field Zeeman lines should therefore be found at frequencies:

$$\nu=\frac{W_F-W_{F-1}}{h}+(m_F+m_{F-1})\frac{g_J}{2i+1}\frac{\mu_0 H}{h}. \quad (4)$$

For $^2S_{\frac{1}{2}}$ states ($g_J=2$) we have two sets of lines corresponding to the π and σ lines of spectroscopy. The π lines, for which $\Delta m=\pm 1$, have frequencies,

$$\nu=\Delta\nu+\frac{2m\pm 1}{i+\frac{1}{2}}\frac{\mu_0 H}{h} \quad (5)$$

and the σ lines, for which $\Delta m=0$, have frequencies,

$$\nu=\Delta\nu+\frac{2m}{i+\frac{1}{2}}\frac{\mu_0 H}{h}, \quad (6)$$

where in (5) and (6), $\Delta\nu=(W_F-W_{F-1})/h$ and is the frequency corresponding to the energy difference between the two F states, $i+\frac{1}{2}$ and $i-\frac{1}{2}$, (expressed in sec.$^{-1}$) at zero magnetic field.

The π lines represent transitions caused by the component of the oscillating magnetic field perpendicular to the constant field, H, and the σ lines arise from the component parallel to H. This is opposite to the usual assignment because we are dealing with magnetic dipole radiation.

As an example we shall consider the magnetic levels of the h.f.s. multiplet of a $^2S_{\frac{1}{2}}$ state for a nuclear spin of $\frac{3}{2}$. These are indicated in Fig. 1 by means of the customary energy level diagram. The transitions which give rise to the π lines are represented by solid lines and those which give rise to the σ lines by means of dotted lines. The spectrum is indicated in the lower portion of the

[2] J. H. Manley and S. Millman, Phys. Rev. **51**, 19 (1937).

diagram. The energy separation between adjacent magnetic levels is $\mu_0 H/(i+\frac{1}{2})$ and the frequency difference between two adjacent π lines as well as between two adjacent σ lines is $2\mu_0 H/[(i+\frac{1}{2})h]$.

It may be seen by use of Eqs. (5) and (6) or by reference to Fig. 1 that the frequency separation of the two F levels in an h.f.s. doublet at zero field, $\Delta\nu$, is given by the mean of the frequencies of all the lines in the Zeeman pattern at a low magnetic field, by the mean of all the π lines, by the mean of all the σ lines, or by the mean frequency of any symmetrical pair of lines.

When $\Delta F=0$, the frequencies of the lines are given by,

$$\nu=\frac{1}{i+\frac{1}{2}}\frac{\mu_0 H}{h} \tag{7}$$

since $\Delta m=\pm 1$. However we shall present no experiments to fit this case in the weak field region.

In the region of high magnetic field ($\mu_0 H/h \gg \Delta\nu$) the total angular momentum, F, is no longer constant and a more suitable description is given in the manner customarily employed for the Paschen-Back effect, i.e., in terms of m_i and m_J, the components in the direction of H of the nuclear and electronic angular momenta, respectively. The energy of the states is given[3] by the formula,

$$Wm_i m_J = m_i g_i \mu_0 H + m_J g_J \mu_0 H + [\Delta W/(i+\tfrac{1}{2})] m_i m_J. \tag{8}$$

The selection rules for the transitions are $\Delta m_i=\pm 1$, $\Delta m_J=0$ and $\Delta m_i=0$, $\Delta m_J=\pm 1$. From this equation it is clear that at large values of H the transitions for which $\Delta m_i=\pm 1$, $\Delta m_J=0$ give rise to lines whose frequencies become independent of the field and approach the limiting value $\Delta\nu/(2i+1)$, since the term $m_i g_i \mu_0 H$ is still relatively small in comparison with the term $[\Delta W/(i+\frac{1}{2})]m_i m_J$ for the highest fields used in our experiments (about 6000 gauss). This happy circumstance is very important for these experiments because it is then possible to measure $\Delta\nu$ with the use of frequencies which lie in the region of $\Delta\nu/(2i+1)$. One can thus avoid some of the technical difficulties involved in the use of extremely high frequencies.

[3] E. Back and S. Goudsmit, Zeits. f. Physik **47**, 174 (1928).

The preceding considerations are only approximate. To utilize the full power of our experimental method one must employ the exact theory of the energy levels of an h.f.s. multiplet in a magnetic field. We shall follow the customary usage by defining the Landé g factor as the negative ratio of the magnetic moment, expressed in units of μ_0, the Bohr magneton, to the angular momentum expressed in units of $h/2\pi$. The g_J values of the ground states of all the alkali atoms are, therefore, positive, while the g_i values of the alkali atoms are negative, since the moments are positive. The energies of the magnetic levels as a function of the field are given[4] by the formulae:

$$W_{i+\frac{1}{2},m} = -\frac{\Delta W}{2(2i+1)} + g_i \mu_0 H m + \frac{\Delta W}{2}\left(1+\frac{4m}{2i+1}x+x^2\right)^{\frac{1}{2}} \tag{9}$$

for $F=i+\frac{1}{2}$; $m=i-\frac{1}{2}, i-\frac{3}{2}, \cdots -(i-\frac{1}{2})$,

$$W_{i+\frac{1}{2},\pm(i+\frac{1}{2})} = -\frac{\Delta W}{2(2i+1)} \pm g_i \mu_0 H(i+\tfrac{1}{2}) + \frac{\Delta W}{2}(1\pm x) \tag{10}$$

for $F=i+\frac{1}{2}$; $m=\pm(i+\frac{1}{2})$,

$$W_{i-\frac{1}{2},m} = -\frac{\Delta W}{2(2i+1)} + g_i \mu_0 H m - \frac{\Delta W}{2}\left(1+\frac{4m}{2i+1}x+x^2\right)^{\frac{1}{2}} \tag{11}$$

for $F=i-\frac{1}{2}$; $m=i-\frac{1}{2}, i-\frac{3}{2}, \cdots -(i-\frac{1}{2})$, where the parameter x in Eqs. (9), (10) and (11) is defined by

$$x=(g_J-g_i)\mu_0 H/\Delta W. \tag{12}$$

Figs. 2a and 2b exhibit graphically the behavior of the ratio $W_m/\Delta W$ as a function of the parameter x for nuclear spins of $\frac{3}{2}$ and 1, respectively. For weak fields where x^2 and g_i may be neglected, Eqs. (9)–(12) yield the same result as Eqs. (5) and (6).

By taking the differences of the energies of the

[4] S. Millman, I. I. Rabi and J. R. Zacharias, Phys. Rev. **53**, 384 (1938).

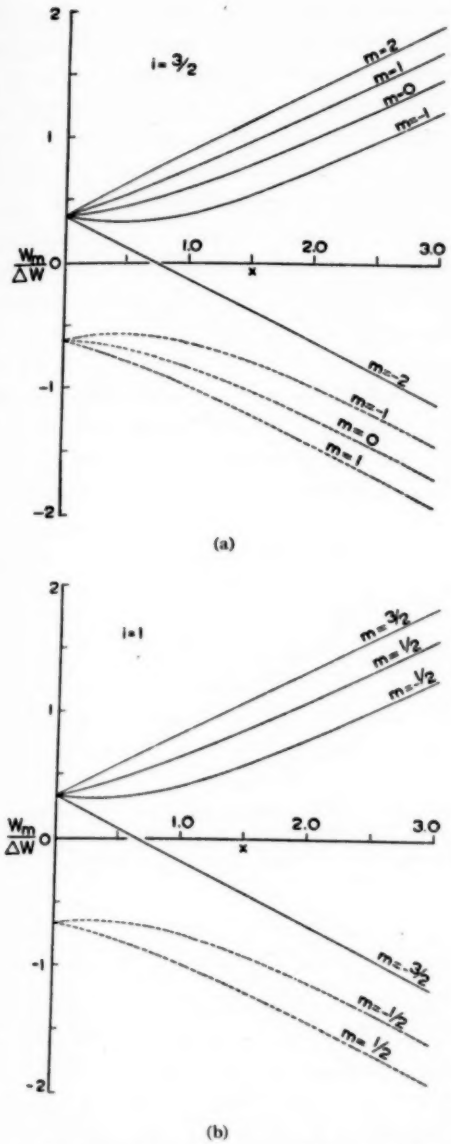

FIG. 2. The variation with magnetic field of the energy of magnetic levels of a normal h.f.s. doublet of a $^2S_{\frac{1}{2}}$ state. (a) describes the case when $i=\frac{3}{2}$ and (b) the case when $i=1$. The solid lines correspond to the levels arising from the state $F=i+\frac{1}{2}$ and the dotted lines to the levels arising from the state $F=i-\frac{1}{2}$.

states between which transitions are allowed and dividing by h, the frequencies of the lines as a function of the field are obtained. These frequencies are shown in Figs. 3 and 4 in units of $\Delta\nu$, for nuclear spins of $\frac{3}{2}$ and 1, respectively, in the region of the weak field and intermediate field Zeeman effect.

The values of the field, H, corresponding to any value of x may be found from Eq. (12), if $\Delta\nu$ is known. The values of H in Fig. 3 are appropriate to the case of K^{39}. However, the curves apply equally well to any atom in a $^2S_{\frac{1}{2}}$ state whose nuclear spin is $\frac{3}{2}$ if a suitable conversion is made from the field parameter x to the field H. Similarly the values of the field in Fig. 4 correspond to the case of Li^6. The curves apply to the case of any atom in a $^2S_{\frac{1}{2}}$ state whose nuclear spin is 1 for an appropriate conversion of the parameter x to the field. The full lines represent the $\pi(\Delta m=\pm 1)$ components and the dotted lines the $\sigma(\Delta m=0)$ components. The approximate equations (5) and (6) which describe the Zeeman pattern at weak fields give the frequencies of the lines only in that range of the field for which the center of gravity of the Zeeman pattern lies very near to $\Delta\nu$. The center of gravity shifts to higher frequencies for increasing values of x. This corresponds to the Zeeman effect at intermediate fields and Eqs. (9)–(12) must be used to describe this case. Terms in g_i may be neglected in calculations of the Zeeman effect in the weak and intermediate field regions, since at these fields the interaction energy of the nuclear moment with the applied field is small compared to other interaction energies. The two lines $(F, m)\leftrightarrow(F-1, m-1)$ and $(F, m-1)\leftrightarrow(F-1, m)$ are represented by a single line in Figs. 3 and 4. Actually these lines constitute a close doublet, except in the case $m=\pm(i+\frac{1}{2})$, whose frequency separation is $2g_i\mu_0H/h$. This energy cannot be indicated on the scale of our curves, nor could this doubling be experimentally observed at the very small fields at which we observed the Zeeman effect of the line $|F-F'|=1$.

The convergence of the frequencies of all the lines for which $\Delta m_i=\pm 1$, $\Delta m_J=0$, to a value independent of the field can be seen from Figs. 2a and 2b. Table I lists the transitions for the case of a nuclear spin of $\frac{3}{2}$. This case is chosen because it applies to the experiments described in this paper; the extension to other cases can easily be made. In designating the states involved in a transition, the first number in the parenthesis denotes the F value of the state, and the second number, the m value. This designation does not imply that these states are characterized by a definite total angular momentum, but rather that each of these states is derived from a

definite (F, m) state by an "adiabatic" transformation. The expressions for the frequencies of the lines in Table I are derived from Eqs. (9)–(11) and are valid for all values of x. However, when $x^2 \gg 1$ a simple expansion of the terms in the frequency expressions indicates that the frequencies approach limiting values of $\Delta\nu/4$ independent of field, except for the term $g_i\mu_0 H/h$. In the general case the limiting frequency is $\Delta\nu/(2i+1)$.

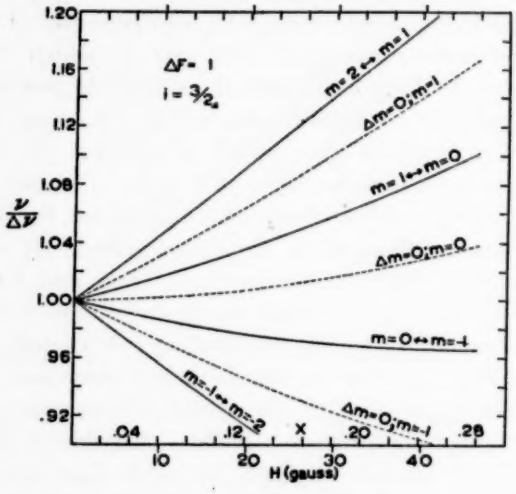

FIG. 3. The frequencies of the components of the Zeeman pattern of the line $|\Delta F| = 1$ as a function of the magnetic field. The values of x are appropriate to any atom in a $^2S_{\frac{1}{2}}$ state with a spin of $\frac{3}{2}$, but the indicated values of H correspond to the case of K^{39} only.

Figures 5 and 6 give the frequencies of the lines, in units of $\Delta\nu$, associated with the transitions $\Delta m_i = \pm 1$, $\Delta m_J = 0$ as a function of the field parameter x, for K^{39} and Li^7, respectively. The curves have been calculated by use of the expressions in Table I. The two sets of curves are different for the two atoms, even though their nuclear spins are the same, because the term $g_i\mu_0 H/h$, though small, is not negligible and has a different value for each nucleus. The values of g_i which have been used in these calculations are $-0.260/1837$[5] and $-2.167/1837$[1] for K^{39} and Li^7, respectively. The range of x covered in each of these figures is such as to include an experimentally convenient range of field, and the indicated values of field are appropriate only to the one nucleus in question. Since x itself may be expressed in terms of the field through the use of Eq. (12), $\Delta\nu$ can be calculated from the frequency observed for any one transition at some known field. The value of g_i need not be known with great precision since the contribution of the term $g_i\mu_0 H/h$ to the total frequency is small. Moreover, the magnetic field need not be accurately determined since the transition frequencies vary slowly with field for large values of H, and in certain regions are practically independent of field.

For each transition $(F, m) \leftrightarrow (F, m-1)$, there will be a pair of lines, one arising for $F = i+\frac{1}{2}$ and the other arising for $F = i-\frac{1}{2}$, provided only that m does not have the value $i+\frac{1}{2}$ and that $m-1$ does not have the value $-(i+\frac{1}{2})$, since the m values $\pm(i+\frac{1}{2})$ do not exist for the state $F = i-\frac{1}{2}$. At a fixed field the expression for the mean frequency of each pair of such lines does not depend on the value of the nuclear g factor. These pairs of lines are identified in Figs. 5 and 6 by the fact that at low fields the two members of the pair have very nearly equal frequencies. The line originating in the state $F = i+\frac{1}{2}$ is indicated by a full line, and that originating in the state $F = i-\frac{1}{2}$ by a dotted line. Regardless of the value of the nuclear spin all of the lines arising from the transitions $\Delta m_i = \pm 1$, $\Delta m_J = 0$, except the lines $(i+\frac{1}{2}, -i-\frac{1}{2}) \leftrightarrow (i-\frac{1}{2}, -i+\frac{1}{2})$ and $(i+\frac{1}{2}, i+\frac{1}{2}) \leftrightarrow (i+\frac{1}{2}, i-\frac{1}{2})$ may be arranged in such pairs. It may be seen by reference to Table I that the sum of the mean frequencies of all the pairs of lines added to the sum of the frequencies of the single lines is identically equal to $\Delta\nu$, for a constant value of x. This is true not only for our case where $i = \frac{3}{2}$, but for any atomic system described by Eqs. (9)–(12). This property permits the determination of $\Delta\nu$ even if neither g_i

TABLE I. *The transitions $\Delta m_i = \pm 1$, $\Delta m_J = 0$ for an atom in a $^2S_{\frac{1}{2}}$ state whose nuclear spin is $\frac{3}{2}$, and the expressions for the frequencies of these lines.*

TRANSITIONS	EXPRESSION FOR FREQUENCIES
$(2,2) \leftrightarrow (2,1)$	$\frac{1}{2}\Delta\nu[(1+x)-(1+x+x^2)^{\frac{1}{2}}]+g_i\mu_0 H/h$
$(2,1) \leftrightarrow (2,0)$	$\frac{1}{2}\Delta\nu[(1+x+x^2)^{\frac{1}{2}}-(1+x^2)^{\frac{1}{2}}]+g_i\mu_0 H/h$
$(1,1) \leftrightarrow (1,0)$	$\frac{1}{2}\Delta\nu[(1+x+x^2)^{\frac{1}{2}}-(1+x^2)^{\frac{1}{2}}]-g_i\mu_0 H/h$
$(2,0) \leftrightarrow (2,-1)$	$\frac{1}{2}\Delta\nu[(1+x^2)^{\frac{1}{2}}-(1-x+x^2)^{\frac{1}{2}}]+g_i\mu_0 H/h$
$(1,0) \leftrightarrow (1,-1)$	$\frac{1}{2}\Delta\nu[(1+x^2)^{\frac{1}{2}}-(1-x+x^2)^{\frac{1}{2}}]-g_i\mu_0 H/h$
$(2,-2) \leftrightarrow (1,-1)$	$\frac{1}{2}\Delta\nu[(1-x+x^2)^{\frac{1}{2}}-(1-x)]-g_i\mu_0 H/h$

[5] P. Kusch, S. Millman and I. I. Rabi, Phys. Rev. **55**, 1176 (1939).

nor the value of the field is known, by the simple expedient of observing the frequencies of all the lines at some fixed field and making the appropriate summation.

If the field is known the value of g_i can be found from the frequency separation of the members of each pair of lines. Such a determination will not be very accurate since we are measuring the rather small frequency difference, $2g_i\mu_0 H/h$, between two lines whose total frequency is large compared to this difference. With the molecular-beam magnetic-resonance method for determining nuclear g values, the quantity $g_i\mu_0 H/h$ was measured directly as a first-order effect and could, therefore, be determined much more precisely than in the present experiments.

Method

In order to detect the transitions between the energy levels, produced by the oscillating magnetic field, we utilize the change in atomic magnetic moment produced by the transitions. As in the molecular-beam magnetic-resonance method, the atoms are deflected in an inhomogeneous magnetic field, then pass through a homogeneous field and are finally deflected in the opposite direction by a second inhomogeneous field to strike a detecting filament. The transitions occur within the homogeneous field region where the oscillating field is situated. Transitions cause a drop of intensity at the detector only if the moment of the atom in the second deflecting field is appreciably different from its value in the first.

This experiment is different from the previous experiments in which molecules were studied because the magnetic moment of the atom is a function of the magnetic field and therefore the deflections in the inhomogeneous fields depend not only on the gradient but also on the magnitude of these fields. For example, we consider a transition which at high fields may be regarded as one in which m_i changes by one unit (Eq. (8)). Clearly at high fields the atomic moment remains practically unchanged because m_J, and therefore the electronic moment, is the same in both states. If the second deflecting field is large ($x \gg 1$) there will be almost no difference between the paths of atoms which have made these transitions and

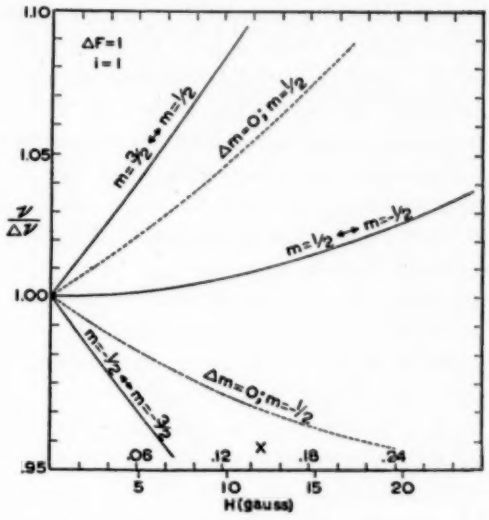

FIG. 4. The frequencies of the components of the Zeeman pattern of the line $|\Delta F| = 1$ as a function of the magnetic field. The values of x are appropriate to any atom in a $^2S_{\frac{1}{2}}$ state with a spin of 1, but the values of H correspond to the case of Li^6 only.

the paths of atoms which have not. However, if the deflecting field is small ($x \sim 1$) the difference in magnetic moment between the two states is great and the paths correspondingly different.

The magnetic moment of the atoms as a function of the magnetic field may be obtained from the Eqs. (9)–(12), since $\mu_{F,m} = -\partial W_{F,m}/\partial H$. These are:

$$\frac{\mu_{i+\frac{1}{2},m}}{\mu_0} = -g_i m - \frac{x+2m/(2i+1)}{2[1+4mx/(2i+1)+x^2]^{\frac{1}{2}}}(g_J - g_i) \quad (13)$$

for $F = i+\frac{1}{2}$; $m = i-\frac{1}{2}, i-\frac{3}{2}, \cdots -(i-\frac{1}{2})$,

$$\frac{\mu_{i+\frac{1}{2},\pm(i+1)}}{\mu_0} = \mp\left(\frac{g_J}{2}+g_i i\right) \quad (14)$$

for $F = i+\frac{1}{2}$; $m = \pm(i+\frac{1}{2})$, and

$$\frac{\mu_{i-\frac{1}{2},m}}{\mu_0} = -g_i m + \frac{x+2m/(2i+1)}{2[1+4mx/(2i+1)+x^2)]^{\frac{1}{2}}}(g_J - g_i) \quad (15)$$

for $F = i-\frac{1}{2}$; $m = i-\frac{1}{2}, i-\frac{3}{2}, \cdots -(i-\frac{1}{2})$, where $\mu_{F,m}/\mu_0$ is the magnetic moment of the atom in units of the Bohr magneton, for any state

characterized by the quantum numbers F and m. Figs. 7a and 7b show a plot of these moment values for spins of $\frac{3}{2}$ and 1, respectively. For the use to which these moment values are to be put, we can safely neglect the term in mg_i. It can be seen from the formulae, and from the curves which they describe, that in cases where $\Delta\nu$ is small (0.01 cm^{-1}), the inhomogeneous field must be relatively weak, since the field corresponding to any value of x is proportional to $\Delta\nu$. For K^{39}, for example, a value of the inhomogeneous field of about 50 gauss ($x=0.3$) would be appropriate for the detection of transitions for which $\Delta m_i=\pm 1$, $\Delta m_J=0$. The resonance frequencies required for the production of transitions depend only on the magnitude of the homogeneous field and not on the values of the field in the deflecting magnets. The choice of field values in the latter merely determines the ease with which the transitions in the homogeneous field are detected.

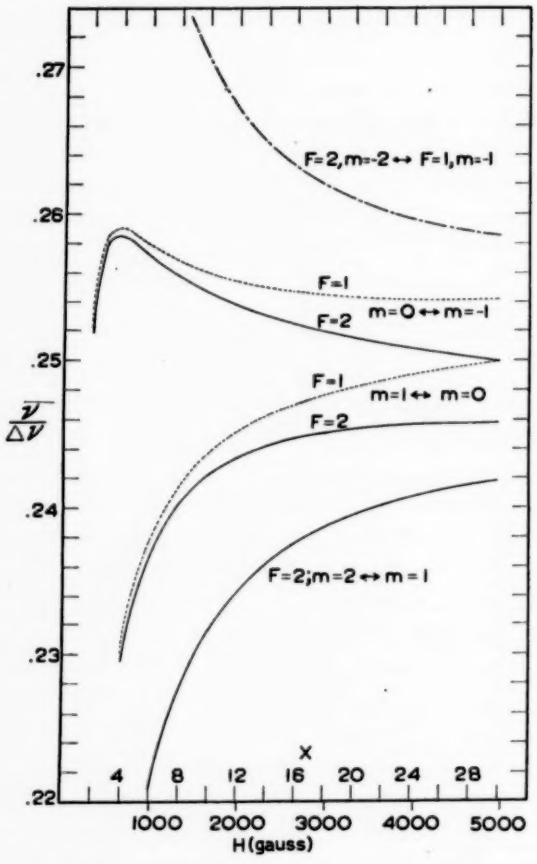

FIG. 5. The field dependence of the frequencies of the lines associated with the spectrum of K^{39} resulting from the transitions $\Delta m_i=\pm 1$, $\Delta m_J=0$.

APPARATUS AND EXPERIMENTAL PROCEDURE

The apparatus used in these experiments was the same as that used in the determination of nuclear magnetic moment by the molecular-beam magnetic-resonance method. The inhomogeneous fields were about 50 cm long. At the position of the beam, fields of about 12,000 gauss and gradients of the order of 10^5 gauss per cm could be attained. These long magnets and high field gradients were required in the older experiments because the systems which were to be deflected had moments of the order of a nuclear magneton. In the present experiments where the moments are of the order of a Bohr magneton, such deflecting power is unnecessary; in fact, these same fields were used in the older experiments, with beams produced by evaporating the alkali metals, to remove the atomic portion of the beam and to permit the study of molecules. The reduction of deflecting power for the present experiments is easily accomplished by limiting the currents in the field coils to very small values. The field values varied from 50 to 100 gauss. The ratio of field gradient to field was about 8. While the field values in the deflecting magnets need not, in general, be critically adjusted for observing atomic transitions, special care must be taken for some particular cases. For example, for the case $i=\frac{3}{2}$ the transition $(F, 0)\leftrightarrow(F', -1)$ will yield no change in the moment of the atom in the deflecting field if it corresponds to the value of the field parameter x of about 0.27. For such a field value the transition cited would be unobservable.

The high frequencies which were required in these experiments were produced by a tuned-plate tuned-filament oscillator with Western Electric 316A tubes. The design of the oscillator followed closely that suggested by the manufacturers of the tube. The frequency of the oscillator was continuously variable and could be set to any desired value to better than one part in 20,000. All frequency measurements were made by use of a General Radio heterodyne frequency meter, Type 620-A. The accuracy of frequency determinations is governed by the precision with which one can set on a zero beat frequency and read the scale. This precision for a single setting was about one part in 20,000. In

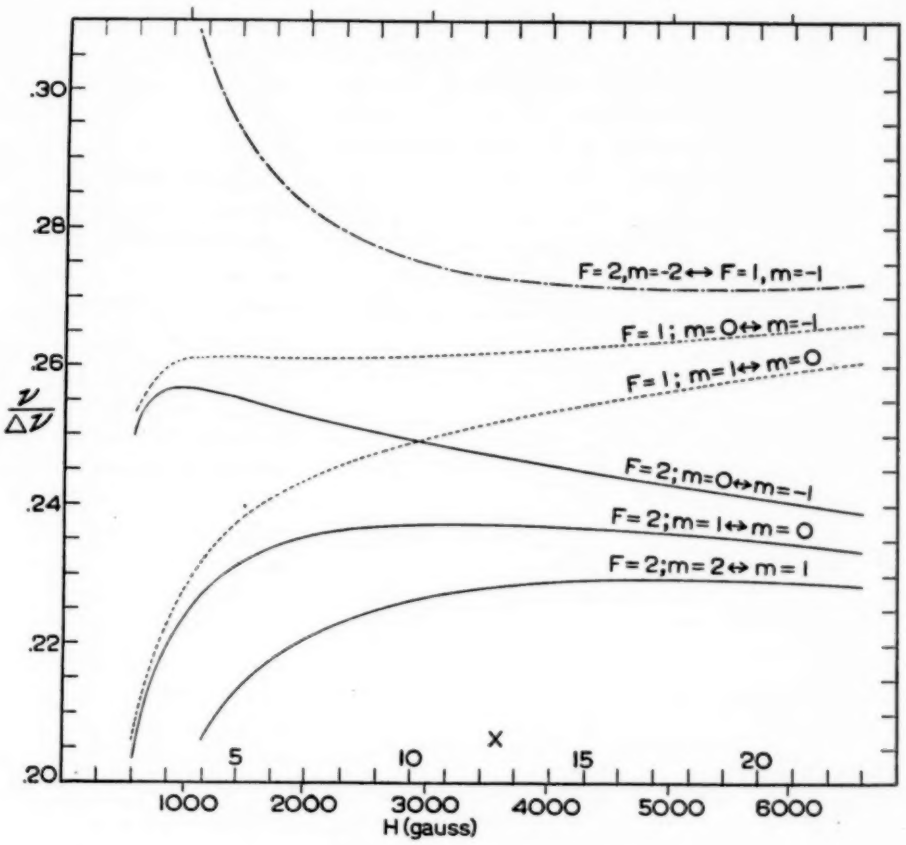

FIG. 6. The field dependence of the frequencies of the lines associated with the spectrum of Li^7 resulting from the transitions $\Delta m_i = \pm 1$, $\Delta m_J = 0$.

practice, however, determinations of frequency were made by observing the position of zero beat frequency between the high frequency oscillator and several harmonics of the wave meter. The frequencies so deduced showed excellent internal consistency and the average of observations on several harmonics of the meter probably gives a frequency with a precision of better than one part in 20,000. The frequency of the quartz crystal against which the wave meter is calibrated is known to better than one part in 100,000 and therefore introduces no error within the precision of our measurements. The stability of the oscillator was so great that no detectable change in frequency occurred over a period of several minutes. The high order of stability is also evident from several examples of the Zeeman pattern to be presented later.

The oscillating magnetic field was produced, as in the previous experiments,[6] by the passage of the oscillating current through two flattened parallel tubes in the gap of the magnet which supplied the homogeneous magnetic field. The oscillating field was approximately perpendicular to the fixed field. The presence of a component of the oscillating field parallel to the fixed field was probably due to the circumstance that the atomic beam did not traverse the field at a point midway between the two wires as well as to the fact that the current distribution in the tubes at very high frequency is considerably different from that at low frequencies. It is to be expected that both π and σ transitions would occur, even though the σ transitions will be considerably weaker than the π transitions.

The oscillating fields required to induce the transitions $\Delta F = \pm 1$ are much smaller than those used in the previous experiments on molecules. The reason for this is that the torque per gauss exerted on the electron is much greater than on the nucleus, since nuclear moments are of the order of 1/1000 as great as the electronic moment, while the change in angular momentum and the

[6] S. Millman, Phys. Rev. **55**, 628 (1939).

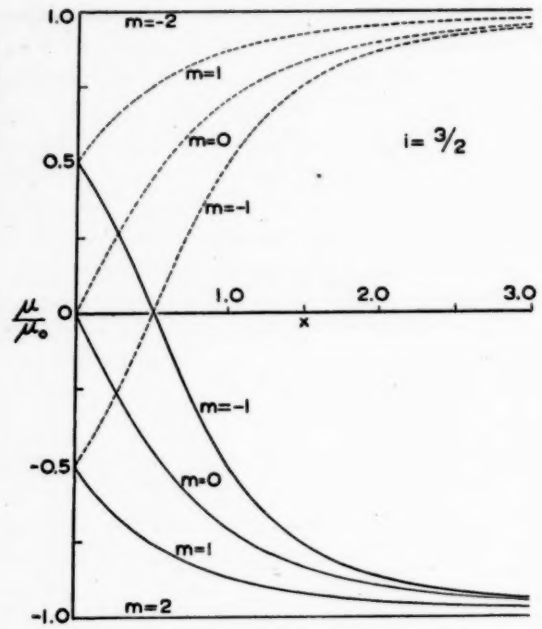

(a)

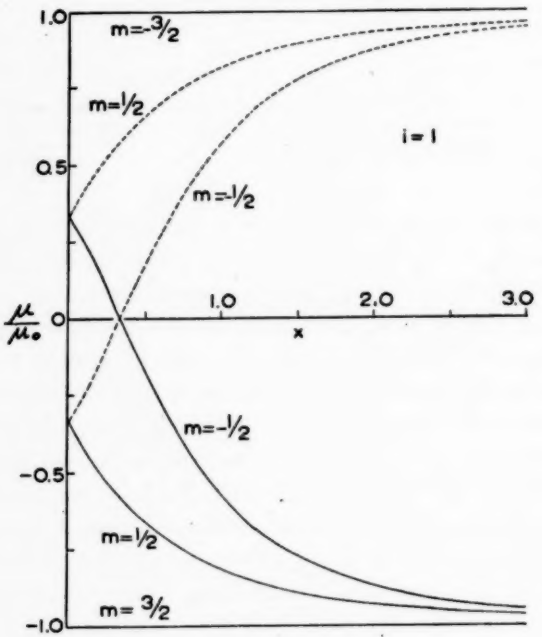

(b)

FIG. 7. The variation of magnetic moment of an atom in a $^2S_{\frac{1}{2}}$ state with magnetic field. (a) describes the case when $i=\frac{3}{2}$ and (b) the case when $i=1$.

time during which the torque acts is approximately the same for the two cases. This is a very fortunate circumstance because it obviates the necessity of using high power ultra-high frequency oscillators. Indeed, the transitions occurred with oscillating currents of only a few milliamperes.

RESULTS

K^{39}

Figures 8–11 show the weak field Zeeman patterns of the line $F \leftrightarrow F-1$ of K^{39} under various experimental conditions. That of Fig. 8 was obtained for a fixed field of 0.25 gauss and an oscillating field sufficiently large to show the σ components. It is to be noted that only two of the three possible σ lines appear. The reason for the absence of the line $(2, -1) \leftrightarrow (1, -1)$ can easily be found by an inspection of Fig. 7a, where it is seen that when the value of x in the deflecting fields is about 0.5 ($H \sim 80$ gauss for K^{39}) no change in the magnetic moment of the atom will result in this transition. Even though the calibration constants for the deflecting magnets at low field values were not known with any degree of accuracy, the above explanation was easily verified by increasing the current in the deflecting magnets by about 50 percent. This increase resulted in a field value at which all transitions were accompanied by appreciable moment changes. Fig. 9 shows the resulting pattern, with none of the expected lines missing. The fixed field value in this case, as calculated from the separations of the lines, was about 0.2 gauss. The intensity of all the σ lines in Figs. 8 and 9 is low since the component of oscillating field parallel to the fixed field is quite small compared with the perpendicular component. The lines $(F, -1) \leftrightarrow (F', 0)$ and $(F, 0) \leftrightarrow (F', -1)$ are most intense since F can take on the two values, 2 and 1, and each of the lines is really an unresolved doublet. The separation between the members of a doublet in a field of 0.2 gauss is only about 100 sec.$^{-1}$ for K^{39} so that the line is not measurably affected in width but is merely raised in intensity.

The half-widths of the lines in the Zeeman patterns shown in Figs. 8 and 9 are considerably greater than can be expected by use of the relationship,

$$\Delta\nu\Delta\tau \sim 1 \qquad (16)$$

where $\Delta\tau$ is the time spent by the atoms in the radiation field and $\Delta\nu$ is roughly the half-width of the curve in frequency units. For potassium

atoms at a temperature of about 550°K the average time spent in a radiation field 4 cm in length is approximately 7×10^{-5} sec., so that the lines should have a half-width of the order of 1.5×10^{4} sec.$^{-1}$. The experimental widths range from 15×10^{4} to 30×10^{4} sec.$^{-1}$ and are chiefly due to the large oscillating fields used in the observation of these curves. When the oscillating field is made extremely small, a pattern of the type shown in Fig. 10 is observed. The component of oscillating field parallel to the fixed field is so small that the σ lines are no longer observable. The two inner lines have a half-width of about 2×10^{4} sec.$^{-1}$ and the two outer lines of about 4×10^{4} sec.$^{-1}$. This well resolved Zeeman pattern was observed for a field of about 0.05 gauss. Fig. 11 shows an unresolved Zeeman pattern at a field slightly greater than that used for the pattern in Fig. 10. The lack of resolution is due to the excess of oscillating field.

In Table II are listed the expected transitions and the observed frequencies of the centers of the lines shown in Figs. 8, 9 and 10. It is seen that

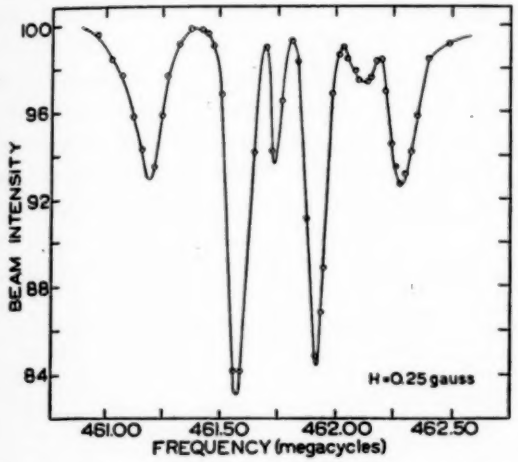

FIG. 8. The Zeeman pattern of the line, $|\Delta F|=1$, of K^{39}.

the frequency differences between the successive lines are constant within the precision of measurement of the frequencies of the lines. This is in agreement with the predictions of Eqs. (5) and (6). From the observation of a large number of curves of the type shown in Figs. 8, 9 and 10 we find for $\Delta\nu$ of the ground state of K^{39} the value $(461.75\pm0.02)\times10^{6}$ sec.$^{-1}$ or 0.015403 cm^{-1} if we take the velocity of light[7] as 2.99776×10^{10} cm/sec.

[7] F. G. Dunnington, Rev. Mod. Phys. **11**, 65 (1939).

The $\Delta\nu$ of K^{39} has also been determined by observations on transitions for which $\Delta m_i=\pm1$, $\Delta m_J=0$, at high magnetic fields. The frequencies of these transitions as a function of the field are indicated in Fig. 5. In Table III are listed the frequencies observed for these lines at a field of 3950 gauss. The third column lists the mean frequencies of the double lines together with the frequencies of the single lines. $\Delta\nu$ is the sum of the frequencies listed in this column. In column 4 of

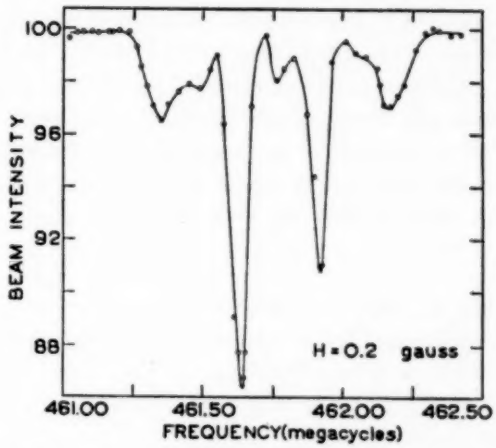

FIG. 9. The Zeeman pattern of the line, $|\Delta F|=1$, of K^{39}, observed for a larger value of the inhomogeneous field than that of Fig. 8.

Table III we list the values $\nu/\Delta\nu$ appropriate to the mean frequency of each of the doublets for a field of 3950 gauss. The last column gives the calculated $\Delta\nu$. From the evaluation of three sets of similar observations we obtain for $\Delta\nu$ the value $(461.75\pm0.02)\times10^{6}$ sec.$^{-1}$. The complete agreement between the two independent methods of calculating $\Delta\nu$ indicates that the high field method of obtaining the h.f.s. separation of the ground state is as reliable as the method involving the measurement of the energies of the transitions between different F levels at very weak fields.

If the frequency interval between the two components of any double line is measured for a known field, the value of g_i can be obtained as explained in an earlier section. The value which we obtain from such measurements for g_i of K^{39} is $-0.261/1837$. This is to be compared with the value $-0.260/1837$ obtained by the molecular beam magnetic resonance method. The present value is the less accurate because the field values were not very well known and the frequency

difference between two lines is subject to considerable error, even though the frequencies of the lines themselves are very well known.

K^{41}

The hyperfine structure separation of the ground state of K^{41} was measured in fields of 0.15 to 0.5 gauss in the same way as the $\Delta\nu$ of K^{39} was determined at low magnetic fields. The nuclear spin is the same for both isotopes of potassium and Eqs. (5) and (6) apply to K^{41} as well as to K^{39}. We find the value $(254.02\pm0.02)\times10^6$ sec.$^{-1}$ or 0.008474 cm^{-1} for the $\Delta\nu$ of K^{41}. The ratio $(\Delta\nu)_{41}/(\Delta\nu)_{39}$ is 0.55012 ± 0.00006. This value is also the ratio of the nuclear moments of the two isotopes if we assume that hyperfine structure is due solely to the magnetic interaction of the nucleus with the atomic electrons.

Li^6

The hyperfine structure separation of the ground state of Li^6 was measured in fields of 0.25 to 1.5 gauss. Since the spin of this nucleus is 1, the Zeeman pattern will contain only five components, three π lines and two σ lines. Fig. 4 indicates the expected frequencies of these lines, in units of $\Delta\nu$, as a function of H. The observed Zeeman pattern for a field of 0.24 gauss is given in Fig. 12. The central component does not vary in frequency with the field for very small values of H. The frequency associated with this π line, therefore gives $\Delta\nu$ of Li^6 without any further calculation. The same result is, of course, obtained by averaging the frequencies of the outside π lines, or by averaging the frequencies of the two σ components. Table IV contains a list of frequencies of the observed lines. The slight departure from the expected uniformity of the spacing of the lines can be explained on the basis of the observation that the outer π lines are broader than any of the inner lines. These outer

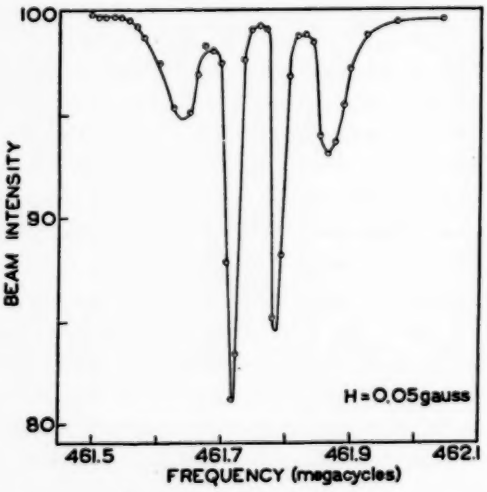

FIG. 10. The Zeeman pattern of the line, $|\Delta F|=1$, of K^{39}, observed for very low amplitude of oscillating field. Only the π components appear.

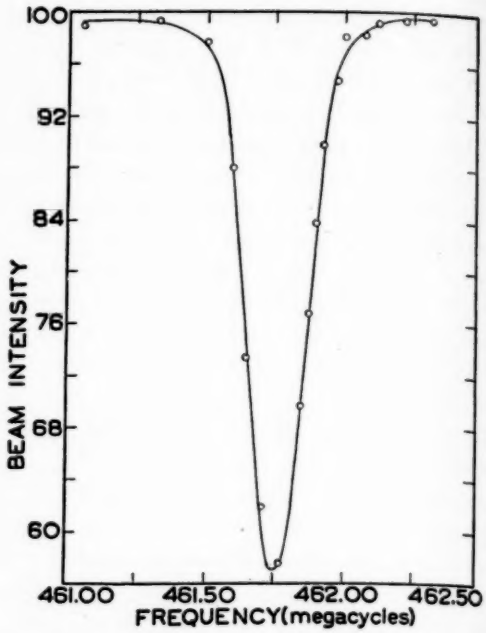

FIG. 11. The Zeeman pattern of the line, $|\Delta F|=1$, of K^{39}, for approximately the same fixed field as in Fig. 10, but for a very much larger amplitude of oscillating field.

TABLE II. *Lines in the Zeeman patterns of* K^{39} *shown in Figs. 8, 9 and 10, and their observed frequencies.*

Transition	Observed frequencies (megacycles)		
	Fig. 8	Fig. 9	Fig. 10
$(2,-2)\leftrightarrow(1,-1)$	461.21		461.64
$(2,-1)\leftrightarrow(1,-1)$	missing		
$(2,-1)\leftrightarrow(1,0)$ $(2,0)\leftrightarrow(1,-1)$	461.58	461.64	461.72
$(2,0)\leftrightarrow(1,0)$	461.74	461.76	
$(2,1)\leftrightarrow(1,0)$ $(2,0)\leftrightarrow(1,1)$	461.91	461.92	461.79
$(2,1)\leftrightarrow(1,1)$	462.12		
$(2,2)\leftrightarrow(1,1)$	462.28		461.87

lines, therefore, overlap the adjacent σ lines to a greater degree than does the central π line. This circumstance leads to a slight shift of the outer π lines toward the center of the pattern and a shift of the σ lines away from the center. The value of $\Delta\nu$ is found to be $(228.22\pm0.01)\times10^6$ sec.$^{-1}$ or 0.007613 cm^{-1}.

Li^7

The $\Delta\nu$ of Li^7 was first measured in strong fields by observing the transitions for which $\Delta m_i=\pm1$, $\Delta m_J=0$. As has already been pointed out, this procedure enables one to obtain $\Delta\nu$ with the use of applied frequencies in the neighborhood of $\Delta\nu/(2i+1)$ which in the case of Li^7 are about 200 megacycles. Fig. 6 indicates the expected frequencies of transition, in units of $\Delta\nu$, as a function of the field parameter x.

In Table V are listed the transitions for the values of the field used in these experiments. By reference to Fig. 6 it may be seen that the frequencies of transition do not vary rapidly with the field for the fields used in these experiments. The first column lists the transitions. The second column lists the corresponding frequencies of the lines at a field of 3060 gauss. Column 3 lists the frequencies of the single lines and the mean frequencies of the double lines. The sum of the frequencies in this column yields $\Delta\nu$. The fourth column lists $\nu/\Delta\nu$ calculated from the

TABLE III. *The frequencies observed for the lines $\Delta m_i=\pm1$, $\Delta m_J=0$ for K^{39} at a field of 3950 gauss and the $\Delta\nu$ calculated from these lines. In the third column, marked ν', are tabulated the frequencies of the single lines and the mean frequencies of the double lines. The sum of the frequencies in this column is equal to $\Delta\nu$. The quantity $\nu/\Delta\nu$ tabulated in the fourth column is that appropriate to the mean frequencies of the double lines.*

TRANSITION	ν OBSERVED FREQUENCY (MEGACYCLES)	ν' (MEGACYCLES)	$\nu/\Delta\nu$	$\Delta\nu$ (MEGACYCLES)
$(2,-2)\leftrightarrow(1,-1)$	119.904	119.904		
$(1,0)\leftrightarrow(1,-1)$	117.347	116.562	0.252439	461.74
$(2,0)\leftrightarrow(2,-1)$	115.776			
$(1,1)\leftrightarrow(1,0)$	114.961	114.167	0.247235	461.78
$(2,1)\leftrightarrow(2,0)$	113.374			
$(2,2)\leftrightarrow(2,1)$	111.115	111.115		
	Sum 461.75			

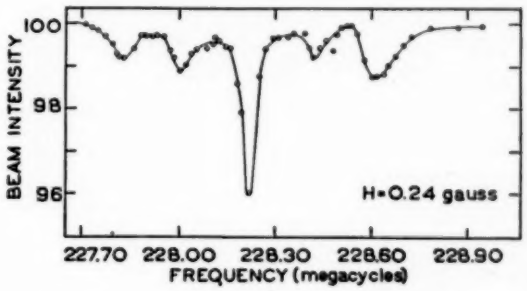

FIG. 12. The Zeeman pattern of the line, $|\Delta F|=1$, of Li^6.

expressions listed in Table I, while the fifth column gives $\Delta\nu$ as obtained from columns 2 and 4. A similar set of data is given in the last four columns of the table. For this latter set of observations the field did not remain constant. This drift in field occurred because of the rather long time required to observe the shape of the resonance line as well as to find its frequency.

A number of sets of observations similar to those given in Table V was made. In addition observations were made on the lines $(1,0)\leftrightarrow(1,-1)$ and $(2,0)\leftrightarrow(2,-1)$ in the neighborhood of $x=3.5$ where the frequencies of the lines take on maximum values and therefore do not vary rapidly with H. From all observations we find for $\Delta\nu$ of the ground state of Li^7 the value $(803.54\pm0.04)\times10^6$ sec.$^{-1}$ or 0.026805 cm^{-1}.

The lines tabulated in the second half of Table V are shown in Fig. 13. The average half-width of the lines is 4.7×10^4 sec.$^{-1}$. The temperature of the oven from which the lithium issued was about 1000°K, so that the most probable velocity of the lithium atoms is about 1.7×10^5 cm/sec. By use of Eq. (16) we find that the theoretical width of the lines is about 4.3×10^4

TABLE IV. *Lines in the Zeeman pattern of Li^6, shown in Fig. 12, and their observed frequencies.*

TRANSITIONS	OBSERVED FREQUENCY (MEGACYCLES)
$(\frac{3}{2},-\frac{3}{2})\leftrightarrow(\frac{1}{2},-\frac{1}{2})$	227.83
$(\frac{3}{2},-\frac{1}{2})\leftrightarrow(\frac{1}{2},-\frac{1}{2})$	228.01
$(\frac{3}{2},-\frac{1}{2})\leftrightarrow(\frac{1}{2},\frac{1}{2})$ and $(\frac{3}{2},\frac{1}{2})\leftrightarrow(\frac{1}{2},-\frac{1}{2})$	228.22
$(\frac{3}{2},\frac{1}{2})\leftrightarrow(\frac{1}{2},\frac{1}{2})$	228.43
$(\frac{3}{2},\frac{3}{2})\leftrightarrow(\frac{1}{2},\frac{1}{2})$	228.62

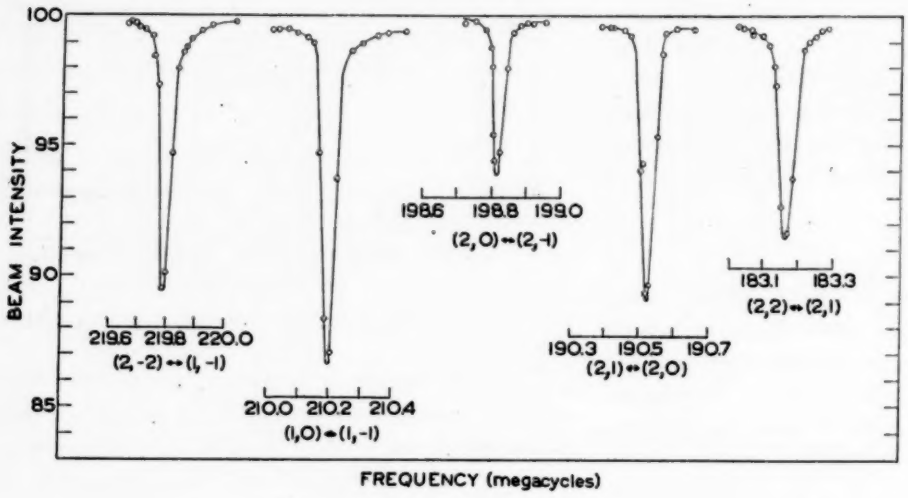

FIG. 13. Contours of the lines in the Paschen-Back spectrum of Li^7 corresponding to Fig. 6.

sec.$^{-1}$. The observed half-widths are thus in agreement with those theoretically expected.

The value of g_i which we obtain for Li^7 is $-2.18/1837$. This value is to be compared to the value $-2.167/1837$ obtained from the molecular beam magnetic resonance method.[1] The agreement is satisfactory in view of the errors in the determination of this quantity by the present method as discussed in the case of K^{39}.

Subsequent to our measurement of the h.f.s. of the ground state of Li^7 by the methods indicated in the preceding paragraphs, Jackson and Kuhn[8] have obtained the value 0.0275 ± 0.0003 cm^{-1} from observations of the splitting of the atomic lines $^2S_{\frac{1}{2}}-{}^2P_{\frac{1}{2}}$ and $^2S_{\frac{1}{2}}-{}^2P_{\frac{3}{2}}$. Their result differs from our value of 0.026805 cm^{-1} by considerably more than their experimental error. It, therefore, seemed worth while to measure the $\Delta\nu$ of the ground state of Li^7 by direct observation of the Zeeman pattern of the line $F \leftrightarrow F-1$ at very low magnetic fields. Such measurements required frequencies in the neighborhood of 800 megacycles, which lie above the upper frequency limit of the Western Electric 316A tube. However, in view of the very small amplitudes of oscillating field required for this work, we attempted to utilize the second harmonic of an oscillator whose fundamental frequency range was in the neighborhood of 400 megacycles. We were able to observe the π components, but because of the small amplitudes of the oscillating field which induced the transitions, the σ lines

[8] D. A. Jackson and H. Kuhn, Proc. Roy. Soc. **A173**, 278 (1939).

TABLE V. *The lines resulting from the transitions $\Delta m_i = \pm 1$, $\Delta m_J = 0$ for Li^7 at high magnetic fields and the $\Delta\nu$ calculated from these lines. The columns marked ν contain the observed frequencies in megacycles. The column headed ν' lists the frequencies of the single lines and the mean frequencies of the double lines. The sum of these frequencies is equal to $\Delta\nu$. All observations recorded in the left-hand side of the table were made at a field of 3060 gauss. The lines on the right-hand side of the table are shown in Fig. 13, and were observed at the indicated fields.*

TRANSITION	ν MC	ν' MC	$\nu/\Delta\nu$	$\Delta\nu$ MC	ν MC	H GAUSS	$\nu/\Delta\nu$	$\Delta\nu$ MC
(2, 2) ↔ (2, 1)	182.38	182.38	0.226937	803.46	183.18	3455	0.227985	803.46
(2, 1) ↔ (2, 0)	190.51	195.58	0.237075	803.58	190.52	3450	0.237087	803.58
(1, 1) ↔ (1, 0)	200.65		0.248666	803.58				
(2, 0) ↔ (2, −1)	199.78	204.87	0.249693	803.42	198.82	3440	0.247388	803.66
(1, 0) ↔ (1, −1)	209.96		0.261284	803.56	210.19	3420	0.261572	803.58
(2, −2) ↔ (1, −1)	220.72	220.72	0.274705	803.66	219.79	3410	0.273570	803.42
	Sum 803.55		Mean 803.54				Mean 803.54	

were not observed. Fig. 14 shows the Zeeman pattern of the line $F \leftrightarrow F-1$ at a field of 0.15 gauss. The frequencies of the observed lines are tabulated in Table VI. The average half-width of the lines is 5×10^4 sec.$^{-1}$ in agreement with the theoretical expectations. The value for $\Delta\nu$ of Li^7 which we obtain from a number of sets of observations similar to that of Fig. 14 and Table VI is $(803.54\pm0.03)\times10^6$ sec.$^{-1}$ or 0.026805 cm^{-1}. The result is in excellent agreement with that obtained from observations at high field.

From the measured values of the $\Delta\nu$ of Li^6 and Li^7 we obtain for the ratio $(\Delta\nu)_7/(\Delta\nu)_6$ the value 3.5209. Using the expression for the ratio of the nuclear magnetic moments of two isotopes of the same element, we obtain:

$$\frac{\mu_7}{\mu_6}=\frac{(2i/2i+1)_7}{(2i/2i+1)_6}\frac{(\Delta\nu)_7}{(\Delta\nu)_6}=3.9610\pm0.0004. \quad (17)$$

This is to be compared with the moment ratio of 3.963 ± 0.004 obtained from the direct moment measurements by the molecular beam magnetic resonance method.

In view of the accuracy with which the ratio of the $\Delta\nu$'s was determined with the present methods it was decided to improve the directly measured moment ratio. Accordingly resonance curves of Li^6 and Li^7 were obtained in LiCl by keeping the homogeneous field fixed and varying the oscillating frequency. The ratio of the g values of the two nuclei is given directly by the ratio of the frequencies at which the minima occurred. No knowledge of the field is required. In the earlier experiments the frequency remained fixed and resonance minima were observed by varying the current in the exciting coils of the homogeneous magnet. Since the value of the magnetic field depends not only upon the current in the coils but also on the previous history of the magnet it was found that errors due to nonreproducibility of the field were of the order of 0.1 percent. The results obtained with the improved procudure give for the ratio μ_7/μ_6 the value 3.9601 ± 0.0015.

Comparison with Previous Measurements

These results are, in the main, in excellent agreement with the results of hyperfine structure measurements by spectroscopic and atomic beam methods, which have previously been made on the same atoms. Since the present results are of far greater precision they can serve as a criterion of the spectroscopic and atomic beam methods. It appears that the precision of these experimental methods was sometimes overestimated. In the case of K^{39}, the present results agree with those of Jackson and Kuhn[9] and of Meissner and Luft[10] who used spectroscopic methods, and with the results of Millman[11] and of Fox and Rabi[12] who worked with the atomic beam methods of zero moments. Our result for the $\Delta\nu$ of K^{41} is in good agreement with that determined by Manley[13] by atomic beam methods. However, the ratio $(\Delta\nu)_{41}/(\Delta\nu)_{39}$ here obtained is in slight disagreement with his results. The discrepancy falls outside his limits of error which were more stringent for the ratio than for the absolute values.

For Li^7 there exist the h.f.s. measurements by Jackson and Kuhn[8] and the atomic beam measurements of Fox and Rabi.[12] The present result is in agreement with the result of the atomic beam methods, and is lower by some three percent than the value of Jackson and Kuhn.[8] Manley and

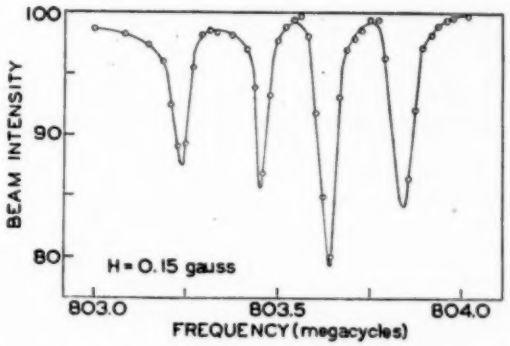

FIG. 14. The Zeeman pattern of the line, $|\Delta F|=1$, of Li^7. A very small amplitude of oscillating field was used, so that the σ-lines do not appear.

Millman[2] measured the ratio $(\Delta\nu)_7/(\Delta\nu)_6$ with atomic beam methods. Their value is lower than ours by about 2 percent.

[9] D. A. Jackson and H. Kuhn, Proc. Roy. Soc. **A165**, 303 (1938).
[10] K. W. Meissner and K. F. Luft, Zeits. f. Physik **106**, 362 (1937).
[11] S. Millman, Phys. Rev. **47**, 739 (1935).
[12] M. Fox and I. I. Rabi, Phys. Rev. **48**, 746 (1935).
[13] J. H. Manley, Phys. Rev. **49**, 921 (1936).

TABLE VI. *Lines in the Zeeman pattern of* Li^7 *shown in Fig. 14 and their observed frequencies.*

TRANSITION	OBSERVED FREQUENCY MEGACYCLES
$(2, -2) \leftrightarrow (1, -1)$	803.22
$(2, -1) \leftrightarrow (1, 0)$ $(2, 0) \leftrightarrow (1, -1)$	803.45
$(2, 1) \leftrightarrow (1, 0)$ $(2, 0) \leftrightarrow (1, 1)$	803.64
$(2, 2) \leftrightarrow (1, 1)$	803.84

DISCUSSION

The measurements of the ratio μ_7/μ_6 show that the ratio of the nuclear moments of the isotopes of lithium derived from h.f.s. measurements is in excellent agreement with the directly measured ratio. Within the limits of experimental error, there is no indication that nonelectromagnetic interactions between the electron spin and the nucleus, if they exist at all, have any measurable effect on atomic energy levels. This result does not preclude the possibility of a spin independent force of the nonelectromagnetic type. Such interactions with the nuclear constituents would not be revealed by these experiments since they would merely cause an equal shift of both h.f.s. levels of a given atomic energy state and would not, therefore, affect the h.f.s. separation of the state.

The precise agreement between the values of the h.f.s. splitting as determined from observations at high and at low magnetic fields shows that the quantum-mechanical expressions for the variation of the energies of the magnetic levels of h.f.s. multiplets in external magnetic fields are accurate to at least one part in 10^4. This is the most searching test to which these expressions have been subjected. As a consequence the procedure may be inverted and the Zeeman effect of the hyperfine structure used as a field measuring device for other purposes, such as the more exact determination of nuclear moments.

As indicated by the results of these experiments, the radiofrequency method applied to the measurement of hyperfine structure is capable of greater precision than other known methods. The resolution, or the power of distinguishing between very close levels, as here exhibited appears to represent an advance by a factor greater than 10^4. This is shown by the ease with which a well-resolved Zeeman pattern is obtained in fields as low as 0.05 gauss. It should be possible to increase the precision of frequency measurements even further by a more refined high frequency technique. These methods should be applicable to the study of nuclear quadrupole moments of light atoms which produce only small departures from the interval rule and may, therefore, escape detection by other methods.

This research has been aided by a grant from the Research Corporation.

On the Seasonal and the Atmospheric Temperature Effect in Cosmic Radiation

VICTOR FRANCIS HESS
Fordham University, New York, New York

(Received January 24, 1940)

By analysis of the observations of the cosmic-ray ionization on the Hafelekar (2300 meters above sea level, 48° North geomagnetic lat.) during five years the existence of a seasonal variation with an amplitude of ±0.9 percent has been proved. Reduction of the monthly means to the annual mean temperature diminishes the amplitude of the 12-month wave to one-half without eliminating it. This agrees with Vallarta and Godart's interpretation of the seasonal effect. A very marked seasonal change in the temperature coefficient of the cosmic radiation has been found, recurring every year. In winter the coefficients are about −0.12, in summer −0.055 percent per degree centigrade. The correlation between temperature and ionization is in winter twice as great as in summer. Derivation of the temperature coefficient from hourly observations gives too low absolute values because of the diurnal changes involved. With unscreened ionization chambers and also with coincidence counter arrangements (triangle position), smaller temperature coefficients are found, which become positive in summer. It is thus not possible to explain the normal negative temperature effect of cosmic radiation completely on the basis of the mesotron disintegration hypothesis.

DURING the Symposium on Cosmic Rays in Chicago (June, 1939) I reported on some difficulties which arise with Blackett's otherwise so attractive interpretation of the atmospheric temperature effect on cosmic-ray intensity based on the mesotron disintegration hypothesis.[1] Meanwhile I have received additional experimental data through the courtesy of Fr. F. X. Roser (Rio de Janeiro), who sent me his thesis which had been worked out in Innsbruck in 1937 and 1938 under my supervision. This thesis contains the full, hitherto unpublished results of our cosmic-ray registrations in the Hafelekar Observatory (Tyrol), 2300 meters above sea level, up to the end of 1937. These data comprise now the fifth year of almost continuous cosmic-ray registration with the Steinke Standard apparatus (1932, 1933, 1934, 1936 and 1937) and enable me to discuss fully the whole complex of questions connected with the temperature effect on cosmic-ray intensity, using also results of other observations with apparatus of the same type with and without complete screening and observations with Geiger-Müller counters, published elsewhere by several of my collaborators.[2]

It is especially noteworthy that a qualitative interpretation of the temperature (air mass) effect is possible without resorting to the hypothesis of mesotron disintegration. I have in fact freely made use of such an explanation in our first publications on the temperature effect,[3] where the existence of this effect was proved beyond doubt.

The interpretation given at that time was to ascribe the increase of cosmic-ray ionization at lower temperatures (after correcting all values to standard pressure) to an enhanced scattering in the lowest part of the atmosphere, due to the increased density of air therein. It was, of course, not feasible to attempt a quantitative discussion of such an effect at that time, since I had no information on the mass distribution of air above the apparatus except that given by the air temperature near the ground.

I. THE SEASONAL EFFECT

The seasonal variation of cosmic-ray intensity (about 2 percent in the course of the year) is now a well-established fact,[4] and recent findings of W. P. Jesse[5] seem to indicate a seasonal variation of even greater range (10 percent) for the rays

[1] V. F. Hess, Rev. Mod. Phys. **11**, 153 (1939).
[2] J. A. Priebsch and H. Kramer, Anzeig. Wien, Akad. d. Wiss., Jan. 14, 1937; A. Demmelmair, Wien. Sitz. Ber. Akad. d. Wiss., **146**, 643 (1937); J. A. Priebsch and W. Baldauf, Wien. Sitz. Ber. Akad. d. Wiss. **145**, 583 (1936).
[3] V. F. Hess and R. Steinmaurer, Berlin. Sitz. Ber. **15**, 521 (1933); V. F. Hess, H. Graziadei and R. Steinmaurer, Wien. Sitz. Ber. **143**, 313 (1934).
[4] See V. F. Hess, H. Graziadei and R. Steinmaurer reference 3.
[5] W. P. Jesse, Rev. Mod. Phys. **11**, 167 (1939).

entering the higher parts of the stratosphere. For the lower parts of the atmosphere it is very difficult to state definitely whether the seasonal variations are entirely or partly due to the atmospheric temperature effect; what we know with certainty is only the existence of a rather close negative correlation between temperature near the ground and ray intensity. The correct way of finding out more about the existence of a real nonthermal seasonal effect of the cosmic rays is to analyze the magnitude of the temperature effect for shorter periods of, for instance, from one to three months and to compare the results with those obtained from analysis of observational data of one or more years. This was attempted by two of my co-workers[6] who found, using exact statistical methods (method of multiple correlation), that in 25 series of data consisting of the daily mean values of cosmic-ray intensity for one or two months the temperature coefficients from these shorter periods did *not* differ essentially from those derived from a whole year. This would indicate that on the Hafelekar, in 2300 meters above sea level, the seasonal variations are mainly due to the temperature effect. This would be in a way contradictory to a true seasonal effect in Jesse's stratosphere observations, but could be explained by assuming that only the softer part of the primary radiation is subject to the large seasonal change which he suspects.

It is very interesting to note that a seasonal effect was also found in the Southern Hemisphere by Schonland, Delatitzky and Gaskell[7] with the minimum cosmic-ray intensity in midsummer (January). It has been shown also by Schonland, Hess and their collaborators that the seasonal variation is greatly reduced but not completely eliminated when all monthly means are corrected for temperature effect.

TABLE I. *Seasonal variation of cosmic-ray intensity, Hafelekar (Tyrol), 2300 m above sea level, 1932 to 1937.*

MONTH	C.R. INTENSITY	C.R. INTENSITY REDUCED TO ANNUAL MEAN TEMPERATURE
I	2769 mI	2757 mI
II	2772 "	2757 "
III	2771 "	2755 "
IV	2764 "	2761 "
V	2728 "	2734 "
VI	2719 "	2731 "
VII	2725 "	2744 "
VIII	2723 "	2739 "
IX	2734 "	2746 "
X	2748 "	2741 "
XI	2756 "	2750 "
XII	2770 "	2761 "

Table I and Fig. 1 show the seasonal variation of cosmic radiation on the Hafelekar in an average taken from five years of observations (1932–1934, 1936, 1937). These data, hitherto unpublished, are all reduced to normal pressure (580 mm Hg, on the Hafelekar). The observations in the first three years were taken with a Steinke ionization chamber (10 atmos. CO_2), shielded with 10 cm lead from all sides. In 1936 and 1937 an additional shield of 7 cm iron was used. The latter data were reduced to 10 cm lead shielding by using a constant factor derived from the comparison of the yearly means with 10 cm Pb alone and with 10 cm Pb plus 7 cm Fe. In the table all values of the cosmic-ray intensity are given in mI (1 mI = 0.001 ion pairs/cc. sec. in air of NPT). These data are shown by the heavy curve in Fig. 1. If all these data are reduced to the same outdoor temperature (annual mean $-1°$ centigrade), using a uniform temperature coefficient of -2.4 mI (-0.9 percent) per degree centigrade, as found in the average from the monthly means of all five years, the seasonal variation is much reduced, but not completely eliminated. This can be seen from Fig. 1, where the thin line is the temperature corrected curve.

The experimental curve (cf. Fig. 1, heavy curve) shows a rather abrupt change from winter to summer while the increase from summer to late fall is more gradual. W. P. Jesse has also noticed a rather sudden change from April to May in his measurements in the stratosphere.

The amplitude of the uncorrected seasonal variation on the Hafelekar (48.4° North geomagnetic lat.) in the five year average is ± 25 mI or about ± 0.91 percent of the total intensity. The thin curve (with temperature correction) would give an amplitude of only half of this magnitude (± 0.46 percent).

These figures essentially agree very well with the results from other stations where data have

[6] J. A. Priebsch and W. Baldauf, reference 2, p. 594.

[7] B. F. J. Schonland, B. Delatitzky and J. Gaskell, Terr. Mag. **42**, 137 (1937).

been collected for sufficiently long periods (not less than one year) with Compton's model *C* cosmic-ray meters.[8,9] In Cheltenham (Maryland) the amplitude was ±2.15 percent, in Teoloyucan (Mexico), in 2300 meters altitude it was ±0.86 percent, at Christchurch (43.5° S lat.), New Zealand and in Huancayo the amplitudes were much lower, ±0.27 and ±0.15 percent, respectively. Schonland in Capetown (South Africa), 32° geom. lat. S reported an amplitude of ±0.8 percent.

Seasonal changes were also studied on the numerous voyages of Compton and of Millikan and their co-workers on the Pacific Ocean. *It seems that at lower geomagnetic latitudes, the seasonal variations as well as the temperature effect itself become much smaller.* Millikan, Neher and Smith[10] found no seasonal effect on cosmic-ray intensity between Los Angeles (lat. 41° N) down to the Straits of Magellan (42° S) exceeding the normal fluctuations of observations. Between Los Angeles and Vancouver (B.C.), however, an increase of 2 to 3 percent was observed in winter and spring, in accordance with observations at other stations, in latitudes beyond the "knee," as discussed above. In summer and autumn no such change, exceeding 1 percent, was noticeable.

It may be mentioned that it has been shown recently[11] that the seasonal variation of cosmic radiation is also closely correlated with the corresponding regular variations of the horizontal intensity of the earth's magnetic field. In our observations in 1936 to 1937 the correlation coefficient between cosmic-ray ionization and horizontal intensity was -0.752 ± 0.126, while the regression coefficient of this effect turned out to be -0.1 percent of the cosmic-ray ionization per gamma ($1\gamma=10^{-5}$ gauss). The ratio of the relative variation of cosmic-ray ionization I to that of the horizontal force H was here $\Delta I/I : \Delta H/H = -22$. Theoretically it seems that a strong negative correlation of this magnitude cannot be explained,[12] and it is rather probable that the seasonal variations of I and H are not causally related to one another.

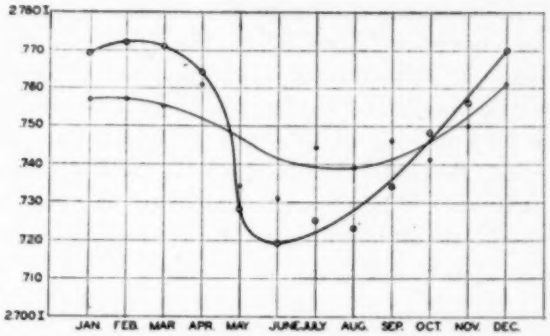

FIG. 1. Five-year mean monthly values of cosmic-ray ionization observed at 2300 m elevation, geomagnetic latitude 48° N. Heavy curve, corrected only to mean barometer. Thin curve, corrected to both mean barometer and mean temperature.

Recently M. S. Vallarta and O. Godart[13] have published the first quantitative theoretical explanation of time variations in cosmic-ray intensity. From this it seems that the solar magnetic field does not account fully for the seasonal variation with a twelve-month period, and that, although a seasonal variation with a six-month wave (maxima in March and September) is predicted by this theory, neither the amplitude nor the phase actually found is in agreement with it. Vallarta and Godart conclude: "It is thus clear that other influences are at work for the seasonal variations in addition to the direct influence of the sun's magnetic field." These influences which also should account for the observed seasonal variations in the lower latitudes are, according to the authors, possible ionospheric influences and the temperature effect. The possibility of ionospheric influences on time variations of cosmic-ray ionization has been brought up six years ago also by other authors.[3]

II. THE TEMPERATURE EFFECT

According to Blackett,[14] the temperature coefficient is

$$\alpha \equiv -\frac{1}{I}\frac{dI}{d\theta} = -\frac{1}{L}\frac{dz}{d\theta},$$

where dz denotes the change in the mean height

[8] S. E. Forbush, Phys. Rev. **54**, 975 (1938).
[9] P. S. Gill, Phys. Rev. **55**, 429 (1939).
[10] R. A. Millikan, H. V. Neher and D. O. Smith, Rev. Mod. Phys. **11**, 167 (1939).
[11] V. F. Hess, A. Demmelmair and R. Steinmaurer, Sitz. Ber. Akad. d. Wiss, Wien **147**, 89 (1938).
[12] T. A. Johnson, Rev. Mod. Phys. **10**, 229 (1938).
[13] M. S. Vallarta and O. Godart, Rev. Mod. Phys. **11**, 180 (1939).
[14] P. M. S. Blackett, Phys. Rev. **54**, 973; Nature **142**, 992 (1938).

of the mesotron-producing layer for a temperature change $d\theta$, and dI is the corresponding change in ionization. L, is the distance traveled by the mesotron during its mean life. Using $L=32$ km, and $dz/d\theta=0.05$ to 0.064 km per degree, Blackett calculates values of α as from -0.16 to -0.20 percent, which are of the observed order of magnitude. More recent measurements[15] have indicated a much lower value for L (8.5 km), but corresponding changes in the estimated value of $dz/d\theta$ leave the calculated value of α not greatly altered. It is noteworthy that Blackett's prediction of a decreased value of α near the equator, arising from a greater value of L appropriate to the higher mean cosmic-ray energies at low latitudes, has been confirmed by the observations of Compton and his collaborators.[16]

The seasonal extremes of the 5-year average ionization at Hafelekar are 2.770 and 2.720 I, corresponding to monthly mean temperature extremes of $-9°$ and $+8°$C. We may thus calculate directly

$$\alpha=\delta I/I\delta\theta=-0.107 \text{ percent per degree,}$$

which differs only slightly from the more rigidly computed value of -0.9 percent per degree given above.

This value is somewhat less than that predicted by Blackett. Compton and Gill[16] find yet smaller values of α in the equatorial zone, which however rises to a maximum of about -0.25 percent per degree at latitudes beyond the knee of the latitude effect curve. The considerably smaller effect present in our data, taken at geomagnetic latitude 48.4° N, cannot be ascribed to the relatively high location of the observatory, since in the neighboring Inn valley, some 1700 m lower, the values of α were essentially the same (-0.11 percent per degree).[17] In light of the finding of Clay and Bruins[18] that at Amsterdam the temperature coefficient is reduced from -0.21 percent per degree to zero as the shield is increased from 12 cm to 110 cm of iron, the relatively small effect which we find may be partly ascribable to our relatively heavy shield. Also the small surface atmospheric temperature changes on the ocean should increase the numerical value of the temperature coefficient as observed by Compton and Gill. Our results are thus not inconsistent with the data of other observers.

When the top shield is removed from the ionization chamber, our earlier studies[19] have shown an entirely different kind of temperature effect, the coefficient becoming positive in the warmer months. The results for 1932 to 1939 for the temperature coefficients on the Hafelekar, (unshielded from above, 10 cm Pb on sides and bottom) are in percent per degree; winter, -0.060, spring, $+0.051$, summer, $+0.057$, autumn $+0.054$. Observations with unscreened Geiger-Müller counters in triangle arrangements made by my collaborators[20] also show the positive effect in summer and negative effect in winter. Thus it appears improbable that the positive effect found with our unshielded chamber is wholly ascribable to the variable radon content of the atmosphere.

A careful analysis of the vast observational material on which the present study is based shows that a somewhat similar seasonal variation of the temperature effect occurs likewise when the ionization chamber is fully shielded. The results of the analysis are summarized in Fig. 2 (for details, see references 2). The coefficients corresponding to each datum point were derived by the method of multiple correlation, taking I, B (barometer), and θ (outdoor temperature) as the three variables, and calculating the correlation and multiple regression coefficients for each month for the five years (except November, 1936, and April, 1937, when the data were unreliable).

It is evident that the general feature of larger coefficients in the cold season and smaller in the summer repeats itself regularly every year. The lower absolute values observed in 1936/37 are due primarily to a difference in the method of calculation. For 1932/34 the temperature coefficients were derived from the *daily* mean values

[15] B. Rossi, H. Van Norman Hilberry and J. Barton Hoag, Phys. Rev. **56**, 837 (1939).
[16] A. H. Compton and P. S. Gill, Rev. Mod. Phys. **11**, 136 (1939); P. S. Gill, Phys. Rev. **55**, 1154 (1939).
[17] R. Steinmaurer, Gerlands Beitr. z. Geophys. **45**, 148 (1935).
[18] J. Clay and E. M. Bruins, Rev. Mod. Phys. **11**, 158 (1939); Physica **6**, 628 (1939).
[19] J. Priebsch and R. Kramer, Anzeig. Wien, Akad. d. Wiss. Jan. 14, 1937.
[20] Dissertations of R. Sommer and of L. Jaeger, University of Innsbruck (unpublished), 1935 and 1936.

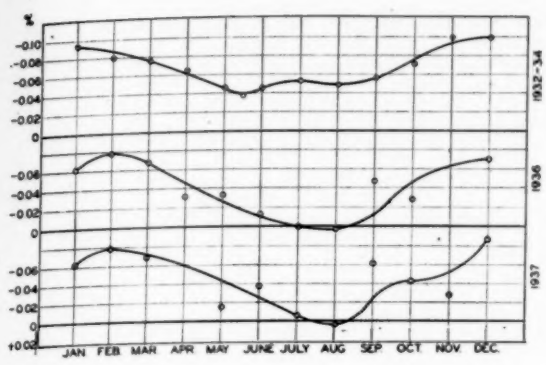

FIG. 2. Monthly values of temperature coefficient of cosmic rays. 1932–34, J. Priebsch and W. Baldauf; 1936, A. Demmelmair; 1937, F. X. Roser.

(reduced to normal pressure), while in 1936/37 the *hourly* values were used. In the latter case the data include the regular diurnal variation of intensity and temperature, both of which reach a maximum shortly after noon. This introduces a positive correlation, and reduces the numerical value of the "real" temperature effect, which is on the whole negative. As has likewise been pointed out by Barnóthy and Forró,[21] it is thus clear that a reliable absolute value of the temperature effect can only be derived from daily mean values or from values for hours when the diurnal temperature change is small. Following Priebsch and Baldauf,[2] therefore, who used the daily mean values for 1932/34, we may consider their values of α of -0.12 percent per degree in winter and -0.055 in summer to be the most reliable.

It is noteworthy that Priebsch-Baldauf and Roser find twice as great correlation between ionization and temperature in winter ($R_{i,t}=-0.044$) as in summer ($R_{i,t}=-0.024$), and at all times a much lower correlation than that between ionization and barometer, which always exceeds -0.8.

If we use the seasonal values of α just given instead of the uniform coefficient from which the thin curve of Fig. 1 was calculated, the residual seasonal changes after the temperature correction has been applied remain just as prominent as with the simpler calculation. It thus seems rather certain that part of the seasonal wave amplitude (± 0.4 percent, as in Fig. 1) is *not* caused by a temperature effect. That is, *if all ionization values are reduced to normal pressure and to annual mean temperature, there remains a marked difference between the cosmic-ray ionization values in winter and in summer; the latter being invariably lower than the former by a difference amounting to about 22 mI (0.8 percent).*

The present study nevertheless confirms previous investigations in ascribing a part of the seasonal effect to temperature changes in the atmosphere. We now have, however, additional and apparently conclusive evidence that *the temperature coefficient varies with the season by a factor of about 2.*

To account for this change in the temperature coefficient on the basis of Blackett's theory would seem to mean that the average height of the mesotron-producing layer likewise changes by a factor of 2, an assumption that would be quite inadmissable. Recently Loughridge and Gast[22] have found changes in cosmic-ray intensity associated with the so-called cold and warm fronts in the atmosphere, from which they estimate changes dz in the height of the mesotron producing layer of from 0.2 to 0.4 km. It may be hoped that such studies will eventually reveal the true nature of the temperature effect of cosmic radiation, which is mainly governed by the mass distribution in the column of air above the point of observation.

Certainly the temperature effect on cosmic-ray intensity is a much more complicated phenomenon than has hitherto been assumed, and existing theories do not account for its varied aspects.

[21] J. Barnóthy and M. Forró, Zeits. f. Physik **104**, 534 (1937).

[22] D. H. Loughridge and Paul Gast, Phys. Rev. **56**, 1169 (1939).

$L\alpha$ Satellite Lines for Elements Mo(42) to Ba(56)

CHARLES A. RANDALL AND LYMAN G. PARRATT
Cornell University, Ithaca, New York

(Received September 9, 1939)

The x-ray satellite lines accompanying the $L\alpha_{1,2}$ emission for elements Mo(42) to Ba(56) have been systematically studied with a two-crystal vacuum spectrometer. Integrated relative intensities of the satellite group agree qualitatively but differ by a factor of about six with previous photographic measurements. The abrupt intensity change at $Z=50$ (the element at which the Coster-Kronig "cross-over" occurs) further confirms qualitatively the Coster-Kronig interpretation of Auger production of the initial state in satellite emission. The observed satellite contour for each element has been resolved arbitrarily into constituent component lines and wave-lengths and relative intensities measured. A few hitherto unreported satellite components are found: Theory predicts fifteen $L\alpha$ satellite components for Au(79), about twice as many as are included in the present analyses for the intermediate atomic numbers. The components farthest removed from the $L\alpha_1$ line seem not to exhibit the abrupt intensity change at $Z=50$ and, therefore, may not be from the $L_{III}M_{IV,V}$ initial state. These components may be Wentzel-Druyvesteyn satellites from another initial state or they may be Richtmyer satellites.

INTRODUCTION

THE Wentzel-Druyvesteyn theory seems to explain satisfactorily the origin of most and perhaps all of the numerous satellite lines in x-ray spectra.[1] Accordingly, satellites arise in radiative transitions between atomic states of double- or multiple-ionization of inner electron shells. A crucial test of the theory is the comparison of the predicted and observed intensities of each of the various groups of satellites. Prior to 1935 the strongest objection to the theory was its apparent failure to account for the curious intensity anomolies for certain ranges of atomic numbers: in particular, for the intensities of the $L\alpha$ and $L\beta_2$ satellites for atomic numbers near $Z=50$ and $Z=75$. In 1935 Coster and Kronig[2] suggested that radiationless transitions share with direct electron (or photon) impact the responsibility for the production of the initial satellite state. The probability of occurrence of the radiationless transitions that produce the doubly-ionized $L_{III}M_{IV,V}$ state was shown to agree sensibly with the observed[3–5] $L\alpha$ and $L\beta_2$ satellite intensities.

As yet, however, only qualitative agreement between the theoretical and experimental satellite intensities has been demonstrated. The assumptions and computations have not yet been refined in quantitative theoretical evaluations; and experimental information of L series satellites has been limited with few exceptions[1, 6, 7] to data obtained with the photographic method and with spectrographs of relatively low resolving power. Illustrative of the uncertainty in measurements of intensity are the following data for Ag(47): Hirsh[4] finds the intensity of the $L\alpha$ satellites to be 15.5 percent of the intensity of the $L\alpha_1$ line; Hirsh and Richtmyer[3] report 33 percent; Parratt,[8] from 6 to 16 percent depending on the choice of background.

The present paper reports systematic measurements of the $L\alpha$ satellites for a range of elements Mo(42) to Ba(56) that includes the Coster-Kronig "cross-over" at $Z=50$. These measurements were obtained from ionization curves recorded with a two-crystal spectrometer of high resolving power. The integrated relative intensities of the satellite group for the various elements agree qualitatively but differ by a factor of about six with the photographic measurements of Hirsh.[4] Also, in the present study, the observed satellite contour for each element has been resolved into constituent component lines and the component wave-lengths and relative intensities measured. Some component lines are found whose relative intensities do not

[1] F. K. Richtmyer, Rev. Mod. Phys. **9**, 391 (1937) and references.
[2] D. Coster and R. de L. Kronig, Physica **2**, 13 (1935).
[3] F. R. Hirsh and F. K. Richtmyer, Phys. Rev. **44**, 955 (1933).
[4] F. R. Hirsh, Phys. Rev. **48**, 722 (1935).
[5] Mrs. A. W. Pearsall, Phys. Rev. **46**, 695 (1934).
[6] L. G. Parratt, Phys. Rev. **54**, 99 (1938).
[7] F. K. Richtmyer and R. Shrader, Science **89**, 398 (1939); Phys. Rev. **55**, 605A (1939).
[8] L. G. Parratt, Phys. Rev. **50**, 598 (1936).

seem to exhibit the Coster-Kronig enhancement as the atomic number is decreased below 50. These components must be members of a different satellite group.

Experimental

The two-crystal vacuum spectrometer used in the present work has been described elsewhere.[6]

The calcite crystals, crystals A_4B_4 as noted in previous studies,[6,9] have again deteriorated, spectrometrically speaking, in the eighteen months since they were last etched. This decrease in degree of crystal perfection, as indicated by the crystal reflectivities, is shown in Table I. The importance of the spectrometric perfection of the crystals lies in the fact that it is our only measure of, or index to, the resolving power of the spectrometer,[9] the vertical divergence of the x-ray beam having been limited to relative unimportance. For purposes of standardization, the data of Table I are given for Mo $K\alpha_1$ radiation, $\lambda = 0.71$A. The decrease in the effective resolving power due to the crystal imperfections indicated in Table I is probably less[9] for the wave-lengths of the present study, 2.8 to 5.4A, than for 0.71A. When we consider, first, that the present $L\alpha$ lines are rather wide (the smallest width, 2.5 x. u., being more than nine times the $d\lambda$ interval of the crystals for the wave-length in question) and, second, that the uncertainty in the satellite background is many times greater than the uncertainties due to finite resolving power, we conclude that the resolving power used in the present satellite study is effectively infinite.

The x-ray tube targets of the various elements were prepared as follows: An 8-mil Mo(42) sheet was spot-welded to a 0.6-mil Ni sheet which was then soft-soldered to the water-cooled copper target carriage. Bits of pure Ru(44) were pressed with a hydraulic press into a roughened Cu sheet which was soft-soldered to the target carriage. Rh(45), Pd(46) and Ag(47) in sheet form, 4 to 10 mils thick, were each soft-soldered directly to the carriage. Cd(48), In(49) and Sn(50) were melted and flowed with rosin flux directly on to the carriage. Sb(51) was electroplated from a hot solution on to a Ni-coated Cu sheet which was soft-soldered to the carriage. Te(52) powder was pressed into a 15-mil sheet of Ag and heated to form a silver telluride. Pure Ba(56) powder, moistened with benzene, was pressed into a 5-mil sheet of Ag and the barium then oxidized by heating in air. The target of I(53) was produced by holding the previously warmed copper carriage in sublimated vapor from gently heated pure iodine crystals. The iodine and barium targets were operated with a power dissipation of 500 watts; the other targets, 600 watts. The focal-spot, fairly uniform in emission, was about 3×7 mm in size.

It has been shown[10] that an x-ray tube voltage of 2 to $2\frac{1}{2}$ times the excitation voltage gives a constant maximum satellite intensity relative to the intensity of the parent $L\alpha_{1,2}$ lines. For each of the elements of the present study the maximum satellite intensity was assured with a tube voltage of 10 kv above the L_{III} excitation voltage. The applied voltage was rectified and filtered, the ripple being about 1 percent.

In the ionization chamber argon gas was used at such pressures that 98 percent of the x-ray beam was absorbed. Since the wave-length of the K-absorption edge of argon, 3.866A, is within the wave-length range of the $L\alpha$ lines of the present study, the argon pressure in the chamber was varied between the limits of 128 cm of Hg (for Cd(48)) and 13 cm of Hg (for In(49)).

Reproduced in Fig. 1 are ionization curves for the $L\alpha$ spectral regions for Rh(45) and for I(53). These two curves are typical of the satellite regions for elements $41 < Z < 51$ and for elements $50 < Z < 57$, respectively.

Throughout the recording of an ionization

Table I. *Reflectivities of etched calcite crystals for* Mo $K\alpha$ *radiation,* $\lambda = 0.71A$.

	1935 Cleavage Surfaces Etched	1937 18 mo. Later Before Re-etching	1937 18 mo. Later After Re-etching	1938 18 mo. Later in Present Work
(1, −1) full width	5.2″	8.0″	5.0″	—
(1, +1) full width	21.0″	27.0″	21.0″	25.1″
(2, −2) full width	1.1″			2.1″
Percent reflection, first order	66.		67.	54.
Percent reflection, second order	49.			29.

[9] L. G. Parratt, Rev. Sci. Inst. **6**, 387 (1935).

[10] D. Coster, H. H. Kuipers and W. J. Huizinga, Physica **2**, 870 (1935).

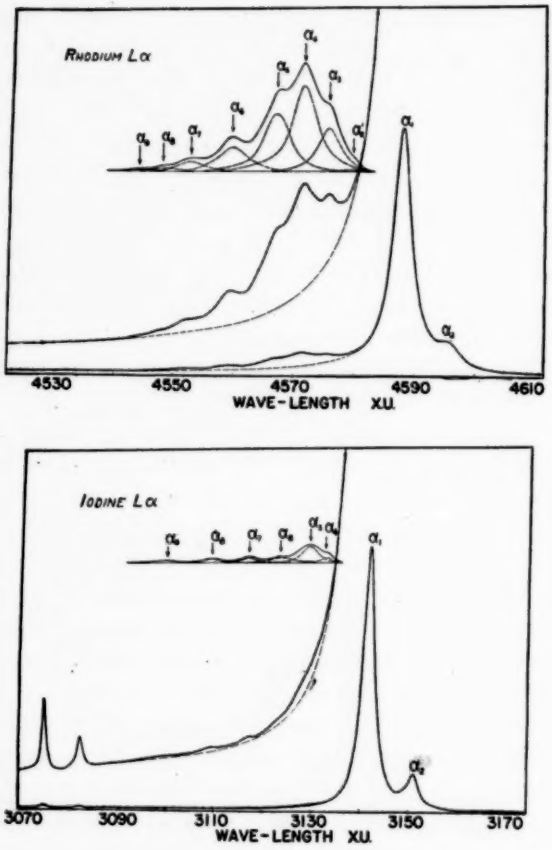

FIG. 1. Ionization curves of the $L\alpha$ regions for Rh(45) and for I(53). The satellite groups are recorded on an intensity scale 8.44 and 28.4 times the scale of the respective $L\alpha_{1,2}$ lines. (In the curve for I(53) the two spurious lines at the left are the Cu$K\alpha_{1,2}$ doublet in second-order reflection.)

curve the tube voltage and current were maintained constant within 1.5 percent by manual control. Before and after each curve was recorded, a time interval of about 4 hours, the maximum ordinate of the $L\alpha_1$ line was measured to detect any uncontrolled intensity change.* The greatest intensity change was for Mo(42), *viz.*, 1.8 percent; for the other elements the intensity change was less than 1 percent.

MEASUREMENTS AND RESULTS

Before we can make any satellite measurements we must resolve the satellites from the parent lines. The overlapping which is illustrated in Fig. 1 is an inherent characteristic of the spectral region and would not have been appreciably less had the resolving power of the spectrometer been infinite. The difficulty of drawing the satellite background has been discussed elsewhere.[8] In the present analyses, the background for each element is the "most reasonable" of many "reasonable" arbitrary curves. The arbitrariness of this choice introduces the greatest uncertainty in the present intensity measurements. The satellite contours, after the background subtractions, are reproduced in Fig. 2. The wave-length scale in x. u. is measured for each contour from the peak of the $L\alpha_1$ line; the intensity scale is arbitrary in each case.

The satellite contours in Fig. 2 are resolved into component lines in the more or less arbitrary manner discussed in a previous paper.[8] The criterion for the existence of a component is that a specific irregularity be observed in the contour and/or that all components be "reasonably" symmetrical. In designating the component satellites we have followed the usual system of

* E.g., any tungsten from the filament condensed on the target results in seriously decreased intensity because of absorption; and, in some cases, a target may melt or pit or its powder gradually disappear.

TABLE II. *Wave-lengths in x. u. of the Lα satellites. The wave-lengths of the $L\alpha_1$ line are taken from the measurements of Hjalmar, Zeits. f. Physik 7, 341 (1921).*

ELEMENT	Z	$L\alpha_1$	α'_2	α_3	α_4	α_5	α'_5	α_6	α_7	α_8	α_9	α'_9
Mo	42	5395.0	5388.8	5383.3	5380.0	5374.8	—	5371.1	5362.9	—	—	—
Ru	44	4835.7	4827.2	4822.8	4817.8	4813.3	—	4804.7	4797.9	—	—	—
Rh	45	4587.8	4579.4	4575.4	4571.1	4566.6	—	4559.1	4552.1	4547.5	4543.4	—
Pd	46	4358.5	4349.7	4347.0	4342.7	4338.1	4334.9	4331.4	4324.0	4319.8	4313.0	—
Ag	47	4145.6	4136.6	4134.7	4131.0	4126.5	4123.6	4119.6	4112.3	4107.8	—	—
Cd	48	3947.8	3939.7	3937.2	3933.8	3929.6	3926.5	3922.9	3917.8	3914.5	3910.0	—
In	49	3763.7	—	3573.7	3750.6	3744.6	3743.9	3739.4	3732.1	3725.1	3720.6	—
Sn	50	3592.2	—	3584.5	3579.7	3575.8	3571.3	3566.2	3561.8	3557.7	—	—
Sb	51	3431.8	—	—	3419.6	3416.2	3413.1	3409.2	3402.2	3397.4	3393.3	3387.2
Te	52	3282.0	—	—	3270.9	3267.7	—	3260.7	3252.6	3248.6	3242.7	3234.7
I	53	3141.7	—	—	3132.4	3129.0	—	3123.5	3116.6	3108.8	3099.3	—
Ba	56	2769.6	—	—	—	2758.0	—	2755.1	2743.2	2736.3	2728.3	2719.8

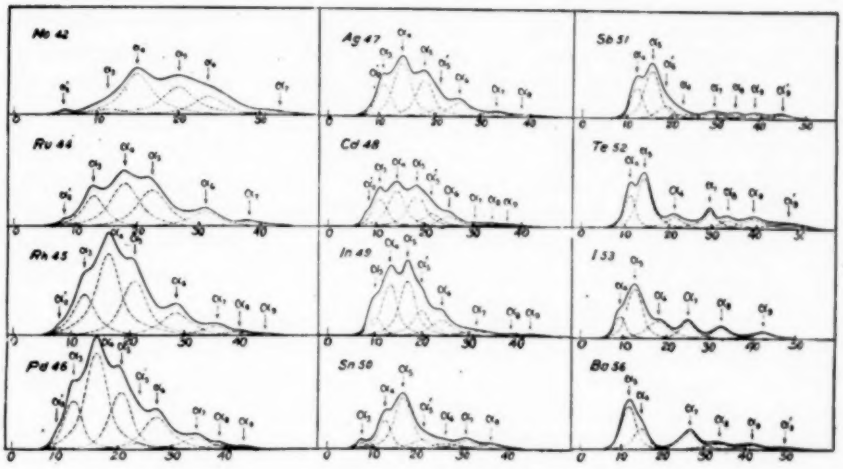

FIG. 2. Contours of the $L\alpha$ satellite groups with backgrounds subtracted. The abscissa scale is in x. u. measured from the $L\alpha_1$ peak; the ordinate scale of each contour is arbitrary.

numeral subscripts and primes. Semi-Moseley graphs are of help in tracing a given component from element to element. These graphs, $(\Delta\nu/R)^{\frac{1}{2}}$ *vs.* Z, where $\Delta\nu$ is measured from the peak of the $L\alpha_1$ line, are shown in Fig. 3. The wave-length positions of the components are listed in Table II.

The integrated intensity of the satellite group relative to the intensity of the $L\alpha_{1,2}$ lines is the ratio of the area contained under the satellite contour divided by the area under the $L\alpha_{1,2}$ lines. Listed in Table III are these integrated relative intensities together with the uncertainties due to the "reasonable" limits in choice of background. These data are shown graphically in Fig. 4. Corrections for differential absorption, reflection coefficients of the crystals, etc., are much less than the above-mentioned uncertainties and so have not been made in these data. Qualitatively the shape of the curve in Fig. 4 agrees well with the curve obtained by Hirsh[4] but the magnitudes of the relative intensities reported by Hirsh are about six times larger for $Z>50$ than those found in the present study.

According to the Wentzel-Druyvesteyn theory, the initial state for $L\alpha$ satellite emission is $L_{\text{III}}M_{\text{IV,V}}$. This state may be produced by any

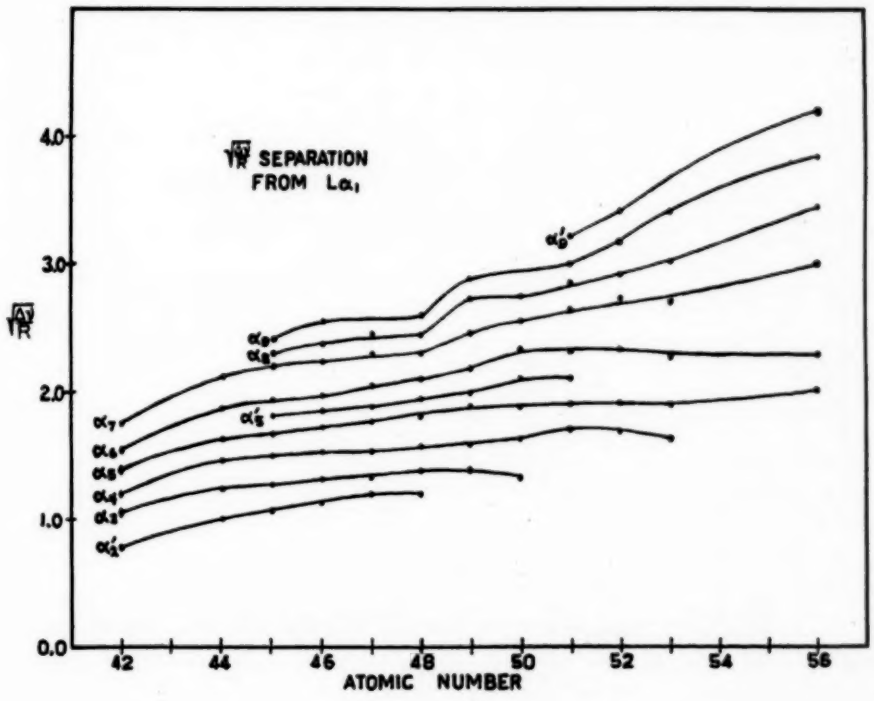

FIG. 3. Semi-Moseley graphs for the component satellites.

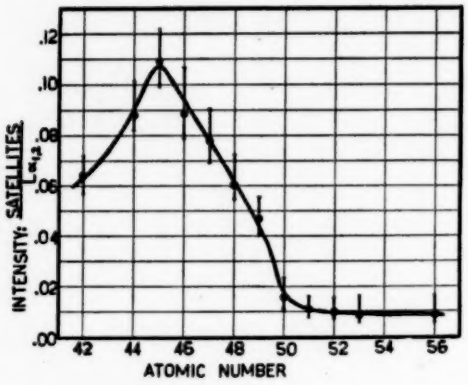

FIG. 4. Integrated intensity of the $L\alpha$ group of satellites relative to the intensity of the $L\alpha_{1,2}$ lines.

one of various methods. For elements $Z<50$ the probability of occurrence of the Auger or radiationless transition $L_{\mathrm{I}}\rightarrow L_{\mathrm{III}}M_{\mathrm{IV,V}}$ is relatively large[11] and is responsible apparently for almost all of the satellite intensity, at least to $Z=42$. The maximum in the curve in Fig. 4 is correlated with the maximum in the Auger probability. For elements $Z>50$ the Auger probability is extremely small and single electron impact is the likely ionizing process.

Figure 5 shows the ratio of the intensity of the various individual satellite components to the intensity of the $L\alpha_{1,2}$ lines. From Figs. 3 and 5 it is evident that α_8, α_9 and α_9', the components farthest removed from the $L\alpha_1$ line, and α_2', the component nearest the $L\alpha_1$ line, seem *not* to exhibit the abrupt intensity change at $Z=50$. These components, therefore, may not arise from the $L_{\mathrm{III}}M_{\mathrm{IV,V}}$ initial state; they may be Wentzel-Druyvesteyn type of satellites from another initial state, or they may be satellites arising from a "double-jump" transition according to

[11] See the Coster-Kronig diagram, Fig. 14 of reference 1.

TABLE III. *Integrated intensity of the $L\alpha$ satellite group relative to the $L\alpha_{1,2}$ lines. The column headed "Uncertainty" contains the respective maximum deviations due to the "reasonable" limits of background choice.*

ELEMENT	ATOM. NO.	RELATIVE INTENSITY OF SATELLITE GROUP	UNCERTAINTY	
Mo	42	0.064	+0.015	−0.010
Ru	44	0.080	+0.020	−0.070
Rh	45	0.109	0.020	0.070
Pd	46	0.089	0.020	0.070
Ag	47	0.078	0.015	0.010
Cd	48	0.060	0.013	0.009
In	49	0.047	0.010	0.007
Sn	50	0.015	0.008	0.006
Sb	51	0.011	0.008	0.004
Te	52	0.010	0.006	0.004
I	53	0.0079	0.006	0.004
Ba	56	0.0091	0.006	0.004

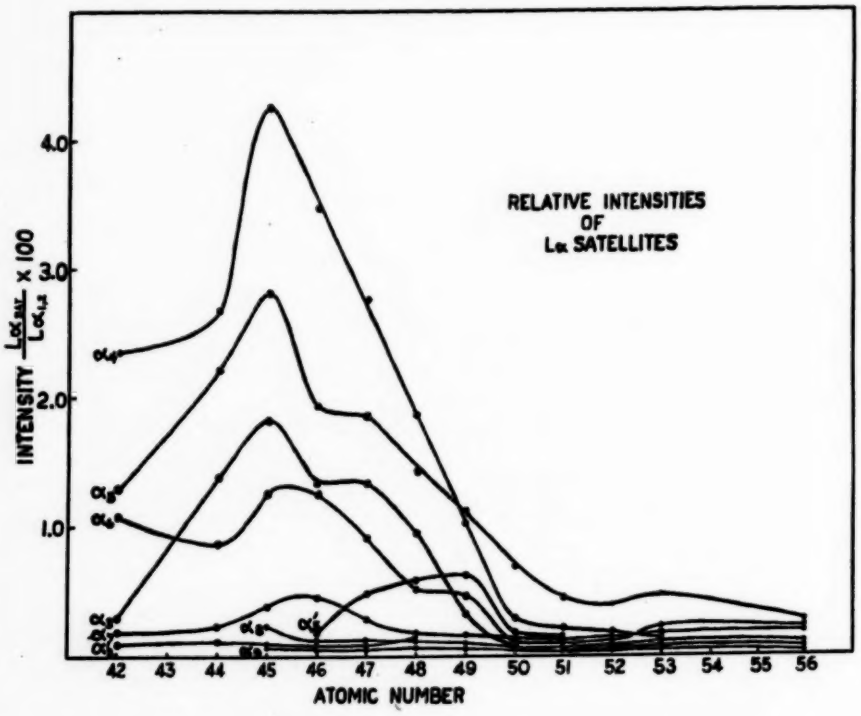

FIG. 5. Intensity of each satellite component relative to the intensity of the $L\alpha_{1,2}$ lines. Components α'_2, α_8, α_9 and α'_9 do not show the Coster-Kronig enhancement of intensity at $Z=50$.

the hypothesis of Richtmyer.[12] The accuracy of the measurements of these weak components is seriously impaired by the uncertainty of the backgrounds and corroborative results would be welcome.

It would be an idle gesture to claim uniqueness for the component resolutions in the present analyses. It is obvious that slightly different resolutions would eliminate most of the deviations from smooth curves in Figs. 3 and 5. Such juggling of the data has not been done because, first, we do not know which values to change, and second, the deviations may have real physical significance because of different atomic forces, e.g., due to chemical binding or crystal structure, in the actual targets of the elements.

[12] F. K. Richtmyer, J. Frank. Inst. **208**, 325 (1929).

MAY 1, 1940 PHYSICAL REVIEW VOLUME 57

Binding Energy of Li⁷ *

K. G. CARROLL†
Sloane Physics Laboratory, Yale University, New Haven, Connecticut
(Received December 26, 1939)

A first-order Hartree calculation based upon a reasonable set of nuclear constants yields only one-third the known binding energy of Li⁷. It is of interest to know whether this discrepancy is a real failure of assumed nuclear forces or merely a result of an inadequate method of calculation. The present note reports the effect of including higher orders in the perturbation treatment. In the final result about half the discrepancy remains and may be attributed to the exchange forces here assumed.

A. INTRODUCTION

IN spite of recent difficulties which the theory of nuclear forces has encountered, initial success has been obtained in explaining the mass defect curve for light nuclei. For nuclei of the two, three, and four-body types, mass defects based upon theory are in rather good agreement with experiment. However, the necessarily large number of arbitrary parameters contained in the nuclear Hamiltonian require for their determination most of the known properties of these nuclei. Application of the theory based on these lightest nuclei to other problems may be hoped to lead to a more satisfactory picture of nuclear forces, capable, among other things, of yielding quantitative information on the energy levels of light nuclei. The present work deals with the binding energy of Li⁷. The Hartree method is improved by the use of Schrödinger perturbation theory, as in former work.[1,2] The information sought is whether the symmetric nuclear Hamiltonian, composed of exchange potentials of the Gauss type, is capable of yielding the correct binding energy for this problem when a more adequate method of calculation than the simple Hartree method is employed. Notation used here will be similar to that in a previous paper on Li⁶.[2]

B. FIRST-ORDER HARTREE CALCULATION

The interaction between a pair of nuclear particles is taken as

$$V_{ij}=-A\exp\left[-r_{ij}^2/a^2\right]\times(w+mP_{ij}+bQ_{ij}+hP_{ij}Q_{ij}). \quad (1)$$

For Li⁷ the ground state ($^2P_{3/2}$) in the Hartree approximation is a linear combination of the six harmonic oscillator functions belonging to the configuration $(1s)^4(2p)^3$. The ^2P state for two neutrons and one proton is a combination of

* Part of a dissertation presented to the Faculty of the Graduate School of Yale University in candidacy for the degree of Doctor of Philosophy.

† Now at North Carolina State College, Raleigh, North Carolina.

[1] D. R. Inglis, Phys. Rev. **51**, 531 (1937).

[2] H. Margenau and K. G. Carroll, Phys. Rev. **54**, 705 (1938).

TABLE I. *First-order calculation of the binding energy as a function of σ, for various sets of nuclear constants. $-H_{00}$ (Mev).*

$\sigma=$	0.8	0.9	1.0	1.1	1.2	1.3	1.4
(a)	9.75	10.75	11.48	11.93	12.13	12.08	11.79
(b)	8.50	9.36	9.94	10.26	10.33	10.16	9.76
(c)	5.98	6.45	6.59	6.41	5.91	5.12	4.05

neutron and proton terms which may be written

$$a(^1S^2P)+b(^1D^2P),$$

the first term referring to the neutrons, the second to the protons. The coefficients a and b can be determined by minimizing the Hamiltonian. In the present work they have been chosen so that the coordinate part of the ground state function becomes symmetrical. This has little effect upon the energy but simplifies higher order calculations. Numerically, $a=\frac{1}{3}\sqrt{5}$, $b=\frac{2}{3}$. In accordance with the Pauli principle the ground state function is antisymmetrized by writing each term in determinantal form. Oscillator functions of the individual particles all contain the spread parameter σ; $\sigma^{-\frac{1}{2}}$ is a measure of the size of the nucleus. It is determined by minimizing the total energy of the system.

Many restrictions on the force parameters w, m, b, and h arise from the saturation requirements of heavy nuclei.[3] Of these the most restrictive are the inequalities of Kemmer, and of Breit and Feenberg:

$$\begin{aligned} m+h-2w-2b&\geq 0,\\ m+2h-4w-2b&\geq 0. \end{aligned} \qquad (2)$$

Former calculations have shown that maximum binding energy is obtained by taking the equality signs in (2). When this is done all the force parameters may be expressed in terms of the single quantity $g=b+h$, which measures the relative strength of spin-dependent forces. First-order (Hartree) calculation then gives

$$H_{00}=6T\sigma-A(\sigma u)^{\frac{1}{2}}(1-g)(9+3u+11u^2)+1.43\sigma^{\frac{1}{2}},$$

where

$$T=\hbar^2/Ma^2, \quad u=1/(\sigma+2). \qquad (3)$$

The terms are, respectively, kinetic, potential, and Coulomb energies, the last of which may be neglected in higher orders.

Table I lists the numerical results in this approximation with the following three sets of nuclear constants:

Choice (a)
$A=35.6$ Mev, $a=2.25\times10^{-13}$ cm, $g=0.20$,
Choice (b)
$A=35.6$ Mev, $a=2.25\times10^{-13}$ cm, $g=0.22$,
Choice (c)
$A=43.7$ Mev, $a=1.93\times10^{-13}$ cm, $g=0.22$.

Choice (a), as in previous work on Li^6, gives maximum stability to the nucleus, and is in close agreement with experimental mass defects in H^2, H^3, and He^4.[4] Choice (c) includes the shorter range and greater depth of interaction recently suggested by Breit, Thaxton and Eisenbud on the basis of their analysis of proton-proton scattering data.[5]

It is seen from Table I that a slight increase in relative magnitude of spin-dependent forces (from $g=0.20$ to 0.22) reduces the binding considerably without, however, changing the size of the nucleus (value of σ at minimum of H_{00}). If, in addition, the range is decreased and the depth increased, as in choice (c), the first-order energy is nearly halved and the nucleus somewhat enlarged. In view of the experimental binding energy for Li^7(39 Mev) it is apparent that the simple Hartree representation of the ground state is here inadequate, as it is for other nuclei containing particles outside the closed s shell of He^4. In the next section the corrections to the Hartree result will be considered.

A much more flexible trial wave function for the ground state can be constructed from that used above by introducing a separate spread parameter, λ, in the orbitals of the p particles. Then the process of minimizing the first-order energy with respect to the variation parameters σ and λ allows the formation of separate orbits for s particles in the alpha-group and the three p particles outside that group. This is equivalent to using a trial wave function which recognizes

[3] These have been collected and summarized; cf. G. Breit and E. Wigner, Phys. Rev. **53**, 998 (1938).

[4] H. Margenau and D. T. Warren, Phys. Rev. **52**, 790 (1937); D. T. Warren and H. Margenau, Phys. Rev. **52**, 1027 (1937); H. Margenau and W. A. Tyrrell, Phys. Rev. **54**, 422 (1938).

[5] G. Breit, H. M. Thaxton and L. Eisenbud, Phys. Rev. **55**, 603 (A) (1939).

the shell structure evidenced in light nuclei. One might expect that, at the minimum, λ would be less than σ, indicating as in atoms that the natural orbits of the p particles are larger than those of the s particles. Exclusive of a small Coulomb energy term, this improved Hartree calculation yields

$$H_{00}=(3/14)T(12\sigma+15\lambda)+(3/7)TF_1 -A(1-g)\left[6\left(\frac{\sigma}{\sigma+2}\right)^{\frac{1}{2}} +\left(\frac{\lambda}{\lambda+2}\right)^{\frac{1}{2}}\frac{3\lambda^2+6\lambda+11}{(\lambda+2)^2}+9F_2\right], \quad (4)$$

where $F_1=16\sigma(\sigma\lambda)^{5/2}/(\sigma+\lambda)^5$,

$$F_2=32\lambda(\sigma\lambda)^{\frac{1}{2}}[(\sigma+\lambda+2)^2-4]^{-5/2}.$$

For any choice of nuclear constants Eq. (4) gives a substantial improvement in binding energy over the previous one-parameter Hartree calculation. However, the energy surface as a function of σ and λ shows no minimum, having its lowest value at $\lambda=0$. This indicates repulsion at all distances of the p particles by the tightly bound alpha-group. Hence with this type of function stability of Li^7 is not to be attained, because of the saturation character of exchange forces.

Unfortunately higher order calculations are not feasible when both spread parameters are retained. In the work which follows only one parameter is employed in the oscillator functions, the shell structure in the Hartree function being sacrificed to gain mathematical simplification. The one-parameter set of harmonic oscillator functions has the desirable properties of orthogonality and completeness.

C. Higher Orders of Perturbation Calculation

States which combine with the normal state fall into classes of even excitation, i.e., doubly, quadruply, etc., excited states. These "excited" functions form, along with that of the ground state employed above, a complete set of functions. Inclusion of higher functions in the ground state energy calculation produces a further lowering of that state, and, in the limit, must yield the correct energy for the problem, quite independent of the poorness of the initial Hartree approximation. In this problem perturbation treatment has been used to determine the effect of higher states. Details of the calculation need not be repeated here (see reference 2).

In Table II are listed all the doubly-excited configurations of Li^7 which combine with the ground state. Their contributions to the energy of the ground level in second order are tabulated for values of σ near the energy minimum, under two extreme choices of nuclear constants. It is to be noted that the second-order contribution of this one lowest lying group of states is of the same order of magnitude as the first-order Hartree result. At this stage of the calculation a convergence limit is completely out of sight. Two aspects of convergence must be investigated before any definite conclusions may be formed: (1) the total second-order contribution of the quadruply, sextuply, etc., excited states, and (2) the relative magnitudes of higher orders in perturbation theory, if, indeed, they converge.

In regard to the first of these, it is possible to secure a fairly good bound to the combined effect in second order of all excited states. Since all functions of a given excitation have the same unperturbed (harmonic oscillator) energies, the second-order perturbation energy of the ground state may be written

$$E_0^{(2)}=\sum_i{}'\frac{H_{0i}^2}{E_0^0-E_i^0} =\frac{S_2}{E_0^0-E_2^0}+\cdots+\frac{S_n}{E_0^0-E_n^0}+G_n,$$

where $S_n=\sum_i H_{0i}^2$, the summation extending

TABLE II. *Second-order perturbation contributions from doubly excited states.* $-E_D^{(2)}$ *(Mev).*

Configuration	No. of Functions	Choice (a) $\sigma=1.0$	Choice (a) $\sigma=1.2$	Choice (c) $\sigma=1.0$
$(1s)^4(2s)^2 2p$	3			
$(1s)^4(3d)^2 2p$	36	0.47	0.39	0.43
$(1s)^4(2p)^2 3p$	18	0.03	0.16	0.20
$(1s)^2(2p)^2 2s$	54	0.88	0.81	0.79
$(1s)^2(2p)^2 3d$	149	6.17	6.47	6.46
$(1s)^4(2p)^2 4f$	27	0.29	0.22	0.25
$(1s)^2(2p)^5$	54	3.01	3.13	3.22
Totals	341	10.85	11.18	11.35
$-H_{00}$		11.48	12.13	6.59
$-H_{00}-E_D^{(2)}$		22.33	23.31	17.94

TABLE III. *Upper bounds to second-order perturbation.*

	$\sigma=1.0$	$\sigma=1.2$
$(V^2)_{00}$	4.447 (mA)^2	5.897 (mA)^2
$(V_{00})^2$	3.872	5.155
S_2	0.389	0.519
$-G_2<$	$\frac{0.186\ (\text{mA})^2}{4T\sigma}$	$\frac{0.223\ (\text{mA})^2}{4T\sigma}$
$-G_2$ (choice a)	5.78 Mev	5.77 Mev
$-G_2$ (choice c)	6.26	

over all states of excitation n. By the multiplication rule for Hermitian matrices

$$(H^2)_{00}=\sum_i H_{0i}^2=(H_{00})^2+S_2+S_4+\cdots+S_n+\cdots.$$

Hence

$$-G_n<\frac{(H^2)_{00}-(H_{00})^2-S_2-S_4\cdots-S_n}{E_0^0-E_{n+2}^0}.$$

Since no kinetic energy terms appear in the H_{0i} beyond doubly excited states, calculation of $(H^2)_{00}$ may be restricted to the potential part, $(V^2)_{00}$, provided, of course, that similar restrictions are placed on $(H_{00})^2$ and S_2. For the present problem, then, a bound is provided for the combined second-order perturbation effect of states above the doubly excited group in the form

$$-G_2<\tfrac{1}{4}T\sigma[(V^2)_{00}-(V_{00})^2-S_2].$$

Only the Majorana term in the potential interaction (1) has been employed in the calculation of $(V^2)_{00}$. It is to be expected that the detailed form of the interaction is of minor importance here, where convergence of the sequence of functions to the true ground state wave function is in question. Added support is given this procedure by a similar calculation for He^5, in which the full interaction (1) was retained.[6] Taking

$$V=-\sum_{i<j}(mA)\exp[-r_{ij}^2/a^2]P_{ij}$$

terms in $(V^2)_{00}$ fall into classes involving the coordinates of two, three, and four particles. Integrals of the three-particle type give cumbersome expressions containing the parameter σ, necessitating a numerical evaluation of $(V^2)_{00}$ for each value of σ. Table III summarizes the calculations. Numerical values of G_2 have been obtained by adjusting (mA), the "equivalent depth" of the Majorana interaction, to produce the same first-order energy as the full interaction (1). Although this procedure is somewhat arbitrary, final bounds are not very sensitive to the exact manner of adjustment. Referring to the last line of Table II, it is seen that the inclusion of the bounds G_2 lowers the ground state energies at most to 28.11, 29.08, and 24.20 Mev. Convergence of the second-order perturbation by excited states is slower under assumption of the shorter range of forces in choice (*c*) of nuclear constants. Under the most favorable assumptions leading to choice (*a*), the binding energy still remains far short of the actual value.

In order to investigate the second aspect of convergence, that of the various orders of perturbation theory, a third-order calculation was made with a selected group of doubly excited functions which were most important in second order. Consideration was restricted to choice (*c*) of constants, since they result in slower convergence than the others. Majorana forces alone were retained for the purpose. Of the configurations $(1s)^2(2p)^3 3d$ and $(1s)^2(2p)^5$ sixty-one functions which in second-order produced nearly half the total lowering (11.35 Mev) of the ground level, were found in third order to raise that level by about 0.6 Mev. Among the noncombining subgroups of these functions the third-order effect was in no case greater than 25 percent of the second order and always of the opposite sign. This result is in harmony with findings in Li^6 where a variational procedure served as a guide to the convergence of orders. In view of the above it appears probable that the ultimate theoretical ground level of Li^7 lies but slightly higher than that given by second-order perturbation theory. General conclusions based upon this and similar work in other light nuclei have recently been given in a letter to the editor of this journal.[7]

The author takes great pleasure in acknowledging the generous assistance and advice of Professor Henry Margenau, under whose guidance this work was done.

[6] W. A. Tyrrell, Phys. Rev. **56**, 250 (1939).

[7] W. A. Tyrrell, K. G. Carroll, and H. Margenau, Phys. Rev. **55**, 790 (1939).

Preliminary Experimental Study of New Diffraction Maxima in X-Ray Photographs*

STANLEY SIEGEL AND W. H. ZACHARIASEN
Ryerson Physical Laboratory, University of Chicago, Chicago, Illinois

(Received February 1, 1940)

A revised theoretical treatment of the diffuse scattering of x-rays by crystals predicts a rapid variation of intensity with scattering angle, thus leading to intensity maxima in specific directions. The new diffraction maxima were observed with a rocksalt crystal and Cu $K\alpha$ radiation. The peak intensities and the half-widths were studied as functions of the direction of incidence. The observations were found to be in general agreement with theory.

IN a recent[1] paper a new intensity expression for the diffuse scattering of coherent x-rays by crystals has been found. According to this theory intensity maxima are to be expected in certain specific directions. The present article describes the results of experiments designed to test the theoretical predictions. These investigations are preliminary to a detailed study of the diffuse scattering which has been begun by one of us (S. S.).

The theory shows that a given intensity maximum becomes sharper and more intense as the directions of incidence approaches a Bragg direction. However, the maximum cannot be directly observed when the Bragg equation is satisfied because of coincidence with the much more intense Bragg maximum. The best condition for observing the new diffraction maximum is accordingly attained when the direction of incidence is made to deviate from the Bragg direction by an amount just sufficient to completely suppress the Bragg scattering.

EXPERIMENTAL PROCEDURE

An x-ray beam from a copper target tube was filtered by nickel foil, passed through a narrow slit (0.04 mm wide, 1 mm high and 30 mm deep) and allowed to fall on the cleavage plane of a stationary rocksalt crystal under a glancing angle of $\theta_B+\Delta$, where θ_B is the Bragg angle for the (200) reflection and Cu $K\alpha$ radiation. The scattered radiation was registered on a photographic plate placed normal to the incident beam. The slit was mounted normal to the plane of incidence and the intensity distribution in this plane near the Bragg scattering angle $2\theta_B$ was obtained from photometer recordings of the photographic plates. The angle was varied in the range from -80 to $+80$ minutes of arc.

In order to obtain a better definition of the orientation of the lattice planes the more heavily warped surface layers of the crystal were removed by etching. With this precaution the distribution function representing the orientation of the

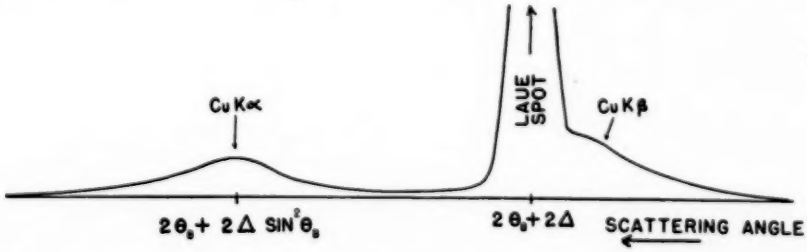

FIG. 1. Photometer tracing showing the intensity maximum due to Cu $K\alpha$ radiation diffusely scattered by a rocksalt crystal. Δ is $-68'$ and the half-width is $29'$. When the crystal is set at the Bragg angle the half-width of the Cu $K\alpha$ line (due to horizontal divergence) is only $1'$. The enhanced intensity maximum due to Cu $K\beta$ is seen close to the Laue spot. The exposure time for this photograph was 10 hours; for the sake of comparison it may be mentioned that the Cu $K\alpha$ line is easily observed after a few seconds exposure when Δ is zero so that Bragg scattering takes place.

* The results given in this article were presented at the Chicago Meeting of the American Physical Society, December 1, 1939.

[1] W. H. Zachariasen, Phys. Rev. **57**, 597 (1940).

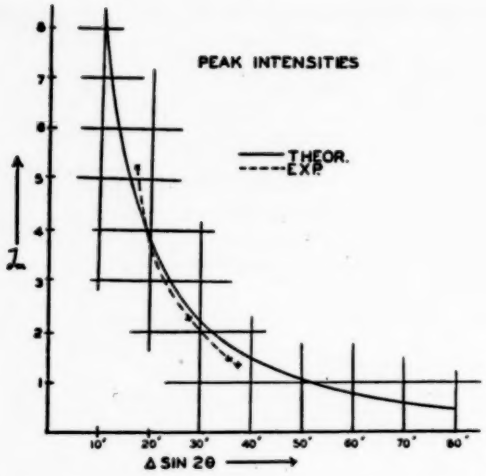

FIG. 2. Variation of peak intensity with $|\Delta|$.

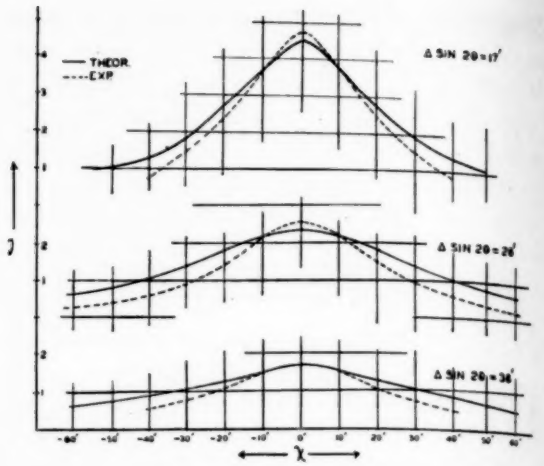

FIG. 3. Shape of the diffraction maximum for different values of $|\Delta|$.

various sections of the lattice planes about the mean normal showed a half-width of about two minutes of arc. But in order to completely get rid of the Bragg reflection of Cu $K\alpha$ in long exposed photographs, it was necessary to make $|\Delta|$ greater than 30′.

The filtered incident radiation naturally was not monochromatic; but the intensity of the continuous radiation was very small in comparison with that of the Cu $K\alpha$ line. In long exposed photographs the continuous radiation did give rise to intense Laue spots, while the diffuse scattering of the continuous radiation could be neglected.

RESULTS

The direction of scattering corresponding to an intensity maximum of the diffuse radiation lies, according to theory, in the plane of incidence with a scattering angle of $2\theta_m = 2\theta_B + 2\Delta \sin^2 \theta_B$. If the incident beam is a narrow pencil the intensity near a maximum is given by the expression

$$J_2 = \frac{K}{(\Delta \sin 2\theta_B)^2 + \chi^2 + \varphi^2}, \qquad (1)$$

where χ and φ measure the angular deviations from the maximum in the plane of incidence and normal to it. As long as Δ, χ and φ remain small quantities, K may be treated as a constant. In our experiments a slit rather than a pinhole was used, so that Eq. (1) cannot be directly applied. Since the intensity measurements were made in the median plane of incidence, Eq. (1) must be integrated with respect to φ, and one finds accordingly

$$J_2 \propto \tan^{-1}(\varphi_m/y)/y; \quad y \equiv [(\Delta \sin 2\theta_B)^2 + \chi^2]^{\frac{1}{2}} \qquad (2)$$

with $\varphi_m = l/2R$. The height of the slit is l and R is the distance from crystal to point of observation. It is seen from Eq. (2) that the half-width of the intensity peak varies from $\Delta \sin 2\theta_B$ for a pinhole to $3^{\frac{1}{2}}\Delta \sin 2\theta_B$ for an infinitely tall slit. The actual value of φ_m was 65′ in our experiments.

Figure 1 shows the photometer tracing of a typical photograph. The observed variation of the peak intensity with $|\Delta|$ agrees well with

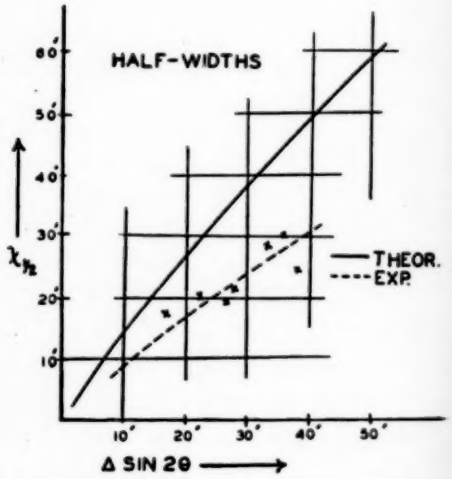

FIG. 4. Variation of half-width with $|\Delta|$.

theory as shown in Fig. 2. Fig. 3 gives the shape of the diffraction maxima. The increasing diffuseness with $|\Delta|$ is well illustrated; but the numerical values for the half-widths are—as Fig. 4 shows—smaller than the theory demands. This discrepancy may be real, but more likely is due to the limited accuracy of our photographic measurements.

More accurate and more extensive measurements, including observations at different temperatures and with different crystals, are of course desirable and are already under way. It may be mentioned that we have observed the new diffraction maxima with calcite crystals and that the maxima show the same general behavior as Δ is varied. Indeed, the theory of diffuse scattering should apply also to perfect crystals since the coupling interaction between incident and scattered radiation is weak when no Bragg scattering takes place.

MAY 1, 1940 PHYSICAL REVIEW VOLUME 57

The Equations of Motion in Electrodynamics

L. INFELD AND P. R. WALLACE
Department of Applied Mathematics, University of Toronto, Canada
(Received December 28, 1939)

A formulation of the equations of motion of singularities in classical electromagnetic theory is obtained. The general method introduced by Einstein, Infeld and Hoffmann leads in a simple way, without any difficulty with "infinities," to the equations of motion obtained before by Dirac. It is shown further that Dirac's introduction of the inertial term into the equations of motion correspond in this method to the assumption of an energy-momentum tensor of matter. The attempt to remove this arbitrary assumption leads in a simple and natural way to the general theory of relativity, in which the equations of motion are obtained from the Einstein-Maxwell field equations.

1. INTRODUCTION

IN Maxwell's theory the motion of charged particles represented as singularities of the field is not determined by the field equations. Dirac[1] has shown that the equations of motion are suggested by the conservation law for the electromagnetic energy-momentum tensor. By virtue of this law, it is demonstrated that the integral representing the flux of energy and momentum over a thin tube surrounding the world-line of a singularity (electron) depends only on the conditions at the ends of the tube. Then the equations of motion are obtained by assuming a simple expression for this flux. However, the integral takes an infinite value as the tube shrinks to the world-line, and Dirac is compelled to remove this difficulty artificially by equating the flux to an expression containing an infinite term and a finite term representing the product of mass and acceleration. This, and the formal complications of the paper, constitute its weak points.

The above procedure leads to familiar equations for the motion of electrons, but whereas these equations were formerly considered to be approximate, Dirac concludes that there is good reason to assume them exact.

The general method of obtaining equations of motion in the theory of relativity introduced by Einstein, Infeld and Hoffmann[2] appears at first sight fundamentally different from that of Dirac. It is shown here, however, that the former method can be adapted to the problem of motion in an electromagnetic field. The method involves only two-dimensional and not three-dimensional surface integrals, avoids the difficulties of "infinities," and leads in a simple manner, without the use of δ-functions, to the results obtained by Dirac. But we believe that the advantage of the

[1] P. A. M. Dirac, Proc. Roy. Soc. **A167**, 148 (1938).

[2] Einstein, Infeld and Hoffmann, Ann. Math. **39**, 65 (1938).

method used in this paper lies not only in the simplification of the derivation of the equations of motion. It gives also a natural transition to the problem of motion of charged particles in the general theory of relativity.

We have tried to formulate the argument in such a way that it may be understood without a knowledge of the quoted papers.

2. The Surface Integrals and the Equations of Motion

Throughout this section we shall use an essentially 3-dimensional notation, Latin letters running from 1 to 3, and repetition of an index implying summation over this range. The notation "$, n$" and "$, o$" will be used to denote ordinary derivatives with respect to the coordinates x^n and time, respectively. The velocity of light is taken as unity throughout.

We write down the conservation laws for the electromagnetic energy-momentum tensor:

$$T_{mn,\,n} = T_{mo,\,o}, \tag{2.1}$$

$$T_{on,\,n} = T_{oo,\,o}, \tag{2.2}$$

where

$$T_{mn} = \text{Maxwell stress tensor} = F_{ms}F_{ns} - F_{mo}F_{no} - \tfrac{1}{4}\delta_{mn}F_{rs}F_{rs} + \tfrac{1}{2}\delta_{mn}F_{so}F_{so}, \tag{2.3}$$

$$T_{on} = \text{Poynting vector} = F_{so}F_{sn}, \tag{2.4}$$

$$T_{oo} = \text{Energy density} = \tfrac{1}{2}F_{so}F_{so} + \tfrac{1}{2}F_{rs}F_{rs}, \tag{2.5}$$

$$\left(\delta_{mn} = \begin{cases} 1 & \text{if } m = n \\ 0 & \text{if } m \neq n \end{cases}\right).$$

$F_{so} = E_s$ and $F_{mn} = \epsilon_{mns}H_s$ where E_s and H_s are the electric and magnetic field, respectively, and ϵ_{mns} is the "permutation symbol" defined in the following manner: $\epsilon_{mns} = 0$ when two of m, n, s are the same, $= 1$ when m, n, s form an even permutation of 1, 2, 3, $= -1$ when m, n, s form an odd permutation of 1, 2, 3.

Equations (2.1) and (2.2) break down only at the point occupied by the singularity, which we assume to be a simple electric pole. Let us surround the singularity with a small sphere, and accept the validity of the equations everywhere outside. Furthermore, let us choose a Lorentz frame of reference in which the singularity is instantaneously at rest at the origin at some moment t. All our calculations will refer to this moment t and to this coordinate system. It is because of this special choice of coordinate system that it is convenient to use throughout the three-dimensional notation.

We introduce now a vector ψ_m and a scalar ψ_o satisfying the equations

$$\Delta\psi_m = -T_{mo,\,o}, \tag{2.6}$$

$$\Delta\psi_o = -T_{oo,\,o}, \tag{2.7}$$

where Δ is the Laplacian operator. Both ψ_m and ψ_o will always exist outside the small sphere if we assume the electromagnetic field to be known, and the T's to be calculated from it. We can therefore write (2.1) and (2.2) in the form

$$(T_{mn} + \psi_{m,\,n})_{,\,n} = 0, \tag{2.8}$$

$$(T_{on} + \psi_{o,\,n})_{,\,n} = 0. \tag{2.9}$$

Assuming that the energy-momentum tensor vanishes rapidly enough at infinity, we obtain from Green's theorem, by virtue of Eqs. (2.8) and (2.9), that the four surface integrals

$$\int (T_{mn} + \psi_{m,\,n})\lambda^n dS, \tag{2.10}$$

$$\int (T_{on} + \psi_{o,\,n})\lambda^n dS, \tag{2.11}$$

(where λ^n are the direction-cosines of the normal to the surface of integration), are independent of the shape and size of the surface chosen, and hence can depend only on quantities characterizing the singularity, in particular the coordinates of the singularity and their time-derivatives. We see from (2.6) and (2.7) that ψ_m and ψ_o are both arbitrary to within a harmonic function. The only solid harmonic function which can give a contribution to the surface integrals is one of the form $f(t)/r$ where $r^2 = x^s x^s$. If we take as the surface of integration a sphere with center at the singularity (the origin) the contribution to the surface integral of a term of this type is $-4\pi f(t)$, i.e., an arbitrary function of t. For

$(f(t)/r)_{,\,n} = -(x^n/r^3)f(t)$, $\lambda^n = x^n/r$, and $dS = r^2 d\omega$,

where $d\omega$ is the element of solid angle subtended at the origin. Hence

$$\int (f(t)/r)_{,\,n}\lambda^n dS = -\int f(t)\,d\omega = -4\pi f(t).$$

It follows, then, that we can give the integrals (2.10) and (2.11) arbitrary values by choosing appropriately the functions $f(t)$.

To assign consistent values to the four integrals means to determine the motion of the singularity, because the integrals depend only on the coordinates of the singularity and their derivatives. We proceed in the following manner: we assume that the integrals are equal to zero—

$$\int (T_{mn}+\psi_{m,n})\lambda^n dS=0, \tag{2.12}$$

$$\int (T_{on}+\psi_{o,n})\lambda^n dS=0, \tag{2.13}$$

and shift the task of determining the motion to the choice of the arbitrary harmonic functions. We could equally well assume any value for the integral, making a corresponding change in the arbitrary harmonic function. Therefore our assumptions (2.12) and (2.13) do not imply any loss of generality.

The apparent anomaly of having four equations where three would appear to determine the motion completely may be met by choosing the arbitrary function in the last equation in such a way that no new restriction is placed on the motion.

We will write

$$\psi_m=\Psi_m-\bar{\psi}_m, \tag{2.14}$$

$$\psi_o=\Psi_o-\bar{\psi}_o, \tag{2.15}$$

where $\bar{\psi}_m$, $\bar{\psi}_o$ are the arbitrary harmonic functions, and Ψ_m, Ψ_o are the solutions of the Poisson equation which do not contain in their development with respect to r an harmonic function of the type $1/r$.

We let the coordinates of the singularity be $\eta^r(t)$, where $\eta^r(t)=0$, $\dot{\eta}^r(t)=0$ in our special coordinate system, at the instant to which our calculations refer. (Dots indicate derivatives with respect to time.) We assume that the field of the singularity is represented by the advanced or retarded potential, and that the external field is superimposed upon this.

We are now prepared to determine the equations of motion by choosing the arbitrary function $\bar{\psi}_m$. Since $\eta^r(t)=0$ and $\dot{\eta}^r(t)=0$ the simplest possible assumption aside from the trivial one which omits this term altogether is

$$\bar{\psi}_m=m_o(\ddot{\eta}^m/r);$$

with this choice the equations of motion (2.12) become

$$m_o\ddot{\eta}^m=-\frac{1}{4\pi}\int (T_{mn}+\Psi_{m,n})\lambda^n dS, \tag{2.16}$$

where the integral on the right-hand side is taken over an arbitrary surface surrounding the singularity.

The form taken by the equations of motion will depend upon the actual field from which T_{mn} is calculated. The usual procedure is to divide the field into two parts, the "external" field (which Dirac calls the "incoming" field) and the field of the singularity, taken as a retarded potential. This procedure is, however, arbitrary. From the formal point of view the solution corresponding to $\frac{1}{2}$ (retarded+advanced) potential, which is known as the "standing wave" solution and which does not specify a privileged direction for the flow of time, is the simplest which can be gained from the use of the "new approximation method."[3] It was this solution which was discussed at the time of Bohr's theory, since it represented an orbital motion without radiation. The addition of radiation seems from this point of view arbitrary, being obtained by superimposing upon the "standing field" a field equal to $\frac{1}{2}$ (retarded-advanced) potential.

The complete calculation of the equations of motion is carried out in Appendix I. If we use the "standing wave" solution for the field of the electron we obtain from (2.16) the equations

$$m_o\ddot{\eta}^m=e_{\text{ext}}\bar{E}_m, \tag{2.17}$$

where ${}_{\text{ext}}\bar{E}_m$ is evaluated at $x^e=0$ and at the moment t.

With regard to the fourth equation (2.13), the contribution from the field is identically zero (Appendix I), and hence the added harmonic function $\bar{\psi}_o$ must be taken equal to zero, since we have laid down the condition that this equation should place no new restriction upon the motion.

Hence the equations of motion formulated by (2.12) and (2.13) and by the choice of the harmonic functions $\bar{\psi}_m=m_o(\ddot{\eta}^m/r)$ and $\bar{\psi}_o=0$

[3] L. Infeld, Phys. Rev. **53**, 836 (1938).

leads through the "standing wave" solution to (2.17) for the special coordinate system in which the equations are formulated.

In the case where we take the retarded potential and leave the harmonic functions as before (2.16) leads to the equations

$$m_o\dot{u}^m = e_{\text{ext}}\bar{E}_m + \tfrac{2}{3}e^2\ddot{u}^m, \tag{2.18}$$

where $u^m = \dot{\eta}^m$; and (2.13) again imposes no new restriction upon the motion.

We wish to remove the restriction imposed by the choice of a particular coordinate-system. This will involve a change to four-dimensional notation. We will consider a four-space with coordinates x^μ. Greek letters will be assumed to take the values 0, 1, 2, 3 where x^o is the time-coordinate and x^1, x^2, x^3 are the space-coordinates, as before. We will assume that the four-space has signature $+---$. The vector v^μ will be defined as the four-dimensional velocity-vector of the electron. Accents will indicate differentiation with respect to arc-length in space-time. Then it may be shown that in the "standing wave" case the equations of motion may be written

$$m_o v'^\mu = e_{\text{ext}}\tilde{F}_\nu{}^\mu v^\nu \tag{2.19}$$

and in the case in which the retarded-potential solution is chosen, they become

$$m_o v'^\mu = e_{\text{ext}}\tilde{F}_\nu{}^\mu v^\nu + \tfrac{2}{3}e^2 v''^\mu + \tfrac{2}{3}e^2 v'^2 v^\mu, \tag{2.20}$$

where ${}_{\text{ext}}\tilde{F}_\nu{}^\mu$ is evaluated at the world-point of the singularity. We can prove this by verifying that these equations reduce to (2.17) and (2.18), respectively, in the particular coordinate system chosen.

In this special coordinate-system in which our calculations have been carried out, since $\dot{\eta}^r = 0$, we have the following values for the components of v^μ and their derivatives:

$$\begin{aligned} &v^o = 1, \quad v'^o = 0, \quad v''^o = \dot{u}^r\dot{u}^r, \\ &v^m = 0, \quad v'^m = \dot{u}^m, \quad v''^m = \ddot{u}^m. \end{aligned} \tag{2.21}$$

Hence

$$v'^2 = v'^o v'^o - v'^m v'^m = -\dot{u}^m\dot{u}^m. \tag{2.22}$$

Now Eqs. (2.19) can be written

$$m_o v'^o = e_{\text{ext}}\tilde{F}_\nu{}^o v^\nu, \quad m_o v'^m = e_{\text{ext}}\tilde{F}_\nu{}^m v^\nu.$$

In our special coordinate-system the first of these is an identity. The second reduces to

$$m_o\dot{u}^m = e_{\text{ext}}\tilde{F}_o{}^m = e_{\text{ext}}\bar{E}_m,$$

which is precisely (2.17).

Consider the additional terms $(\frac{2}{3}e^2 v''^\mu + \frac{2}{3}e^2 v'^2 v^\mu)$ which occur in (2.20). From (2.21) and (2.22) we have:

$$\tfrac{2}{3}e^2 v''^o + \tfrac{2}{3}e^2 v'^2 v^o = \tfrac{2}{3}e^2\dot{u}^r\dot{u}^r - \tfrac{2}{3}e^2\dot{u}^r\dot{u}^r = 0$$

and

$$\tfrac{2}{3}e^2 v''^m + \tfrac{2}{3}e^2 v'^2 v^m = \tfrac{2}{3}e^2\ddot{u}^m;$$

therefore (2.20) is likewise an identity when $\mu = 0$ and it reduces to (2.18) when $\mu = m$.

Hence Eqs. (2.19) and (2.20) are valid in one coordinate-system. Since they are vector equations, it follows that they are valid in all Lorentz coordinate-systems, and therefore give the general form of the equations of motion.

Dirac assumes that (2.20) and not (2.19) represent the rigorous equations of motion. The present discussion tends to show that any choice between them is from the formal point of view arbitrary.

3. The Energy-Tensor of Matter

In order to obtain the equations of motion we have made three fundamental assumptions: (1) A special choice for the arbitrary additive harmonic functions in (2.12) and (2.13). (2) A division of the field into "external" or "incoming" field, and the field of the electron. (3) A special choice for the field of the electron ("standing" or "retarded").

The second and third assumptions cannot be removed, since they are characteristic of the whole structure of electrodynamics. This is not true, however, of the first assumption. We ask how we may generalize our scheme of equations to rid ourselves of this assumption, and obtain a logically simpler though formally more complicated scheme.

We may show first that the assumption (1) corresponds to the choice of an energy-momentum tensor for matter. From Eq. (2.12) we had

$$\int T_{mn}\lambda^n dS + \int \psi_{m,n}\lambda^n dS = 0,$$

where $\psi_m = \Psi_m - \bar{\psi}_m$, $\bar{\psi}_m$ being a harmonic function.

If we define a "mechanical" energy-momentum tensor

$$M_{mn}=-\bar{\psi}_{m,n}-\bar{\psi}_{n,m}+\delta_{mn}\bar{\psi}_{s,s}, \tag{3.1}$$

where $\bar{\psi}_m=m_0\ddot{\eta}^m/r$, then M_{mn} is symmetric in m and n and satisfies the condition

$$M_{mn,n}=0. \tag{3.2}$$

Then $\int M_{mn}\lambda^n dS$ taken over any surface enclosing the singularity is independent of the size or shape of the surface. If a sphere with center at the singularity is again used, it follows immediately that the contribution to the integral of the last two terms of M_{mn} vanishes identically. The first term yields $\int \bar{\psi}_{m,n}\lambda^n dS$, which has the value $-4\pi m_0\ddot{\eta}^m$. Hence (2.12) can now be written

$$\int (E_{mn}+M_{mn})\lambda^n dS=0, \tag{3.3}$$

E_{mn} being $T_{mn}+\Psi_{m,n}+\Psi_{n,m}-\delta_{mn}\Psi_{s,s}$. Furthermore (2.13) may be put into the form

$$\int (E_{on}+M_{on})\lambda^n dS=0 \tag{3.4}$$

if we take $M_{on}=0$, $T_{on}+\Psi_{o,n}=E_{on}$ in the particular coordinate-system employed.

We now prove a lemma:

If we have a set of functions $B_{ab\cdots kl}$, skew-symmetric in the indices k and l, the surface integral

$$\int_{(S)} B_{ab\cdots kl,l}\lambda^k dS$$

taken over an arbitrary closed surface S which may enclose but may not pass through a singularity of the field, vanishes identically.

For let us set

$$B_{ab\cdots 23}=C_1, \quad B_{ab\cdots 31}=C_2, \quad B_{ab\cdots 12}=C_3.$$

Then we can write the integral

$$\int_{(S)} \mathrm{curl}_n\, \mathbf{C}\, dS,$$

which may be transformed by Stokes' theorem into a line integral around the rim of the surface; but since the surface is closed this rim must have zero length, so that the integral vanishes identically.

By virtue of the lemma, we deduce that if the T's satisfy relations of the form

$$E_{mn}+M_{mn}=K_{mnl,l}, \tag{3.5}$$

$$E_{on}+M_{on}=K_{onl,l}, \tag{3.6}$$

where K_{mnl}, K_{onl} are skew-symmetric in the indices n and l, then the equations of motion have the form (3.3) and (3.4). Such relations are therefore sufficient to ensure that the equations of motion have this form.[4]

4. The Equations of Motion of a Charged Particle in General Relativity

The difficulty which still remains is the arbitrariness of the choice of the tensor M_{mn}. We shall show now how this may be removed by an appeal to the general relativity theory.

Let us attempt to derive equations of motion from field equations by a method similar to that used by Einstein and Infeld.[5] We start from the Einstein-Maxwell field equations

$$G_{\mu\nu}+kT_{\mu\nu}=0, \tag{4.1}$$

where $G_{\mu\nu}=R_{\mu\nu}-\frac{1}{2}g_{\mu\nu}R$, $R_{\mu\nu}$ being the Ricci tensor and $T_{\mu\nu}$ the electromagnetic energy-momentum tensor. We shall take $k=1$, as may obviously be done if we choose appropriately the units of mass and charge.

If Eq. (4.1) above be contracted, since $T=0$ it follows that $R=0$, and hence the field equations may be written

$$R_{\mu\nu}+T_{\mu\nu}=0. \tag{4.2}$$

We shall write the fundamental metric tensor of general relativity in the form

$$g_{\mu\nu}=\eta_{\mu\nu}+h_{\mu\nu}, \tag{4.3}$$

where

$$\eta_{\mu\nu}=\eta^{\mu\nu}=\begin{pmatrix}1&0&0&0\\0&-1&0&0\\0&0&-1&0\\0&0&0&-1\end{pmatrix}.$$

We shall make the following assumptions: (i) We neglect nonlinear gravitational terms in $R_{\mu\nu}$. (ii) We neglect gravitational-electromagnetic interactions. The second assumption is equivalent to treating the term $T_{\mu\nu}$ as though the metric tensor of space-time were $\eta_{\mu\nu}$.

[4] Cf. M. H. L. Pryce, Proc. Roy. Soc. **A168**, 302 (1938).
[5] A. Einstein and L. Infeld, Ann. Math. (In print.)

Now Eq. (4.2) are six independent equations in the ten unknowns $h_{\mu\nu}$. Hence we may add to these equations four nontensorial "coordinate conditions" on the $h_{\mu\nu}$. We introduce the quantities

$$\gamma_{\mu\nu}=h_{\mu\nu}-\tfrac{1}{2}\eta_{\mu\nu}\eta^{\rho\sigma}h_{\rho\sigma}. \tag{4.4}$$

The coordinate conditions which will be imposed are

$$\eta^{\nu\rho}\gamma_{\mu\nu,\,\rho}=0. \tag{4.5}$$

With the aid of the assumption (i) and the coordinate conditions, we derive the relation[6]

$$R_{\mu\nu}=\tfrac{1}{2}\Box\gamma_{\mu\nu}, \tag{4.6}$$

where $\Box$ is the d'Alembertian operator

$$\eta^{\rho\sigma}(\partial^2/\partial x^\rho\partial x^\sigma).$$

Hence the field equations become

$$-\Box\gamma_{\mu\nu}=2T_{\mu\nu}. \tag{4.7}$$

We may write these as follows:

$$\begin{aligned}&\text{(a)}\quad \gamma_{mn,\,ss}-\gamma_{mn,\,oo}=2T_{mn},\\ &\text{(b)}\quad \gamma_{on,\,ss}-\gamma_{on,\,oo}=2T_{on},\\ &\text{(c)}\quad \gamma_{oo,\,ss}-\gamma_{oo,\,oo}=2T_{oo},\end{aligned} \tag{4.8}$$

and the coordinate conditions (4.5) may be written:

$$\begin{aligned}&\text{(a)}\quad \gamma_{mn,\,n}-\gamma_{mo,\,o}=0,\\ &\text{(b)}\quad \gamma_{on,\,n}-\gamma_{oo,\,o}=0.\end{aligned} \tag{4.9}$$

Now

$$(\gamma_{mn,\,s}-\gamma_{ms,\,n}),_s=\gamma_{mn,\,ss}-\gamma_{ms,\,ns}=\gamma_{mn,\,ss}-\gamma_{mo,\,no}$$

and

$$(\gamma_{on,\,s}-\gamma_{os,\,n}),_s=\gamma_{on,\,ss}-\gamma_{os,\,ns}=\gamma_{on,\,ss}-\gamma_{oo,\,no},$$

by virtue of the coordinate-conditions (4.9) (a), (4.9) (b), respectively. Hence (4.8) (a) and (4.8) (b) may be written

$$\begin{aligned}&\text{(a)}\quad K_{mns,\,s}=(\gamma_{mn,\,s}-\gamma_{ms,\,n}),_s\\ &\qquad\qquad =2T_{mn}+\gamma_{mn,\,oo}-\gamma_{mo,\,no}.\\ &\text{(b)}\quad K_{ons,\,s}=(\gamma_{on,\,s}-\gamma_{os,\,n}),_s\\ &\qquad\qquad =2T_{on}+\gamma_{on,\,oo}-\gamma_{oo,\,no}.\end{aligned} \tag{4.10}$$

As a consequence of the lemma of §2 we have, since K_{mns}, K_{ons} are skew-symmetric in the indices n and s,

$$\begin{aligned}&\text{(a)}\quad \int K_{mns,\,s}\lambda^n dS=0,\\ &\text{(b)}\quad \int K_{ons,\,s}\lambda^n dS=0,\end{aligned} \tag{4.11}$$

the integrals being over surfaces surrounding the singularity of the field at $\eta^r(x^o)$. Because of the field-equations (4.10) the equations (4.11) lead to

$$\begin{aligned}&\text{(a)}\quad \int(\gamma_{mn,\,oo}-\gamma_{mo,\,no}+2T_{mn})\lambda^n dS=0,\\ &\text{(b)}\quad \int(\gamma_{on,\,oo}-\gamma_{oo,\,no}+2T_{on})\lambda^n dS=0,\end{aligned} \tag{4.12}$$

and we call Eqs. (4.12) the "equations of motion" of the electron. For, as in §3, the integrals are independent of the shape and size of the surface of integration, and so can depend only on quantities characterizing the singularity, in particular the coordinates of the singularity and their time derivatives.

These equations of motion are obtained by virtue of *both* the field equations and the coordinate conditions. In fact, the equations of motion (4.12) are conditions which ensure the consistency of Eqs. (4.8) and (4.9). Or, to formulate it differently, (4.8) and (4.9) can be satisfied only by virtue of the equations of motion. This becomes evident if we attempt to solve the equations completely by means of the "new approximation method."[7]

Thus we see that we are led to "equations of motion" in general relativity theory without any such assumptions as the first one in §3. This is because the general theory of relativity has provided us with an energy tensor of matter, derived from the Ricci tensor $R_{\mu\nu}$.

We may write the solutions of the field equations (4.7) in the form

$$\gamma_{\mu\nu}=\Gamma_{\mu\nu}+\bar{\gamma}_{\mu\nu}, \tag{4.13}$$

where $\Gamma_{\mu\nu}$ are particular solutions of Eqs. (4.8) obtained by a process of direct calculation and

[6] A. S. Eddington, *Mathematical Theory of Relativity* (Cambridge University Press, second edition, 1930), pp. 128–129, (57.4) and (57.5).

[7] This has been done by Mr. P. R. Wallace in a thesis at present in preparation.

$\bar{\gamma}_{\mu\nu}$ are solutions of the corresponding homogeneous set:

$$\Box\bar{\gamma}_{\mu\nu}=0. \tag{4.14}$$

The quantities $\Gamma_{\mu\nu}$ are purely electromagnetic in nature. On the other hand, the $\bar{\gamma}_{\mu\nu}$ may be solved by retarded (or "standing") potentials of the same form as those given for the electromagnetic potentials. In choosing the solution we are guided by the consideration that when the particle is not charged, i.e., when $e=0$, the field must reduce, in the first approximation, to the Newtonian gravitational field. Therefore the $\bar{\gamma}_{\mu\nu}$ represent the gravitational field of a particle of mass m and zero charge.

Neither $\Gamma_{\mu\nu}$ nor $\bar{\gamma}_{\mu\nu}$ will be chosen to satisfy the coordinate conditions separately, but solutions may be obtained such that their sum satisfies them by virtue of the equations of motion.

Because of our simplifying assumptions, involving neglect of nonlinear gravitational terms and electromagnetic-gravitational interactions, we have been able to obtain a "splitting" of the field into gravitational and electromagnetic parts. With these assumptions, the problem demonstrates a formal similarity to that of §3. The field equations (4.10) may be written, as in (3.5) and (3.6), in the form

$$E_{mn}+M_{mn}=K_{mns,s}, \quad E_{on}+M_{on}=K_{ons,s},$$

where K_{mns}, K_{ons} are skew-symmetric in n and s. The $E_{\mu\nu}$ may be considered as arising from the $T_{\mu\nu}$ and the $\Gamma_{\mu\nu}$, and the $M_{\mu\nu}$ as coming from the $\bar{\gamma}_{\mu\nu}$. Then the equations of motion (4.12) take the form of (3.3) and (3.4). But if the problem had been attempted in its most general form, the energy-momentum tensor would have appeared in a form involving electromagnetic-gravitational interactions, and could not have been split in the above manner.

Thus the theory of relativity provides a scheme which includes both the gravitational and electromagnetic fields, whereas before the gravitational field was introduced merely through an arbitrary harmonic function and defined only in a special coordinate system.

The coordinate conditions (4.5) are invariant under a Lorentz transformation, from which it follows that we may, as before, choose a coordinate-system in which the electron is instantaneously at rest at some time t, and carry out the calculation of the surface integrals with reference to this particular coordinate-system and this particular time. The removal of this restriction, once the integrals have been calculated, will be carried out precisely as in §2.

The calculation of the equations of motion from Eqs. (4.12) involves the computation of three types of integrals: (i) those arising from $\Gamma_{\mu\nu}$, (ii) those arising from the $\bar{\gamma}_{\mu\nu}$, (iii) the integrals of T_{mn}, T_{on}. The latter have already been calculated in Appendix I. In Appendix II it is shown that the integrals of type (i) are all zero, while from those of type (ii) there is a contribution of $m_o\ddot{\eta}^m$ to the equation of motion (4.12) (a), and no contribution to (4.12) (b). It follows that the equations of motion of the electron, derived from (4.12) (a), are exactly the same as those derived in §2, and that, as required, (4.12) (b) is an identity, and places no new restriction upon the motion.

We have therefore shown that the equations of motion of an electron in an external field, as deduced under stated assumptions from the general theory of relativity, may have the form either of (2.19) or of (2.20).

The whole problem has concerned the development of the equations of a single electron. The method is easily generalized to deal with the problem of n electrons in an external field. In determining the equations of motion of one of the electrons, one has merely to add to the external field the fields of the other electrons.

Appendix I

All the integrals in these Appendices are evaluated over a sphere with center at the singularity. Only expressions of the order $1/r^2$ in the integrands can give contributions to the integrals, since the integrals of other expressions would necessarily depend on the size of the sphere of integration and must therefore vanish. All integrations then correspond to the spherical surface of integration and to the terms of order $1/r^2$ in the integrands. The final result refers, of course, to an arbitrary surface.

We wish (i) to evaluate $(1/4\pi)\int T_{mn}\lambda^n dS$ and $(1/4\pi)\int T_{on}\lambda^n dS$, and (ii) to show that $\int \Psi_{m,n}\lambda^n dS$ and $\int \Psi_{o,n}\lambda^n dS$ are both zero. For the former, it is necessary to calculate the terms of order $1/r^2$ in T_{mn} and T_{mo}, omitting those which contain u^r which is zero. For the latter, we have to calculate the terms of order $1/r^3$ in T_{mo} and T_{oo}, omitting those which contain u^r more than once. (This may be seen from an examination of (2.6) and (2.7).) Now

$$F_{mn}=\gamma_{m,n}-\gamma_{n,m}+{}_{\text{ext}}F_{mn}, \tag{I.1}$$

$$F_{mo}=\gamma_{m,o}-\gamma_{o,m}+{}_{\text{ext}}F_{mo}, \tag{I.2}$$

where γ_o is the electromagnetic scalar potential and γ_m the vector potential of the field of the electron and ${}_{\text{ext}}F_{\mu\nu}$ is the external field. Since none of F_{mn}, F_{mo} approach infinity faster than $1/r^2$ as r approaches zero, and they appear quadratically in the T's, F_{mn} and F_{mo} influence the first calculation only through terms of order -2, -1 and zero in r.

The solutions for the potentials satisfying Maxwell's equations are:[3]

$$\gamma_o=e\sum_{l=1}^{\infty}\frac{1}{(2l-2)!}\frac{d^{2l-2}}{dt^{2l-2}}(r^{2l-3})-e\sum_{l=1}^{\infty}\frac{1}{(2l-1)!}\frac{d^{2l-1}}{dt^{2l-1}}(r^{2l-2}), \tag{I.3}$$

$$\gamma_m=-e\sum_{l=1}^{\infty}\frac{1}{(2l-2)!}\frac{d^{2l-2}}{dt^{2l-2}}(\gamma^{2l-3}u^m)+e\sum_{l=1}^{\infty}\frac{1}{(2l-1)!}\frac{d^{2l-1}}{dt^{2l-1}}(r^{2l-2}u^m), \tag{I.4}$$

where the first sum in each case represents the solution: ($\frac{1}{2}$ retarded$+\frac{1}{2}$ advanced) potential, i.e., the "standing wave" solution, and the second represents the solution: ($\frac{1}{2}$ retarded$-\frac{1}{2}$ advanced) potential. Therefore the complete expressions represent the retarded potential solutions.

The symbol "$\sim$" will be used to designate the relevant terms of an expression. Also, when an expression is divided into two parts by a comma, the part preceding the comma will be understood to have arisen from the "standing wave" solution alone, while the part following it will represent the terms added when the retarded potential solution is used.

From the above expressions for the potentials we derive, keeping only terms which can influence the calculations (i) or (ii):

$$\gamma_o\sim\frac{e}{r}-\frac{e}{2}\frac{(x^s-\eta^s)}{r}\dot{u}^s+\frac{3e}{8}\frac{(x^l-\eta^l)(x^s-\eta^s)}{r}\dot{u}^l\dot{u}^s+\frac{3e}{8}r\dot{u}^s\dot{u}^s,\ -eu^s\dot{u}^s+\frac{e}{3}(x^s-\eta^s)\ddot{u}^s, \tag{I.5}$$

$$\gamma_m\sim-\frac{e}{r}u^m+\frac{e}{2}\frac{(x^s-\eta^s)}{r}\dot{u}^su^m+\frac{e}{2}\frac{(x^s-\eta^s)}{r}u^s\dot{u}^m-\frac{e}{2}r\ddot{u}^m,\ +e\ddot{u}^m-e(x^s-\eta^s)\dot{u}^s\dot{u}^m. \tag{I.6}$$

We deduce the relevant terms of

$$F_{mo}\sim{}_{\text{ext}}F_{mo}+e\frac{x^m}{r^3}-\frac{e}{2}\frac{1}{r}\dot{u}^m-\frac{e}{2}\frac{x^sx^m}{r^3}\dot{u}^s+\frac{e}{4}\frac{x^s}{r}\dot{u}^su^m-\frac{3e}{8}\frac{x^m}{r}\dot{u}^su^s+\frac{3e}{8}\frac{x^lx^sx^m}{r^3}\dot{u}^l\dot{u}^s,\ +\frac{2}{3}e\ddot{u}^m, \tag{I.7}$$

and

$$F_{mn}\sim{}_{\text{ext}}F_{mn}+e\frac{x^n}{r^3}u^m-e\frac{x^m}{r^3}u^n-\frac{e}{2}\frac{x^sx^n}{r^3}(\dot{u}^su^m+u^s\dot{u}^m)+\frac{e}{2}\frac{x^sx^m}{r^3}(\dot{u}^su^n+u^s\dot{u}^n)-\frac{e}{2}\frac{x^n}{r}\ddot{u}^m+\frac{e}{2}\frac{x^m}{r}\ddot{u}^n,\ +0. \tag{I.8}$$

In these latter expressions we have put $\eta^r=0$ throughout.

Of the expressions occurring in the various integrands, the only ones whose integrals are not zero are those of the form

$$x^{S_1}x^{S_2}\cdots x^{S_p}/r^{p+2},\quad (S_1, S_2, \cdots S_p=1, 2, 3),$$

where p is an odd integer. Hence, so far as the calculation (i) is concerned we may write

$$-T_{mn}\sim e\frac{x^m}{r^3}\,{}_{\rm ext}F_{no}+e\frac{x^n}{r^3}\,{}_{\rm ext}F_{mo}-\delta_{mn}e\frac{x^s}{r^3}\,{}_{\rm ext}F_{so},\quad +\frac{2}{3}e^2\frac{x^m}{r^3}\ddot{u}^n+\frac{2}{3}e^2\frac{x^n}{r^3}\ddot{u}^m-\frac{2}{3}\delta_{mn}e^2\frac{x^s}{r^3}\ddot{u}^s, \tag{I.9}$$

$$T_{on}\sim e\frac{x^s}{r^3}\,{}_{\rm ext}F_{sn}. \tag{I.10}$$

Consequently the integrals arising from (I.9) and (I.10) are $e_{\rm ext}F_{mo}$, $+\frac{2}{3}e^2\ddot{u}^m$, and

$$\frac{1}{4\pi}\int T_{on}\lambda^n dS=e\delta_{mn}\,{}_{\rm ext}\widetilde{F}_{mn}=0,$$

since ${}_{\rm ext}\widetilde{F}_{mn}$ is skew-symmetric.

Let us now consider (ii). The equations satisfied by Ψ_m, Ψ_o are

$$\Delta\Psi_m=-T_{mo,\,o}, \tag{2.6}$$

$$\Delta\Psi_o=-T_{oo,\,o}. \tag{2.7}$$

Using the expressions (I.7) and (I.8) to form $T_{mo,\,o}$ and $T_{oo,\,o}$ and remembering that we are interested only in terms of order $1/r^3$, we have

$$T_{mo,\,o}=(F_{ms}F_{os})_{,o}\sim 2e^2\frac{x^s}{r^4}\dot{u}^s\dot{u}^m-\frac{1}{2}e^2\frac{x^m}{r^4}\dot{u}^s\dot{u}^s-\frac{3}{2}e^2\frac{x^mx^lx^s}{r^6}\dot{u}^l\dot{u}^s,$$

and

$$T_{oo,\,o}=\tfrac{1}{2}(F_{so}F_{so}+F_{rs}F_{rs})_{,o}\sim -e^2\frac{x^s}{r^4}\ddot{u}^s$$

if we omit terms which contain u^r. It follows that all the terms of $\Psi_{\mu,\,n}$ will contain an even number of factors x^s, and hence that their integrals will vanish μ.

Appendix II.

By inspection of the integrals (4.12) we see that only the following types of terms in the $\gamma_{\mu\nu}$ could give nonzero contributions to the integrals: (i) terms of γ_{mn} of order $1/r$ and not containing $\dot{\eta}^s$; or terms of order $1/r^2$, which may contain $\dot{\eta}^s$ at most twice. (ii) terms of γ_{on} of order $1/r$ which contain $\dot{\eta}^s$ once only or not at all; or terms of order $1/r^2$ which may contain $\dot{\eta}^s$ at most twice. (iii) terms of γ_{oo} of order $1/r$, only if they contain a single $\dot{\eta}^s$ or higher derivative of η^s.

Consider first $\Gamma_{\mu\nu}$. The following solutions of (4.8) may be verified, where we include only terms of the above types, and omit also terms whose divergence vanishes identically:

$$\text{(a)}\quad \Gamma_{oo}=\left[\frac{e^2}{r^2}\right]+e^2\frac{(x^s-\eta^s)}{r^2}\ddot{\eta}^s+\cdots,$$

$$\text{(b)}\quad \Gamma_{on}=-\frac{e^2}{r^2}\dot{\eta}^n+e^2\frac{(x^n-\eta^n)}{r^2}\dot{\eta}^s\ddot{\eta}^s+2e^2\frac{(x^r-\eta^r)(x^s-\eta^s)(x^n-\eta^n)}{r^4}\dot{\eta}^m\ddot{\eta}^s+\cdots, \tag{II.1}$$

$$\text{(c)}\quad \Gamma_{mn}=\frac{e^2}{r^2}\dot{\eta}^m\dot{\eta}^n+e^2\frac{(x^m-\eta^m)(x^s-\eta^s)}{r^4}\dot{\eta}^n\dot{\eta}^s+e^2\frac{(x^n-\eta^n)(x^s-\eta^s)}{r^4}\dot{\eta}^m\dot{\eta}^s-\frac{3e^2}{2}\frac{(x^m-\eta^m)}{r^2}\ddot{\eta}^n$$
$$-\frac{3e^2}{2}\frac{(x^n-\eta^n)}{r^2}\ddot{\eta}^m+2\delta_{mn}e^2\frac{(x^s-\eta^s)}{r^2}\ddot{\eta}^s+\cdots.$$

If now we calculate $(\Gamma_{mn,\,oo}-\Gamma_{mo,\,no})$ and $(\Gamma_{on,\,oo}-\Gamma_{oo,\,no})$ omitting from them all terms which involve $\dot{\eta}^s$, it will be found that the remaining terms are all of the types whose surface integrals are zero.

The omission of terms whose divergence vanishes identically is justified, since the surface integrals of such terms must also vanish identically.

The solutions (II.1) were obtained by the "new approximation method,"[3] adopting the same procedure by which the potentials (I.3) and (I.4) were determined.

Thus we have shown that the $\Gamma_{\mu\nu}$ give no contribution to the integrals occurring in the equations of motion (4.12). Let us now turn to the $\bar{\gamma}_{\mu\nu}$.

The retarded potentials which we choose to satisfy (4.14) are:[3]

$$\text{(a)}\qquad \bar{\gamma}_{oo}=-2m_0\sum_{l=1}^{\infty}\frac{1}{(2l-2)!}\frac{d^{2l-2}}{dx^{o\,2l-2}}(r^{2l-3})+2m_0\sum_{l=1}^{\infty}\frac{1}{(2l-1)!}\frac{d^{2l-1}}{dx^{o\,2l-1}}(r^{2l-2}),$$

$$\text{(b)}\qquad \bar{\gamma}_{on}=2m_0\sum_{l=1}^{\infty}\frac{1}{(2l-2)!}\frac{d^{2l-2}}{dx^{o\,2l-2}}(r^{2l-3}\dot{\eta}^n)-2m_0\sum_{l=1}^{\infty}\frac{1}{(2l-1)!}\frac{d^{2l-1}}{dx^{o\,2l-1}}(r^{2l-2}\dot{\eta}^n), \tag{II.2}$$

$$\text{(c)}\qquad \bar{\gamma}_{mn}=-2m_0\sum_{l=1}^{\infty}\frac{1}{(2l-2)!}\frac{d^{2l-2}}{dx^{o\,2l-2}}(r^{2l-3}\dot{\eta}^m\dot{\eta}^n)+2m_0\sum_{l=1}^{\infty}\frac{1}{(2l-1)!}\frac{d^{2l-1}}{dx^{o\,2l-1}}(r^{2l-2}\dot{\eta}^m\dot{\eta}^n).$$

If we inspect (II.2) (a), (b), and (c) for terms of the types specified above, we find that there are none of type (i) or type (iii). Only one term of type (ii) is to be found, and this is the first term of the first sum of (II.2) (b). This will not contribute to the integral (4.12) (b), since its contribution to $\bar{\gamma}_{on,\,oo}$ will contain $\dot{\eta}^r$ which is zero. It will, however, give a contribution to (4.12) (a), for

$$-\frac{1}{4\pi}\int 2m_0\left(\frac{1}{r}\right)_{,\,n}\ddot{\eta}^m\lambda^n dS=2m_0\ddot{\eta}^m.$$

This is the source of the inertial term in the equation of motion.

The same obviously holds when we take in (II.2) the "standing" rather than the "retarded" gravitational potentials.

If the solutions given in (II.1) are pushed one step further, so as to involve terms which do not become infinite near the singularity, and the $\gamma_{\mu\nu}$ are formed from these and (II.2), it may be verified that in the neighborhood of the singularity and in our special coordinate system we have

$$\gamma_{on,\,n}-\gamma_{oo,\,o}=0$$

and

$$\gamma_{mn,\,n}-\gamma_{mo,\,o}=-\frac{2}{r}(m_0\ddot{\eta}^m-e_{\text{ext}}\tilde{F}_{mo})=0^7$$

by virtue of the equations of motion.

We would like to thank Professor J. L. Synge for his helpful discussions and criticism.

Solutions of Equations for Particles of Spin Zero or One When No Field Is Present

A. H. TAUB
University of Washington, Seattle, Washington

(Received February 13, 1940)

Belinfante's four-component spinor form of the equations investigated by Kemmer for particles of spin zero and one are obtained in general coordinate systems. These equations are then solved when no external field is present by means of two simple spinors which satisfy Dirac equations for particles of spin one-half. The results previously obtained for the vector case hold for the pseudo-scalar case with one additional condition which says that the spins must be oppositely oriented. The pseudo-vector and scalar cases have similar conditions. In these cases the results differ from the previous two in that if one particle of spin one-half satisfies a Dirac equation with a positive mass term then the other satisfies one with a negative mass term.

1. INTRODUCTION

IN a recent paper Kemmer[1] has shown that the four types of equations (two for the case of spin zero, and two for the case spin one) he had previously investigated[2] for the meson of charge e and mass m in an electromagnetic field described by a vector potential φ_μ could be written as

$$\beta^\mu \pi_\mu \Psi = ik\Psi \quad (\mu = 1, 2, 3, 4), \tag{1.1}$$

where

$$\pi_\mu = \frac{\partial}{\partial x^\mu} - \frac{ie}{\hbar c}\varphi_\mu, \quad k = \frac{mc}{\hbar}, \quad x^4 = ct;$$

c is the velocity of light, $\hbar$ is Planck's constant divided by 2π, we have used the summation convention and β^μ are a set of four matrices defined by the commutation rules given by Duffin:[3]

$$\beta^\mu\beta^\nu\beta^\rho + \beta^\rho\beta^\nu\beta^\mu = \beta^\mu g^{\nu\rho} + \beta^\rho g^{\nu\mu} \tag{1.2}$$

and in a preferred coordinate system $g^{\mu\nu} = 0$ unless $\mu = \nu$ and then

$$-g^{11} = -g^{22} = -g^{33} = g^{44} = 1.$$

Belinfante[4] has been able to write the equations for the vector and pseudo-scalar cases in terms of a second-order four-component spinor by essentially solving Eqs. (1.2) as follows:

$$\beta^\mu = \tfrac{1}{2}[(\gamma^\mu \times 1) + (1 \times \gamma^\mu)], \tag{1.3}$$

where the cross denotes the direct product of matrices and γ^μ are four four-dimensional matrices satisfying

$$\tfrac{1}{2}(\gamma^\mu\gamma^\nu + \gamma^\nu\gamma^\mu) = g^{\mu\nu} \cdot 1. \tag{1.4}$$

The β^μ given by Eqs. (1.3) are 16-dimensional matrices and if these values are substituted in Eq. (1.1), Ψ is to be considered as a 16-component spinor which can be obtained from a second-order four-component spinor by ordering the latter lexicographically.

In this paper we use Eqs. (1.3) without specializing the matrices γ^μ and obtain invariant conditions that distinguish each of the four types of spinor equations corresponding to the vector equations investigated by Kemmer. It will then be shown, as in the Proca case,[5] that when no external field is present each of the spinor equations can be solved by using two simple four-component spinors which satisfy Dirac equations for particles of spin one-half and masses m_1 and m_2.

In the notation used here the four types of equations investigated by Kemmer[2] are; the scalar case

$$\pi_\sigma \varphi = k\chi_\sigma, \quad \pi_\sigma \chi^\sigma = -k\varphi, \tag{1.5a}$$

the vector or Proca case,

$$\pi_\mu U_\nu - \pi_\nu U_\mu = kG_{\mu\nu}, \quad \pi_\nu G^{\mu\nu} = kU^\mu, \tag{1.5b}$$

the pseudo-vector case,

$$\pi_\alpha G_{\beta\gamma} + \pi_\beta G_{\gamma\alpha} + \pi_\gamma G_{\alpha\beta} = kU_{\alpha\beta\gamma}, \quad \pi_\mu U^{\alpha\beta\mu} = kG^{\alpha\beta}, \tag{1.5c}$$

and the pseudo-scalar case,

$$\pi_\mu \chi_{\sigma\tau\nu} + \pi_\sigma \chi_{\tau\nu\mu} + \pi_\tau \chi_{\nu\mu\sigma} + \pi_\nu \chi_{\mu\sigma\tau} = -k\varphi_{\mu\sigma\tau\nu}, \quad \pi_\alpha \varphi^{\tau\mu\nu\alpha} = -k\chi^{\tau\mu\nu}, \tag{1.5d}$$

where all quantities have the tensor transforma-

[1] N. Kemmer, Proc. Roy. Soc. **173**, 91 (1939).
[2] N. Kemmer, Proc. Roy. Soc. **166**, 127 (1938).
[3] R. J. Duffin, Phys. Rev. **54**, 1114 (1938).
[4] F. J. Belinfante, Physica **6**, 870 (1939).
[5] A. H. Taub, Phys. Rev. **56**, 799 (1939), hereafter referred to as *A*.

tion laws indicated by their indices and those with more than one index are antisymmetric in all their indices.

Equations (1.5*d*) and (1.5*c*) are dual forms of Eqs. (1.5*a*) and (1.5*b*), respectively, as may be seen by writing

$$\begin{aligned} &G^{\dagger\mu\nu}=\tfrac{1}{2}g^{-\frac{1}{2}}\epsilon^{\mu\nu\sigma\tau}G_{\sigma\tau} \quad \text{or} \quad G_{\mu\nu}=\tfrac{1}{2}g^{\frac{1}{2}}\epsilon_{\mu\nu\sigma\tau}G^{\dagger\sigma\tau},\\ &U^{\dagger\mu}=(1/3!)g^{-\frac{1}{2}}\epsilon^{\mu\nu\sigma\tau}U_{\nu\sigma\tau} \quad \text{or} \quad U_{\nu\sigma\tau}=g^{\frac{1}{2}}\epsilon_{\mu\nu\sigma\tau}U^{\dagger\mu},\\ &\chi^{\dagger\mu}=(1/3!)g^{-\frac{1}{2}}\epsilon^{\mu\nu\sigma\tau}\chi_{\nu\sigma\tau} \quad \text{or} \quad \chi_{\nu\sigma\tau}=g^{\frac{1}{2}}\epsilon_{\mu\nu\sigma\tau}\chi^{\dagger\mu},\\ &\varphi^{\dagger}=(1/4!)g^{-\frac{1}{2}}\epsilon^{\mu\nu\sigma\tau}\varphi_{\mu\nu\sigma\tau} \quad \text{or} \quad \varphi_{\mu\nu\sigma\tau}=g^{\frac{1}{2}}\epsilon_{\mu\nu\sigma\tau}\varphi^{\dagger}, \end{aligned} \tag{1.6}$$

where $g^{\frac{1}{2}}$ is the square root of the determinant of $g_{\mu\nu}$ and is $+(-1)^{\frac{1}{2}}$ in a preferred coordinate system and $\epsilon^{\mu\nu\sigma\tau}$ is the completely antisymmetric relative tensor defined in A. By using Eqs. (1.6) and the identities[6]

$$\begin{aligned} &\epsilon_{\alpha\beta\gamma\delta}\epsilon^{\mu\nu\sigma\tau}=\delta^{\mu\nu\sigma\tau}_{\alpha\beta\gamma\delta}, \quad \epsilon^{\mu\nu\sigma\tau}\epsilon_{\mu\nu\alpha\beta}=2\delta^{\sigma\tau}_{\alpha\beta},\\ &\epsilon^{\mu\nu\sigma\tau}\epsilon_{\mu\alpha\beta\gamma}=\delta^{\nu\sigma\tau}_{\alpha\beta\gamma}, \quad \epsilon^{\mu\nu\sigma\tau}\epsilon_{\mu\nu\sigma\alpha}=3!\delta^{\tau}_{\alpha}, \end{aligned} \tag{1.7}$$

where the δ's are the generalized Kronecker delta's,[6] we find that Eqs. (1.5*d*) and (1.5*c*) may be written as

$$\pi_\sigma\varphi^{\dagger}=k\chi_\sigma{}^{\dagger}, \quad \pi_\sigma\chi^{\dagger\sigma}=-k\varphi^{\dagger}, \tag{1.8a}$$

and

$$\pi_\mu U_\nu{}^{\dagger}-\pi_\nu U_\mu{}^{\dagger}=kG_{\mu\nu}{}^{\dagger}, \quad \pi_\nu G^{\dagger\mu\nu}=kU^{\dagger\nu}, \tag{1.8b}$$

respectively. Moreover these equations imply (1.5*d*) and (1.5*c*), respectively.

It should be noticed that the quantities with a dagger before their indices obey a tensor transformation law if the determinant of the transformation is positive whereas under a transformation with a negative determinant they transform as

$$\lambda^{\dagger\mu\nu\cdots\rho *}=-\lambda^{\dagger\sigma\tau\cdots\alpha}\frac{\partial x^{\mu *}}{\partial x^{\sigma}}\frac{\partial x^{\nu *}}{\partial x^{\tau}}\cdots\frac{\partial x^{\rho *}}{\partial x^{\alpha}}.$$

Also the process of taking the dual commutes with the process of raising and lowering indices.

In the following we shall refer to four-component spinors, and denote their components by using lower case latin letters which shall have the range 1, 2, 3 and 4. We shall introduce such coordinate systems in the four-dimensional spin space so that the simple four-component spinors are related to two two-dimensional simple spinors in the manner given in §3 of A. This means that the transformation,

$$\psi^{*}=T\psi, \tag{1.9}$$

is the spin image of the Lorentz transformation

$$x^{\sigma}=L^{\sigma}{}_{\tau}x^{\tau} \tag{1.10}$$

if and only if

$$\gamma^{\tau}L^{\sigma}{}_{\tau}=T\gamma^{\sigma}T^{-1}. \tag{1.11}$$

Further, if

$$\gamma_5=-(g^{\frac{1}{2}}/4!)\epsilon_{\mu\nu\sigma\tau}\gamma^{\mu}\gamma^{\nu}\gamma^{\sigma}\gamma^{\tau}, \tag{1.12}$$

then

$$\gamma_5\gamma_\mu+\gamma_\mu\gamma_5=0 \quad (\gamma_5)^2=1 \tag{1.13}$$

and

$$T\gamma_5T^{-1}=L\gamma_5, \tag{1.14}$$

where L is the determinant of the matrix $\|L^{\sigma}{}_{\tau}\|$ and is $+1$ if (1.10) is a proper Lorentz transformation and -1 if it is improper.

The antisymmetric matrix $B=\|B_{ab}\|$ is determined up to a factor[7] by the equations

$$B\gamma^{\sigma}=-(B\gamma^{\sigma})', \quad B\gamma_5=-(B\gamma_5)' \tag{1.15}$$

and may be used to raise and lower four component spin indices. The rules for raising and lowering spin indices are

$$\psi_a=B_{ac}\psi^{c}, \quad \psi^{c}=\psi_aB^{ac}, \tag{1.16}$$

where $B_{ad}B^{ac}=\delta_d{}^{c}$ or

$$\|B^{ac}\|=-\|B_{ac}\|^{-1}=\|B_{ac}\|'^{-1}=B^{\circ} \tag{1.17}$$

and the prime denotes the transposed matrix. The symbol $^{\circ}$ after a matrix will hereafter denote the transposed inverse matrix.

From Eq. (1.11) it follows that the matrix T is determined up to an arbitrary factor. This factor is usually determined[8] by the requirement

$$T(L)B^{\circ}T'(L)=B^{\circ}. \tag{1.18}$$

However, in order to take account of improper Lorentz transformations as was done in A we replace this requirement by

$$T(L)B^{\circ}T'(L)=LB^{\circ}. \tag{1.19}$$

This replacement amounts to making the spin transformation

$$\varphi=(1/2^{\frac{1}{2}})(1+i\gamma_5)\psi=D\psi, \tag{1.20}$$

which amounts to replacing a matrix $P(L)$ satisfying (1.18) by

$$T(L)=DP(L)D^{-1}, \tag{1.21}$$

[6] O. Veblen, *Invariants of Quadratic Differential Forms* (Cambridge, 1927), p. 9.

[7] See A and the references given there for a more complete discussion of this matrix.

[8] R. Brauer and H. Weyl, Am. J. Math. **57**, 433 (1935).

which satisfies (1.19). The transformation may be thought of as the spin image of the transformations (1.6) for if we transform the matrices γ^μ by it we have

$$\gamma^{\mu *} = D\gamma^\mu D^{-1} = \tfrac{1}{2}(1+i\gamma_5)\gamma^\mu(1-i\gamma_5) = i\gamma_5\gamma^\mu = (1/3!)g^{-1}\epsilon^{\mu\nu\sigma\tau}\gamma_\nu\gamma_\sigma\gamma_\tau. \tag{1.22}$$

The last of these equations may be proved by verifying it in the coordinate system used in A.

2. The Spinor Equations

In order to obtain the spinor form of Eqs. (1.5a) and (1.5b) we use the fact that an arbitrary contravariant second-order spinor may always be written as[9]

$$\Psi^{\cdot\cdot} = \|\Psi^{ab}\| = \tfrac{1}{4}[\tfrac{1}{2}iG_{\mu\nu}\gamma_5\gamma^{\mu\nu}B^\circ + U_\tau\gamma_5\gamma^\tau B^\circ + \chi_\tau{}^\dagger\gamma^\tau B^\circ + i\varphi^\dagger B^\circ + \rho\gamma_5 B^\circ], \tag{2.1}$$

where

$$\gamma^{\mu\nu} = \tfrac{1}{2}(\gamma^\mu\gamma^\nu - \gamma^\nu\gamma^\mu), \quad (\gamma_5\gamma^{\mu\nu}B^\circ)' = \gamma_5\gamma^{\mu\nu}B^\circ, \quad (\gamma_5\gamma^\tau B^\circ)' = \gamma_5\gamma^\tau B^\circ, \tag{2.2}$$

and we placed dots to indicate the position of indices not written in. It follows from Eq. (2.1) that if

$$\Psi^{\cdot\cdot *} = T(L)\Psi^{\cdot\cdot}T'(L), \tag{2.3}$$

then

$$\Psi^{\cdot\cdot *} = \tfrac{1}{4}[\tfrac{1}{2}iG_{\mu\nu}{}^*\gamma_5\gamma^{\mu\nu}B^\circ + U_\tau{}^*\gamma_5\gamma^\tau B^\circ + \chi_\tau{}^\dagger\gamma^\tau B^\circ + i\varphi^{\dagger *}B^\circ + \rho^*\gamma_5 B^\circ], \tag{2.4}$$

where the starred tensor quantities are the transforms of the tensor quantities of Eq. (2.1) under the corresponding Lorentz transformation.

The second-order four-component spinors, Ψ^{ab}, are in one to one correspondence with simple sixteen-component spinors. To go from the former to the latter we take the first row of the matrix $\|\Psi^{ab}\|$ as the first four components of the latter, the second row as the next four and so on. Using this fact and Eq. (1.3) we are able to write Eqs. (1.1) as the matrix equation:

$$\tfrac{1}{2}\pi_\sigma(\gamma^\sigma\Psi^{\cdot\cdot} + \Psi^{\cdot\cdot}\gamma^{\sigma\prime}) = ik\Psi^{\cdot\cdot}. \tag{2.5}$$

For ease of computation we let

$$\Psi^{\cdot}{}_{\cdot} = \|\Psi^a{}_b\| = \|\Psi^{ac}B_{bc}\| = \tfrac{1}{4}[\tfrac{1}{2}iG_{\mu\nu}\gamma_5\gamma^{\mu\nu} + U_\tau\gamma_5\gamma^\tau + \chi_\tau{}^\dagger\gamma^\tau + i\varphi^\dagger + \rho\gamma_5]. \tag{2.6}$$

Then Eqs. (2.5) become

$$\tfrac{1}{2}\pi_\sigma(\gamma^\sigma\Psi^{\cdot}{}_{\cdot} + \Psi^{\cdot}{}_{\cdot}\gamma^\sigma) = ik\Psi^{\cdot}{}_{\cdot}. \tag{2.7}$$

From Eqs. (2.2), (1.4), (1.13) and

$$\tfrac{1}{2}(\gamma^\sigma\gamma_5\gamma^{\mu\nu} + \gamma_5\gamma^{\mu\nu}\gamma^\sigma) = \gamma_5\tfrac{1}{2}(\gamma^{\mu\nu}\gamma^\sigma - \gamma^\sigma\gamma^{\mu\nu}) = g^{\nu\sigma}\gamma^\mu - g^{\mu\sigma}\gamma^\nu.$$

It follows from (2.7) and (2.6) that

$$i\pi_\sigma G^{\mu\sigma}\gamma_5\gamma_\mu + \pi_\sigma U_\tau\gamma_5\gamma^{\tau\sigma} + \pi_\sigma\chi_\tau{}^\dagger g^{\tau\sigma} + \pi_\sigma i\varphi^\dagger\gamma^\sigma = ik(\tfrac{1}{2}iG_{\tau\sigma}\gamma_5\gamma^{\tau\sigma} + U^\mu\gamma_5\gamma_\mu + \chi_\sigma{}^\dagger\gamma^\sigma + i\varphi^\dagger + \rho).$$

From the linear independence of the matrices it follows that, $G^{\mu\sigma}$ and U^τ describe a particle satisfying Eqs. (1.5b), $\chi_\tau{}^\dagger$ and $\varphi_\tau{}^\dagger$ describe a particle satisfying (1.8a), and $\rho = 0$.

This result may be stated as follows: If Ψ^{ab} is a second-order spinor satisfying Eqs. (2.5) then

$$B_{bc}\gamma_5{}^{ca}\Psi^{ab} = \text{trace } (B\gamma_5\Psi^{\cdot\cdot}) = 0, \tag{2.8}$$

the antisymmetric tensor $G_{\mu\nu}$ and the vector U_ν defined by the equations

$$U_\tau = \text{trace } (B\gamma_5\Psi^{\cdot\cdot}), \quad G_{\mu\nu} = -i \text{ trace } (B\gamma_5\gamma_{\mu\nu}\Psi^{\cdot\cdot}) \tag{2.9}$$

satisfy Eqs. (1.5b), and the pseudo-scalar $\varphi^\dagger$ and pseudo vector $\chi_\mu{}^\dagger$ defined by the equations

$$\varphi^\dagger = -i \text{ trace } (B\Psi^{\cdot\cdot}), \quad \chi_\mu{}^\dagger = \text{trace } (B\gamma_\mu\Psi^{\cdot\cdot}) \tag{2.10}$$

satisfy Eqs. (1.8a). Moreover since the transposed matrix $\Psi^{\cdot\cdot\prime}$ satisfies (Eqs. (2.5) if $\Psi^{\cdot\cdot}$ does, it follows that the restrictions $\Psi^{ab} = \pm\Psi^{ba}$ are consistent with Eqs. (2.5). If Ψ^{ab} is restricted to be symmetric then $\varphi^\dagger = \chi_\mu{}^\dagger = 0$ but if it is restricted to be antisymmetric then $U_\tau = G_{\mu\nu} = 0$. Eqs. (2.8), (2.9) and (2.10) determine the spinor Ψ^{ab} uniquely and it can be shown by using the identities given by Veblen and also by Pauli[10] that if (Eqs. (1.5b) and (1.8a) are satisfied then Eqs. (2.5) follow. Belinfante[4] proves this by solving Eqs. (2.9) and (2.10) in a special coordinate system for Ψ^{ab} and then showing that Eqs. (1.5b) and (1.8a) imply (2.5).

[9] This follows directly from the fact that 1, γ^μ, γ_5, $\gamma^{\mu\nu}$, $\gamma_5\gamma^\mu$ form a basis for all four-dimensional matrices. The symmetry properties of the matrices follow from Eqs. (1.15). See §3 of A and the references given there.

[10] O. Veblen, Proc. Nat. Acad. Sci. **19**, 979–989 (1933); W. Pauli, *Zeeman Verhandlingen* (Nijhoff, 1935).

Since Eqs. (1.5a) and (1.8b) differ from (1.8a) and (1.5b), respectively, only in that U_τ is replaced by $U_\tau^\dagger$, $G_{\mu\nu}$ by $G_{\mu\nu}^\dagger$, $\varphi^\dagger$ by φ and $\chi_\mu^\dagger$ by χ_μ, this suggests that we consider the quantity

$$\Psi^{\dagger\cdots}=\tfrac{1}{4}[\tfrac{1}{2}iG_{\mu\nu}^\dagger\gamma_5\gamma^{\mu\nu}B^0+U_\tau^\dagger\gamma_5\gamma^\tau B^0+\chi_\tau\gamma^\tau B^0+i\varphi B^0+\rho^\dagger\gamma_5 B^0]. \tag{2.11}$$

If we now compute

$$\Psi^{\dagger\cdots *}=T(L)\Psi^{\dagger\cdots}T'(L) \tag{2.12}$$

we find

$$\Psi^{\dagger\cdots *}=(L/4)[\tfrac{1}{2}iG_{\mu\nu}^{\dagger *}\gamma_5\gamma^{\mu\nu}B^0+U^{\dagger}_{\tau}{}^{*}\gamma_5\gamma^\tau B^0+\chi_\tau{}^{*}\gamma^\tau B^0+i\varphi^* B^0+\rho^{\dagger *}\gamma_5 B^0]. \tag{2.13}$$

This implies that $\Psi^{\dagger\cdots *}$ is not the same linear combination of the starred tensor quantities as $\Psi^{\dagger\cdots}$ was of the unstarred ones and hence $\Psi^{\dagger\cdots}$ differs from $\Psi^{\cdots}$ in this respect (cf. Eqs. (2.4)). However, the quantity

$$\Phi^{\cdots}=\gamma_5\Psi^{\dagger\cdots}=\tfrac{1}{4}[\tfrac{1}{2}iG_{\mu\nu}^\dagger\gamma^{\mu\nu}B^0+U_\tau^\dagger\gamma^\tau B^0+\chi_\tau\gamma_5\gamma^\tau B^0+i\varphi\gamma_5 B^0+\rho^\dagger B^0] \tag{2.14}$$

has the same transformation properties as $\Psi^{\cdots}$, as may readily be verified from Eqs. (1.14), (2.12) and (2.13).

The relation between Eqs. (2.5) and (1.5a) and (1.8b) may be stated either in terms of the "pseudo-spinor" $\Psi^{\dagger\cdots}$ or in terms of the spinor $\Phi^{\cdots}$. The former are identical with those given above for the case of the spinor $\Psi^{\cdots}$ when we replace $\Psi^{\cdots}$ by $\Psi^{\dagger\cdots}$ and replace all tensors by pseudo-tensors and conversely.

In terms of the spinor $\Phi^{\cdots}$ Eqs. (2.5) become

$$\tfrac{1}{2}\pi_\sigma(\gamma^\sigma\gamma_5\Phi^{\cdots}+\gamma_5\Phi^{\cdots}\gamma^{\sigma\prime})=ik\gamma_5\Phi^{\cdots};$$

multiplying by γ_5 on the left and using Eq. (1.13) we obtain

$$\tfrac{1}{2}\pi_\sigma(-\gamma^\sigma\Phi^{\cdots}+\Phi^{\cdots}\gamma^{\sigma\prime})=ik\Phi^{\cdots}, \tag{2.15}$$

which may be written in 16-component notation as

$$\beta^{\mu *}\pi_\mu\Phi=\tfrac{1}{2}\pi_\sigma[(-\gamma^\sigma\times 1)+(1\times\gamma^\sigma)]=ik\Phi \tag{2.16}$$

and

$$\beta^{\mu *}=(\gamma_5\times 1)\beta^\mu(\gamma_5\times 1).$$

We now have the result: If Φ^{ab} is a second-order spinor satisfying Eqs. (2.15) then

$$\text{trace}\,(B\Phi^{\cdots})=0, \tag{2.17}$$

the pseudo-antisymmetric tensor $G_{\mu\nu}^\dagger$ and the pseudo-vector $U_\nu^\dagger$ defined by the equations

$$\begin{aligned}U_\tau^\dagger&=\text{trace}\,(B\gamma_\tau\Phi^{\cdots}),\\ G_{\mu\nu}^\dagger&=-i\,\text{trace}\,(B\gamma_{\mu\nu}\Phi^{\cdots})\end{aligned} \tag{2.18}$$

satisfy Eqs. (1.8b), and the scalar, φ and vector χ_μ defined by the equations

$$\begin{aligned}\varphi&=-i\,\text{trace}\,(B\gamma_5\Phi^{\cdots}),\\ \chi_\mu&=-\text{trace}\,(B\gamma_5\gamma_\mu\Phi)\end{aligned} \tag{2.19}$$

satisfy Eqs. (1.5a).

Since $\Phi^{\cdots\prime}$ does not satisfy (2.15) as a consequence of $\Phi^{\cdots}$ satisfying it, the restriction to the pseudovector case or the scalar case are no longer obtained by the requirement that $\Phi^{ab}=\Phi^{ba}$ or $\Phi^{ab}=-\Phi^{ba}$, respectively. In terms of $\Psi^{\dagger\cdots}$ these restrictions are obtained by setting $\Psi^{\dagger\cdots}=\pm\Psi^{\dagger\cdots\prime}$. Hence

$$\Phi^{\cdots}=\gamma_5\Phi^{\cdots\prime}\gamma_5' \tag{2.20}$$

is the condition that restricts us to the pseudovector case and

$$\Phi^{\cdots}=-\gamma_5\Phi^{\cdots\prime}\gamma_5' \tag{2.21}$$

is the condition that restricts us to the scalar case.

3. Solutions When No Field Is Present

In order to solve Eqs. (2.5) and (2.15) in terms of solutions of the Dirac equations for particles of spin one-half we must solve them for $\pi_\sigma\gamma^\sigma\Psi^{\cdots}$. This has been done by Belinfante[4] using the 16-component notation. In terms of the four-component notation his method amounts to computing

$$\begin{aligned}\tfrac{1}{2}\pi_\tau(\gamma^\tau\Psi^{\cdots}-\Psi^{\cdots}\gamma^{\tau\prime})&=(1/4ik)\{\pi_\tau\gamma^\tau[\pi_\sigma\gamma^\sigma\Psi^{\cdots}+\pi_\sigma\Psi^{\cdots}\gamma^{\sigma\prime}]-\pi_\tau[\pi_\sigma\gamma^\sigma\Psi^{\cdots}+\pi_\sigma\Psi^{\cdots}\gamma^{\sigma\prime}]\gamma^{\tau\prime}\}\\ &=-(e/8mc^2)f_{\tau\sigma}[\gamma^{\tau\sigma}\Psi^{\cdots}-\Psi\gamma^{\tau\sigma\prime}+2\gamma^\tau\Psi^{\cdots}\gamma^{\sigma\prime}],\end{aligned}$$

where

$$f_{\tau\sigma}=\partial\varphi_\sigma/\partial x^\tau-\partial\varphi_\tau/\partial x^\sigma$$

and is the tensor representing the electromagnetic field strengths. Adding this equation to (2.5) we obtain

$$\pi_\tau\gamma^\tau\Psi^{\cdots}=ik\Psi^{\cdots}-(e/8mc^2)f_{\tau\sigma}[\gamma^{\tau\sigma}\Psi^{\cdots}-\Psi^{\cdots}\gamma^{\tau\sigma'}+2\gamma^\tau\Psi^{\cdots}\gamma^{\sigma'}]. \tag{3.1}$$

Similarly we may obtain from Eqs. (2.15)

$$\pi_\tau\gamma^\tau\Phi^{\cdots}=-ik\Phi^{\cdots}+(e/8mc^2)f_{\tau\sigma}[\gamma^{\tau\sigma}\Phi^{\cdots}-\Phi^{\cdots}\gamma^{\tau\sigma'}-2\gamma^\tau\Phi^{\cdots}\gamma^{\sigma'}]. \tag{3.2}$$

In case no external field is present Eqs. (3.1) may be written as

$$\gamma^\tau(h/i)(\partial/\partial x^\tau)\Psi^{\cdots}=mc\Psi^{\cdots}. \tag{3.3}$$

If we restrict $\Psi^{\cdots}$ to be symmetric (vector case) then it follows from A that particular solutions of Eqs. (3.3) of the type

$$\Psi^{ab}=\Psi^{ab}(p)\exp(ip_\sigma x^\sigma/\hbar) \tag{3.4}$$

may be written as

$$\Psi^{ab}=\Psi_1{}^a\Psi_2{}^b+\Psi_1{}^b\Psi_2{}^b, \tag{3.5}$$

where

$$\Psi_1{}^a=\Psi_1{}^a(p_1)\exp(ip_{1\sigma}x^\sigma/\hbar),\quad \Psi_2{}^a=\Psi_2{}^a(p_2)\exp(ip_{2\sigma}x^\sigma/\hbar), \tag{3.6}$$

and $\Psi_1{}^a$ and $\Psi_2{}^a$ both satisfy the Dirac equations for free particles of spin one-half, of masses m_1 and m_2, respectively, that is,

$$\gamma^\sigma p_{1\sigma}\Psi_1(p_1)=m_1c\Psi_1(p_1),\quad \gamma^\sigma p_{2\sigma}\Psi_2(p_2)=m_2c\Psi_2(p_2). \tag{3.7}$$

We must have in addition:

$$\begin{gathered}m=m_1+m_2,\quad p_\sigma=p_{1\sigma}+p_{2\sigma},\quad p_\sigma p^\sigma=m^2c^2,\quad p_{1\sigma}=(m_1/m)p_\sigma,\quad p_{2\sigma}=(m_1/m)p_\sigma,\\ \Psi_1{}^a(p_1)\gamma_b{}^b{}_a\Psi_{2b}(p_2)=0.\end{gathered} \tag{3.8}$$

In A the additional requirement that

$$\Psi_1{}^a(p_1)\Psi_{2a}(p_2)\neq 0$$

was also imposed. This condition is not necessary as may be seen as follows: If the condition is violated then we may take $\Psi_1{}^a(p_1)=\rho\Psi_2{}^a(p_2)$ substituting (3.6) in (3.4) and this in turn in (3.3) we have

$$(2/\rho)\Psi_1{}^c(p_1)\gamma^{\tau a}{}_b p_\tau\Psi_1{}^b(p_1)=(2mc/\rho)\Psi_1{}^c(p_1)\Psi_1{}^a(p_1),$$

since $\Psi_1{}^c(p_1)$ is not identically zero we must have

$$\gamma^\sigma p_\sigma\Psi_1(p_1)=mc\Psi_1(p_1),$$

and similarly

$$\gamma^\sigma p_\sigma\Psi_2(p_2)=mc\Psi_2(p_2).$$

Examining the consistency of these equations with (3.7) as was done in *A* we are led to (3.8). Conversely (3.8) are sufficient to insure that (3.5) are solutions of (3.3).

The analogous results for $\Psi^{ab}=-\Psi^{ba}$ (pseudo-scalar case) will now be obtained. In this case it follows from Eqs. (2.6), (3.3) and (3.4) that

$$\Psi(p)^{\cdot}{}_{\cdot}=\|\Psi(p)^a{}_b\|=\tfrac{1}{4}(\chi_\tau{}^\dagger(p)\gamma^\tau+i\varphi^\dagger(p))=\frac{i\varphi^\dagger(p)}{4}\left(\frac{p_\sigma}{mc}\gamma^\sigma+1\right),$$

hence

$$\text{trace }(\Psi(p)^{\cdot}{}_{\cdot})=i\varphi^\dagger$$

and

$$(\Psi(p)^{\cdot}{}_{\cdot})^2=\tfrac{1}{2}\text{ trace }(\Psi(p)^{\cdot}{}_{\cdot})\Psi^{\cdot}{}_{\cdot}.$$

From the last of these equations and the fact that not all $p_\sigma=0$ we have that the determinant of $\Psi(p)^{\cdot}{}_{\cdot}$ is zero. Hence Ψ^{ab} is a singular antisymmetric spinor of second order and therefore can be written as

$$\Psi^{ab}(p)=\Phi_1{}^a(p_1)\Phi_2{}^b(p_2)-\Phi_1{}^b(p_1)\Phi_2{}^a(p_2). \tag{3.9}$$

The equations determining $\Phi_1{}^a(p_1)$ and $\Phi_2{}^a(p_2)$ are,

$$\Psi^{ab}(p)\Phi_{1b}(p_1)=\Phi_2{}^b(p_2)\Phi_{1b}(p_1)\Phi_1{}^a(p_1),\quad \Psi^{ab}(p)\Phi_{2b}(p_2)=\Phi_2{}^b(p_2)\Phi_{1b}(p_1)\Phi_2{}^a(p_2),$$

since $$\Phi_1{}^a\Phi_{1a}=\Phi_2{}^a\Phi_{2a}=0.$$

In order for $\Psi^{ab}(p)$ not to vanish identically we must have (cf. the vector case)

$$\Phi_1{}^a(p_1)\Phi_{2a}(p_2)\neq 0. \tag{3.10}$$

Substituting (3.9) in (3.4) and this in turn in (3.3) we obtain

$$\gamma^{\sigma a}{}_b p_\sigma(\Phi_1{}^b(p_1)\Phi_2{}^c(p_2)-\Phi_1{}^c(p_1)\Phi_2{}^b(p_2))=mc(\Phi_1{}^a(p_1)\Phi_2{}^c(p_2)-\Phi_1{}^c(p_1)\Phi_2{}^a(p_2)). \tag{3.11}$$

Multiplying by first $\Phi_{1c}(p_1)$ and summing, and then by $\Phi_{2c}(p_2)$ and summing, and using (3.10) we find that this equation may be written as two equations

$$\begin{aligned}\gamma^\sigma p_\sigma\Phi_1(p_1)&=mc\Phi_1(p_1),\\ \gamma^\sigma p_\sigma\Phi_2(p_2)&=mc\Phi_2(p_2).\end{aligned} \tag{3.12}$$

Equations (3.12) are fully equivalent to (3.11).

In order that $\Phi_1{}^a$ and $\Phi_2{}^b$ be interpreted as the wave functions for particles of spin one-half and masses m_1 and m_2, respectively, they must satisfy Eqs. (3.7) as well as (3.12). The necessary and sufficient conditions for this are the same as for the vector case and are summarized in Eqs. (3.8). Hence a particle satisfying the pseudo-scalar equations is equivalent to two Dirac particles of spin one-half, provided Eqs. (3.8) and (3.10) are satisfied. If we go over to the two component notation used in A we find that Eq. (3.10) and the last of Eqs. (3.8) imply that $\psi_A\chi^A\neq 0$. If we now interpret this condition in terms of the spin functions introduced on pages 805 and 806 we find that this means that the two particles must have their spins oriented in opposite directions. This follows from the fact that $\psi_A\chi^A\neq 0$ means that ψ_A and χ_A cannot be proportional.

An arbitrary solution of Eqs. (3.3) of the form (3.4) may be considered as the sum of a symmetric one and an antisymmetric one. Each of these may be treated as above. We would then have

$$\begin{aligned}\Psi^{ab}(p)=&\tfrac{1}{2}[\Psi_1{}^a(p_1)\Psi_2{}^b(p_2)+\Psi_1{}^b(p_1)\Psi_2{}^a(p_2)]\\ &+\tfrac{1}{2}[\Phi_1{}^a(p_1)\Phi_2{}^b(p_2)-\Phi_1{}^b(p_1)\Phi_2{}^a(p_2)].\end{aligned}$$

The relations between the four simple spinors, each of which satisfies a Dirac equation for particles of spin one-half, would then be determined by the rank of the matrix $\|\Psi^{ab}(p)\|$.

The corresponding results for the pseudo-vector and scalar cases may be obtained by considering the solutions of Eqs. (3.2) when no external field is present. However since the cases cannot be separated by using the symmetry properties of the spinor Φ^{ab} it is simpler to treat these cases by using Eqs. (3.3) but remembering that we now must use the pseudo-spinor $\Psi^{\dagger ab}$. In a particular coordinate system $\Psi^{\dagger ab}$ has the same properties as Ψ^{ab}. Hence if $\Psi^{\dagger ab}$ is symmetric and of the form (3.4) it must be possible to write it in the form (3.5) and if it is antisymmetric, it must be possible to write it in the form (3.9), in a particular coordinate system. However, in both cases not both of the single index quantities can transform as simple spinors, for if this were so $\Psi^{\dagger ab}$ would transform as a second-order spinor. Since $\Psi^{\dagger ab}$ transforms according to the representation $LT(L)\times T(L)$, we see that it is possible that one of these single index quantities be a simple spinor and then the other must be the substitution of the representation $LT(L)$.

Hence in the symmetric case we may write

$$\Psi^{\dagger ab}=\Psi_1{}^a\Psi_2{}^{\dagger b}+\Psi_1{}^b\Psi_2{}^{\dagger a}$$

or

$$\Psi^{\dagger ab}=\Psi_1{}^{\dagger a}\Psi_2{}^b+\Psi_1{}^{\dagger b}\Psi_2{}^a \tag{3.13}$$

and in the antisymmetric case we may write

$$\Psi^{\dagger ab}=\Phi_1{}^a\Phi_2{}^{\dagger b}-\Phi_1{}^b\Phi_2{}^{\dagger a}$$

or

$$\Psi^{\dagger ab}=\Phi_1{}^{\dagger a}\Phi_2{}^b-\Phi_1{}^{\dagger b}\Phi_2{}^a. \tag{3.14}$$

It will be sufficient to determine how $\Psi^{\dagger a}$ transforms in the symmetric case.

To do this we restrict ourselves to $\Psi^{\dagger ab}=\Psi^{\dagger ba}$ (pseudo-vector case) and go over to the two component theory in the manner given in §3 of A

Let us write

$$\|\Psi^{\dagger ab}\| = \left\| \begin{array}{cc} \|A_{1\cdot\cdot}\| & \|B^{\dagger}{}_{\cdot\cdot}\|' \\ \|B^{\dagger}{}_{\cdot\cdot}\| & -\|\bar{A}_{2}{}^{\cdot\cdot}\| \end{array} \right\|, \tag{3.15}$$

then from Eqs. (2.11) it follows that

$$\begin{aligned} A_{1AB} &= \tfrac{1}{8} G_{\mu\nu} S^{\mu\nu}{}_{AB}, \\ \bar{A}_{2}{}^{AB} &= \tfrac{1}{8} G_{\mu\nu} \bar{S}^{\mu\nu AB}, \quad (A, B = 1, 2). \\ B^{\dagger A'}{}_{B} &= \tfrac{1}{4} U^{\dagger\sigma} g_{\sigma}{}^{A'}{}_{B}, \end{aligned} \tag{3.16}$$

Eqs. (3.3) when written in two-component form now become the same as (2.1) to (2.4) of A with $B^{A'}{}_{B}$ replaced by $B^{\dagger A'}{}_{B}$ and $A_{2}{}^{AB}$ replaced by $-A^{AB}$.

We now write

$$A_{1AB} = \psi_{1A}\psi_{2B} + \psi_{1B}\psi_{2A}, \tag{3.17}$$

as can always be done, and introduce two other spinors by the equations

$$B^{\dagger A'B} = \bar{\varphi}_{1}{}^{A}\psi_{2}{}^{B} - \bar{\varphi}_{2}{}^{A}\psi_{1}{}^{B}. \tag{3.18}$$

This differs from the procedure of A in that the minus sign occurs in the right member instead of the plus sign (Cf. Eq. (2.12) of A.) However, the sign must be minus since under the transformation (1.24) of A which corresponds to the improper Lorentz transformation (1.25) of A we must have

$$B^{\dagger A'B} \rightarrow B^{\dagger A'B*} = -B^{\dagger B'A}$$

because $B^{\dagger A'B}$ is the spin image of a pseudo-vector. The position of the minus sign is undetermined, that is we may equally well write

$$B^{\dagger A'B} = \bar{\varphi}_{2}{}^{A}\psi_{1}{}^{B} - \bar{\varphi}_{1}{}^{A}\psi_{2}{}^{B}. \tag{3.19}$$

Instead of showing directly how the two-component form of Eqs. (3.3) may be solved by means of the simple two-component spinors introduced by means of Eqs. (3.17) and (3.18) we need only determine $\Psi_{1}{}^{a}$ and $\Psi_{2}{}^{\dagger a}$ (or $\Psi_{1}{}^{\dagger a}$ and $\Psi_{2}{}^{a}$) in terms of these two-component spinors. Substituting Eqs. (3.17) and (3.18) in (3.15) and comparing with the first of (3.13) we find, $\Psi_{1}{}^{a}$ is the four-component spinor formed from ψ_{1A} and $\bar{\varphi}_{1}{}^{A}$, and

$$\Psi_{2}{}^{\dagger a} = \gamma_{5}{}^{a}{}_{b}\Psi_{2}{}^{b},$$

where $\Psi_{2}{}^{b}$ is the four-component spinor formed from ψ_{2A} and $\bar{\varphi}_{2}{}^{A}$. If we had used Eqs. (3.19) instead of (3.18) and the second of (3.13) instead of the first, we would have obtained

$$\Psi_{1}{}^{\dagger a} = \gamma_{5}{}^{a}{}_{b}\Psi_{1}{}^{b}.$$

We may summarize our result as follows: When no field is present in the pseudo-vector case solutions of Eqs. (3.2) of the type

$$\Phi^{ab} = \Phi^{ab}(p) \exp(ip_{\sigma}x^{\sigma}/\hbar) \tag{3.20}$$

may be written as

$$\begin{aligned} \Phi^{ab} &= \gamma_{b}{}^{a}{}_{c}\Psi_{1}{}^{c}\gamma_{5}{}^{b}{}_{d}\Psi_{2}{}^{d} + \Psi_{1}{}^{b}\Psi_{2}{}^{a} \\ &\quad (\text{or } = \Psi_{1}{}^{a}\Psi_{2}{}^{b} + \gamma_{5}{}^{b}{}_{c}\Psi_{1}{}^{c}\gamma_{5}{}^{a}{}_{d}\Psi_{2}{}^{d}), \end{aligned} \tag{3.21}$$

where

$$\begin{aligned} \Psi_{1}{}^{a} &= \Psi_{1}{}^{a}(p_{1}) \exp(ip_{1\sigma}x^{\sigma}/\hbar), \\ \Psi_{2}{}^{a} &= \Psi_{2}{}^{a}(p_{2}) \exp(ip_{2\sigma}x^{\sigma}/\hbar), \end{aligned} \tag{3.22}$$

and $\Psi_{1}{}^{a}$ and $\gamma_{5}{}^{a}{}_{b}\Psi_{2}{}^{b}$ (or $\gamma_{5}{}^{a}{}_{b}\Psi_{1}{}^{b}$ and $\Psi_{2}{}^{b}$) both satisfy the Dirac equations for particles of spin one-half and masses m_{1} and m_{2}, respectively. In addition we must have all but the last of Eqs. (3.8) holding. The last condition is replaced by $\Psi_{1}{}^{a}\Psi_{2a} = 0$.

Similarly, when no field is present, in the scalar-case solutions of Eqs. (3.2) of the type of (3.20) may be written as

$$\begin{aligned} \Phi^{ab} &= \gamma_{5}{}^{a}{}_{c}\Phi_{1}{}^{c}\gamma_{5}{}^{b}{}_{d}\Phi_{2}{}^{d} - \Phi_{1}{}^{b}\Phi_{2}{}^{a} \\ &\quad (\text{or } = \Phi_{1}{}^{a}\Phi_{2}{}^{b} - \gamma_{5}{}^{b}{}_{c}\Phi_{1}{}^{c}\gamma_{5}{}^{a}{}_{d}\Phi^{d}), \end{aligned} \tag{3.23}$$

where

$$\begin{aligned} \Phi_{1}{}^{a} &= \Phi_{1}{}^{a}(p_{1}) \exp(ip_{1\sigma}x^{\sigma}/\hbar), \\ \Phi_{2}{}^{a} &= \Phi_{2}{}^{a}(p_{2}) \exp(ip_{2\sigma}x^{\sigma}/\hbar), \end{aligned} \tag{3.24}$$

and $\Phi_{1}{}^{a}$ and $\gamma_{5}{}^{a}{}_{b}\Phi_{2}{}^{b}$ (or $\gamma_{5}{}^{a}{}_{b}\Phi_{1}{}^{b}$ and $\Phi_{2}{}^{a}$) both satisfy Dirac equations for particles of spin one-half and masses m_{1} and m_{2}, respectively. In addition Eqs. (3.8) must hold with the last equation of (3.8) replaced by $\Phi_{1}{}^{a}\Phi_{2a} = 0$. However, this case differs from the pseudo-vector case above as the pseudo-scalar did from the vector in that we have an additional condition; namely,

$$\Phi_{1}{}^{a}\gamma_{5}{}^{b}{}_{a}\Phi_{2}{}^{a} \neq 0.$$

The condition that $\gamma_{5}{}^{a}{}_{b}\Psi^{b}$ satisfy the Dirac equation is

$$\gamma^{\sigma}p_{\sigma}\gamma_{5}\Psi = mc\gamma_{5}\Psi \tag{3.25}$$

or in virtue of Eqs. (1.13)

$$\gamma^{\sigma}p_{\sigma}\Psi = -mc\Psi. \tag{3.26}$$

That is, the condition is equivalent to the statement that Ψ satisfy a Dirac equation with the sign of the mass changed. Thus the two Dirac particles whose wave functions can be compounded to form the wave functions of a pseudovector particle or a scalar particle must be such that one of them satisfies a Dirac equation with the sign of the mass differing from the other. It may be of interest to note that the matrix γ_5 is the spin image of the extended Lorentz transformation

$$x^{\sigma *} = -x^{\sigma}$$

which interchanges past and future.

MAY 1, 1940 PHYSICAL REVIEW VOLUME 57

The Cross Section for Change of Charge and Ionization by High Velocity Metallic Ions in Hydrogen and Helium

CHALMERS W. SHERWIN
Ryerson Physical Laboratory, University of Chicago, Chicago, Illinois
(Received March 1, 1940)

An experimental method was developed in which the primary ionization and change of charge effects of a beam of positive ions can be studied separately. The cross sections for change of charge and for ionization have been measured for Be^{+}, B^{+}, B^{++}, C^{+}, C^{++}, Al^{+}, Al^{++}, K^{+}, Fe^{+}, Fe^{++}, Fe^{+++}, Cu^{+}, Cu^{++}, and Cu^{+++} ions moving through hydrogen and helium with velocities corresponding to accelerating potentials between 6000 and 24,000 volts. The determination of the cross section for change of charge was shown to be independent of the size and shape of the collectors used in the measurements, and the effects of scattered incident ions and of secondary electrons from various sources were shown to be negligible. A large energy difference was found between the ions formed in the gas by primary ionization and those formed by the change of charge process, the former having energies of the order of 10 ev and the latter having energies of about 0.1 ev or less. The cross-section values depend upon the type of ion and upon the accelerating voltage, and have magnitudes varying from less than 0.01 to 23×10^{-16} cm^2 for hydrogen, and from less than 0.01 to 10×10^{-16} cm^2 for helium.

1. INTRODUCTION

MEASUREMENTS of the rate at which charged ions of various types become neutralized in passing through gases at low pressures find application in several fields. In ion sources for high voltage apparatus, the ion beams must be accelerated through the low voltage range and may be much weakened in that process. In mass spectrographs the ions often describe paths of a meter or more in length. The rate of neutralization is specially important for this latter instrument, for if various ions are neutralized at different rates in the residual gas, the relative abundance of the ions detected may be quite different from the relative number of the ions originally produced. The dependence of the rate of neutralization on velocity is also of great importance for accurate measurements of isotope abundances, for, in the ordinary methods, the isotopes whose intensities are compared move through the residual gas with different velocities. It is possible by tests in each case to see whether a pressure effect is present or not,[1] but definite information on the rate of neutralization and its dependence on velocity would be desirable.

Experiments on the rate of neutralization of positively charged atoms of helium, neon, argon and krypton with energies up to 22,000 volts have been made by Rudnick[2] and Batho.[3] They found that the free path for neutralization in the same gas as the charged atom was between four and six times the kinetic theory free path. Experiments by Ramsauer, Kollath and Lilienthal,[4] Kallmann and Rosen,[5] Wolf,[6] Penning and Ven-

[1] A. O. Nier, Phys. Rev. **52**, 933 (1937).
[2] P. Rudnick, Phys. Rev. **38**, 1342 (1931).
[3] H. F. Batho, Phys. Rev. **42**, 753 (1932).
[4] Ramsauer, Kollath and Lilienthal, Ann. d. Physik **8**, 709 (1931).
[5] H. Kallmann and B. Rosen, Zeits. f. Physik **61**, 61 (1930); **64**, 806 (1930).
[6] F. Wolf, Zeits. f. Physik **72**, 42 (1931); **74**, 574 (1932); Ann. d. Physik **34**, 355 (1939).

nemans,[7] and Jordan[8] with rare gas ions with energies less than 1000 volts have given shorter free paths, in some cases less than the kinetic theory free path.

Ionization by high velocity positive ions in the sense of producing both a free electron and a free positive ion in the gas has seldom been distinguished from the production of a positively charged atom in the gas by the capture of an electron by the positively charged atom moving through it. Experiments by Wolf[6] and Brasefield[9] have attempted to distinguish the effect at low velocities while Goldmann[10] has studied it for 400–4000-volt protons. Most experiments on ionization by positive ions have used alkali ions, and have been directed almost exclusively to the observation of the lowest potential at which ionization occurs.[11,12] In this paper several cases will be discussed in which these two phenomena can be studied separately.

In this investigation, the rate of neutralization and the efficiency of free electron production have been studied with the following ions: Be^+, B^+, B^{++}, C^+, C^{++}, Al^+, Al^{++}, K^+, Fe^+, Fe^{++}, Fe^{+++}, Cu^+, Cu^{++}, Cu^{+++}, moving in hydrogen and helium accelerated by potentials between 6000 and 24,000 volts.

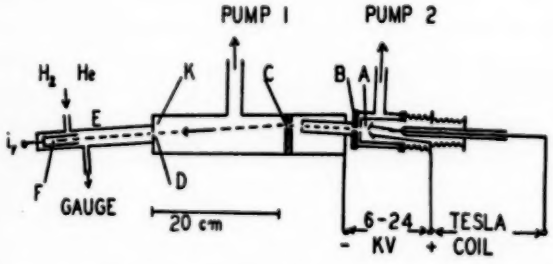

FIG. 1. Mass spectrograph. The ions are produced in the spark A, accelerated to B, deflected at C and studied in chamber E.

2. PRODUCTION OF THE ION BEAMS

Ions were created in the high frequency spark A (Fig. 1), accelerated to B, sorted out by Thomson's method of crossed electric and magnetic deflections at C, and finally directed into the chamber E where measurements were made.[13] The different ions enter the measuring chamber E through the small hole D which is enlarged beyond the point where the beam has been defined. This enlarged part prevents the secondary electrons created at the defining aperture from reaching the electrodes in E. The main beam is collected by the deep cylinder electrode F which prevents the escape of secondary electrons. The

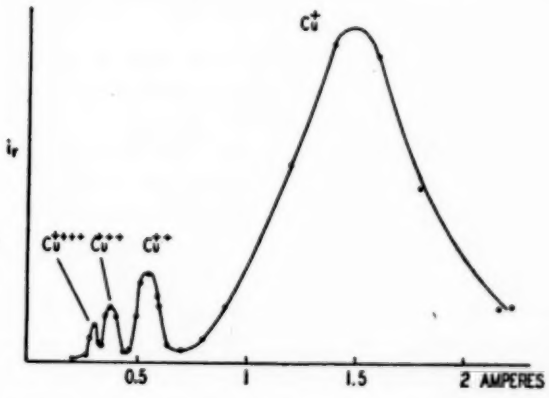

FIG. 2. Ion current to F (Fig. 1) as the current to the magnet is varied, showing the separation of the ions with different charge. Copper electrodes in spark, 12,000 volts.

current to F (i_F), due to ions from a copper spark, as the magnetic field is varied, is shown in Fig. 2, which shows that the copper ions with different charges could be well separated.

The hydrogen and helium gases were purified by passage through activated charcoal at liquid-air temperatures and then introduced into the measuring chamber through a capillary tube. For some of the measurements with hydrogen a palladium valve was used in place of the capillary.

Gas pressure measurements were made with an ionization gauge which was directly calibrated by a McLeod gauge. It was found that both the change of charge and ionization cross sections were constant over the range of pressures used in the experiment (10^{-4} to 5×10^{-4} mm of Hg), provided the original pressure was less than about 2×10^{-6} mm. This original low pressure was obtained by means of a side tube on the measuring chamber immersed in liquid air. Most of the cross-section measurements were made at pressures of about 5×10^{-4} mm of Hg.

[7] F. M. Penning and C. F. Vennemans, Zeits. f. Physik **62**, 746 (1930).
[8] E. B. Jordan, Phys. Rev. **47**, 467 (1935).
[9] C. J. Brasefield, Phys. Rev. **42**, 11 (1932).
[10] F. Goldmann, Ann. d. Physik **10**, 460 (1931).
[11] O. Beeck and J. C. Mouzon, Ann. d. Physik (5) **11**, 737, 858 (1931).
[12] R. N. Varney, Phys. Rev. **47**, 483 (1935); **50**, 159 (1936).
[13] Sheng-Lin Ch'u, Phys. Rev. **50**, 212 (1936).

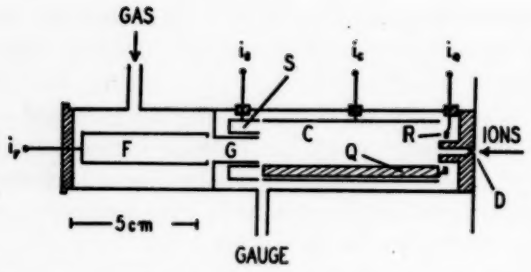

FIG. 3. Measuring chamber used to collect most of the data in Table I. An electric field between "quarter-cylinder" Q and cylinder C can be used to sweep out the positive ions and electrons formed along the path of the original ion beam.

3. PRELIMINARY EXPERIMENTS

Three different ionization chambers (Figs. 3, 5, and 7) were used at E (Fig. 1) to study the changes that occur in the beam of ions entering at D (Fig. 1) and the ionization produced in the gas. A comparison of these observations demonstrated the possibility of avoiding complicating effects—scattered ions, photoelectric emission, and secondary emission from the impact of ions on metallic parts—and showed how to allow for them in cases where they could not be completely avoided.

In the chamber shown in Fig. 3, the ions enter at D and pass through the cylinder C to the Faraday chamber F. The electrode Q is a "quarter cylinder" having the same curvature and length as cylinder C, but having only one-fourth the area. It is mounted about 1 mm from the bottom of C, and supported at the extreme right by the ring R through which connection is made to the outside. The electrode S is a Faraday chamber formed by the annular space between two cylinders and was used to observe any scattered ions. It is protected from the slow ions formed along the path of the main beam by the shield G.

When the gas in the measuring chamber is hydrogen (pressure $=5\times10^{-4}$ mm of Hg) no scattered ions can be detected at S. The currents to quarter-cylinder Q (per unit current to F) are given in Fig. 4, curve Q. The field sweeping out the ions is that between the quarter-cylinder Q and the cylinder C (Fig. 3). The abscissa V is the voltage with respect to ground of the collector Q when collectors C and S are grounded. When, however, C and Q are connected together, forming a complete cylinder, and have no potential applied to them, a positive current (per unit current to F) due to neutralization of the ions is observed (point $C+Q$, Fig. 4). The rapidly moving ion picks up an electron from the gas, leaving a positively charged hydrogen molecule behind which charges up the $C+Q$ cylinder. When, however, collector Q is negative it attracts a positive current in excess of the amount $C+Q$. This excess of positive current is exactly the same in magnitude as the negative current picked up by Q when it is made positive. These positives and negatives appearing in equal numbers can only be due to ionization. Note that about 10 volts is required to saturate both the positive ions and the electrons. With this interpretation, the two different effects, change of charge and ionization, can be separated. Since collector S indicates zero current, the effect of scattering is negligible. In all cases studied in hydrogen, with the exception of K^+, curves of the same form and interpretation as Fig. 4 were obtained. The potential on Q necessary for saturation varied between 10 and 25 volts.

Experiments confirming these interpretations were made in which the collector Q is replaced by a fine wire W, 1 mm in diameter. (See Fig. 5.) Various potentials V are applied to W, with C and S grounded, and the currents received on the wire are shown in curve W, Fig. 6. When S and W are grounded, and C is at zero potential, it (C) receives a positive current of the same magnitude as the combination $C+Q$ (Fig. 3). This is because of the negligible area of the wire W. Quarter-cylinder Q (Fig. 3), on the other hand, has an appreciable area and receives about one-fourth the current (at zero potential) that goes to the combination $C+Q$ (see Fig. 4). This indicates that

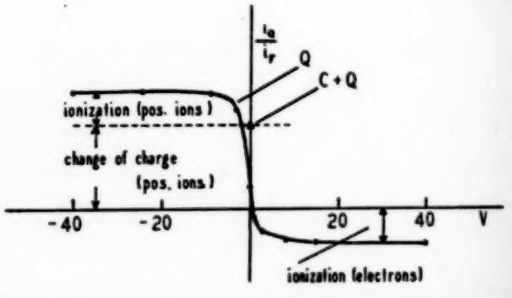

FIG. 4. Current received by Q (Fig. 3), when it is fixed at different potentials, compared to that received by $C+Q$ (Fig. 3) when it is at zero potential. B^+ ions in hydrogen; 12,000 volts.

the ions formed along the beam diffuse radially in a uniform manner. The current to electrode C, at zero potential, is shown at C, Fig. 6. The current to W (i_W) does not saturate at the voltages shown in Fig. 6. These ions and electrons have a maximum energy of about 10 volts as is seen from Fig. 4, where they are saturated by that potential. The small wire is a very inefficient collector for ions with an initial kinetic energy of their own. The field deviates them from their path but they pass by the wire and strike the cylinder unless the applied potentials are very great. The wire W fails to capture all these 10-volt ions even though the potential of W is 320 volts. The curve W, Fig. 6, does, however, show a sharp bend at P ($V=-3$ volts, approximately) indicating the presence of slow ions due to change of charge which are easily saturated by this small voltage. From the effectiveness of the wire W in capturing the 10-volt ions, when charged to 320 volts, the maximum energy of these slow ions must be less than 0.1 volt. These slow ions form a current very nearly equal to that picked up on C, which current is due to change of charge. For all of the ions studied, in both hydrogen and helium, the i_W at bend P (Fig. 6) corresponded closely to the current due to change of charge. We are thus led to the conclusion that the majority of the ions formed from the originally neutral gas atoms or molecules by the change of charge process have energies much less than one volt. On the other hand, positive ions and electrons formed by the ionization events have energies ranging up to 10 volts or more. The saturation curve for the positive ions due to ionization and electrons due to the same cause are similar, although the electrons appear to saturate more easily. Thus Fig. 6 shows the existence of three different classes of

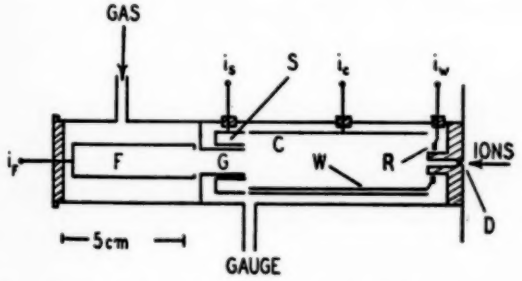

FIG. 5. Measuring chamber used to study the energy distribution of the positive ions and electrons created by the incident ion beam. W is a fine wire.

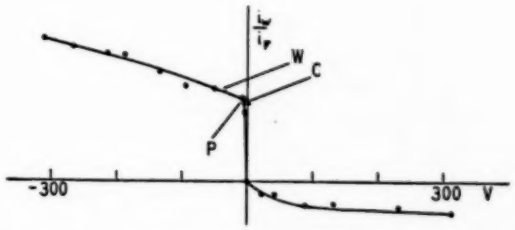

FIG. 6. Current received by W (Fig. 5), when it is fixed at different potentials, compared to that received by C (Fig. 5) when it is at zero potential. The bend at P shows the presence of two groups of ions with widely different energies. B^+ ions in hydrogen; 12,000 volts.

charged particles formed in a gas by a beam of high velocity ions: (1) slow positive ions, created by the change of charge process, which have energies much less than 1 volt,[14] (2) fast positive ions due to ionization events which have energies ranging up to 10 volts or more,[15] and (3) fast electrons due to ionization events which also have energies up to 10 volts or more.

As a further confirmation of the assumption that the currents picked up on collectors $C+Q$ (Fig. 3) and on C or $C+W$ (Fig. 5), when they are at zero potential, are to be attributed entirely to change of charge, a cylinder of different dimensions was employed, C (Fig. 7). Whereas the cylinders so far described had a length of 7.0 cm and a diameter of 2.4 cm, the cylinder in Fig. 7 had a length of 21.6 cm and a diameter of 0.95 cm. If there is an "end effect" which makes the effective length of the cylinder different from its measured length, this effect for the long narrow cylinder should be of much less importance than with the short cylinder of larger diameter. The long cylinder will, however, be more easily affected by scattered ions since the solid angle of the opening at the end H (Fig. 7) as seen from D is only about 1/80 the corresponding solid angle for the short cylinder. It is found that in many cases the long and the short cylinders give the same result for the change of charge cross section. Examples are given later. In cases where there is a divergence between the long and short cylinders, the long cylinder always picks up more cur-

[14] An attempt to measure the momentum transferred in the related process of light excitation by fast ions, by measurements of the Doppler effect in the light excited, led to zero velocity. See W. Wien, Ann. d. Physik **43**, 955 (1914).

[15] Positive ions, with energies up to 8 volts, produced in a gas by the impact of slow (~50-volt) electrons were found by Tate and Lozier, Phys. Rev. **39**, 254 (1932).

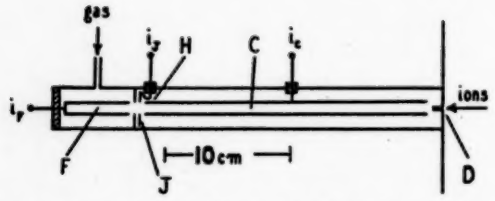

FIG. 7. Measuring chamber with the long cylinder. The cross sections for change of charge determined with this cylinder are compared to the values obtained with the short cylinder in Figs. 3 or 5.

rent than would be expected, judging from the currents with the short cylinder, indicating that it is receiving scattered ions, while the short cylinder is known to be free from scattering effects when S (Figs. 3 and 5) receives no current. In cases where divergence occurs the electrode J (Fig. 7) receives measurable currents when the cylinder C is removed, indicating scattering.

The conservation of energy and momentum are sufficient to give the maximum angle through which an ion of mass M may be scattered by an atom of mass m.[16] The maximum possible angle ϕ is given by $\sin\phi = m/M$. For the cylinder in Fig. 3, the angle ϕ was approximately $\sin^{-1} 1/6$. Thus with helium no ions of mass 24 or more, and with hydrogen no ions of mass 12 or more can reach C, and the number for lighter ions is probably extremely small, depending on the law of force. Scattered ions may, however, reach the surface G (Fig. 3) or the end H of the long cylinder C (Fig. 7) and give rise to secondary electrons in the first case and charging in the second.

The ions collected by $C+Q$ and Q (Fig. 3) when Cu^{++} ions pass through helium are shown in Fig. 8. The left-hand part due to positive ions is very similar to Fig. 4. The right-hand side shows a large excess of electrons. A magnet at G greatly reduced this negative current. The electrons are probably secondary electrons from G. It was shown that they are not produced on the interior surface of C or Q by photoelectric emission or metastable helium atoms[17] by alternately collecting the electrons on the large and small collectors. The curve in Fig. 8 was the same in both cases, although the areas of the surfaces of Q and C differ by a factor of four.

[16] Rutherford, Chadwick and Ellis, *Radiations from Radioactive Substances* (Cambridge University Press, 1930), p. 241.

[17] M. Oliphant, Proc. Roy. Soc. **A127**, 373 (1930).

From the curve Q in Fig. 8, it is possible to determine both the ionization and the change of charge from the left-hand side of the curve due to positive ions. The point marked $C+Q$ is the current observed due to change of charge when C and Q are joined together and are at zero potential. The difference between this and the saturation current is due to positive ions produced by ionization. Ions in helium all gave curves similar to Fig. 8.

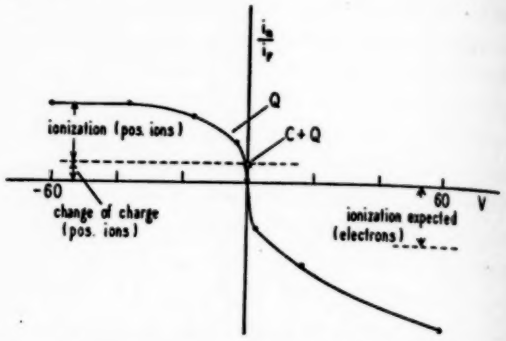

FIG. 8. Current received by Q (Fig. 3), when it is fixed at different potentials, compared to that received by $C+Q$ (Fig. 3) when it is at zero potential. Cu^{++} ions in helium; 12,000 volts. The excess of electrons is due to secondaries from G (Fig. 3).

4. MEASUREMENT OF THE CROSS SECTIONS

Since an ion beam is attenuated exponentially due to change of charge effects, the measurement of the intensity at two points is sufficient to determine the cross-section value. Referring for example to Fig. 7, the sum of the currents to C and F is proportional to the intensity at D, while the current to F is proportional to the intensity at the end H.

The ratio of the currents to C and to F (Figs. 3, 5 or 7) was measured using the circuit in Fig. 9. As C and F charge up, the two electrometers are kept at zero by adjusting R_1. R_2 and the pointer P. (See Fig. 9.) After any length of time the ratio of the charges Q on C and F is given by $Q_c/Q_f = kR_2/(R_1+R_2)$ where k is defined by $C_2 = kC_1$. This method is similar to that used by Bailey[18] and Vanderberg.[19]

The currents used to determine the cross section for an ionization event were taken from those values marked "ionization" as in Figs. 4 and 8.

[18] V. A. Bailey, Phil. Mag. **50**, 831 (1929).

[19] R. M. Vanderberg, M.A. Thesis, University of Chicago, 1940.

In calculating the cross-section values allowance has been made for the appearance, for example, of neutral, singly, and doubly charged ions in a beam consisting originally of only triply charged ions. Also, the appearance in the beam, of ions of higher multiplicity of charge than the original ions has been investigated. Using the photographic method described by Ch'u,[13] evidence was found showing that a small number of singly charged ions were changing to doubly charged ions without having their initial direction altered. This process rarely occurs for slow ions, but is a well-known phenomenon for ions of very high energies. This effect was found for singly charged ions of Be, B, C, Al, Fe, and Cu when passing through both hydrogen and helium. The results indicate, however, that this effect was of negligible importance compared to the loss of charge effect.

5. Results

A. Metallic ions in hydrogen

It has been shown above that there are three ways of measuring the change of charge cross section using (1) the value of the saturation currents as in Fig. 4 (the magnitude of the current due to electrons produced by ionization is subtracted from the total current due to positive ions giving that part of the positive ions due to the change of charge process), (2) the positive ion current received by the short cylinder, and (3) the positive ion current received by the long cylinder, when both cylinders are at zero potential. These methods are compared in Fig. 10 which is for the case of Fe^{++} ions in hydrogen. Further examples are shown in Figs. 11 and 12. It is seen that the agreement in these cases is good. Agreement between the values deduced from ionization and those deduced from the currents to the short cylinder was found for all the positive ions in hydrogen with the exception of K^+ which seemed to scatter more easily than the others, creating secondaries at G (Fig. 3). Agreement between the short and long cylinders was less good due to the extreme sensitiveness of the long collector to scattered ions.

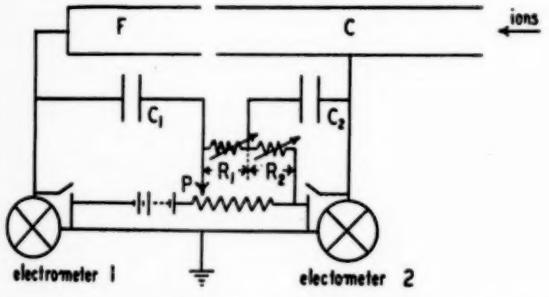

Fig. 9. Electrical circuit used to compare the currents received by C and F.

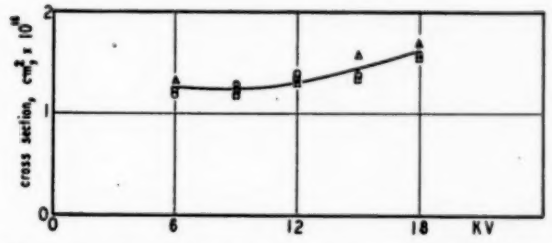

Fig. 10. Comparison of the three methods used to determine the cross section for change of charge (2→1 transition) for Fe^{++} ions in hydrogen at different accelerating potentials. ○—7.0-cm cylinder at zero potential; Δ—21.6-cm cylinder at zero potential; □—values deduced using ionization currents as in Fig. 4.

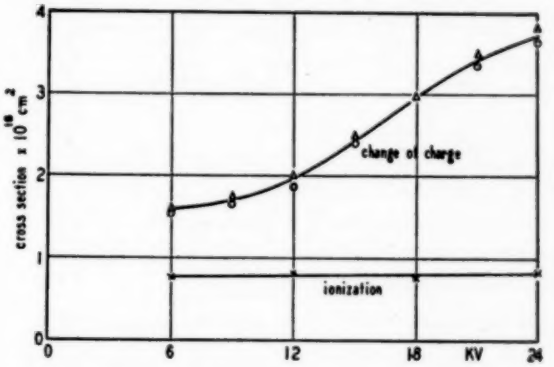

Fig. 11. Change of charge (1→0 transition) and ionization cross sections for C^+ ions in hydrogen at different accelerating potentials. ○—7.0-cm cylinder at zero potential (change of charge); Δ—21.6-cm cylinder at zero potential (change of charge); ×—cross section for ionization. This is a typical example of the variation of the ionization cross section with accelerating voltage.

The tabulated values of the change of charge and ionization cross sections are given in Table I in the columns labeled "hydrogen." It turned out that the variation of the cross section with accelerating voltage is very nearly linear in most cases—at least to within experimental error (2 to 6 percent depending on the ion). Consequently it is necessary to give only two values for the cross section (namely, the values at 6000 volts and at either 18,000 or 24,000 volts) which then determine the variation of the cross section with velocity. A notable exception to this linear

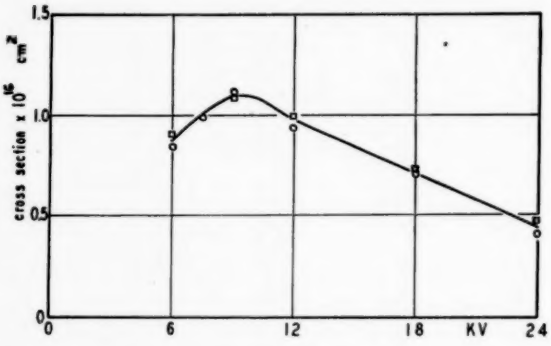

FIG. 12. Change of charge (1→0 transition) cross sections for Al^+ ions in hydrogen at different accelerating potentials. This is an unusual curve inasmuch as the variation with accelerating potential is usually linear (or nearly so) over this range. ○—7.0-cm cylinder at zero potential; □—values deduced using ionization currents as in Fig. 4.

type of relation is Al^+ in hydrogen which is shown in detail in Fig. 12.

The variation of the cross section with velocity for an ionization event is usually small. A typical curve is shown in Fig. 11 which is for C^+ ions in hydrogen.

The data in Table I, except for the case of Al^{++}, have certain characteristics in common. (1) The cross section for both change of charge and ionization increase rapidly with increasing multiplicity of charge on the incident ion. (2) Both of the cross sections either remain constant or increase with increasing accelerating voltage, the change of charge cross sections for the Fe^{+++}, C^+ and Be^+ ions showing a particularly large increase.

B. Metallic ions in helium

With helium in place of hydrogen in the measuring chamber three important changes were found. (1) The scattering increased greatly. (2) The cross sections for both ionization and change of charge were reduced. (3) The shape of the cross section *vs.* accelerating voltage curve was in some cases greatly altered (e.g. Fe^{+++}).

For all ions of multiplicity greater than one, there was no appreciable scattering to the collectors C or Q since collector S (Fig. 3) received currents less than about 3 percent of those received by $C+Q$. Consequently the cross-section determinations for these ions are about as reliable as those for hydrogen. These values are given in Table I, since it is again found that the variation of cross section with velocity is nearly linear, with the exception of Fe^{+++} which is shown in Fig. 13.

The case of singly charged ions in helium is different, however. Here the change of charge is very small and consequently the scattering to S (Fig. 3) is often of the same order of magnitude as the currents to $C+Q$, and the secondaries created at both G and S (Fig. 3) are sufficiently numerous to render uncertain the true value of

TABLE I. *Collected data for the change of charge and ionization cross sections in hydrogen and helium. Since the variation of the cross sections with accelerating potential is nearly linear, only two values are given. For singly charged ions, σ is the cross section for the 1→0 transition, for doubly charged ions σ is the cross section for the 2→1 transition, and for triply charged ions, it is the cross section for the 3→2 transition. σ_i is the cross section for an ionization event. The value 0 means $\sigma<0.01\times10^{-16}$ cm².*

Ion	In Hydrogen				In Helium			
	$\sigma\times10^{16}$ cm²		$\sigma_i\times10^{16}$ cm²		$\sigma\times10^{16}$ cm²		$\sigma_i\times10^{16}$ cm²	
	6 kv	24 kv	6 kv	24 kv	6 kv	24 kv	6 kv	24 kv
Be^+	0	0.29	0.06	0.41			0.23	0.37
B^+	0.83	1.3	0.64	1.3			0.22	0.50
B^{++}	15	15	3.2	3.2	1.7	3.2	0.46	1.5
C^+	See Fig. 11		0.90	0.90			0.81	1.7
C^{++}	15	15	1.9	2.0	6.2	13	1.4	5.5
Al^+	See Fig. 12		0.22	0.51			0.18	0.35
Al^{++}	3.9	5.1			2.2	3.3		
K^+	0.35	0.25	0.19	0.45				
	6 kv	18 kv	6 kv	18 kv	6 kv	18 kv	6 kv	18 kv
Fe^+	0	0	0.32	0.48			0.23	0.23
Fe^{++}	1.2	1.6	0.52	0.84	0	0.05	0.28	0.28
Fe^{+++}	11	23	3.2	4.8	See Fig. 13		See Fig. 13	
Cu^+	0	0	0.16	0.26			0.18	0.39
Cu^{++}	3.8	4.0	0.33	0.58	0.1	0.1	0.23	0.42
Cu^{+++}	22	23	1.6	2.6	8.2	6.5	1.5	2.2

the $C+Q$ current from which the change of charge cross sections are deduced. These secondaries are usually numerous enough, relative to the small number of positive ions formed by the change of charge process, to make the $C+Q$ currents negative by small amounts. The small cross section for the change of charge of these ions is consequently not listed in Table I. The cross sections for ionization can still be determined with fair accuracy, however, since the currents from which they are deduced are 5 to 10 times the magnitude of those due to change of charge, and are not appreciably masked by the secondaries from G.

As an example of the application of these results, the attenuation over a one-meter path, due to change of charge, is computed for a beam of Fe ions passing through hydrogen at a pressure of 10^{-3} mm of Hg. For 12,000-volt Fe^{+}, Fe^{++}, and Fe^{+++} ions, the attenuation amounts to 0.01 percent, 0.5 percent and 7 percent, respectively. In helium at the same pressure the Fe^{++} and Fe^{+++} ion beams are attenuated 0.1 percent and 0.6 percent, respectively. The mean free paths for charge transfer, calculated from the cross-section values in Table I vary widely with reference to the kinetic theory value. For example, in hydrogen, Fe^{+} has a free path for change of charge several hundred times, and Fe^{++} about 20 times the kinetic theory value for Ag atoms in air, and Fe^{+++} has a free path about 2 times this amount. The mean free paths measured for the rare gas ions by Batho,[3] and for Li^{+} by Thompson[20] cover nearly as great a range.

For electrons in hydrogen at 1 mm pressure the maximum efficiency of ionization occurs at about 70 volts[21] where 3.6 ions are produced per centimeter of path. For 12,000-volt Fe^{+}, Fe^{++}, Fe^{+++}, ions the corresponding numbers are 1.4, 2.5, 12.5.

6. Reference to Theory

Quantum-mechanical calculations of the cross sections for change of charge for slow (<400-volt) protons in hydrogen,[22] and in helium[23] have been made. The calculations have not been extended to more complicated electron configurations, although the cross section for charge transfer from a $1S$ to a $1S$ state has been computed by Brinkmann and Kramers[24] for high velocity ions. The general theory does predict a variation in the cross-section value as the ion velocity is varied. For slow protons in hydrogen the first approximation theory predicts a maximum which was found by Bartels[25] although at too high a voltage. The explanation of the maximum found for Al^{++} in hydrogen (Fig. 12) might be similar.

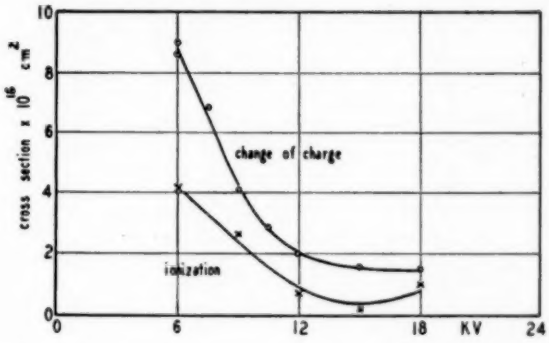

FIG. 13. Change of charge (3→2 transition) and ionization cross sections for Fe^{+++} ions in helium at different accelerating potentials. This is the only case observed where the ionization cross section decreased with increasing accelerating potential.

The cross section for primary ionization has been theoretically calculated for fast ($>10^6$ ev) positive ions,[26] and decreases with increasing velocity, but for any velocity increases as the square of the charge on the ion. These experiments indicate that there is no decrease in the ionization cross section with increasing ion velocity for 10^4-ev ions (except for Fe^{+++} in helium) but rather an increase is usually observed. The second effect, namely, the increase of cross section for ionization with the charge on the incident ion, is found in all cases, the increase being roughly as the square of the charge in agreement with the theory for the fast ions.

The author wishes to thank Professor A. J. Dempster, who proposed this problem, for his advice and assistance throughout the investigation.

[20] J. S. Thompson, Phys. Rev. **35**, 1196 (1930).
[21] J. Tate and P. Smith, Phys. Rev. **39**, 270 (1932).
[22] N. F. Mott and H. S. W. Massey, *Theory of Atomic Collisions* (Oxford University Press, 1933), p. 239.
[23] H. S. W. Massey and R. A. Smith, Proc. Roy. Soc. **142**, 142 (1933).
[24] N. F. Mott and H. S. W. Massey, reference 22, p. 228.
[25] H. Bartels, Ann. d. Physik **13**, 373 (1932).
[26] N. F. Mott and H. S. W. Massey, reference 22, p. 225.

The Influence of Discharge Chamber Structure Upon the Initiating Mechanism of the High Frequency Discharge

SHERWOOD GITHENS, JR.*
The University of North Carolina, Chapel Hill, North Carolina
(Received November 25, 1939)

It is shown that a breakdown in a rarefied gas with high frequency e.m.f. of the order of megacycles may occur through three different processes. Mode *a* is characterized by a breakdown voltage of about half the d.c. discharge value. Mode *b* occurs at lower gas densities and is characterized by breakdown at a voltage somewhat above the corresponding d.c. discharge value. Mode *c* is the high frequency counterpart of the Paschen law phenomenon, in that when the density is too low to support an inter-electrode discharge, the latter seeks a longer path. It is shown that all three of these modes may operate in the same discharge chamber, sometimes simultaneously, and that the breakdown-process may shift from one mode to another with change in pressure or frequency. Many of the baffling complexities in earlier h.f. striking-voltage data may thus be understood. It is pointed out that mode *c* breakdowns are of little value for quantitative interpretation. A type of discharge chamber is described in which the breakdown may be held definitely to modes *a* and *b*.

INTRODUCTION

THERE have been marked discrepancies in the striking voltages observed by various workers, under apparently similar conditions, in a rarefied gas, with high frequency e.m.f. of the order of megacycles. The variations in V_s with change in pressure and especially with change in frequency have been baffling and contradictory. Darrow remarks[1] that "the data do not form a complete or coherent system." A definite choice between the several proposed pictures of the mechanism of the breakdown,[2–12] or between the accompanying mathematical predictions of the striking voltage, is impossible. Enough variety exists in the data both to give some support to, and to create some difficulties for, each of the current explanations.

Some of the disagreements may be attributed to the use of unreliable potential-measuring methods. The difficulties involved have been recognized.[7, 13, 14] It is believed by the writer, as a result of his investigation of the potential-measuring devices used by earlier workers, that in some cases, reported values and variations in striking voltage did not exist and were falsely indicated because of harmonic resonances in the apparatus used. This has probably delayed a better understanding of the h.f. discharge mechanism. Therefore, a calibrated high frequency generator was built especially for use on this problem and was designed so as to eliminate or minimize the error-producing factors. It has been described.[15]

MODES OF DISCHARGE

An extensive study has been made of the influence of discharge chamber and electrode structure upon the initiating process of the h.f. discharge. It appears that there are three modes of h.f. breakdown, which may be described or localized as follows.

Mode *a*: Where the breakdown occurs between the electrodes, with the application of a peak potential difference approximately equal to half of the voltage required to produce a d.c. discharge under otherwise identical conditions.

Mode *b*: Where the breakdown occurs between the elec-

* Now at Wake Forest College, Wake Forest, North Carolina.

[1] K. K. Darrow, Bell Sys. Tech. J. **12**, 91 (1933).
[2] Bergen Davis, Phys. Rev. **17**, 501 (1903).
[3] Bergen Davis, Phys. Rev. **20**, 129 (1905).
[4] E. O. Hulbert, Phys. Rev. **20**, 127 (1922).
[5] J. J. Thomson, Phil. Mag. **4**, 1128 (1927).
[6] John Thomson, Phil. Mag. **10**, 280 (1930).
[7] John Thomson, Phil. Mag. **18**, 696 (1934).
[8] Fritz Kirchner, Ann. d. Physik **77**, 287 (1925).
[9] Fritz Kirchner, Ann. d. Physik **7**, 798 (1930).
[10] Lothar Rohde, Ann. d. Physik **12**, 569 (1932).
[11] J. S. Townsend and R. H. Donaldson, Phil. Mag. **5**, 178 (1928.)
[12] John Thomson, Phil. Mag. **23**, 1 (1937).
[13] Lothar Rohde, Zeits. f. tech. Physik **12**, 263 (1931).
[14] P. Mercier and G. Joyet, Helv. Phys. Acta **8**, 310 (1935) (also in Bulletin de l'asso. Suisse des Electriciens No. 25 (1935).
[15] Sherwood Githens, Rev. Sci. Inst. **8**, 48 (1937).

trodes, with the application of a peak potential difference somewhat greater than the d.c. discharge voltage.

Mode *c*: Where the breakdown takes a longer path than the inter-electrode space and occurs in the area between the electrodes and the walls of the chamber.

It is found that the mode of the discharge depends upon the chamber and electrode structure, the pressure, and the frequency of the applied e.m.f.; and that two or all three of these modes may occur, separately or concurrently, in the same discharge chamber. Most of the earlier work presupposed a single initiating mode.

There appears to exist for each of these h.f. modes of discharge a single-minimum V_s–*vs.*–p relationship resembling that of the d.c. discharge. For example, consider the 5-megacycle striking voltages observed in chamber *A* (described later) shown in Fig. 1. The V_s–*vs.*-p curves for the three modes are indicated, partly by dashed lines. Near the intersections of the curves the striking voltage is lower than it would be for either mode acting alone, and follows the portions marked *ab* and *bc*.

The shift of the breakdown mechanism from one mode to another as the pressure is changed produces a plurality of minima in the unanalyzed V_s–*vs.*–p relationship. Such plurality has been observed by several workers.[12,16-18] The possibility of various types of discharge has been noted,[12] and the work of Gill and Donaldson[16] strongly suggests a dependence upon the electrode and discharge chamber orientation, but a

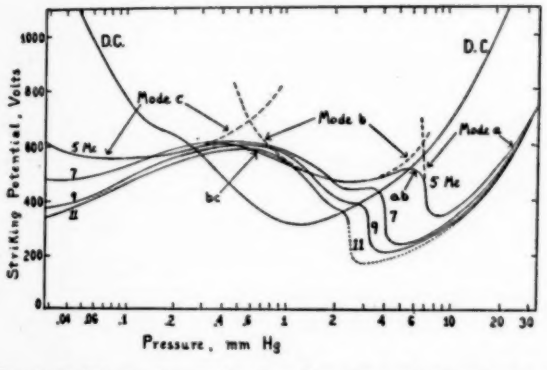

FIG. 1. Striking voltages in chamber *A* in neighborhood of the critical pressure. Electrode separation = 10.5 mm.

[16] E. W. B. Gill and R. H. Donaldson, Phil. Mag. **12**, 719 (1931).
[17] C. and H. Gutton, Comptes rendus **186**, 303 (1928).
[18] C. J. Brasefield, Phys. Rev. **35**, 92, 1073 (1930).

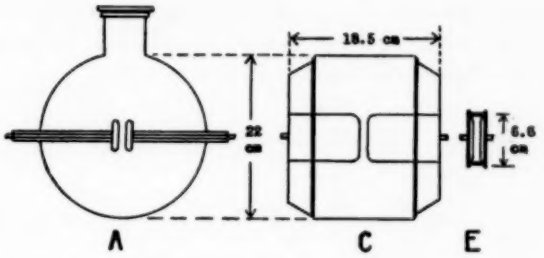

FIG. 2. Central longitudinal cross sections of three discharge chambers, to scale.

systematic analysis of this plurality has not been reported.

Over 11,000 observations of striking voltage have been made by the writer with a number of chambers falling into 7 types. The salient facts concerning the modes of discharge and the influence of chamber construction can be observed in the behavior of the type *A*, *C* and *E* chambers. The others yielded information of a corroborative nature.

THE DISCHARGE CHAMBERS

Several types of chamber yielded capricious values of striking voltage or relationships defying interpretation. It was learned that such results are caused by: (1) Chamber walls of too extensive area; (2) electrodes of complicated design; (3) insufficient radii of curvature at the edges of electrodes; (4) electrodes of such large capacity as to disturb the action and voltage calibration of the h.f. oscillator.

Five types of chamber which avoid these faults yielded useful information. They may be described as follows, with the aid of scale drawings in Fig. 2: Chamber *A* is a spherical 5-liter Pyrex flask. Its electrodes are supported by brass rods surrounded by Pyrex tubing. Chamber *C* is composed of a Pyrex cylinder and two Pyrex pie plates (dimensions shown on diagram) united with Apiezon wax *W*. Type *E* is a short length of 65-mm Pyrex tubing to which end plates, rounded as shown, are waxed. Chambers *B* and *D*, not illustrated, are identical with *C* except that *B* possesses a longer cylinder and longer electrodes, to give an over-all length of 28.5 cm; while *D* has no central cylinder at all, shorter electrodes, and an over-all length of 5.5 cm.

All electrodes are of polished brass, those in *B* and *C* being hollow. The flat portion of their

interfaces is 25 mm in diameter in *A*, and 55 mm in the others. The electrode separations used mostly were as follows:

Chamber	*A*	*B*	*C*	*D*	*E*-1	*E*-2
d (in mm)	10.5	9.5	9.6	10.2	10.0	9.8 .

In assembling, the faces of the electrodes were polished on a lathe with fine emery and rouge cloth and the parts of the chamber immediately assembled untouched by the hands, the glass parts having been prepared with bichromate acid cleaning solution and well washed with distilled water.

Auxiliary Apparatus, Procedure and Accuracy

The breakdowns were observed in hydrogen at pressures ranging from 0.001 to 150 mm Hg. This gas was selected to facilitate comparisons, for the earlier work was done preponderantly with hydrogen. It is admitted into the vacuum system from a steel cylinder through an electrically-heated palladium tube at a temperature just sufficient to pass the hydrogen. The gas thus filtered is extremely pure. The pumps and manometers employ Apiezon oil to avoid the possibility of mercury contamination.[7] The production of hydrocarbon vapors by the breakdown of Apiezon products under the influence of the discharge is apparently insufficient to influence the breakdown potential to a noticeable extent. As an added precaution, a low temperature trap has been used between the pumps and the rest of the system. Evacuation and as much baking-out as is possible is continued for a couple of days after the time when a discharge within the system cannot be produced with a three-inch spark coil.

The system and chamber are filled to the highest pressure to be investigated. The plate voltage of the oscillator is slowly raised until a breakdown occurs, whereupon it is immediately switched off. The reading of an ammeter in the oscillator circuit at the moment of discharge is recorded, to be converted into voltage later by calculation. Two to six such observations are made at each of 12 evenly-distributed frequencies in the range from 5 to 11 megacycles, and also with d.c. Some of the hydrogen is then pumped out and a similar set of observations is made. The pressure is thus lowered in about 15 steps, until a discharge is no longer producible. This large number of repeated observations is made with the same sample of gas without evidence of contamination. The absence of a change in the nature of the gas has been verified frequently by re-evacuation and insertion of new hydrogen at lower pressures. The new striking-potential curves have always matched the old within three percent. This variation is considered normal, for earlier observers have reported variations between different samples of hydrogen ranging up to five percent.[7,19,20]

The pressure is measured in one of three ways, depending upon its magnitude: by an open mercury manometer with a few centimeters of Apiezon oil floating on top of the mercury; by a differential oil manometer; or by calculations based upon a process of sharing between two chambers of known volume. The accuracy ranges from 1/10 of one, to one percent.

The oscillator produces h.f. potential ranging from about 100 to 2500 peak volts. All potentials quoted are voltages between electrodes, the value at the peak of the cycle. The relative accuracy in voltage measurement as a function of frequency is within 1.5 percent. The absolute accuracy varies directly as the magnitude of the deflection of the r.f. ammeter used in the oscillator. Two such meters, having a rated accuracy of two percent of full scale value, were employed in the work reported on. Their ranges were selected so that the average error below 600 volts is less than two percent, and is within three percent above this value; although in a few individual cases, because of extremely small meter deflection, the error is known to rise as high as eight percent. On the whole, the accuracy obtained is ample for the present work, since in general we are interested in qualitative values.

In analyzing the data obtained the average breakdown voltages for a given pressure were plotted first as a function of the *frequency* of the e.m.f.; i.e., isobaric curves were made. Then the voltages appearing on these curves at the frequencies of 5, 7, 9 and 11 Mc were plotted again as a function of *pressure*, in two ways: The strik-

[19] F. L. Jones and J. P. Henderson, Phil. Mag. **28**, 185 (1939).
[20] F. L. Jones, Phil. Mag. **28**, 192 (1939).

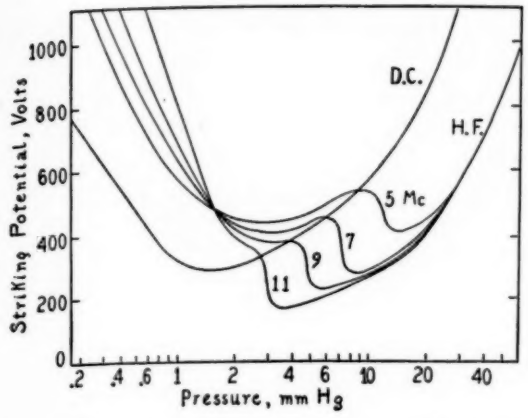

FIG. 3. Striking voltages in chamber E in neighborhood of the critical pressure. Electrode separation = 10.0 mm.

ing potentials at the higher pressures were plotted with a linear pressure scale; while those at the lower pressures were plotted against a logarithmic scale, to produce a convenient spreading of the data in this region of pressure.

V_s AT THE HIGHER PRESSURES (ABOVE 40 MM HG)

In all five of the chambers described above it is found that when the pressure is high enough for the breakdown to fall distinctly in the mode a class, the striking voltage is essentially independent of the frequency. With a 10-mm gap and frequencies between 5 and 11 Mc, and between pressures of 40 and 150 mm Hg: (1) The h.f. discharge voltage is independent of the frequency; (2) The h.f. and d.c. V_s–*vs.*–p curves are linear; (3) The h.f. values are almost exactly one-half as great as the d.c. values. Grouping together the data for all five chambers in these ranges, the ratio of the h.f. to the d.c. breakdown voltage is 0.49 ± 0.03. This is tantamount to saying that the h.f. and d.c. linear portions are not parallel, as in a previously reported case,[7] but that they intersect, and do so on the pressure axis. With the chambers and gaps herein reported on, this intersection fell at -17 ± 3 mm Hg. The slope of the h.f. linear portion is 12.2 ± 1.0 volts per mm Hg per cm gap length, and that of the d.c. curve of course is twice as great.

STRIKING VOLTAGE AT THE LOWER PRESSURES

Results of typical runs made at low pressures with chambers E-1 and A are shown in Figs. 3 and 1, respectively. In Fig. 3, we see: (1) The transitions from mode a to mode b. The lower the frequency, the higher the pressure at which the transition occurs. (2) A convergence and crossing of the mode b curves at the pressure of 1.55 mm, which is also the critical pressure on the d.c. curve. (3) The rapid rise in striking voltage below the critical pressure; the higher the frequency, the more rapid the rise.

In Fig. 1, illustrating chamber A discharge potentials, it is to be observed first that, down to 2 mm pressure, the nature of the variation in V_s with pressure and frequency is identical with that in the type E chamber; second that below 2 mm, the h.f. curves fail to converge as they do in Fig. 3. The striking voltage, instead of rising rapidly, falls below the d.c. curve again and follows a mode c type of curve. It is also noted that in the mode c range of pressure, the lower frequency curves rise first, which is the same order as is observed in the mode a to b transitions.

CHANGES IN APPEARANCE OF THE DISCHARGE

It must be emphasized that individual appearances cannot be correlated closely with striking voltages, for the voltage drops 5 to 80 percent immediately upon ignition. Conditions under sustained discharge are quite different from those at the moment of initiation. However, the *succession* of changes in appearance as the pressure is decreased is quite suggestive. The appearances of the discharge in chamber A are shown photographically in Fig. 4. At the highest pressures the glow is a narrow, striated column, which spreads out laterally as the pressure is decreased until it finally fills the chamber. The letters just above the pressure axis in Fig. 1 show the *approximate* pressures at which each appearance occurs. It is to be noted that: (1) The glow emerges from between the electrodes at about the pressure at which mode c initiation is encountered. (2) The 5-Mc discharge goes through this succession of appearances from one to two steps ahead of the 11-Mc discharge, as the pressure is decreased. This agrees with the fact that the lower frequency striking potentials go through their succession of changes ahead of the higher frequencies.

Of course, in chamber E the succession of ap-

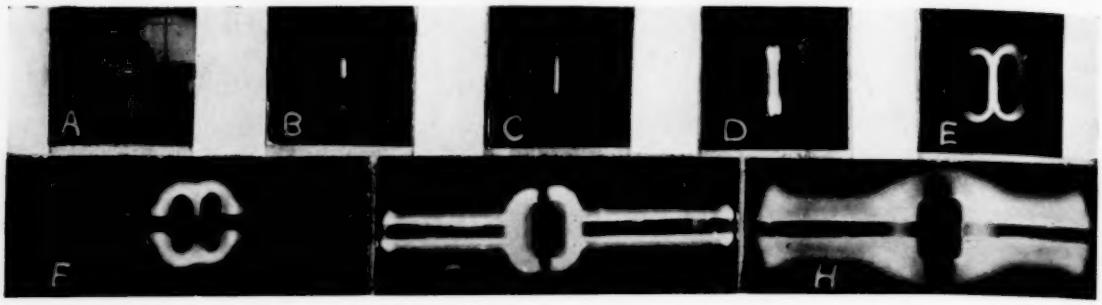

FIG. 4. Successive appearances of the glow discharge in chamber *A* as the pressure is decreased. Stage *I*, not shown, consists of a dull glow extending throughout the chamber except for darkness between the electrodes and at the inner surface of the Pyrex sphere.

pearances gets no further than stage *D*. Here the glow becomes fluttery, jumps around inside the chamber, and rapidly refuses to strike at all as the pressure is further decreased. This behavior is in agreement with the curves shown in Fig. 3 and is to be expected from Paschen's law.

STABILITY AND CONSISTENCY OF STRIKING VOLTAGE

In a type E chamber

The voltage at which breakdown occurs is sharply defined at all pressures above the critical value (1.55 mm in Fig. 3) except during the transitions from mode *a* to *b*, where the curves are steep. Here, individual trials may vary from the mean by as much as five percent. The striking potential below the critical pressure becomes progressively more poorly defined as the pressure is decreased, and at the lowest pressure the range of values obtained on successive observations may equal 30 percent of the mean. The time interval allowed between observations does not affect the striking potentials.

In the type A chamber

Observations may be made in rapid succession only at pressures above 10 mm, approximately. Below this pressure, if the potential is applied too soon after a previous discharge, the glow may strike at a subnormal voltage, from 10 to 50 percent lower than the value it would have had if a certain amount of time had been allowed to elapse. The necessary recovery time is a function of the frequency of the e.m.f. applied, as well as of the pressure. Subnormal discharges may be avoided by making observations periodically with a clock. Table I shows the times between observations which were found satisfactory. When these periods are employed, the sharpness of definition of the h.f. striking voltage in chamber *A* agrees favorably with that described above for the type *E* chamber.

In both types of chamber the d.c. striking potentials are very sharply defined above the critical pressure but show increasing randomness below this value, though not to such a marked extent as in the h.f. case. When the insertion of a new sample of gas results in a slight uniform change in the h.f. striking voltages as mentioned earlier, the d.c. values shift also.[19]

MODE *c* DISCHARGE AN EXTRA-ELECTRODE PROCESS

There is much evidence to indicate that the mode *c* discharge does not occur between the electrodes but is produced in the electric field which extends from the sides or backs of one electrode to those of the other or toward the walls of the chamber. In addition to the appearance of the discharge in the mode *c* pressure region, and to the fact that mode *c* initiation is encountered in every type of chamber *except* type *E*, which is the *only* type that does not possess an extra-electrode space, we have the following facts.

(1) In chamber *A*, if the electrode gap is reduced, the h.f. striking voltages in the mode *a* and *b* regions of pressure are considerably lessened, while the reverse is true if the gap is increased. But in the mode *c* regions of pressure the striking voltage remains the same. The gap

length does not appreciably affect the mode *c* discharge voltage.

(2) Subnormal discharges are never experienced in pure cases of mode *a* or *b* discharge, while they are always encountered in mode *c*, *bc* and *ac* discharges. They are evidently caused by the presence of charged residues on the nonconducting walls of a discharge chamber.[7,21] Locher's theory[22] and Paetow's work[23] are of interest in this connection. The presence of the charges would aid a discharge in which the walls play a part, but would be of little consequence when the initiating process is localized between the electrodes. The increasing troublesomeness of the subnormal discharge phenomenon as the pressure is lowered indicates that the neutralization and dispelling of these charges takes longer as the hydrogen density decreases.

Interelectrode Nature of Mode *a* and *b* Discharges

Since modes *a* and *b* are both found in the *E* type chambers it necessarily follows that both must be inter-electrode in nature, by virtue of the construction of this type of chamber.

The mode *a* discharge appears to be associated with the *oscillatory* motion of charged particles, for the pressure at which mode *a* becomes impossible is dependent upon both the electrode separation *and* the frequency of the applied e.m.f. At the higher pressures there is ample space between the electrodes for this oscillatory motion. That the breakdown is accomplished with about half as much voltage as the d.c. discharge would require is no doubt due to the trapping of space charge between the electrodes. As the pressure is decreased the electrode separation becomes too short for the necessary oscillatory amplitude, and when insufficient space charge can be built up to create a mode *a* discharge, the breakdown can occur only by mode *b*. The order of the frequencies at which this transition occurs agrees with considerations of the motion of a charged particle in an oscillatory field: with or without an effective resistive force due to collisions with gas molecules, the lower the frequency, the greater the amplitude of oscillation, other conditions being equal. This analysis is borne out further by the fact that when the electrode separation is *decreased*, the pressures of transition from mode *a* to *b* all shift to *higher* pressures; and conversely.

It is evident that at some frequency below 5 Mc the trapping effect and build-up of space charge between the electrodes must cease, and the striking voltage will rise to the d.c. value.

A similarity between the mechanism of the mode *b* breakdown and that of the d.c. discharge is indicated. It would be expected that if the breakdown is of the static type and occurs during a half-cycle, the voltage required to strike would be greater than the corresponding d.c. voltage because of the short duration of the half-cycle. The convergence of the mode *b* curves at a common point, at a pressure equal to the critical pressure on the d.c. discharge curve, was observed in both of the type *E* chambers. Whether this last feature was due to chance remains to be further investigated.

Overlapping of Modes of Discharge

When there is a considerable expanse of electrode side-surface the breakdown at pressures normally favorable (on the basis of electrode gap and frequency) for mode *a* or *b* discharge, may occur in part through extra-electrode ionization. The two processes acting simultaneously (mode *ac* or *bc* discharge) result in striking potentials lower than the mode *a* or *b* values. This is shown by typical striking voltages for chamber *C*, Fig. 5. Between 0.5 and 10 mm pressure the values are all considerably lower than the corresponding mode *a* and *b* values in Figs. 1 and 3. In the data pertaining to chamber *D*, the shortest chamber of this type, this depression of the striking volt-

Table I. *Time required between observations in chamber A to give consistent striking voltages.*

Pressure mm Hg	Frequency of e.m.f. 4.96–6.67 Mc	7.86–9.15 Mc	10.47 Mc
3–130	1 min.	1 min.	1 min.
2	1	2	2
0.3–1.2	1	2	3
0.17	2	2	3
0.072–0.037	3	3	4
0.019	4	5	5
0.0009		5–7 min.	
0.0046		8–10 min., or longer.	

[21] John Thomson, Phil. Mag. **21**, 1057 (1936).
[22] See L. B. Loeb, *Fundamental Processes of Electrical Discharges in Gases* (Wiley, New York, 1939), p. 498.
[23] H. Paetow, Zeits. f. Physik **111**, 770 (1939).

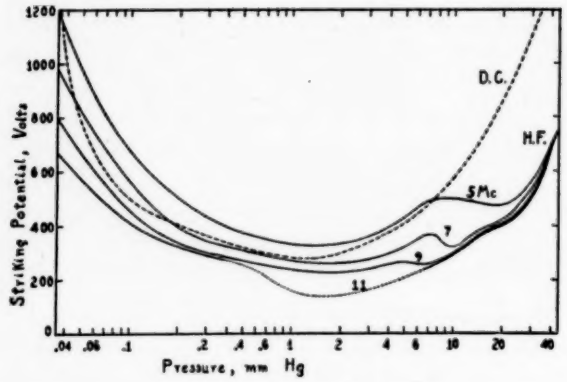

FIG. 5. Striking voltages in chamber *C* in neighborhood of the critical pressure. Electrode separation = 9.6 mm.

age is much less marked; while in the case of chamber *B*, the longest of this type, the depression is extreme, and exists up to 50 mm pressure for the higher frequencies.

Furthermore, in these three chambers considerable difficulty with subnormal strikings is encountered when taking observations in these regions of voltage-depression. Long waiting periods between observations are required. In chambers *B* and *C*, periods ranging up to one hour are necessary at the very lowest pressures to prevent subnormal discharges.

When the breakdown in what should be the mode *a* or *b* pressure region is thus assisted by extra-electrode-gap ionization, the "effective striking distance" is not equal to the electrode separation. Therefore a quantitative interpretation of the *bc* or *ac* type of breakdown is difficult if not impossible.

RELATIONSHIP TO EARLIER DATA

By considering the structure of the discharge chambers employed, most of the qualitative features of the striking voltage data obtained by earlier workers can be recognized and classified into the suggested modes. The bulk of the work appears to have fallen in the mode *c*, *bc* or *ac* classes.

In the most accurate work in this field, that by Thomson,[12] there appears to be one excellent example of pure mode *a* and *b* discharges, shown in curve 1 of his Fig. 7, which was obtained with 1.8-Mc potential. That the transition from mode *a* to *b* occurs at the low pressure of 5.5 mm is to be expected because of the larger electrode gap (25.8 mm). As noted above, the transition-pressure shifts to a lower value upon increasing the electrode separation, and vice versa. The gradients of the linear portions of curve 1 are about 13 and 12 volts per mm pressure per cm electrode separation, for modes *a* and *b*, respectively. These values agree nicely with the value 12.2 ± 1.0 quoted earlier in this article.

It therefore would appear that Thomson's other curves represent mode *c*, *bc* or *ac* discharges. If so, their gradients should not be compared with the value 12.2 ± 1.0, which applies to mode *a* discharge. Whatever the mode, the curves indicate clearly that as long as the frequency was high enough to avoid mode *a* or *b* discharges, the breakdown stayed in the same mode and in the linear portions was independent of the frequency.

Further measurements with type *E* chambers of varying sizes and gap lengths are planned, for it appears that further treatment of the mechanism of the h.f. discharge can best be accomplished with chamber conditions which produce pure mode *a* and *b* discharges.

The writer is grateful to Dr. Otto Stuhlman, Jr., who suggested this problem, and to Dr. Arthur E. Ruark for advice on the apparatus and facilities.

Properties of Rochelle Salt

HANS MUELLER
Massachusetts Institute of Technology, Cambridge, Massachusetts

(Received February 19, 1940)

In a qualitative way the anomalous properties of Rochelle salt can be explained on the basis of four different theories: (*a*) on the dipole theory, (*b*) by assuming polymorphic transitions at the Curie points, (*c*) by postulating an anomalous piezoelectric effect, and (*d*) with an interaction theory which assumes that the structure and the fundamental properties of the crystal have no unusual characteristics and which ascribes the observed anomalies to an accidental degeneration of the piezoelectric interaction between the elastic deformation and the electric polarization. The existence of a polymorphic transition at the upper Curie point is demonstrated in a new experiment and it is shown that this transition is a spontaneous elastic deformation. It can be explained on the basis of either one of the four theories. A quantitative analysis of the experimental data, which leads to a new interpretation of the elastic and piezoelectric measurements, shows that the theories (*b*) and (*c*) are not valid for Rochelle salt. The experimental data verify the conclusions of the dipole theory insofar as they lead to the result that Rochelle salt would show an abnormal temperature dependence of the dielectric constant even if the crystal were not piezoelectric or if the piezoelectric deformations could be suppressed. However, it is doubtful whether the clamped crystal has a Curie point. The observed Curie points of the free crystal result from the lattice-dipole coupling as described by the interaction theory.

THE DIPOLE THEORY OF ROCHELLE SALT

THREE theories have been advanced to account for the well-known anomalous properties[1] of Rochelle salt. The commonly accepted theory, due to Kurtschatow[2] and Fowler,[3] assumes that the phenomena are due to the Lorentz interaction between rotating polar molecules and that the lower Curie point is caused by the gradual freezing-in of the dipoles. Against this theory several objections can be raised.[4] We possess no conclusive evidence that the anomalies are due to free dipoles. On the contrary, the discovery of electric Curie points in H_2KPO_4 and H_2KAsO_4[5] shows that they occur also in crystals which contain no polar molecules. The most serious deficiency of Fowler's theory (and also of Onsager's[6] theory for H_2KPO_4) lies in the fact that it assumes a rigid lattice structure. It neglects the large piezoelectric effects which occur in all ferroelectric crystals.[7] The theory, therefore, does not relate to the commonly measured properties of Rochelle salt but rather to the properties of the strain free crystals, i.e., of crystals which are clamped rigidly in such a way that no piezoelectric deformations can take place. The measured quantities, however, are those of free crystals in which the stresses are zero. Sawyer and Tower,[8] David[9] and the writer[10] have shown that a partial suppression of the piezoelectric deformations greatly reduces the dielectric constant in the para-electric state and almost completely suppresses the hysteresis loops in the ferroelectric temperature range. The properties of the clamped crystals differ so radically from those of the free crystals that it is doubtful whether a rigidly clamped crystal would show any anomalies whatever, and hence it is questionable whether the dipole theory of Rochelle salt in its present form can be justified.

POLYMORPHISM OF ROCHELLE SALT

The second theory, due to Jaffe,[11] postulates that Rochelle salt undergoes a polymorphic

[1] For reviews see: I. V. Kurtschatow, *Seignette Electricity* (Moscow, 1933). French translation entitled: *Le champs moléculaire dans les diélectriques* (Paris, 1936). H. Staub, Naturwiss. **23**, 728 (1935). W. G. Cady, Am. Phys. Teacher **6**, 227 (1938). P. Scherrer, Zeits. f. Elektrochem. **45**, 171 (1939) and the forthcoming review by the writer in the *Annals New York Academy of Science*.

[2] P. Kobeko and J. Kurtschatow, Zeits. f. Physik **66**, 192 (1930).

[3] R. H. Fowler, Proc. Roy. Soc. **A149**, 1 (1935).

[4] Other deficiencies of Fowler's theory have been pointed out by Busch, Hablützel and Scherrer, Helv. Phys. Acta **10**, 330 (1937).

[5] G. Busch, Helv. Phys. Acta **11**, 269 (1938).

[6] L. Onsager, Symposium on Dielectrics, to appear in *Annals New York Academy of Science*.

[7] W. Lüdy, Zeits. f. Physik **113**, 302 (1939) shows that H_2KPO_4 has a piezoelectric anomaly similar to that of Rochelle salt.

[8] C. B. Sawyer and C. H. Tower, Phys. Rev. **35**, 269 (1930).

[9] R. David, Helv. Phys. Acta **8**, 431 (1935).

[10] H. Mueller, Phys. Rev. **47**, 175 (1935).

[11] H. von R. Jaffe, Phys. Rev. **51**, 43 (1937); **53**, 917 (1938).

transition at the Curie points. It assumes that the normally orthorhombic structure becomes monoclinic through a slight change of the angle between the b and c axes. Jaffe estimated that at 0°C this angle should deviate from 90° by about 2.7′. To test this hypothesis we have measured this angle as a function of temperature. Four plane mirrors were glued to the b and c faces of a rectangular block of Rochelle salt of the dimensions $l_a=4$ cm, $l_b=l_c=1$ cm. Two electrodes were attached to the a faces and connected together to avoid electric fields due to pyroelectric charges. The crystal was mounted, with the a axis vertical, within a small temperature bath with four windows and placed on the prism table of a Geneva precision spectrometer. By the usual method of autocollimation, employing a Huygens ocular, it was possible to measure the angles between the mirrors to an accuracy of 5″. The crystal was kept for over 10 hours at constant temperature, namely at 0°, 11°, 25°, 34° and 45°C. The measurements were repeated twice with increasing and decreasing temperatures, the results agreed within 15″. Although the mirrors on opposite faces were not exactly parallel (180±1.5°) the angles between them varied with temperature by less than 20″. The angles between neighboring faces, however, showed a very marked temperature variation. They stayed approximately (±20″) constant between 45° and 25°C, but below the Curie point the angle between the $+b$ and $+c$ directions diminished (and the other angles increased or decreased accordingly) by about 3′ at 11°C and by 3′45″ at 0°C.[12] These deviations are considerably larger than the experimental errors of maximal 30″. The results must be considered as the first direct verification of Jaffe's hypothesis.

The polymorphic transition of Rochelle salt is of a very unusual type. According to the x-ray evidence[13] it does not involve any marked structural changes, it has no latent heat of transition and it is not accompanied by a sudden change of the optical properties. It is a transition of the second kind in which the specific heat[14] and the temperature gradient of the birefringence[10] have a discontinuity at the Curie point. Especially significant is the fact that one can produce artificially, at temperatures above the Curie point, the same type of polymorphic transition which occurs spontaneously below the Curie point. This can be accomplished by applying either an electric field in the direction of the a axis or a shearing strain in the b, c plane. In either case the angle between the b and c axes is slightly changed, the optical properties are altered and the crystal becomes pyroelectric. To realize that the latter statement is true we recall that above the Curie point the dielectric and piezoelectric constants show a large temperature variation. Hence if a constant field or stress is applied the electric polarization of the crystal varies with temperature. The writer has shown[10] that the relation between the spontaneous polarization and the change of birefringence (spontaneous Kerr effect) is the same as between dielectric polarization and Kerr effect[15] above the Curie point. It appears most likely that also the relation between deformation and polarization is the same. A comparison of the dielectric and piezoelectric (static) measurements indicates that above the Curie point the relation $y_x=\delta\cdot P_x$ is valid, where $\delta=1\pm0.4\times10^{-6}$. Within the accuracy of the available data this relation holds also for the spontaneous polarization and deformation. For instance, at 0°C we found $y_x=3'45''=0.001$ and the spontaneous moment is $P=800$ e.s.u. (from the hysteresis loops), whence $\delta=1.2\times10^{-6}$.

We conclude therefore that the polymorphic transition is simply a spontaneously occurring elastic deformation. It can be explained on the basis of the dipole theory: The spontaneous deformation is the inverse piezoelectric effect produced by the spontaneous polarization. However, this argument can also be reversed, and

[12] Jaffe expected that these angular changes could be detected only if the crystals were grown at temperatures below the Curie point. Our determination was carried out on a crystal which had previously been used to measure the pyroelectric effect. More accurate measurements by a different method are in progress.

[13] H. M. Krutter and B. E. Warren, Phys. Rev. **43**, 500 (1933); H. Staub, Physik. Zeits. **34**, 292 (1933); Helv. Phys. Acta **7**, 1, 480 (1934).

[14] P. Kobeko and J. Nelidow, Physik. Zeits. Sowjetunion **1**, 382 (1932); A. Rusterholz, Helv. Phys. Acta **8**, 39 (1935); A. J. C. Wilson, Phys. Rev. **54**, 1103 (1938); J. F. G. Hicks and J. G. Hooley, J. Am. Chem. Soc. **60**, 2994 (1938).

[15] It is questionable whether the name "Kerr effect" is appropriate. The observed change of birefringence could also be termed a quadratic photoelastic effect. Actually, in view of Pockels' results on other piezoelectric crystals, the optical changes are most probably the result of both, mechanical and electrical, deformations.

since we have, so far, no means of deciding whether the polarization or the elastic deformation is the primary effect, we can explain the phenomena also as follows:

At the Curie points the orthorhombic lattice of Rochelle salt becomes unstable against elastic deformations, i.e., an elastic anomaly is the intrinsic cause of the abnormal properties. Our experimental results imply indeed, since the crystal gets a shearing strain without a stress being applied, that the elastic modulus s_{44} becomes infinitely large at the Curie point. Below the Curie point the lattice has two elastically stable states. An alternating field can force it to flop from one position into the other, hence the hysteresis loops. If this interpretation of Jaffe's theory is correct, the final solution of the problem of Rochelle salt must be found in its lattice structure and the lattice forces, and not in the dipole-dipole interaction.

The Piezoelectric Theory of Rochelle Salt

The third theory of Rochelle salt makes the abnormally large piezoelectric effect responsible for the anomalies. This theory was first proposed by Cady[16] and has been the guiding idea in the work of Schulwas-Sorokin and Posnov.[17] Cady pointed out that the electric susceptibility κ_F in the a direction of a free crystal is larger than that, κ_{cl}, of a clamped crystal. In a free crystal the piezoelectric deformation gives rise to an additional polarization $P'=e_{14}y_z$, where $y_z=d_{14}E$ is the deformation caused by the electric field. Hence $P_F=\kappa_F E=P_{cl}+P'=(\kappa_{cl}+e_{14}d_{14})E$. By writing this equation in the form

$$P_F=\kappa_{cl}[E+(e_{14}\cdot d_{14}P_F/\kappa_{cl}\cdot\kappa_F)]$$

one recognizes the analogy with the Lorentz equation $P=N\alpha(E+fP)$, which leads to a Curie point when $N\alpha f=1$.

The lattice theory offers a simple physical interpretation of Cady's formal theory. According to Born[18] the piezoelectric effect is the result of the so-called "inner displacements" of ions. Another way of stating the conclusions of this theory is: An elastic deformation produces a reversible change of the equilibrium orientation and magnitude of the dipole moment of the unit cell, and vice versa, a change of this moment creates an elastic deformation (homogeneous disturbance in Born's notation). The dipole moment of the unit cell is not necessarily due to the presence of polar molecules; the basic cell of most ionic lattices (NaCl) has a moment. If now an electric field is applied on a free crystal the following changes in the basic cell occur successively: First the moment is oriented; this creates an elastic deformation which in turn alters the equilibrium position of the dipole in such a way that the field can orient it still further. An additional polarization creates additional deformation and shifts the equilibrium position still further, and so on, and it is readily seen how such an "autocatalytic" reaction might eventually result in a spontaneous alignment of the moments.

This type of mechanism is essentially different from that of the dipole or the elastic theory. Though polar molecules might be involved, they are not necessary. In any case no free or hindered rotation must be assumed. In the piezoelectric theory of Rochelle salt the dipole-lattice interaction is responsible for the observed anomalies.

The Interaction Theory of Rochelle Salt

To these three older theories we now can add a fourth one. This fourth theory is a special case of Cady's theory. The formulation of this new aspect of the problem of Rochelle salt also furnishes the basis on which it is possible to decide which theory is the correct one.

The following considerations apply to the state of Rochelle salt above the upper and below the lower Curie point where the structure is orthorhombic. We consider the change Φ of the free energy of 1 cc when the crystal is deformed by a uniform strain with the components x_z, y_z, and simultaneously polarized in an arbitrary direction

[16] W. G. Cady, Phys. Rev. **33**, 278 (1929). Some writers have, erroneously, credited this theory to me. Professor Cady apparently has abandoned this theory in favor of the dipole theory (see reference 1). Partly as a matter of convenience, we shall here nevertheless refer to it as "Cady's theory."

[17] R. D. Schulwas-Sorokin, Zeits. f. Physik **77**, 541 (1932); Physik. Zeits. Sowjetunion **12**, 685 (1937); and M. V. Posnov, Phys. Rev. **47**, 166 (1935).

[18] M. Born and M. Göppert-Mayer, *Handbuch der Physik*, Vol. 24, 634–8, or M. Born, *Problems of Atomic Dynamics* (Mass. Inst. of Tech., 1926), pp. 139–154. Born's discussion of zinc blende can be generalized to fit the case of Rochelle salt and leads to the formulation given in the next section.

by a uniform electric field. By referring all quantities to a system of axes in which the x, y, z directions coincide with the crystallographic a, b, c axes, respectively, and by taking into account the symmetry properties of the orthorhombic class we obtain, in first approximation,

$$\begin{aligned}\Phi=&\tfrac{1}{2}(c_{11}x_x^2+c_{22}y_y^2+c_{33}z_z^2)\\&+(c_{23}y_yz_z+c_{31}z_zx_x+c_{12}x_xy_y)\\&+\tfrac{1}{2}(c_{44}y_z^2+c_{55}z_x^2+c_{66}x_y^2)\\&+(f_{14}y_zP_x+f_{25}z_xP_y+f_{46}x_yP_z)\\&+\tfrac{1}{2}(\chi_1P_x^2+\chi_2P_y^2+\chi_3P_z^2).\end{aligned}\quad(1)$$

P_x, P_y, P_z are the components of the polarization and c_{ik}, f_{ik}, χ_i are characteristic constants of the crystal. By differentiation we obtain the stresses $-Y_z=\partial\Phi/\partial y_z$, and the components of the electric field $E_x=\partial\Phi/\partial P_x$. This furnishes nine equations, three each of the following form

$$-X_x=c_{11}x_x+c_{12}y_y+c_{13}z_z,\quad(2a)$$

$$-Y_z=c_{44}y_z+f_{14}P_x,\quad(2b)$$

$$E_x=f_{14}y_z+\chi_1P_x,\quad(2c)$$

or by solving this system of linear equations

$$-x_x=s_{11}X_x+s_{12}Y_y+s_{13}Z_z,\quad(3a)$$

$$-y_z=s_{44}Y_z+d_{14}E_x,\quad(3b)$$

$$P_x=d_{14}Y_z+\kappa_1E_x.\quad(3c)$$

The relations between the first and second set of constants are of the following types

$$\begin{aligned}s_{23}&=(c_{12}c_{13}-c_{11}c_{23})/D_{13},\\c_{23}&=(s_{12}s_{13}-s_{11}s_{23})D_{13},\end{aligned}\qquad D_{13}=\begin{vmatrix}c_{11}&c_{12}&c_{13}\\c_{12}&c_{22}&c_{23}\\c_{13}&c_{23}&c_{33}\end{vmatrix},$$

$$s_{44}=\chi_1/D_{14},\quad(4a)\qquad D_{14}=c_{44}\chi_1-f_{14}^2\quad(4d)$$

$$d_{14}=f_{14}/D_{14},\quad(4b)\qquad=1/(s_{44}\kappa_1-d_{14}^2).$$

$$\kappa_1=c_{44}/D_{14},\quad(4c)$$

The two sets of six constants c_{11} to c_{23} and s_{11} to s_{23} are the elastic constants and compliance coefficients, and the three constants d_{ik} are the piezoelectric moduli, as defined in the usual theory. $\chi_i=1/\kappa_{cl}$ are the reciprocal of the principal electric susceptibilities of the clamped crystal (when $y_z=0$) while κ_i are the susceptibilities of the free crystal (when $Y_z=0$). In place of the more logical[19] piezoelectrical constants f_{ik} the usual theory employs the quantities e_{ik} defined by $-Y_z=e_{14}E_z$ (if $y_z=0$) or $-P_z=e_{14}y_z$ (if $E_z=0$). Comparison with Eqs. (2) and (3) shows that

$$f_{14}=\chi_1e_{14}=\chi_1d_{14}/s_{44}.\quad(5)$$

The two sets of constants c_{44}, c_{55}, c_{66} and s_{44}, s_{55}, s_{66} require special attention. They are not identical with the corresponding quantities in the usual theory, because we note that the commonly employed relation $s_{44}=1/c_{44}$ is not valid. According to Eq. (2b) c_{44} is the elastic constant for a shearing deformation during which $P_x=0$. In order to carry out such a deformation it would be necessary to apply simultaneously an electric field $E_x=f_{14}y_z$ in order to suppress the production of a polarization. The constant c_{44} (and similarly c_{55} and c_{66}) characterizes the "true" elastic properties of the crystal, because it relates to a deformation in which the piezoelectric effect plays no role.

The constant s_{44}, on the other hand, is the compliance for a deformation during which the applied field is zero. In order to measure this constant it is necessary to cover the crystal with a grounded electrode. Therefore we shall call s_{44} the compliance of the foiled crystal. It is not a true elastic constant, because even in a foiled crystal a deformation creates a piezoelectric polarization. The foil serves only to compensate for the induced surface charges but does not suppress the polarization.

We have previously pointed out that the susceptibilities κ_i of the free crystal depend on the elastic deformation. They are therefore not suitable constants to characterize the true dielectric properties of the crystal. In their stead we must use the constants χ_i. For similar reasons we consider f_{ik} as the true piezoelectric constants, because d_{14} is the moment P_x for a stress $Y_z=1$ when $E_x=0$ and depends therefore on the deformation.

The problem of finding the origin of the anomalous properties of Rochelle salt consists therefore in determining which one of the three quantities c_{44}, f_{14} or χ_1 shows an abnormal behavior.

[19] It is logical to express the energy change (1) either in terms of inner parameters (z_y, P_z) or external parameters (Y_z, E_z). Voigt's definition of e_{ik} involves a mixing of parameters (E, y_z). This inconsistency of the usual theory is the root of many misunderstandings, particularly in connection with the problem of Rochelle salt. The f_{ik} constants were introduced by Mason, Phys. Rev. 55, 783 (1939).

(We know that none of the other quantities has an unusual value.) Thus the decision between the three theories depends simply on which one of these three constants has an abnormal temperature dependence.

Unfortunately neither c_{44}, f_{14} nor χ_1 has been measured in a direct way. The experiments furnish s_{44}, d_{14} and κ_1. It is well known that κ_1 and d_{14} become extremely large at the Curie point, and our new experiment shows that also s_{44} reaches an infinite value at this temperature. According to Eqs. (4) these facts permit only one interpretation, namely, that none of the fundamental constants becomes zero or infinite at the Curie point, but that the determinant $D_{14}=c_{44}\chi_1-f_{14}^2$ vanishes at this critical temperature. This can occur even if all three parameters have normal values[20] and normal temperature gradients. Thus we are led to a fourth theory of Rochelle salt, which assumes that the structure and the properties of the crystal have no unusual characteristics. The occurrence of the anomalies is accidental. It is the result of an unusual combination of circumstances and has its origin in the lattice-dipole interaction as discussed in the preceding section. This fourth theory does not exclude any of the earlier theories, because it is possible that D_{14} vanishes because either c_{44} or χ_1 becomes unusually small or because f_{14} is abnormally large.

In a qualitative way any one of the four theories is able to account for the dielectric, piezoelectric, pyroelectric, optical, elastic, caloric and electrocaloric anomalies of Rochelle salt. Only a quantitative analysis of the experimental data can decide which one is valid. For this purpose we shall calculate the fundamental quantities c_{44}, χ_1 and f_{14} from the measured values of s_{44}, κ_1 and d_{14}, by using Eqs. (4). But before we can do this, it is necessary to clarify the interpretation of the experimental results.

[20] For most crystals, in particular also for ammonium-sodium tartrate which is isomorphous with Rochelle salt, $c_{44}\sim10^{11}$, $\chi_1\sim1.5$, $f_{14}=3$ to $7\ 10^4$. Hence D_{14} differs only slightly from $c_{44}\chi_1$ and the usual relations $s_{44}=1/c_{44}$, $\chi_1=1/\kappa_1$ are good approximations. But if for instance $c_{44}=2\times10^{10}$ (in some crystals it is even smaller) $\chi_1=0.5$ (corresponds to a dielectric constant of 25) the determinant D_{14} vanishes when $f_{14}=10^5$, and this is not an unusually large value.

The Gap Effect In Rochelle Salt

A crystal of Rochelle salt at a constant temperature above the Curie point is a system with, mainly, two independent variables: The shearing stress Y_x and the electric field E_x. In such a system the dielectric properties depend on the stress, and the elastic properties depend on the electric field. The role of external stresses in the dielectric measurements of Rochelle salt is now generally recognized, but the influence of electric fields on the elastic constants has not been taken into account in the correct manner.[21] For other piezoelectric crystals Cady[22] has discussed this problem in connection with the so-called gap effect. In Rochelle salt this gap effect is unusually large and it can readily be calculated for the experimentally most important cases as follows.

We consider a thin plate of Rochelle salt of thickness T, cut normal to the a direction, and placed between the parallel plates of a condenser with a plate separation $(D+T)$. D is the gap width. V denotes the potential difference between the condenser plates and $E_0=V/(D+T)$ is the field when the crystal is removed. The crystal is deformed by a uniform strain y_x and has therefore a uniform polarization P_x which creates a charge density $\pm P_x$ on the surfaces of the plate. If σ denotes the charge density on the condenser plates, the field intensity in the gap is $E_x'=4\pi\sigma$, and in the crystal $E_x=4\pi(\sigma-P_x)$. Whence $V=4\pi[\sigma D+(\sigma-P_x)T]$. By eliminating σ from the last two equations we obtain

$$E_x=E_0-4\pi P_x D/(D+T). \qquad (6)$$

For the special cases of a foiled or plated crystal, $D=0$, and $E_x=V/T$. For an isolated crystal, $D=\infty$, the surface charges give rise to a depolarization field $E_x=-4\pi P_x$. By inserting E_x from Eq. (6) into Eqs. (3b) and (3c) it is found that these relations can be written

$$-y_x=s_{44}^*Y_x+d_{14}^*E_0, \qquad (3b')$$

$$P_x=d_{14}^*Y_x+\kappa_1^*E_0, \qquad (3c')$$

[21] W. P. Mason, Phys. Rev. **55**, 775 (1939). A. N. Holden and W. P. Mason, Phys. Rev. **57**, 54 (1940). While the experimental work reported in these papers is of superior quality, the writer cannot agree with the theoretical interpretation of the results. It will be shown here that their calculations of the dielectric constant of the clamped crystal and of d_{14} are not justified.

[22] W. G. Cady, Physics **7**, 245 (1936).

where

$$s_{44}^* = s_{44} - 4\pi d_{14}^2 D/(\epsilon_F D + T), \quad (7a)$$

$$d_{14}^* = d_{14}(D+T)/(\epsilon_F D + T) \quad (7b)$$

$$\kappa_1^* = \kappa_1(D+T)/(\epsilon_F D + T), \quad (7c)$$

and where $\epsilon_F = 1 + 4\pi\kappa_1$ is the dielectric constant in the a direction of the free crystal. Eq. (7c) expresses the well-known fact that a small gap between electrode and crystal gives rise to a large error in the determination of the dielectric constant. Eq. (7b) shows that a gap has a similar influence on the determination of the piezoelectric modulus d_{14}. According to Eq. (7a) the elastic compliance coefficient s_{44} is smaller for a crystal held in an air-gap holder than it is for a foiled crystal. Since ϵ_F and d_{14} assume very large values in Rochelle salt, especially near the Curie point, all these changes are enormous, even for a small gap.

Of special interest is the case of an isolated crystal, i.e. when $\epsilon_F D \gg T$. Denoting by s_{44}^i the compliance coefficient of an isolated crystal, one finds from Eqs. (7a) and (4)

$$s_{44}^i = s_{44} - 4\pi d_{14}^2/\epsilon_F = s_{44}\epsilon_{cl}/\epsilon_F = 1/c_{44} + d_{14}^2/\kappa_1\epsilon_F, \quad (8)$$

where ϵ_{cl} is the dielectric constant of the clamped crystal. We can show later[23] that in Rochelle salt $d_{14}^2/\kappa_1\epsilon_F$ is a small correction term, amounting to less than 0.4 percent of $1/c_{44}$. Hence we arrive at the important result that the elastic measurements on the isolated crystal furnish very closely the true elastic properties of Rochelle salt. This is due to the fact that in an isolated crystal the depolarization field $E_x = -4\pi P_x$ prevents almost completely the production of a piezoelectric polarization.

The Elastic Properties of Rochelle Salt

The above considerations are valid only if the electrical conductivity of the crystal and its surface can be neglected. The relations hold therefore if the elastic constants are determined by a dynamic method. For static measurements, as carried out by Mandell,[24] the crystal is neither isolated nor foiled, and it is therefore not surprising that the results differ from those obtained by dynamic methods. The static methods furnish reliable results only if the crystals are foiled or if the applied stress contains no shearing components Y_z, Z_x, X_y. Static measurements of this type have been carried out by Hinz.[25] As shown in Table I his results are in satisfactory agreement with those of Mason.[26]

Elastic measurements by the dynamic method have been made by Davies,[27] Cady,[22] Mikhailov,[28] Mattiat,[29] Hiltscher[30] and Mason.[26] The constant s_{44} is calculated from the resonance frequency $f = \frac{1}{2}(E/\rho)^{\frac{1}{2}}$ of a plate, 1 cm long, for longitudinal vibrations in the direction at 45° to the b and c axes. The density ρ is 1.775 (acc. to Mason) and Young's modulus E for this direction is

$$1/E = S = \tfrac{1}{4}(s_{22} + s_{33} + 2s_{23} + s_{44}^*), \quad (9)$$

whereby s_{44}^* must be replaced by s_{44} if the electrodes are attached to the crystal, or by s_{44}^i if the plate is mounted in a sufficiently wide air-gap holder. Since $s_{44} > s_{44}^* > s_{44}^i$ (Eq. (7a)) the isolated crystal has the highest resonance frequency, f^i, and the foiled crystal has the lowest, f. The data of the various observers differ because many have neglected to take into account the large gap effect. The best data[31] are those of Mason, who

[23] The relation $s_{44}^i = 1/c_{44}$ is obtained if one approximates $\epsilon_F = 4\pi\kappa_1$. Since above the Curie point ϵ_F is nowhere smaller than 70, this approximation involves a very small error.

[24] W. Mandell, Proc. Roy. Soc. **A116**, 623 (1927). Mandell's data are derived from bending and twisting experiments on thin plates, in which it is difficult or impossible to avoid shearing stresses. Mandell reports that the crystals reached a state of constant deformation only after some minutes and he ascribes this to the slow electrical conduction along the surface. However, this leakage was not large enough to eliminate all potential differences, otherwise he would have found the large change of s_{44} at the Curie point of the foiled crystal. Mandell's data, therefore, refer to a crystal in an unknown electric field and cannot be used for a quantitative analysis.

[25] H. Hinz, Zeits. f. Physik **111**, 617 (1938). The values of s_{11}, s_{22}, s_{33}, s_{23}, s_{31}, s_{12} are obtained from measurements of the longitudinal and transversal strains for stresses parallel to the crystallographic axes which create no piezoelectric effects in Rochelle salt. Hinz's values of s_{44}, s_{55} and s_{66} are subject to the same objections as raised against Mandell's data.

[26] W. P. Mason, reference 21. His dynamic measurements on unplated crystals, cut normal to the a axis, furnish s_{11}, s_{22}, s_{33} and $(2s_{23}+s_{44}^i)$, $(2s_{31}+s_{55}^i)$, $(2s_{12}+s_{66}^i)$. Mason's determination of c_{44}, c_{55}, c_{66} neglects the gap effect and is therefore open to criticism. We shall therefore not use his values of s_{23}, s_{31} and s_{12}.

[27] R. M. Davies, Phil. Mag. **16**, 97 (1933).

[28] G. Mikhailov, Tech. Physik USSR **3**, 652 (1936).

[29] O. Mattiat, Hoch: tech. u. Elek: akus. **50**, 115 (1937).

[30] R. Hiltscher, Zeits. f. Physik **104**, 672 (1937).

[31] Other investigators, using a wide gap, find similar values, e.g., Hiltscher finds $f^i = 2.1\times10^5$, Mikhailov 2.12 $\times10^5$; others find smaller values, Mattiat 1.9, Davies 2.07×10^5. In Mason's notation $f^i = f_M$, $f = f_R$.

TABLE I. *Static and dynamic compliance coefficients of Rochelle salt.*

	s_{11}	s_{22}	s_{33}	s_{12}	s_{13}	s_{23}
Static values (Hinz)	5.23×10^{-13}	3.43	3.24	−2.18	−1.68	−1.33
Dynamic values (Mason)	5.18×10^{-13}	3.49	3.34	(−1.53)	(−2.11)	(−1.03)

finds at 30°C $f^i=2.105\times10^5$. This value furnishes $S=3.16\times10^{-12}$ and with the data in Table I and Eq. (8) one derives

$$c_{44}=1/s_{44}{}^i=11.6\times10^{10}.$$

The value of f^i decreases at a uniform rate[32] with increasing temperature. The temperature gradient is somewhat larger than in other crystals, but this can be ascribed to the fact that the crystal is near its melting point. We conclude that the elastic constant c_{44} of Rochelle salt has a normal value and a normal temperature variation. Consequently Jaffe's theory must be discarded. The spontaneous elastic deformation at the Curie point is not caused by an elastic anomaly but it is a secondary effect.

From Mason's data of f, the resonance frequency of the plated crystal, we have calculated in Fig. 1 (see also Table II) the compliance coefficient s_{44} of the foiled crystal. The result confirms our previous conclusion that s_{44} becomes infinite at the Curie point. As shown by the dotted curve in Fig. 1 s_{44} follows a Curie-Weiss law of the form

$$s_{44}-1/c_{44}=\sigma/(t-t_c) \tag{10}$$

with $t_c=23$°C and $\sigma=66.7\times10^{-12}$. σ will be called the "elastic Curie constant." According to Eq. (8) its value is related to the dielectric and piezoelectric constants by the equation

$$\sigma=(t-t_c)d_{14}{}^2/\kappa_1=C(d_{14}/\kappa_1)^2, \tag{11}$$

where C is the electric Curie constant in the law $1/\kappa_1=(t-t_c)/C$.

Mason has established an interesting relation between f, f^i and the anti-resonance frequency f_A of a foiled crystal plate, for longitudinal vibrations at 45° to the b and c direction; namely,

$$\frac{\pi f_A}{2f}\cot\frac{\pi f_A}{2f}=1-(f^i/f)^2=-k^2/(1-k^2). \tag{12}$$

As shown in the appendix this relation can be derived on the basis of the fundamental relations (3). Mason's derivation is not acceptable and the correct expression for the electromechanical coupling coefficient is (according to Eqs. (12), (9) and (8))

$$k^2=1-(f/f^i)^2=4\pi d_{14}{}^2/\epsilon_F(s_{22}+s_{33}+2s_{23}+s_{44})$$
$$=4\pi\rho d_{14}{}^2f^2/\epsilon_F. \tag{13}$$

THE PIEZOELECTRIC PROPERTIES OF ROCHELLE SALT

In this section we shall prove that the true piezoelectric properties of Rochelle salt are normal. According to Eqs. (4)

$$d_{14}/\kappa_1=f_{14}/c_{44}. \tag{14}$$

Since we have already shown that c_{44} is very nearly constant, a normal behavior of f_{14} is ascertained if we can show that the ratio d_{14}/κ_1 has a constant value in the temperature range above the Curie point.

The results of the dielectric measurements at audiofrequencies of the writer,[10] Bancroft,[33] Mason[21] and Hablützel[34] are in satisfactory agreement. The susceptibility κ_1 of the free crystal is therefore known with a good degree of accuracy, but it would be desirable to have further data at radiofrequencies.

The constant d_{14} has been measured by Norgordon[35] by a dynamic method from the inverse piezoelectric effect. He found that in the temperature range between 24° to 33° the piezoelectric effect for small fields (frequency 700 cycles/sec.) follows a Curie-Weiss law

$$-y_z=d_{14}E_x=\Delta E_x/(t-t_c), \tag{15}$$

where $t_c=23$°C and $\Delta=4.25\times10^{-5}$ (from Norgorden's Fig. 11). For the same temperature range the writer[10] has shown that κ_1 (for 1000 cycles) is given by $\kappa_1=C/(t-t_c)=178/(t-23)$.

[32] f^i decreases from 2.12 at 25° to 2.07×10^5 at 50°C. Our consideration is restricted to the temperature range above the Curie point. To explain the small discontinuity of f^i at the Curie point it is necessary to enlarge the present theory.

[33] D. Bancroft, Phys. Rev. **53**, 587 (1938).
[34] J. Hablützel, Helv. Phys. Acta **12**, 489 (1939).
[35] O. Norgorden, Phys. Rev. **49**, 820 (1936); **50**, 782 (1936).

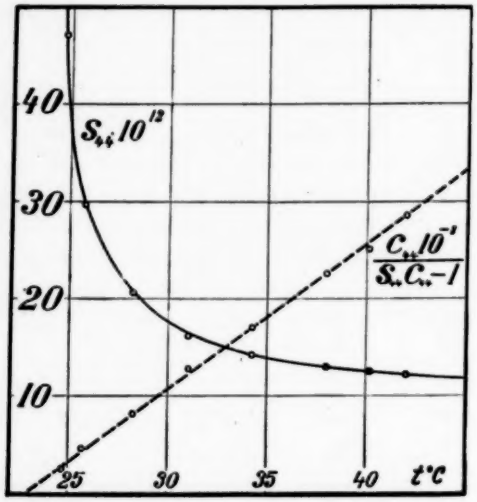

FIG. 1. The Curie-Weiss law for the elastic compliance coefficient s_{44} of a foiled crystal of Rochelle salt. $C_{44}10^{-8}$ should read $C_{44}10^{-10}$.

Hence

$$d_{14}/\kappa_1=\Delta/C=2.4\times10^{-7}$$

is constant and $f_{14}=c_{44}\Delta/C=2.8\times10^{4}$ has no unusually large value and varies but little with temperature.

This result is confirmed by the data of Mikhailov.[36] This investigator measured the change δf of the resonance frequency of a crystal plate with a change $\delta D=D_1-D_2$ of the gap width. The plate is cut normal to the a axis and the vibrations are longitudinal at 45° to the b and c direction. According to Eqs. (9) and (7)

$$\delta f/\delta D=2\pi\rho Tl^2f^3[d_{14}/(T+\epsilon_F D)]^2, \quad (16)$$

where l is the length of the plate and f is the resonance frequency for an intermediate gap D defined by $(T+\epsilon_F D)^2=(T+\epsilon_F D_1)(T+\epsilon_F D_2)$, or, approximately,

$$(T+\epsilon_F D)=4\pi\kappa_1(D_1D_2)^{\frac{1}{2}}$$

and hence

$$(d_{14}/\kappa_1)^2=\frac{8\pi D_1D_2}{\rho Tl^2f^3}\frac{\delta f}{\delta D}. \quad (16')$$

The experiments (Mikhailov's Fig. 2) show that in the entire temperature range δf is practically constant for a fixed δD. By inserting Mikhailov's data $\delta f=280\pm20$, $D_1=1.4\times10^{-2}$, $D_2=1\times10^{-2}$, $f=1.195\times10^{5}$, $l=1.447$, $T=0.2588$ we find $d_{14}/\kappa_1=3.5\times10^{-7}$, and $f_{14}=4\times10^{4}$.

Finally we have Mason's data, from which, according to Eq. (13), we obtain

$$d_{14}^2=k^2\epsilon_F/4\pi\rho f^2. \quad (13')$$

The coupling factor k can be evaluated, according to Eq. (12) either from f and f^i or from f and f_A. Table II presents a complete set of data. f, f^i and f_A are Mason's values,[37] $4S=s_{22}+s_{33}+2s_{23}+s_{44}$ is obtained from f, k_1 results from f and f^i, k_2 from f and f_A. The dielectric data are taken from the writer's measurements. This set of data shows once more that f_{14} is approximately constant and gives $f_{14}=7.2\times10^{4}$. The three methods lead to different values of f_{14}, though all are of the same order of magnitude. The difference is most probably due to the fact that the first value is based on data obtained at audiofrequencies, the second involves only measurements at radiofrequencies, while in the calculation of the third value data from high and low frequency measurements have been mixed. The static measurements[38] of d_{14} lead to a still larger value of f_{14}

[36] G. Mikhailov, Tech. Physik USSR **4**, 461 (1937).

[37] The writer is indebted to Dr. Mason for communicating the original data.

[38] R. D. Schulwas-Sorokin, Zeits. f. Physik **73**, 700 (1932); H. Hinz, Zeits. f. Physik **111**, 617 (1938).

TABLE II. *Elastic, dielectric and piezoelectric data for Rochelle salt above the upper Curie point.*

t°C	$f\times10^{-1}$	$f_A\times10^{-1}$	$f^i\times10^{-1}$	$4S\times10^{12}$	k_1	k_2	ϵ_F	κ_1	$d_{14}\times10^{8}$	$s_{44}\times10^{12}$	χ_1	$(d_{14}/\kappa_1)\times10^{7}$
24.7	10,473	16,434	21,220	51.34	0.868	0.870	1490	119	67.7	47.2	0.046	5.7
25.7	12,916	18,350	21,200	33.76	0.796	0.793	810	64.3	37.2	29.7	0.054	5.8
28.2	15,046	19,380	21,144	24.88	0.704	0.703	430	34.2	20.6	20.8	0.071	6.0
31.0	16,626	19,960	—	20.38	0.617	—	265	21.0	12.8	16.3	0.090	6.1
34.2	17,461	20,160	21,100	18.48	0.557	0.561	181	14.3	9.1	14.4	0.117	6.3
38.0	18,167	20,263	—	17.08	0.493	—	134	10.6	6.65	13.0	0.142	6.3
40.2	18,351	20,270	20,878	16.74	0.473	0.477	116	9.1	5.88	12.6	0.160	6.4
42.0	18,656	20,290	—	16.20	0.438	—	104	8.2	5.07	12.1	0.171	6.2
47.5	18,962	20,320	20,712	15.69	0.400	0.402	80	6.3	4.0	11.6	0.214	6.3
											Average $d_{14}/\kappa_1=6.2\times10^{-7}$	

of about 10×10^4. Compared with other piezoelectric crystals the value of f_{14} is not unusually large. Hence the anomalous properties of Rochelle salt cannot be ascribed to an abnormal piezoelectric effect and we can eliminate Cady's theory.

According to Eq. (8) the relation $s_{44}^i=1/c_{44}$ is not exact but involves a percental error $100\times c_{44}d_{14}^2/\kappa_1\epsilon_F$. This quantity is smaller than $(d_{14}/\kappa_1)^2c_{44}/4\pi$ and the data above show that the error is smaller than 0.35 percent and probably even less than 0.1 percent.

The elastic Curie constant, as defined in Eqs. (10) and (11), is $\sigma=C(d_{14}/\kappa_1)$, where $C=178$ for temperatures near the Curie point. Since here again we mix low and high frequency data, we chose the larger value $(d_{14}/\kappa_1)=6.2\times10^{-7}$ and obtain $\sigma=68\times10^{-12}$. The close agreement with the previously determined value shows that all data are consistent.

Finally it should be pointed out that the commonly used relation $e_{14}=d_{14}/s_{44}$ is valid only if s_{44} is the compliance coefficient of the foiled crystal. All previous calculations of e_{14} are based on s_{44}^i and lead therefore to excessive values.

The Dielectric Properties of the Clamped Crystal

We have already eliminated the elastic and piezoelectric theory of Rochelle salt and have now to make a decision between the dielectric and interaction theories. This is achieved by calculating the reciprocal susceptibility χ_1 of the clamped crystal. According to Eqs. (4*a*) and (4*c*) $\chi_1=c_{44}s_{44}/\kappa_1$, and can be calculated from the experimental data in Table II. The results are given in the table and Fig. 2 shows that the susceptibility of the clamped crystal follows a Curie-Weiss law

$$\chi_1=1/\kappa_{e1}=(t-t_c^*)/C^* \qquad (17)$$

with $t_c^*=18.5$°C and $C^*=136$. All the data which are used to find χ_1, with the exception of s_{23}, have been verified by at least two observers or two methods.[39] A small error in s_{23} does not alter the results.[40]

[39] κ_1 and f^i have been verified by at least three observers, s_{22} and s_{33} by two. The close agreement between k_1 and k_2 (Table II) is ample proof that Mason's values of f are accurate. Only these values and s_{23} are used to find χ_1.

[40] For any value of s_{23} between -1 and -2×10^{-12} the Curie point t_c^* is between 18° and 19° and C^* is unchanged.

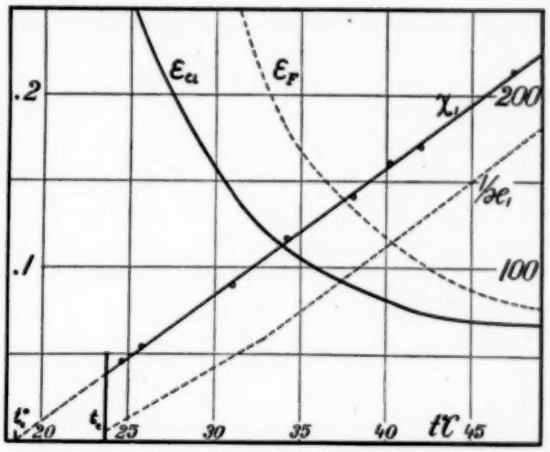

FIG. 2. The dielectric constants and the reciprocal susceptibilities of Rochelle salt for the free and the clamped crystal.

The results in Fig. 2 prove conclusively that the true dielectric properties of the clamped crystal of Rochelle salt are anomalous. However, at the Curie point $t_c=23.7$°C of the free crystal, ϵ_{c1} has a finite value of about 300. The interaction theory is therefore correct insofar as the free crystal becomes spontaneously polarized at a temperature at which the true dielectric, elastic and piezoelectric properties are normal.

Of special interest is the fact that the Curie constant $C^*=136$ of the clamped crystal coincides with that, C, of the free crystal for temperatures above 34°C.[10] That this is not a coincidence is shown by the following consideration: If the dielectric susceptibility of the clamped crystal satisfies a Curie-Weiss law $\chi_1=(t-t_c^*)/C^*$, then according to Eq. (4)

$$1/\kappa_1=(t-t_c^*-C^*f_{14}^2/c_{44})/C^*=(t-t_c)/C,$$

i.e., the clamped and the free crystal have the same Curie constant

$$C^*=C, \qquad (18)$$

We have used Hinz's values $s_{22}+s_{33}+2s_{23}=4\times10^{-12}$; Mason's value 4.9×10^{-12} gives the same C^* and $t_c=18.3$, even Mandell's value 9.4×10^{-12} produces no appreciable change of C^*, but it shifts t_c^* to about 14°C. We have calculated under what circumstances the anomalies could be explained with a constant value of the dielectric constant of the clamped crystal. This would occur if $\epsilon_{c1}=200$ and if $s_{22}+s_{33}+2s_{23}=13\times10^{-12}$. The latter value is incompatible with the measurements because it would require $s_{23}>3\times10^{-12}$. But, since $2s_{23}+1/c_{44}<6\times10^{-12}$ is definitely established by a large number of experiments, this hypothesis would lead to an infinite or negative value of c_{44}. Hence a "pure" interaction theory is excluded.

but the Curie temperature t_c^* of the clamped crystal is lower than that, t_c, of the free crystal by

$$t_c - t_c^* = \delta t = C f_{14}^2 / c_{44} = C c_{44} (d_{14}/\kappa_1)^2. \quad (19)$$

Since we have no reliable value for (d_{14}/κ_1), we cannot test Eq. (19), but it is noteworthy that the value from Table II, when applied to the temperature range above 34°, where $C=136$, $t_c=25°$, furnishes $\delta t=6°$, whence $t_c^*=19°$. Equations (18) and (19) make it possible to discuss the behavior of the clamped crystal below the lower Curie point, in spite of the fact that no elastic and piezoelectric data are available for this temperature range. If the assumption is justified that c_{44} and f_{14} have approximately the same values as they have above the upper Curie point, then the shift of the lower Curie point is found from $\delta t'/\delta t = C'/C$, where $C'=-93.8$ is the Curie constant at the lower Curie point.[10] The lower Curie point of the clamped crystal is therefore higher than that of the free crystal.

The writer[10] has shown that the dielectric data can be represented by a set of Curie-Weiss laws, whereby various temperature ranges give the values C and t_c shown in Table III. Eq. (19) serves to find the corresponding values of δt and t_c^* and we are therefore able to construct the approximate course of the $\chi_1(t)$ curve as shown in Fig. 3.

Figure 3 shows that the difference $\chi_1 - 1/\kappa_1 = 0.05$ is practically constant over the entire temperature range. This result is a consequence of $\chi_1 = c_{44} s_{44}/\kappa_1$ and $s_{44} = 1/c_{44} + d_{14}^2/\kappa_1$, (from Eq. (8)), whence

$$\chi_1 - 1/\kappa_1 = (d_{14}/\kappa_1)^2 c_{44}. \quad (20)$$

By using Eqs. (4) and (5) it is readily shown that (20) is equivalent to Cady's relation $\kappa_1 - \kappa_{el} = d_{14} e_{14}$. Eq. (20) offers the most convenient method for the determination of the dielectric

TABLE III. *Curie constants and Curie temperatures for the free and clamped crystal of Rochelle salt.*

TEMPERATURE RANGE	C	δt	t_c	t_c^*
above 34	136	6.8	25.3	18.5
32 to 24	178	8.9	23.0	14.1
− 18 to − 28	−93.8	−4.7	−17.9	−13.2
− 28 to − 42	−68.5	−3.4	−20.6	−17.2
− 42 to − 80	−47.9	−2.4	−27.1	−24.7
−100 to −140	−80.6	−4.0	16.6	12.6

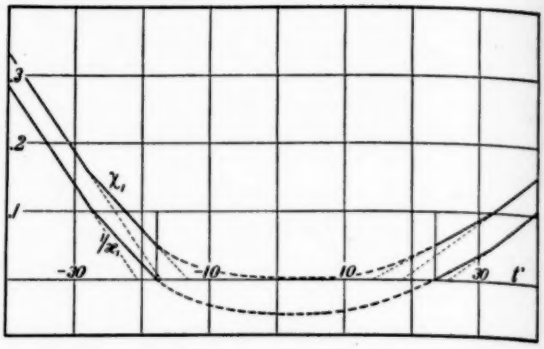

FIG. 3. The reciprocal susceptibility of the free crystal and the approximate course of the $\chi_1(t)$ curve for the clamped crystal of Rochelle salt in the ferroelectric temperature range.

properties of the clamped crystal. The value of χ_1 is obtained by displacing all points of the measured $1/\kappa_1(t)$ curve by an amount $(d_{14}/\kappa_1)^2 c_{44}$. This shift usually will vary with temperature. Its magnitude can be found from elastic measurements, since, with good approximation (use $\epsilon_P = 4\pi\kappa_1$)

$$(d_{14}/\kappa_1)^2 = (1/f^2 - 1/f^{i2})/\rho\kappa_1. \quad (21)$$

Our theory is valid only for the temperature range where the crystal is orthorhombic; i.e., above the upper and below the lower Curie point. In order to give a theory for the ferroelectric state it is necessary to enlarge the present theory by taking into account higher terms in the expression (1) for the free energy. We shall discuss this extension in another paper, in which we shall prove that the relationships between the properties above and below the upper Curie point are essentially those given in an earlier paper.[10] There, (Eq. (23) of our 1935 paper) we have shown that $-1/2\kappa_0 = (t - t_c)/C$, where κ_0 is the susceptibility corresponding to the slope of the saturation branch of the hysteresis loop. Hence by plotting $-1/2\kappa_0$ *versus* t we can interpolate between the two branches of the $1/\kappa_1$ curve in Fig. 3 and obtain the approximate $\chi_1(t)$ curve for the ferroelectric range. According to the result in Fig. 3 it appears most likely that the clamped crystal of Rochelle salt does not become ferroelectric, although its dielectric constant reaches extremely large values between −10° and 10°C.

We conclude therefore that the true dielectric properties of Rochelle salt are anomalous and this anomaly is largely responsible for the spon-

taneous polarization and deformation of the free crystal. The clamped crystal, however, most probably does not become ferroelectric, or if it does, the two Curie points are only a few degrees apart and the clamped crystal will never show a large hysteresis loop. This result is confirmed by the experiments on crystals in which the deformation is suppressed. The large hysteresis loop of the free crystals is mainly due to the piezoelectric interaction between dielectric polarization and elastic deformation.

Appendix

Anti-resonance of a vibrating crystal

We consider the case of a foiled plate of Rochelle salt, 1 cm long, cut normal to the a axis, and in the state of longitudinal vibration in the direction at 45° to the b and c axes. We refer all quantities to a new system of axes in which $x'=x$ and the y' axis points in the direction of vibration. The stress tensor associated with a longitudinal wave has only one component Y_y' and the elastic equations (3) in the new system are[41]

$$\begin{aligned} -y_y' &= s_{22}' Y_y' + d_{12}' E_x, \\ P_x &= d_{12}' Y_y' + \kappa_1 E_x, \end{aligned} \qquad (A)$$

where

$$\begin{aligned} s_{22}' &= \tfrac{1}{4}(s_{22}+s_{33}+2s_{23}+s_{44}), \\ d_{12}' &= \tfrac{1}{2} d_{14}, \end{aligned} \qquad (B)$$

and $E_x = E\cos\omega t$ is the field applied across the condenser plates. If u denotes the displacement in the direction of vibration of a volume element of the crystal, $y_y' = \partial u/\partial y'$, and the principles of mechanics furnish

$$\rho \partial^2 u/\partial t^2 = -\partial Y_y'/\partial y'. \qquad (C)$$

Since for a foiled crystal $\partial E/\partial y' = 0$, (A) and (C) lead to the differential equation of a wave

$$s_{22}' \rho \partial^2 u/\partial t^2 = \partial^2 u/\partial y'^2.$$

The solution which satisfies the boundary conditions $Y_y'(\pm\tfrac{1}{2}) = 0$ is

$$u = a \sin \omega y'/v \cos \omega t, \qquad (D)$$

i.e., a standing wave with the amplitude

$$a = (-v d_{12}' E/\omega) \cos \omega/2v, \qquad (E)$$

and traveling with the velocity $v = (\rho s_{22}')^{-\frac{1}{2}}$.

The field produces within the crystal a displacement current of density

$$i = (1/4\pi)(\partial D/\partial t) = (1/4\pi)(\partial E_x/\partial t) + \partial P_x/\partial t.$$

By inserting u from (D) into $y_y' = \partial u/\partial y'$ and substituting the result in Eqs. (A) one finds after elimination of Y_y'

$$P_x = [(\kappa_1 - d_{12}'^2/s_{22}')E - (a\omega d_{12}'/v s_{22}') \cos \omega y'/v] \cos \omega t.$$

If W is the width of the crystal the total current I passing through the condenser is

$$I = W \int_{-\frac{1}{2}}^{\frac{1}{2}} i\, dy',$$

and this leads to the final result

$$I = (\epsilon_F/4\pi) W (dE_x/dt) \times \left[\left(\frac{2v}{\omega} \tan \frac{\omega}{2v} - 1 \right) \pi d_{14}^2/s_{22}' \epsilon_F + 1 \right].$$

Resonance occurs when $\omega/2v = \tfrac{1}{2}\pi$; i.e., for the frequency $f = \omega/2\pi = \tfrac{1}{2}v = \tfrac{1}{2}(\rho s_{22}')^{-\frac{1}{2}} = \rho^{-\frac{1}{2}}(s_{22}+s_{33}+2s_{23}+s_{44})^{-\frac{1}{2}}$. This is the result used in Eq. (9). Anti-resonance occurs when $I=0$, hence for a frequency $f_A = \omega/2\pi$ for which

$$(2f/\pi f_A) \tan (\pi f_A/2f) = 1 - s_{22}' \epsilon_F/\pi d_{14}^2,$$

and comparison with Eqs. (12) and (13) shows that this is identical with Mason's relation, but the value of k is that given in Eq. (13).

[41] For the equations of transformation see W. P. Mason, Phys. Rev. **55**, 781 (1939).

On the Spark Spectrum of Silver

EBBE RASMUSSEN
Institute for Theoretical Physics, Copenhagen, Denmark
(Received April 1, 1940)

WITH a hollow cathode of pure silver in a neon discharge, a number of new spectral lines were observed, many of which had intensities comparable to the strongest silver arc lines, as shown on Fig. 1. Cooling the cathode with liquid air the strongest of the new lines in the visible and ultraviolet were examined with Fabry-Perot interferometers with silvered or aluminized plates, showing that the lines consisted of doublets with separations 0.05−0.06 cm^{-1}, the components of which had nearly equal intensities. For this reason the new lines were first believed to be combinations with the $d^9s^2\ ^2D$ term of the silver atom, since this term, because of its two s electrons, was expected to show isotope shift according to the two almost equally abundant silver isotopes. However, after the discovery of the $d^9s^2\ ^2D$ term[1] this hypothesis was abandoned because the ^2D splitting could not be found between the lines.

In order to find constant differences between the wave numbers, exposures in the region 9000 to 2000A obtained in the first order of a 21-foot grating were measured out with an accuracy of about 0.01A. By putting together the differences so found in a quadratic scheme it was ascertained that all the strong lines and some of the weaker ones could be classified as combinations between the well-known group of twelve odd terms arising from the $4d^95p$ configuration of the silver ion,

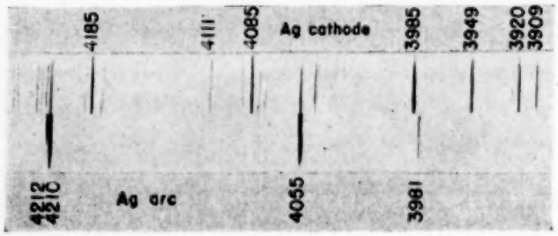

FIG. 1. Spectrum portion of the Ag spectrum showing some new lines brought out with a hollow cathode of pure silver in a neon discharge.

and five higher even terms, which do not occur either in the analysis of the silver spark spectrum by Shenstone[2] or in later supplementary papers by other investigators.[3] In fact, some of the classified lines—especially in the short wave region—have been found as weak lines in the ordinary silver spark spectrum by different observers, and are given in *Kaysers Handbook*. In Table I the intensities, wave-lengths, wave numbers and combinations of all the classified lines are given, while Table II contains the values of the new terms obtained by putting the normal state of the silver ion equal to zero.

As regards the origin of the new levels, it is very probable that the $4d^85s^2$ configuration is responsible for them, since this configuration is expected to give rise to singlet S, D, and G terms and triplet P and F terms similar to those occurring in the arc spectra of Ni, Pd and Pt from d^8s^2 configurations. This interpretation also explains the observed fine structure as an isotopic

TABLE I. *Intensities, wave-lengths, wave numbers, and classifications in the spark spectrum of silver.*

INT.	λ (AIR)	ν (VAC.)	CLASSIFICATION
20	5538.46	18050.56	$4d^95p\ ^1D_2 - 4d^95s^{1}3P_1$
20	5440.89	18374.26	$4d^95p\ ^3F_2 - 4d^95s^{1}3P_2$
15	5373.81	18603.61	$4d^95p\ ^3D_1 - 4d^95s^{1}3P_1$
10	5319.70	18792.84	$4d^95p\ ^3D_1 - 4d^95s^{1}3P_0$
20	5317.21	18801.64	$4d^95p\ ^3D_2 - 4d^95s^{1}3P_2$
10	5198.17	19232.20	$4d^95p\ ^1P_1 - 4d^95s^{1}3P_0$
80	5027.35	19885.67	$4d^95p\ ^1D_2 - 4d^95s^{1}1D_2$
10	4983.27	20061.56	$4d^95p\ ^3D_2 - 4d^95s^{1}3P_1$
5	4891.33	20438.64	$4d^95p\ ^3D_1 - 4d^95s^{1}1D_2$
100	4788.40	20877.98	$4d^95p\ ^1P_1 - 4d^95s^{1}1D_2$
50	4620.46	21636.83	$4d^95p\ ^3P_1 - 4d^95s^{1}3P_2$
80	4620.04	21638.79	$4d^95p\ ^1F_3 - 4d^95s^{1}1D_2$
10	4533.81	22050.34	$4d^95p\ ^3F_2 - 4d^95s^{1}3P_1$
30	4385.06	22798.32	$4d^95p\ ^3P_0 - 4d^95s^{1}3P_1$
20	4211.53	23737.67	$4d^95p\ ^3D_3 - 4d^95s^{1}3P_2$
100	4185.48	23885.41	$4d^95p\ ^3F_2 - 4d^95s^{1}1D_2$
30	4111.89	24312.88	$4d^95p\ ^3D_3 - 4d^95s^{1}1D_2$
80	4085.91	24467.47	$4d^95p\ ^1F_3 - 4d^95s^{1}3F_4$
70	3985.19	25085.84	$4d^95p\ ^3P_2 - 4d^95s^{1}3P_2$
60	3949.43	25312.97	$4d^95p\ ^3P_1 - 4d^95s^{1}3P_1$
70	3920.10	25502.36	$4d^95p\ ^3P_1 - 4d^95s^{1}3P_0$
50	3909.31	25572.75	$4d^95p\ ^3D_2 - 4d^95s^{1}1D_2$
80	3683.34	27141.58	$4d^95p\ ^3D_3 - 4d^95s^{1}3F_4$
75	3682.46	27148.06	$4d^95p\ ^3P_1 - 4d^95s^{1}1D_2$
80	3495.28	28601.86	$4d^95p\ ^3F_3 - 4d^95s^{1}1D_2$
70	3475.82	28761.99	$4d^95p\ ^3P_2 - 4d^95s^{1}3P_1$
10	3339.93	29932.17	$4d^95p\ ^3F_4 - 4d^95s^{1}3F_4$
100	3267.35	30597.05	$4d^95p\ ^3P_2 - 4d^95s^{1}1D_2$
90	3180.70	31430.56	$4d^95p\ ^3F_3 - 4d^95s^{1}3F_4$

[1] E. Rasmussen, Phys. Rev. **57**, 243 (1940).

[2] A. G. Shenstone, Phys. Rev. **31**, 317 (1928).

[3] H. A. Blair, Phys. Rev. **36**, 173 (1930); W. P. Gilbert, Phys. Rev. **47**, 847 (1935).

displacement of about 0.05 cm^{-1} caused by the two s electrons. While the assigned J values for the new terms are quite certain, the L values are of course only tentative and might possibly be altered.

The remarkable enhancement of the combinations with the new levels is explained by a resonance effect of collisions of the second kind between Ne ions and Ag atoms similar to the effect observed by Duffendack and Thomson[4] for other combinations of metals and rare gases. As seen from Table II, the values of the new terms, relative to the normal level of neutral silver, fall very close to the ionization energy of the neon atom, the energy discrepancy being less than one electron volt. As to the term $^3F_4$, which is a little higher than the normal ionization energy of neon, it must be remembered that the neon atom also has a second limit 780 cm^{-1} above the first.

TABLE II. *Values of the new terms in the spark spectrum of silver obtained by putting the normal state of the silver ion equal to zero.*

TERM	TERM VALUE	ENERGY DISCREPANCY	NUMBER OF COMBINATIONS
$4d^95s^2\,{}^3P_2$	105257.9	7567.7 =0.93 volt	5
$4d^95s^2\,{}^3P_1$	108934.0	3891.6 =0.48 volt	7
$4d^95s^2\,{}^3P_0$	109123.3	3702.3 =0.46 volt	3
$4d^95s^2\,{}^1D_2$	110769.1	2056.5 =0.25 volt	10
$4d^95s^2\,{}^3F_4$	113597.8	−772.2 = −0.09 volt	4

A full account of the silver spectra will be published in the *Proceedings of the Royal Society of Denmark*. I wish to express my greatest thanks to Professor Niels Bohr for his kind interest in this work.

[4] O. S. Duffendack and K. Thomson, Phys. Rev. **43**, 106 (1933).

LETTERS TO THE EDITOR

Prompt publication of brief reports of important discoveries in physics may be secured by addressing them to this department. Closing dates for this department are, for the first issue of the month, the eighteenth of the preceding month, for the second issue, the third of the month. Because of the late closing dates for the section no proof can be shown to authors. The Board of Editors does not hold itself responsible for the opinions expressed by the correspondents.

Communications should not in general exceed 600 words in length.

Theory of the Magnetite Light Shutter

In a recent article in this journal[1] Heaps has reported that a fairly coarse magnetite suspension acts in a limited way as a magnetically controlled light shutter. To explain this phenomenon Heaps assumes (1) that the particles are oriented by the magnetic field according to Langevin's theory of a paramagnetic gas, and (2) that individual particles (or small groups of particles) cast a shadow given by $S(\theta)=A\sin\theta+E\cos\theta$ appropriate to a cylinder.[2] The total shadow S cast by all particles is then computed and an expression obtained relating measured light quantities to the applied magnetic field. Heaps finds that this simple theory fails to give the correct law of variation of light with magnetic field.

It has occurred to the writer that it is more reasonable to suppose that the magnetic entities responsible for the effect have, on the average, an ellipsoidal rather than cylindrical shape. It is easy to show that the shadow cast by an ellipsoid of revolution is given by the expression

$$S(\theta)=\{(A^4\sin^2\theta+E^4\cos^2\theta)/(A^2\sin^2\theta+E^2\cos^2\theta)\}^{\frac{1}{2}}$$
$$=E+\{(A^4-E^2A^2)/2E^3\}\sin^2\theta+O(\sin^4\theta)\cdots. \quad (1)$$

On computing the total shadow S, making approximations appropriate to $a=\mu H/kT\gg 1$ and relating S to measured light quantities, the relation

$$l_{||}-l=(1/a)[(l_0-l_\perp)^4-(l_0-l_\perp)^2(l_0-l_{||})^2]/(l_0-l_{||})^3+O(1/a^2)\cdots \quad (2)$$

is obtained, to be compared with Eq. (7) in Heaps' article. Thus, for large a, it is deduced that $(l_{||}-l)\sim H^{-1}$, rather than $(l_{||}-l)\sim H^{-\frac{1}{2}}$ as earlier predicted. Eq. (2) has been tested by plotting corresponding values of $(l_{||}-l)$ and H^{-1} computed from Fig. 1 in which Heaps summarizes his experimental observations. A fairly good straight line is obtained from whose slope the average particle moment μ has been calculated to be $\mu=1.4\times10^{-12}$. This value of μ is in substantial agreement with the value ($\mu=1.0\times10^{-12}$) obtained by Heaps from a direct measurement of the magnetization curve of a more dense suspension. Hence by substituting ellipsoidal for cylindrical particles the simple theory can be retained without resort to a more complicated analysis.

W. C. ELMORE

Department of Physics,
Swarthmore College,
Swarthmore, Pennsylvania,
April 11, 1940.

[1] C. W. Heaps, Phys. Rev. **57**, 528 (1940).
[2] See reference 1 for meaning of symbols used in this note.

Influence of Electrostatic Fields on the Elastic Properties of Rochelle Salt

According to the new interaction theory of Rochelle salt, presented elsewhere in this issue, the strain-stress relation $y_s(Y_s)$ of a foiled crystal should be similar to the dielectric $P_x(E_x)$ relation, i.e., it should show hysteresis loops at temperatures below the Curie point and satisfy a $\frac{1}{3}$ power law at the Curie point. Since the shear modulus or the compliance coefficient s_{44} for small strain variations is determined by the slope of the strain-stress curve, these quantities will be altered when a large constant strain is superposed on the small strain variations. This effect is analogous to the observed variation of the reversible susceptibility when a crystal is subjected to a steady field.

If, therefore, a constant potential is applied across electrodes attached to the a faces of a plate of Rochelle salt, all resonance and anti-resonance frequencies of this plate will be altered, because the static field creates a large piezoelectric strain and hence changes the compliance coefficient s_{44} which enters into the equations determining those resonance frequencies which can be excited by small alternating fields in the a direction. This conclusion has been verified by measurements on a plate of Rochelle salt, 3×5 cm in area and about 1 mm thick in the a direction. The source of steady potential V is connected to the electrodes over large chokes and the crystal is connected to the measuring circuit over large condensors. This crystal

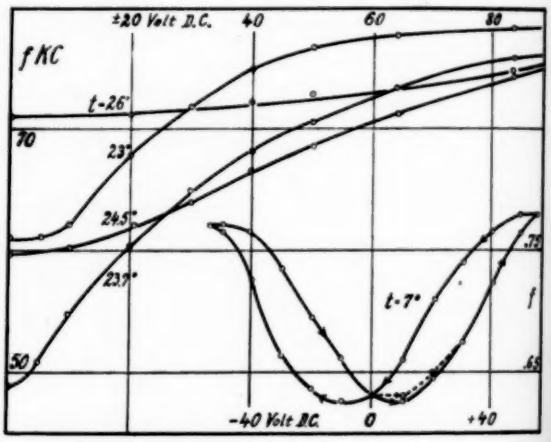

FIG. 1. Change of the resonance frequencies of a foiled plate of Rochelle salt, cut normal to the a axes, with application of a steady potential across the electrodes.

has five resonance frequencies in the range ½ to 100 kilocycles. The various modes of vibration have not been identified. All resonance and anti-resonance frequencies f show the same kind of variations with temperature and potential as shown in Fig. 1 for the highest resonance frequency. The $f(t)$ curves have a sharp minimum at the Curie point $t=23.7$°C. At this temperature the influence of static fields is very large, a field of 800 volt/cm increases the resonance frequency by over 50 percent. The magnitude of the field effect diminishes at lower and higher temperatures. Above the Curie point the changes are independent of the direction of the field and are reversible. Below the Curie point the hysteresis phenomena give rise to curves of the type shown in the figure for the lowest resonance frequency of this crystal.

HANS MUELLER

Physics Department,
Massachusetts Institute of Technology,
Cambridge, Massachusetts,
April 10, 1940.

The Theory of Multiple Scattering of Electrons

The Boltzmann equation governing the change of angular distribution with thickness of scatterer was set up by Bothe.[1] We shall here find its solution, subject to the boundary condition of no scattering at zero thickness.

Let q=total cross section for single scattering, $qp(\theta)d\Omega$ =the cross section for scattering through θ into $d\Omega$, s=thickness already traversed, $f(\Theta, \phi, s)\cos\Theta d\Omega$, $d\sigma$=number of scattered electrons leaving the surface element $d\sigma$ in the solid angle $d\Omega$ (ordinary angles Θ, ϕ) per second, N=number of atoms per cc, and $\nu=Nqs$. If the incident beam strikes normally, and is initially of unit intensity, its intensity at thickness s will be $e^{-\nu}$.

Particles scattered into $d\Omega$ (angles Θ, ϕ) will come (1) directly from the incident beam or (2) indirectly from a solid angle $d\Omega'$ (angles Θ', ϕ'), the angle between $d\Omega$ and $d\Omega'$ to be denoted by θ. The Boltzmann equation is, if we assume all angles in question to be small enough so that $\cos\Theta \cong 1$,

$$(\partial f/\partial\nu) = -f(\Theta) + \int f(\Theta')p(\theta)d\Omega' + p(\Theta)e^{-\nu}. \quad (1)$$

Expand f and p in terms of Legendre polynomials, and apply the addition theorem in evaluating the integral in (1). Set

$$f=(1/4\pi)\Sigma(2l+1)G_l p_l(\cos\Theta)$$

and

$$p(\Theta)=(1/4\pi)\Sigma(2l+1)\bar{p}_l p_l(\cos\Theta).$$

Then $G_l=\int p_l f d\Omega$, and $\bar{p}_l=\int p_l p d\Omega$. Multiply Eq. (1) by p_l and integrate. The result is

$$(dG_l/d\nu) = -Q_l G_l + \bar{p}_l e^{-\nu}, \quad (2)$$

where $Q_l=1-\bar{p}_l$.

The solution of (2), with $G_l(0)=0$, is $G_l=e^{-\nu Q_l}-e^{-\nu}$, as may be verified by direct substitution. The scattering intensity is therefore

$$f=(1/4\pi)\Sigma(2l+1)(e^{-\nu Q_l}-e^{-\nu})p_l(\cos\Theta). \quad (3)$$

Equation (3) differs from that of Goudsmit and Saunderson,[2] who find $G_l=e^{-\nu Q_l}$. If it were allowable to rearrange terms, one could find formally that the difference in scattering intensity would be $\Delta f=(e^{-\nu}/4\pi)\Sigma(2l+1)p_l(\cos\Theta)$. This series is Poisson summable (sum equals zero for $\Theta\neq 0$), but is not convergent,[3] so that the legitimacy of rearrangement is doubtful, and we cannot assert that our expression agrees with that of Goudsmit and Saunderson.

We have derived our equation without recourse to the Poisson formula, and with explicit mention of the boundary conditions. In order to extend the theory to scattering angles of the order of 90° or more, it would probably be advisable to consider the case of oblique incidence, since the experiments have been done with such an arrangement. Complications set in because (1) the Boltzmann equation is changed in detail because of the obliqueness, and (2) the $\cos\Theta$ factor interferes with the orthogonality relations previously prevailing. The theory as at present developed should not be expected to have any validity at these large angles.

JAMES H. BARTLETT, JR.

Department of Physics,
University of Illinois,
Urbana, Illinois,
April 13, 1940.

[1] W. W. Bothe, Zeits. f. Physik **54**, 161 (1929). See also Bethe, Rose and Smith, Proc. Am. Phil. Soc. **78**, 573 (1938).
[2] S. Goudsmit and J. L. Saunderson, Phys. Rev. **57**, 24, 552 (1940).
[3] Hobson, *Spherical Harmonics* (1931), pp. 339–342.

Isotopic Identification of Induced Radioactivity by Bombardment of Separated Isotopes; 37-Minute Cl^{38}

The thermal diffusion method for separating isotopes, discovered by Clusius and Dickel,[1] offers the possibility of bombarding separated isotopes as an excellent method for the isotopic identification of induced radioactivities. The bombardment of separated isotopes should be especially useful in those cases where it is difficult or impossible to make the identification by the ordinary method of "cross bombardments." We have used the thermal diffusion method to effect separation of the chlorine isotopes (mass numbers 35 and 37) in order to make definite a hitherto doubtful isotopic assignment.

A radioactive chlorine of 37-min. half-life which emits negative beta-particles has been formed by the $Cl(n, \gamma)$,[2] $Cl(d, p)$,[3] and $K(n, \alpha)$ [4] reactions. Since all of these reactions can lead to both Cl^{36} and Cl^{38} they do not make possible a definite isotopic assignment. Although the γ, n and $n, 2n$ reactions could lead to Cl^{36} and not Cl^{38} the formation of another activity of almost the same half-life (the 33-minute, positron-emitting Cl^{34} from $Cl^{35}(\gamma, n)$ [5] and $Cl^{36}(n, 2n)$ [6]) might have masked the activity.

Hydrogen chloride gas, a chlorine compound which is well suited to the thermal diffusion method, was introduced at a pressure of one atmosphere into a vertical column, which was connected to a reservoir of 12 liters capacity at the bottom. The column, of the Clusius and Dickel type,[1] was 7.5 meters in length and had an inside diameter of 6.7 mm. This tube was kept at room temperature by means of a water-cooling jacket while an axial, platinum wire (0.40 mm diameter) was kept at a temperature of approximately 650°C by the passage of an electric current through

it. After six days of continuous operation a 10-cc sample was removed from the top end of the column. This sample, which contains the light (HCl^{35}) fraction,[1] was dissolved in water and was activated, together with another solution containing an identical amount of ordinary HCl, with the paraffin-slowed neutrons formed by the bombardment of beryllium with 45 microampere-hours of 16-Mev deuterons in the 60-inch cyclotron of the Crocker Radiation Laboratory. The chloride in these solutions was precipitated as silver chloride and the radioactivity in these precipitates measured with a Lauritsen electroscope. The sample of the enriched HCl^{36} from the top of the column showed a 37-minute activity with an intensity which was only one-fifth as great as that in the sample from ordinary HCl. Bombardment of the silver chloride precipitates, as a confirmatory experiment, gave the same result. The lower intensity in the HCl^{35} sample shows that this activity is to be assigned to Cl^{38}, formed as the result of neutron absorption by the heavier isotope Cl^{37}; the intensities of the radioactivities in the two HCl samples show that the enriched sample contained about 95 percent HCl^{35}.

It is known[7] that chlorine has a larger cross section for the absorption of slow neutrons than can be accounted for by the formation of the 37-minute activity alone and Grahame,[8] in a search for a second neutron-capture activity in chlorine, showed that there is no short-lived isotope. Grahame and Walke[9] have now shown that a very long-lived chlorine is formed as the result of deuteron or neutron bombardment of chlorine. This activity, which undergoes decay by K-electron capture as well as by positron and negative beta-particle emission, is to be assigned to Cl^{36} and removes the anomaly in the slow neutron absorption cross section of chlorine.

The definite assignment of the 37-minute activity to Cl^{38} makes it likely that the high energy (5 Mev) group of beta-particles, originally reported[10] to be associated with A^{41} but shown by Davidson[11] to be inconsistent with mass data, are actually due to Cl^{38} formed in the reaction $A^{40}(d, \alpha)Cl^{38}$. A small amount of Cl^{38} would have been present with the A^{41} in the procedure used in the original energy determination.[10]

We wish to thank Professor Ernest O. Lawrence for his interest in this work and we are grateful to the Research Corporation for financial assistance.

J. W. KENNEDY
G. T. SEABORG

Department of Chemistry,
University of California,
Berkeley, California,
April 16, 1940.

[1] K. Clusius and G. Dickel, Zeits. f. physik. Chemie **B44**, 397 (1939); Naturwiss. **26**, 546 (1938).
[2] E. Amaldi, O. D'Agostino, E. Fermi, B. Pontecorvo, F. Rasetti and E. Segrè, Proc. Roy. Soc. **A149**, 522 (1935).
[3] S. N. Van Voorhis, Phys. Rev. **49**, 889 (1936).
[4] D. Hurst and H. Walke, Phys. Rev. **51**, 1033 (1937).
[5] W. Bothe and W. Gentner, Zeits. f. Physik **112**, 45 (1939).
[6] M. L. Pool, J. M. Cork and R. L. Thornton, Phys. Rev. **52**, 239 (1937).
[7] S. Kikuchi, E. Takeda and J. Ito, Proc. Phys.-Math. Soc. Japan **19**, 43 (1937).
[8] D. C. Grahame, Phys. Rev. **54**, 972 (1938).
[9] D. C. Grahame and H. Walke, private communication.
[10] F. N. D. Kurie, J. R. Richardson and H. C. Paxton, Phys. Rev. **49**, 368 (1936).
[11] W. L. Davidson, Jr., Phys. Rev. **57**, 244 (1940).

Scattering of Light by Liquid Helium

Although London's theory[1, 2] of liquid helium is able to account qualitatively for many of its properties in terms of a Bose-Einstein gas of helium atoms, it cannot be regarded as definitive, and it is of interest to consider other consequences of the theory for possible comparison with experiment. The density fluctuations and intensity of scattered light have recently been discussed in this connection by Goldstein.[3] Since this discussion makes essential use of inconclusive arguments connecting the condensation in coordinate and in momentum space, it seems desirable to give here the results of a detailed calculation.

Heisenberg[4] has used the formalism of quantized waves to calculate the energy fluctuations in a gas of light quanta obeying Bose-Einstein statistics. We have made an analogous calculation of the expectation value of the intensity of light of wave-length λ scattered by a small (spherical) volume $v \gg \lambda^3$, using Born approximation for the light waves. We use London's energy spectrum for the states of the independent atoms: $g(E)dE \propto E^{\sigma-1}dE$, where a fraction, γ, of all the atoms is supposed to be free to take part in the condensation process. The calculation is then straightforward if the wave-functions for the independent atom states are known. We assume them to be Bloch-type functions, having roughly the orthonormality properties of plane waves, and distributed in the space of the propagation vector $\boldsymbol{k}$ with density: $g(E)dE \propto k^2 dk$. This is certainly true for the free-atom case[1] ($\sigma = \frac{3}{2}$, $\gamma = 1$), and appears to be the most reasonable interpretation of London's formalism for the other cases.[2] We then obtain for the ratio R of the intensity of light scattered per unit solid angle at 90° to the intensity of the incident unpolarized light:

$$R = \frac{4\pi^2\gamma v}{\lambda} \frac{(\mu-1)^2}{(\rho\lambda^3)^{1-1/\sigma}} \frac{T}{T_0}\left[1-\left(\frac{T}{T_0}\right)^{\sigma}\right]\left[\frac{3\gamma}{2^{7/2}\pi\zeta(\sigma)\Gamma(\sigma+1)}\right]^{1/\sigma},$$

when the index of refraction μ is close to 1; ρ is the atomic density, and ζ is the Riemann ζ-function. For temperatures T equal to or slightly greater than the temperature T_0 of the lambda-point, R does not strictly vanish, but is smaller than the above by a factor of order $(\rho\lambda^3)^{\alpha}$, where $\alpha = 1-1/\sigma$ for $\sigma \leqq 2$, and $\alpha = 1/\sigma$ for $\sigma \geqq 2$. A similar calculation shows that the relative mean square fluctuation in the density of a small region containing n particles on the average is of order $n^{1/\sigma-1}$, for $T < T_0$.

For liquid helium ($T_0 = 2.19$°K) under its vapor pressure at 2.0°K, $\rho = 2.2\times10^{22}$, $\mu = 1.028$. For $\lambda = 4358$A, the free-atom model ($\sigma = \frac{3}{2}$, $\gamma = 1$) gives $R_1 = 5.6\times10^{-3}$ for a centimeter cube. This corresponds to the scattering found experimentally by Keesom[5] for ethylene 0.36°C above its critical point, and is far too large to have escaped observation. The present calculation must therefore be regarded as a further argument against London's first model.[1] The experimental specific heat curve is reproduced well[2] with $\sigma = 5$, $\gamma = 0.136$; this gives $R_2 = 2.0\times10^{-7}$, which is even smaller than for normal liquids ($R = 2.0\times10^{-6}$ for water under standard conditions), and would be difficult to measure.

The numerical value R_2 calculated on the basis of the independent atom model cannot be regarded as comparable with experiment, since it neglects the correlations between the positions of the atoms that would be expected to play a decisive role in the fluctuations. For comparison with experiment, it is probably correct to employ the usual formula[6] together with the experimentally observed isothermal compressibility;[7] these give $R_3=1.3\times10^{-10}$, a value that is practically unaffected by crossing the lambda-point. However, this is so small as to be quite unobservable experimentally. The large difference between R_2 and R_3 indicates the importance of correlations in the density fluctuations.

The writer is indebted to Professor J. R. Oppenheimer for several helpful discussions of this subject.

L. I. SCHIFF

Department of Physics,
University of California,
Berkeley, California,
April 10, 1940.

[1] F. London, Phys. Rev. **54**, 947 (1938).
[2] F. London, J. Phys. Chem. **43**, 49 (1939).
[3] L. Goldstein, Phys. Rev. **57**, 241, 457 (1940).
[4] W. Heisenberg, Ber. Math.-Phys. d. Sächs. Akad. (Leipzig) **83**, 3 (1931).
[5] W. H. Keesom, Ann. d. Physik **35**, 591 (1911).
[6] R. C. Tolman, *Principles of Statistical Mechanics* (Oxford, 1938), p. 647.
[7] J. Satterly, Rev. Mod. Phys. **8**, 347 (1936).

The Attainment of High Hydrostatic Pressures

In a two-stage cascaded pressure apparatus designed and built by the Geophysical Laboratory hydrostatic pressures were attained in the second inner pressure vessel as predicted from the hypothesis recently published.[1]

In the run made on March 21 with this apparatus a pressure in excess of 200,000 atmospheres was obtained in the second-stage cylinder; no attempt was made to go to higher pressures because this was the limit to which the gages would record. Owing to the jerky behavior of the apparatus with increasing pressure, piston displacement measurements were made only as pressure was released. These measurements indicated that sodium chloride was compressed in excess of 20 percent—perhaps nearer to 30 percent—by this pressure. As a measure of sensitivity the initial volume compressibility to 10,000 atmospheres was obtained as 4.2×10^{-6} which agrees very well with the accepted compressibility of sodium chloride. The Carboloy piston of the second stage was under such high internal stress after this cycle of operations that it shattered on receiving a slight jar.

The first-stage cylinder has two pistons actuated by two presses tied together. One of these pistons is used to develop the hydrostatic pressure in the first-stage cylinder and the second piston is used to force the inner piston down. In the pressure run described above the inner piston diameter was one-eighth inch and the length less than one-quarter inch. The first-stage pressure was about 18,000 atmospheres.

In another run in which the inner piston was made one-half inch long, for a longer stroke, and the first-stage pressure reduced to 15,500 atmospheres the inner piston shattered at about 135,000 atmospheres.

Grateful acknowledgment is made to Dr. J. A. Fleming and Dr. M. Tuve of the Department of Terrestrial Magnetism for their hearty stimulus and cooperation. To Professor F. Bitter of Massachusetts Institute of Technology and Professor P. W. Bridgman of Harvard, we are indebted for the discussions held with them concerning the project involving the use of very high hydrostatic pressures which was begun about a year ago. Our thanks are also due the Carboloy Corporation and others for their kindness in making available to us the necessary alloys and to Mr. F. Rowe who built the apparatus.

ROY W. GORANSON
E. A. JOHNSON

Geophysical Laboratory, (RWG)
Department of Terrestrial Magnetism, (EAJ),
Carnegie Institution of Washington,
Washington, D. C.,
April 18, 1940.

[1] Roy W. Goranson, J. Chem. Phys. **8**, 323 (1940). A condensed version of this paper was presented at the September, 1939, meeting of the International Union of Geodesy and Geophysics.

Proceedings of the Metropolitan Section of the American Physical Society

Minutes of the Columbia University Meeting, April 5, 1940

THE second meeting of the Metropolitan Section of the American Physical Society for the season 1939–1940 was held at 3:00 P.M. on Friday, April 5, 1940, in the Pupin Physics Laboratories of Columbia University. The following papers were presented:

Vacuum Tubes for Decimeter Waves.—A. L. Samuel.
Hollow-Conductor Wave Guides—Theory and Practice.—A. E. Bowen.

The following officers were elected for the season 1940–1941:

Chairman, L. A. Turner.
Vice Chairman, Bernhard Kurrelmeyer.
Secretary-Treasurer, W. S. Gorton.
Members of the Executive Committee,
Edith H. Quimby and H. L. Hull.

W. S. Gorton, *Secretary-Treasurer*